

## Novel broad-spectrum virucidal antivirals

Présentée le 10 décembre 2021

Faculté des sciences et techniques de l'ingénieur  
Laboratoire des nanomatériaux supramoléculaires et interfaces - Chaire Constellium  
Programme doctoral en science et génie des matériaux

pour l'obtention du grade de Docteur ès Sciences

par

**Matteo GASBARRI**

Acceptée sur proposition du jury

Prof. M. Ceriotti, président du jury  
Prof. F. Stellacci, directeur de thèse  
Prof. M. M. Stevens, rapporteuse  
Prof. D. Lembo, rapporteur  
Prof. H.-A. Klok, rapporteur

# Acknowledgements

I always thought that the “acknowledgments” are the most interesting part of a PhD thesis since it tells more about the person and the journey he lived than the science. Indeed, it is usually the first part I read, when I open a PhD thesis. I hope if you are here, you will enjoy reading also some of the thesis, but if not, I hope you will grasp some insights about the PhD journey I lived during my years at EPFL.

This thesis tries in fact to collect the work performed during my PhD in the last 4 years. However, it talks just about the scientific findings, discoveries and achievements, but does not tell about all the rest. And a PhD is usually much more about the rest. My PhD was a very long journey during which I have grown as a person, a human-being, a colleague and as a scientist thanks to all the people, the experiences, the successes and failures I encountered.

Starting from the very end of the journey, I would like to thank the jury members of my PhD defence: prof. Molly Stevens, prof. David Lembo, prof. Harm-Anton Klok and the president prof. Michele Ceriotti. They dedicated some time of their very busy agenda to read my thesis and take part of my defence. I truly enjoyed our discussion and I appreciated each question, because they made the defence a really broad and sharp conversation about my projects and beyond. I only regret that it was only on line, so we could not further proceed our dialogue during a lunch.

This journey would not be possible without my supervisor, prof. Francesco Stellacci. When I applied to EPFL in April 2017, I was a young student from a small university in Rome, applying for a top-10 Materials Science Department in the world. He saw in me something, I was not aware of. I am still wondering what he saw in me at the time. However, he gave me the opportunity to join a top-class university and working in a field far from my background. He gave me trust, responsibility and freedom and he let me grow as a scientist and as a person. Furthermore, he gave me the opportunity to explore my passion for innovation. I enjoyed working in his lab for the exposure to so many projects and collaborations, for his vision and his passion to science, his commitment and motivation. Thanks for letting me embark on this adventure and let me discover that “something” that you saw in me in advance.

I joined the lab, SuNMIL, in September 2017, and at that time it was *SuNMIL 2.0*. Pelin, Nikos, Ula, Ahmet, Zhi, Elif, Evi, Xiaowang, Huayan, Bhadra, Marta, all people that were a part of my first months in SuNMIL. In particular, I want to thank the virus sub-group, with Rosie, Matej and Ozgün, with whom I have shared very insightful discussions at the very beginning of my PhD. A special thanks to Pelin and Rosie, that spent time teaching me first the synthesis of gold nanoparticles and the world of the biolab to a freshman.

At the time of writing SuNMIL changed completely its shape becoming a sort of *SuNMIL 3.0*. Łukasz, Xufeng, Heyun, Ting, Laura, Lixia, Pamina, Cecilia, Hanna, Melis, Yong, Chihui, Weina, and someone that was part of it for a while as Nicolò, Vladimir, Yndia and Colleen or our visiting PhD students Ester, Camilla and Harita. Thank you all for the lunches, the laughs and the discussions. I leave the role of Italian ambassador to Francesca and Vincenzo, please keep defending Italian cuisine! I hope that, apart from my cooking madness, I have also given you good scientific and personal advices.

A special mention goes to Suiyang. Suiyang and I were the two PhD students’ part of the transition from SuNMIL 2.0 to 3.0. We met during the Hiring Days and we shared each and every moment of our PhDs

## Acknowledgements

---

from day 0 until the very end. Thanks for our conversations going from science to basketball from international politics to our life choices.

Two columns of SuNMIL are still there throughout the whole journey: Quy and Paulo. I want to especially thank Paulo for his commitment, his passion and his love for science. I truly enjoyed our discussions, either on science, economics, politics or football. Thanks for your continuous support and help in every aspect of my PhD.

Last, I have to thank the two people with whom I shared the office for more than 3 years, Simone and Anna. Simone was the representation of dedication and stubbornness, and, even with our opposite views of many things, it was special to meet you and share a large part of our PhDs. Anna was the very first person that I met in the office, and she welcomed me. She immediately became a reference for me, scientifically and personally, and a friend, more than a colleague. We shared so many moments inside and outside the lab, from our numerous travels to Ticino with our amazing molecular cuisine experiments to our countless discussions on any possible topic. Thanks a lot for everything I learnt from you.

This PhD and whole the projects I have worked on were possible just thanks to so many collaborations with people, groups and universities all around the world, giving a real sense to the definition of “collaborative science”.

I have to thank prof. Tapparel from University of Geneva for hosting me in her lab multiple times and for the very tight collaboration we have had on many projects. I have spent so many hours working with her postdocs Valeria Cagno and Chiara Medaglia, that we were almost part of the same research group. Valeria was my contact person for each virology-related doubt. I have started asking questions on virology since day 1 and she was always there keen to explain. We have then spent countless hours dressed in Tyvek suite in BSL3, working on SARS-CoV-2, in a very stressful and demanding period. I was lucky to work at your side and take some of your knowledge, motivation and willingness. Chiara, thanks for your mindset, for your positivity and for our discussions that helped deepening our understanding on the projects. Thanks also for bringing our talks always somewhere far from science, being Italian food, holidays venues or books.

I have to thank prof. Rainer Haag from Free University of Berlin and his postdoc Ehsan Mohammadi-far for our long-standing collaboration that brought to very important results. Thanks, Ehsan, for your work, your calm and support during these years.

Thanks to all the other people I collaborated with from University of Groningen (RUG), University of Zurich (UZH), Swiss Federal Institute of Technology Zurich (ETH), Imperial College London (ICL), University of College London (UCL), Vanderbilt University and many others. I want to thank all the people I met in the conferences, seminars and talks I have attended around the world in Singapore, Berlin, Paris, Basel or Rome.

Thanks to NCCR Bio-Inspired Materials for the support. It was great to participate to our annual gathering in Charmey and take part to our scientific discussions. Thanks to Werner Siemens Foundation for the generous support, they gave us during the pandemic, believing in our projects.

During these years I had the possibility to follow and nurture my passion for innovation and technology transfer and I have learnt so much thanks to the many courses I had the chance and privilege to attend. Thanks to Innosuisse, to the Technology Transfer Office of EPFL, to College of Management of Tehcnology and to Catalyze4Life for organizing such great seminars and in particular thanks to prof. de

## Acknowledgements

---

Rassenfosse, Mauro Lattuada, André Catana, Lan Zuo and Gautam Maitra and all the amazing speakers that gave me a glimpse of this fascinating world.

Probably the largest acknowledgement goes to EPFL. Starting from the vision of the president Martin Vetterli and the board, down to each professor, scientist, technician or staff, I had the real privilege to be part of such an amazing community. The exposure to such brilliant pool of talents made me explore how science can be performed at a different level, being at the forefront of research, where real breakthroughs are happening. This was a priceless experience, that makes you feel you are at the centre of the world.

Furthermore, during my PhD, I was Safety Coordinator and BioSafety Officer, so I was exposed to so many offices and roles at EPFL that I really felt the importance of the support coming from all of them. EPFL gives a marvellous assistance to all of us as scientists, that I feel we are almost spoiled. The support coming from each facility is enormous and the knowledge that the scientists and technicians can share is just incredible. During the beginning of the pandemic, I could appreciate even more the impact that each office has on our daily work. Being the chem-shop, the concierge, the maintenance or the head of department, everyone is a gearwheel that allows to do our science in the best possible way and it should never be given as granted.

In particular, I want to acknowledge some people that did a tremendous job to let us work with SARS-CoV-2 at EPFL in April 2020, and with whom I had a continuous interaction during the last years. I want to thank Camille Freyssenet, Eleonora Simeoni, Neeraj Dhar, Vivianne Pardun, Patrick Gerber and all the people from DSPS that take care of our health, safety and prevention. Your help, support, and attitude are extremely valuable and I appreciated and learnt working with each one of you. Thanks.

Thanks to our secretary Chiara Donini and to the EDMX secretary Chrystelle Demierre for the support in everything concerning bureaucracy, reports, invoices, and reimbursements.

Doing a PhD abroad, means much more than the title. It means living in another country, in a different context and in a new environment. Everyone knows that at first, I did not fall in love with Lausanne, being a spoiled roman, in love with his city. However, the time helped me understanding the beauty of this city and this country. The calm, the organization, the lake, the mountains, the nature, the landscapes, the views, the slopes, hiking and skiing. It has been an amazing experience, that would be possible just thanks to all the people with whom I shared these moments.

Thanks to MUPDFQ: Leonardo, Uccello, Alessio, Dani, Presidente, Simo e Fabio. Our conversations, memes, pizzas, dinners were priceless and our support during the pandemic was a large source of laughs. Thanks also to our new friend Gianmarco Tamperi, that after his gold medal at the Olympics wanted to play basketball with us. Thanks to all the Propagandi: Anelli, Grisa, Anna, Antimo, Oliviero, Silvia, Luca, Gloria, Gigi. Our never-ending discussions on science and politics deserves tickets and popcorn, but our Italian dinners could be worth a Michelin star. Thanks to Enri, Fede, Ana, Fra for our beers, Suze, abricotines and endless laughs. Thanks to my first flatmate, Federico, for his passion for research. Thanks to all the people I have met during the journey between PhD retreats, dinners, seminars, aperos: Lorenzo, Daniel, Michele, Oriane, Michele, Nicola, Master-Shen, Matteo, Giulia, Matteo, Lorenzo and many more.

Being far from home, it is not always easy, and during the pandemic this burden was even higher. I am strongly attached to my family and my friends in Rome, and not sharing such an emotionally intense period left its signs. However, thanks to WhatsApp, Facebook, Instagram, Zoom, Skype, we were able to stay

## Acknowledgements

---

in touch with all of them. Thanks to my long-standing friends Colino, Cocco, Rik, Claudio, David, Danilo, Valerio, Andrea that always welcome me back in Rome as nothing changed, even though I missed many pieces of the puzzle. Thanks also to Lollo, Martino, Diego, Eli and all the people around the world that supported me throughout these years. I hope to come and visit you soon.

I thank my family, because I would not be here without them. Their values, their honesty, their will, their support and their love are a true source of inspiration. Thanks to my grandma for always welcoming me with my favourite dishes and for her infinite love, to my aunts for their affection, to my uncle for the curiosity with which he has fed me and for his genuine enthusiasm, to my brother-in-law and my sister-in-law for their fondness, to my brother and my sister for being always at my side, supporting me even without asking, and to my niece and my nephew for their smiles, their tenderness and for their different view on the world.

Thanks to my parents for being what they are. Their constant hidden presence gives me strength and their continuous support and pride keeps me running in this incredible journey.

Last, thanks to Tania, for sharing with me the search for the meaning of the word “together”.

Thanks.

*Lausanne, 3<sup>rd</sup> November 2021*

Matteo Gasbarri

## Abstract

The current COVID-19 pandemic has showed the threats that viruses can cause to the whole world. Over 200 million infections and over 4.5 million deaths and enormous socio-economic impact were the output of the emergence of a single new pathogen: SARS-CoV-2. The development of vaccines is the paramount solution to overcome the pandemic. However, even with extraordinary and unprecedented worldwide efforts, it took almost one year to have a first validated vaccine and it will take longer to have a global vaccination. In addition, vaccines are preventive drugs, that need to be administered before the infection to stimulate the immune-system of the patient. In the meanwhile, in case of an infection, we were harmless in the fight against the virus.

Antivirals are curative drugs, that inhibit one step of the viral replication. Many approaches have been investigated: antibodies, peptides, peptomimics, small molecules. Most of them are specific to a single family of virus, making the development slow and expensive. Entry inhibitors are a class of antivirals that binds to the virus, preventing the attachment to the cell membrane. Such antivirals usually have a broad-spectrum of action, since they mimic cell receptors, such as heparan sulfate proteoglycans (HSPGs), exploited by different viruses. Many compounds have been developed throughout the years; however, the reversible nature of the virus inhibition mechanism has prevented their translation to the clinic.

Our group has recently shown that the simple addition of a long hydrophobic linker makes the inhibition irreversible, proving this hypothesis with two compounds: gold-nanoparticles and beta-cyclodextrins. The goal of this thesis is to develop novel antivirals able to inhibit a broad-spectrum of viruses with an irreversible mechanism of action and to investigate the key features responsible of such properties.

In this thesis, we further expand the broad-spectrum activity of gold-nanoparticles and beta-cyclodextrins showing that they are capable of inhibiting viruses beyond HSPG-dependent ones. In addition, we show their ability of reversibly inactivating SARS-CoV-2. Moreover, we have investigated the role of the hydrophobic linker's length in the virucidal inhibition in case of cyclodextrins, proving the need of such moiety to have an irreversible viral inactivation. Envisioning a translation of such drug, we have performed a preliminar pharmacokinetic study performed via intranasal administration.

A novel class of compounds has been also proposed: sulfated/sulfonated dendritic polyglycerol. A broad investigation of the molecular design rules needed to achieve nanomolar irreversible viral inhibition is discussed. We also show that the most active compound proves to be active against HSV-2 and RSV, thus with a broad-spectrum activity. In addition, we demonstrate that the virucidal activity is leading to the release of viral DNA upon interaction between the virus and our dendritic polyglycerol. A different modification of dendritic polyglycerol, bearing carboxylic acid, showed activity against SARS-CoV-2; such inhibition results to be irreversible. This compound has been further tested in a hamster model, where initial studies confirm its feasibility as antiviral.

In addition to these studies on development of virucidal antivirals, different technological solutions to prevent viral spreading are proposed. In particular, we focused on an antiviral filter and antiviral surfaces.

## Keywords

Antivirals, broad-spectrum, virucidal, entry inhibitors, SARS-CoV-2, HSV-2, nanomaterial, supramolecular



## Riassunto

L'attuale pandemia di COVID-19 ha mostrato le minacce che i virus possono causare al mondo intero. Oltre 200 milioni di infezioni e oltre 4,5 milioni di morti e un enorme impatto socio-economico sono stati l'output dell'emergenza di un unico nuovo patogeno: SARS-CoV-2. Lo sviluppo dei vaccini è la soluzione fondamentale per superare la pandemia. Tuttavia, anche con sforzi mondiali straordinari e senza precedenti, ci è voluto quasi un anno per avere un primo vaccino approvato e ci vorrà ancora più tempo per avere una vaccinazione globale. Inoltre, i vaccini sono farmaci di prevenzione, che devono perciò essere somministrati prima dell'infezione per stimolare il sistema immunitario del paziente. Nel frattempo, in caso di infezione, siamo rimasti senza armi nella lotta al virus.

Gli antivirali sono farmaci curativi, che inibiscono una fase della replicazione virale. Molti gli approcci studiati: anticorpi, peptidi, peptomimici, molecole. La maggior parte di essi è specifica per una singola famiglia di virus, rendendo lo sviluppo lento e costoso. Gli inibitori dell'ingresso sono una classe di antivirali che si lega al virus, impedendo l'adesione alla membrana cellulare. Tali antivirali di solito hanno un ampio spettro d'azione, poiché imitano i recettori cellulari, come i proteoglicani dell'eparano solfato (HSPG), utilizzati da diversi virus. Molti composti sono stati sviluppati nel corso degli anni; tuttavia, la natura reversibile del meccanismo di inibizione del virus ha impedito la loro traslazione clinica.

Il nostro gruppo ha recentemente dimostrato che la semplice aggiunta di un lungo linker idrofobico rende irreversibile l'inibizione, dimostrando tale ipotesi con due composti: nanoparticelle d'oro e beta-ciclodestrine. L'obiettivo di questa tesi è quello di sviluppare nuovi antivirali in grado di inibire un ampio spettro di virus con un meccanismo d'azione irreversibile e di investigare le caratteristiche responsabili di tali proprietà.

In questa tesi, ampliamo ulteriormente l'attività ad ampio spettro delle nanoparticelle d'oro e delle beta-ciclodestrine dimostrando che sono in grado di inibire altri virus oltre a quelli dipendenti da HSPG. Inoltre, mostriamo la loro capacità di inattivare in modo reversibile SARS-CoV-2. Abbiamo quindi studiato il ruolo della lunghezza del linker idrofobico nell'inibizione virucida delle ciclodestrine, dimostrandone la necessità per avere un'inattivazione virale irreversibile. Ipotizzando una traslazione clinica di tale composto, abbiamo condotto uno studio farmacocinetico preliminare effettuato tramite somministrazione intranasale.

È stata inoltre proposta una nuova classe di composti: il poliglicerolo dendritico solfato/sulfonato. In particolare, viene discusso un ampio studio sulle regole di design molecolare necessarie per ottenere una inibizione virale nanomolare. Mostriamo inoltre che il composto più attivo risulta essere efficace contro HSV-2 e RSV, quindi con un'attività ad ampio spettro. Inoltre, dimostriamo che l'attività virucida determina un rilascio di DNA virale in seguito all'interazione tra il virus e il nostro poliglicerolo dendritico. Una diversa modificazione del poliglicerolo dendritico, contenente acido carbossilico, si mostra attiva contro SARS-CoV-2; tale inibizione risulta irreversibile. Questo composto è stato ulteriormente testato in un modello animale di criceto, dove studi iniziali confermano la sua efficacia come antivirale.

Oltre a questi studi sullo sviluppo di antivirali virucidi, vengono proposte diverse soluzioni tecnologiche per prevenire la diffusione virale. In particolare, ci siamo concentrati su un filtro antivirale e superfici antivirali.

## Parole-chiave

Antivirali, ampio spettro, virucidi, inibitori di ingresso, SARS-CoV-2, HSV-2, nanomateriali, sopramolecolari



# Contents

<b>Acknowledgements</b> .....	<b>i</b>
<b>Abstract</b> .....	<b>v</b>
<b>Keywords</b> .....	<b>v</b>
<b>Riassunto</b> .....	<b>vii</b>
<b>Parole-chiave</b> .....	<b>vii</b>
<b>Contents</b> .....	<b>ix</b>
<b>List of figures</b> .....	<b>xiii</b>
<b>List of tables</b> .....	<b>xix</b>
<b>Introduction</b> .....	<b>1</b>
<b>Chapter 1 A journey into the viral world: from a virus to a novel paradigm</b> .....	<b>5</b>
1.1 Virus: between virology and materials science .....	5
1.2 Viral diseases .....	8
1.2.1 Vaccines .....	9
1.3 Antivirals .....	10
1.4 Broad-spectrum .....	10
1.5 Entry inhibitors .....	12
1.5.1 Multivalency .....	13
1.5.2 Virustatic mechanism .....	14
1.6 A superior approach : virucidal antivirals .....	15
1.6.1 Gold Nanoparticles .....	17
1.6.2 Cyclodextrins .....	19
<b>Chapter 2 Materials and methods</b> .....	<b>21</b>
2.1 Amphiphilic gold nanoparticles .....	22
2.1.1 Abstract .....	22
2.1.2 Introduction .....	22
2.1.3 Protocol .....	23
2.1.4 Representative results .....	28
2.2 Beta-cyclodextrins .....	35
2.2.1 Materials .....	35
2.2.2 Synthesis .....	35
2.2.3 Characterization .....	35
2.2.4 Further development .....	37
2.3 Dendritic polyglycerol (dPG) .....	37

2.3.1	Materials.....	37
2.3.2	Synthesis of dPG core .....	38
2.3.3	Synthesis of different dPG strcutures .....	39
2.4	Biological assays .....	50
2.4.1	Cytotoxicity .....	50
2.4.2	Dose-response .....	51
2.4.3	Virucidal assay .....	54
2.4.4	DNA release assay.....	56
2.4.5	Antiviral surfaces testing .....	58
<b>Chapter 3</b>	<b>Gold nanoparticles and beta-cyclodextrins: beyond the state of the art .....</b>	<b>61</b>
3.1	Broad-spectrum activity beyond HSPGs viruses .....	61
3.1.1	Abstract .....	61
3.1.2	Introduction.....	62
3.1.3	Results .....	63
3.1.4	Discussion .....	66
3.1.5	Conclusions.....	67
3.2	SARS-CoV-2 inhibition by sulfonated compounds .....	67
3.2.1	Abstract .....	67
3.2.2	Introduction.....	67
3.2.3	Results .....	69
3.2.4	Discussion .....	71
3.2.5	Conclusions.....	71
3.3	Modified cyclodextrins : a study on the influence of the lenght of the linkers .....	72
3.4	Pharmacokinetic study (PK) .....	74
3.4.1	Results .....	74
3.5	Summary.....	76
<b>Chapter 4</b>	<b>Polyanionic dendritic polyglycerol as novel broad-spectrum virucidal antivirals.....</b>	<b>77</b>
4.1	Abstract .....	77
4.2	Introduction.....	78
4.3	Result and discussion.....	79
4.4	Conclusion .....	84
<b>Chapter 5</b>	<b>Novel virucidal candidate against SARS-CoV-2.....</b>	<b>85</b>
5.1	Abstract .....	85
5.2	Introduction.....	85
5.3	In vitro results.....	86

5.4	In vivo results.....	90
5.5	Conclusions.....	91
<b>Chapter 6</b>	<b>Other antiviral strategies: from filters to surfaces .....</b>	<b>93</b>
6.1	Abstract .....	93
	Introduction .....	93
6.2	Anti-viral filter.....	94
6.3	Anti-viral surfaces .....	97
6.3.1	Graphene-based surfaces .....	98
6.4	Conclusions.....	100
<b>Chapter 7</b>	<b>Conclusions and outlook .....</b>	<b>101</b>
7.1	Achieved results.....	101
7.2	Future development .....	102
<b>References</b> .....		<b>105</b>
<b>List of publications</b> .....		<b>119</b>
<b>List of patents</b> .....		<b>119</b>
<b>Curriculum Vitae</b> .....		<b>121</b>



# List of figures

Figure 0.1 – <b>Cover of <i>Time Magazine</i>, May 2017</b> .....	1
Figure 1.1 – <b>A scheme of the structure of an enveloped virus</b> . It is composed by an external lipid envelope, where specific proteins, needed for the recognition and the infection cycle, are located. Inside the envelope, a nucleocapsid, composed by proteins, contains the viral genome. Adapted from Bruslind (2015). ....	5
Figure 1.2 – <b>Replication cycle of SARS-CoV-2</b> . The virus infects the respiratory system of a person, coming from different possible sources such as air or surfaces. Once it attaches to a host cell, the virus starts the replication cycle, hijacking the replication machinery of the cell. New virions are assembled and then release, ready to infect other cells. Adapted with permission from Tang et al. (2020).....	6
Figure 1.3 – <b>Contributions of materials science during the COVID-19 pandemic</b> : on the left, the development of materials for masks and protective equipment, in the center, the design and optimization of testing both for viral RNA, proteins or antibody, on the right, the advancements on drugs, vaccines and delivery systems. Adapted with permission from Tang et al. (2020).....	7
Figure 1.4 – <b>Timeline of key contributions of materials science to virology</b> . – Adapted with permission from Tang et al. (2020).....	8
Figure 1.5 – <b>Overview of human viral infections</b> . All the organs or tissue can be infected by different families of viruses. ....	9
Figure 1.6 – <b>Different antiviral strategies</b> . On the left "one-drug, one-bug" with the development of solutions tailored for a single virus; on the right, "one-drug, multiple-bugs". This strategy envisions the idea of having an antiviral that could eventually block the replication of multiple viruses. Such strategy can focus on the virus or on the host. Adapted from Bekerman e al. (2015) <sup>32</sup> .....	11
Figure 1.7 – <b>Generic structure of a subunit of heparan sulfate (HS)</b> . The large number of sulfate groups gives rise to the high negative charge. ....	12
Figure 1.8 – <b>Multivalency in action: viruses, cells and drugs</b> . A) binding of a virus to cell surface. B) Monovalent drugs. C) Multivalent drug. Adapted with permission from Fasting et al (2012) <sup>47</sup> .....	13
Figure 1.9 – <b>Hemagglutinin and multivalency</b> . On the left, a trimer of hemagglutinin (HA). On the right the binding dendrimers bearing sialic acid (SA) with different spacing, displaying the importance of the spacing in order to have a stronger interaction, so higher affinity. Adapted with permission from Kwon et al. (2017) <sup>51</sup> . ....	14
Figure 1.10 – <b>Different multivalent scaffold proposed as a viable candidate to design antiviral entry inhibitors</b> . Adapted from Szunerits et al. (2015) <sup>53</sup> . ....	14
Figure 1.11 – <b>Sketch of virustatic mechanism</b> . There is an equilibrium between virus and virustatic nanomaterial, determined by kinetic constants $k_{on}$ and $k_{off}$ , that result in a thermodynamic constant $K_D$ . Modified from <sup>54</sup> .....	15
Figure 1.12 – <b>Sketch of virucidal mechanism</b> . Disinfectants, strong acids, detergents are common virucidal agents. Modified from <sup>54</sup> .....	16
Figure 1.13 – <b>Design principle of our broad-spectrum virucidal antiviral</b> . We combine a multivalent scaffold, with a hydrophobic linker, and a functional group responsible of the recognition of the virus. In our vision, the hydrophobic linker is responsible of the virucidal activity. ....	16
Figure 1.14 – <b>Sketch of virucidal mechanism for entry inhibitors</b> . Between the virus and the virucidal material, there is an equilibrium, determined by kinetic constants $k_{on}$ and $k_{off}$ that then evolves towards an irreversible inactivation (determined by a kinetic constants $k_v$ ) of the virus that lose its infectivity. Modified from <sup>54</sup> .....	17
Figure 1.15 – <b>Antiviral activity of heparin, MES AuNPs and MUS:OT AuNPs against HSV-2</b> . From left to right: chemical structure, HSV-2 inhibition and cytotoxicity and virucidal assay for respectively a) heparin b)	

Mercapto-ethansulfonate (MES) gold nanoparticles (Au NPs) c) 11-Mercapto-undecansulfonate:octanthiol (MUS:OT) gold nanoparticles (Au NPs). Adapted with permission from Cagno et al. (2018)<sup>67</sup>. ..... 18

Figure 1.16 – **Association of MUS:OT NPs with HSV-2** a) using dry negatively stained TEM or b) and c) by cryo-TEM. D) shows the distribution of NPs associated with HSV-2 immediately or 90 min after the incubation. Stage 1: Virus with no NPs associated. Stage 2: virus with some NPs. Stage 3: virus with at least one local cluster of NPs. Stage 4: Deformed virus mostly covered by NPs. Scale bars are 100 nm. Adapted with permission from Cagno et al. (2020)<sup>67</sup>. ..... 19

Figure 1.17 – **Synthesis of modified beta-cyclodextrins bearing MUS**. Adapted from Jones et al. (2020).<sup>68</sup> ..... 19

Figure 1.18 – **Drug resistance assay of CD-MUS and Acyclovir**. HSV-2 passaged eight times in the presence of increasing concentrations of (a) acyclovir or (b) CD-MUS, or no inhibitory compounds were subjected to a dose-response assay. The percentages of infection were calculated by comparing the number of plaques in treated and untreated wells. Results are mean and SEM of at least two independent experiments. Adapted from Jones et al. (2020).<sup>68</sup> ..... 20

Figure.2.1 – **Schematic of MUS synthesis**. MUS synthesis is the key point for the reproducibility of amphiphilic nanoparticle synthesis. If MUS has a high salt content, the stoichiometric ratio of the ligands may deviate.  $X=9$ . ..... 29

Figure 2.2 – **NMR spectra of the molecules after each step in the MUS synthesis** (400 MHz). (A) This panel shows the <sup>1</sup>H-NMR spectrum of sodium undec-10-enesulfonate in D<sub>2</sub>O. (B) This panel shows the <sup>1</sup>H-NMR spectrum of sodium 11-acetylthio-undecanesulfonate in D<sub>2</sub>O. (C) This panel shows the <sup>1</sup>H-NMR spectrum of 11-mercapto-1-undecanesulfonate in D<sub>2</sub>O. In all spectra, \* indicates the solvent peaks. .... 30

Figure 2.3 – **Schematic of the amphiphilic nanoparticle synthesis**. (A) This panel shows the preparation of the one-phase chemical reduction reaction using ethanol as solvent. (B) Gold-thiolate complex is allowed to form before the addition of a reducing agent. At this stage, the solution of gold salt became turbid. (C) During the dropwise addition of the reducing agent, gold nanoparticles are formed. .... 31

Figure 2.4 – **Cleanliness of the nanoparticles from unreacted free ligands**. (A) This panel shows the <sup>1</sup>H-NMR spectrum of the nanoparticles right after the synthesis and vacuum-drying. D<sub>2</sub>O is used as the solvent for the <sup>1</sup>H-NMR analysis. Sharp peaks shown by red arrows indicate the existence of free unbound ligands. (B) This panel shows the <sup>1</sup>H-NMR spectrum of the nanoparticles after a thorough purification (i.e., washes and centrifugation with ethanol and DI water). The red arrow points to the magnified part of the spectrum, in which the peaks are broad, not sharp as before indicating the absence of free ligands. In both spectra, \* indicates the solvent peaks. .... 31

Figure 2.5 – **Size distribution of nanoparticles**. (A) This panel shows a representative TEM image of MUS:OT nanoparticles. The scale bar is 20 nm. (B) This panel shows a histogram of the core size of nanoparticles based on several TEM images. (C) UV-Vis spectra of the nanoparticles showed the characteristic surface plasmon resonance peak of the nanoparticles at around 520 nm. .... 31

Figure 2.6 – **Ligand ratio calculation**. (A) This panel shows representative NMR spectra of combinations of disulfides (as references for ligands after core etching) and peak assignments for different protons in MeOD-d<sub>4</sub>. (B) This panel shows <sup>1</sup>H-NMR spectra of etched nanoparticles in MeOD-d<sub>4</sub>. In all spectra, \* indicates the solvent peaks. .... 32

Figure 2.7 – **Ligand density analysis**. A TGA measurement of the nanoparticles was done to determine the ratio and density of organic material (ligands). The graph of the measurements is plotted as the weight percentage vs. the temperature. OT desorbs first, between 176 °C to 233 °C (vertical lines). MUS degrades to smaller molecules and is totally burned at around 800 °C. The remaining weight percentage corresponds to the gold core of the nanoparticles. .... 33

Figure 2.8 – **Comparison of stoichiometric and NMR ratios of OT on the particles**. It is possible to tune the amphiphilicity of the nanoparticles by changing the starting stoichiometric ratio between MUS and OT in the reaction. The error bars show the upper and lower limit of OT content acquired using the indicated

stoichiometric ratios. Stoichiometric ratios of 10%, 20%, etc., up to 90% OT, were synthesized to observe the limits of OT content on the nanoparticle surfaces. .... 33

Figure 2.9 – **Mass spectrometry characterization of CD-MUS.** HRMS Cold-Spray Ionisation spectrum of CD-MUS in EtOH/H<sub>2</sub>O (50:50), b) HRMS Summary of CD-MUS in EtOH/H<sub>2</sub>O (50:50). Values correspond to the monoisotopic mass..... 36

Figure 2.10 – **CE-UV electropherogram of CD-MUS.** Absorbance acquired at 230 nm with assigned CD species showing 31% of 6 and 69% of 7 sulfonates per CD. .... 37

Figure 2.11 – **Reaction scheme of dPG core** ..... 38

Figure 2.12 – **DLS and GPC measurements of dPG core.** A) Dynamic light scattering measurements shows the hydrodynamic diameter of dPG core in phosphate buffer at concentration of 1 mg/ml. Results are for three measurement series (indicated by triangles, circles and squares). B) Gel permeation chromatography (GPC) diagram of the non-functionalized core dPG (C1). (Mn:7.2 kDa, Mw: 10 kDa, PDI: 1.4)..... 38

Figure 2.13 – **Synthetic route for preparation the of dPG-allyl.** ..... 39

Figure 2.14 – **<sup>1</sup>H-NMR of dPG-allyl.** The degrees of functionalization (DF) in the different reactions were confirmed by <sup>1</sup>H-NMR of the pure product correlating the allyl protons at 5.9 -5.8 ppm with the polyglycerol backbone protons (3.7 - 3.4). .... 39

Figure 2.15 – **Synthetic route for preparation of the dPG-1 (X = 2), dPG-2 (X = 50) and dPG-3 (X = 85).** 40

Figure 2.16 – **<sup>1</sup>H-NMR of dPG-1 in D<sub>2</sub>O.** dPG-1 was functionalized with 11-mercapto-1-undecanesulfonate (MUS) with degree of functionalization of 2%. .... 40

Figure 2.17 – **<sup>1</sup>H-NMR of dPG-2 in D<sub>2</sub>O.** dPG-2 was functionalized with 11-mercapto-1-undecanesulfonate (MUS) with degree of functionalization of 50%. .... 41

Figure 2.18 – **<sup>1</sup>H-NMR of dPG-3 in D<sub>2</sub>O.** dPG-3 was functionalized with 11-mercapto-1-undecanesulfonate (MUS) with degree of functionalization of 85%. .... 41

Figure 2.19 – **Synthetic route for preparation of the dPG-4.** ..... 42

Figure 2.20 – **<sup>1</sup>H-NMR of dPG-4 in D<sub>2</sub>O.** ..... 43

Figure 2.21 – **Synthetic route for preparation of the dPG-5.** ..... 44

Figure 2.22 – **<sup>1</sup>H-NMR of dPG-1 (before sulfation reaction) in DMF-d<sub>6</sub>.** ..... 44

Figure 2.23 – **<sup>1</sup>H-NMR of dPG-5 in D<sub>2</sub>O.** ..... 45

Figure 2.24 – **Synthetic route for preparation of the dPG-6.** ..... 46

Figure 2.25 – **<sup>1</sup>H-NMR of dPG-6 in DMF-d<sub>6</sub> before sulfation.** ..... 46

Figure 2.26 – **<sup>1</sup>H-NMR of dPG-6 in D<sub>2</sub>O after sulfation.** ..... 47

Figure 2.27 – **One-pot approach for the synthesis of the a) dPG-7 b) dPG-8.** ..... 48

Figure 2.28 – **<sup>1</sup>H-NMR of dPG-7 in D<sub>2</sub>O.** ..... 48

Figure 2.29 – **<sup>1</sup>H-NMR of dPG-8 in D<sub>2</sub>O.** ..... 49

Figure 2.30 – **Synthetic route for preparation of the dPG-C10-COO.** ..... 49

Figure 2.31 – **<sup>1</sup>H-NMR of dPG-C10-COO in D<sub>2</sub>O.** ..... 50

Figure 2.32 – **Sketch of a dose-response inhibition assay for HSV-2.** A fixed amount of virus is incubated for a certain amount of time with an increasing concentration of the compound of interest. Then, the mixtures are added onto cells and the virus is let infect. After a given time, the cells are stained and the infection state measured via a plaque assay. Percentage of infection is compared to a non treated control. .... 52

Figure 2.33 – **Example of an inhibition assay curve.** On the y-axis the infectivity (or percentage of infection) is reported, while on the x-axis the concentration the compound in log scale. A fitting with a four-parameter

dose-response curve is performed, in order to identify the IC<sub>50</sub>, i.e. the concentration at which the infection is reduced by 50%..... 53

Figure 2.34 – **Sketch of virucidal assay graphs for virustatic and virucidal drugs.** On top, the effect of virucidal and virustatic drug at the incubation concentration. Both are able to inhibit the viral infection. On the bottom, the viral titer of both cases is reported upon dilution: a clear difference can be detected. For the virustatic drug, the inhibition is lost upon dilution, while there is an irreversible viral inhibition in case of a virucidal compound. .... 55

Figure 2.35 – **Sketch of DNA release assay.** The assay consists of multiple step: a) incubation of virus and virucidal drug b) dilution and addition of DNase with relative buffer c) addition of lysate buffer to stop the activity of DNase and disrupt the virus d) washing and collection of DNA e) quantification of DNA via qPCR. The Ct are the compared to an untreated control. .... 57

Figure 3.1 – **Chemical structure of MUS:OT AuNPs and CD-MUS.** (a) MUS:OT AuNPs, composed of a gold (Au) core covered by the ligands mercaptoundecansulfonate (MUS) and 1-octanethiol (OT). (b) CD-MUS, composed of a cyclodextrin (in blue) conjugated with MUS. .... 62

Figure 3.2 – **Antiviral and virucidal activity of heparan sulfate analogues and MUS:OT NPs and CD-MUS against H1N1 A/Netherlands/602/2009 (a) and VSV (b).** Viruses and compounds were incubated for 1 h at 37°C and subsequently added to cells. Infectivity was evaluated at 24 hpi for both viruses. The percentage of infection was calculated by comparing the number of infected cells for H1N1 or plaques for VSV to those for the untreated controls. (c and d) Virucidal activities of MUS:OT NP, CD-MUS, and K5NOS(H) against H1N1 (c) and MUS:OT NP and CD-MUS against VSV (d). Approximately 10<sup>5</sup> focus-forming units (ffu) (H1N1) or 105 PFU (VSV) were incubated for 1 h at 37°C with the indicated concentrations of the compound and subsequently serially diluted in cells. Infectious titers were evaluated under each treatment condition at dilutions at which the concentration of compound is not active. Results are expressed as means and standard errors of the means (SEM) from three independent experiments performed in duplicate. Statistical significance relative to the untreated control was calculated using one-way ANOVA (\*\*, P < 0.01; \*, P < 0.05). EC<sub>50</sub>, 50% effective inhibitory concentration..... 64

Figure 3.3 – **Mechanisms of action of CD-MUS (a) and MUS:OT NP (b) against VSV.** The compounds were either added to cells for 2 h before infection (pretreatment of cells), incubated with the virus for 1 h and then added to cells at 37°C (pretreatment with virus infection at 37°C), added with the virus to the cells (cotreatment), or preincubated with the virus for 1 h and then added to cells at 4°C for 1 h before shifting to 37°C (pretreatment with virus infection at 4°C). Infectivity was evaluated at 24 hpi. (c) Flow cytometry was performed at 3 hpi with Vero cells infected with VSV expressing GFP (MOI of 5) after pretreatment with MUS:OT NP for 2 h (pretreated cells) or in the presence of MUS:OT NP (cotreatment). Percentages of infection are normalized according to the untreated (UT) conditions. (d) Vero cells that were uninfected (mock) or infected with VSV (MOI of 20) in the absence (UT) or presence of MUS:OT NP (100 µg/ml) were fixed at 1 hpi and subjected to immunostaining with an anti-VSV polyclonal antibody. Green, VSV; red, Evans blue; blue, DAPI. Bars, 10 µm. Results are expressed as means and SEM from two independent experiments performed in duplicate. Statistical significance relative to the untreated control was calculated using one-way ANOVA (\*\*\*\*, P < 0.001)..... 65

Figure 3.4 – **Inhibitory activity of sulfonated nanomaterials against SARS-CoV-2.** a) VSV-CoV-2 or b) SARS-CoV-2 were incubated for 1h at 37°C with different doses of MUS:OT NP or CD-MUS and subsequently serially added on cells. In a), the number of GFP positive cells was evaluated 24hpi while in b) the number of plaques was determined 48hpi. Results are expressed as mean and SEM of three independent experiments.69

Figure 3.5 – **Virucidal activity of sulfonated nanomaterials against SARS-CoV-2.** 10<sup>5</sup> pfu of SARS-CoV-2 were incubated for 1h at 37°C with 300 µg/ml and subsequently serially diluted on cells. Infectious titers were evaluated for each treatment condition at dilutions at which the concentration of compound was not active. Results are expressed as mean and SEM of three independent experiments. .... 70

Figure 3.6 – **Reaction scheme used to synthesis different CD-MXS.** X represents the number of carbon atoms present on the aliphatic chain. N ranged from 2 to 16 resultin in X ranging between 4 and 18..... 72

Figure 3.7 – **Kinetic profiles of the CD-MUS concentrations in plasma and organs**..... 76

Figure 4.1 – <b>Schematic structure of functionalized dendritic polyglycerols (dPGs)</b> . In the scheme the ligands shown are for the most active compound (dPG-5). The ligands structures (R1 and R2) for other compounds are shown at Table 1. ....	80
Figure 4.2 – <b>Antiviral activity and toxicity profile of dPG5</b> . a) <i>In vitro</i> activity of dPG-5 against HSV-2 (blue) and RSV (red). dPG-5 shows an antiviral activity with an EC50 respectively of 0.16 µg/ml and 0.15 µg/ml. b) , the cell viability of dPG-5 against three different cell lines. Data from 2 independent experiments performed in duplicates. ....	82
Figure 4.3 – <b>Virucidal activity and DNA release assay for dPG-5</b> . Virucidal activity of dPG-5 against RSV (a) and HSV-2 (b). In both cases we show the viral titer after 1h incubation with 300 µg/ml of dPG-5. Graph c) show DNA release assay: HSV-2 was incubated in the presence or absence of dPG-5 (µg/ml) for 1 hour at 37°C and then incubated for 30 min with Turbo DNase or only buffer and subsequently subjected to qPCR. Results are expressed in fold change of DNase treated versus untreated. Data from 2 independent experiments performed in duplicates. Shown mean + SD.....	83
Figure 4.4 – <b>Schematic representation of the virucidal mechanism of action</b> (envelope is not represented for clarity). dPG first inter-acts with the virion and then leads to an irreversible step that disrupts the capsid causing the release of viral DNA.....	83
Figure 5.1 – <b>Reaction scheme of dPG-C10-COO</b> . Starting from a dPG-allyl, a 11-mercapto-undecanoic acid react via click reaction catalyzed via UV in order to obtain a fully functionalized dPG.....	86
Figure 5.2 – <b>Cell viability assay of dPG-C10-COO</b> . MTS assay is performed on Vero cells. (24h incubation). Cell viability expressed as percentage relative to the untreated control. ....	86
Figure 5.3 – <b>Structures and antiviral activity of two different carboxylate dendritic polymers</b> . On the left, chemical structure of Z2 and Z9, two different dendritic structures. Z2 is a dPG modified with a short 3 carbon atoms linker terminated with a carboxylic acid. Z9 is a dendritic structure synthesized reacting 2-hydroxypropane-1,2,3-tricarboxylic acid with glycerol. On the right, viral inhibition against SARS-CoV-2 is reported. No inhibition has been detected up to 2mg/ml. ....	89
Figure 5.4 – <b>Post-infection assay of dPG-C10-COO against SARS-COV-2</b> . More than 2 log in viral titer reduction can be detected compared to an untreated control. ....	90
Figure 5.5 – <b>Results of the <i>in vivo</i> experiments against SARS-CoV-2 in hamster</b> . On the y-axis is reported the relative change in body weight (%) every twelve hours, while on the x-axis the days post-infection. ....	91
Figure 6.1 – <b>Schematic of the experimental filtration set-up</b> . ....	94
Figure 6.2 – <b>Infectivity of Φ6 after 1 h of incubation with BLG AF, 30 nm Fe NPs, BLG</b> .....	95
Figure 6.3 – <b>Elimination of infectious enveloped viruses for water filtered through BLG AF–Fe membranes</b> . a–c, Complete elimination of infectious viruses and the corresponding reduction in the genome count for Φ6 (a), H1N1 (b) and SARS-CoV-2 (c) when filtered through BLG AF–Fe membranes (blue, before filtration; grey, after filtration). A limited or no elimination was observed when filtering the same viruses through the cellulose support or the BLG AFs alone. The lower value of the genome count of Φ6 than that of the other two viruses is probably due to both a higher ratio of infectious viruses to genome count than those of the other two viruses and also the low efficiency of the genome extraction from these phages (Supplementary Table 2). Φ6 infectivity represents the plaque count from one plate of a series of dilutions that consist of at least three plates. A replicate of the Φ6 filtration experiment for which the infectivity was calculated using three technical replicas is shown in Supplementary Fig. 3. The genome count for Φ6 represents the average of four technical replicas and the error bars represent the standard deviation (s.d.). The infectivity and genome count of H1N1 as well as the genome count of SARS-CoV-2 represent the average of two technical replicas and the error bars represent the range. The infectivity of SARS-CoV-2 represents the average of four technical replicas and the error bars represent the s.d. LOD, limit of detection; *below the LOD. Representations of the virions are reproduced from pictures on ViralZone .....	96
Figure 6.4 – <b>Surface properties influencing the persistence of viruses</b> . These include physical properties (including light exposure, temperature and humidity), chemical properties (such as pH or antiviral coatings)	

and biological properties (depending on the virus vulnerabilities, e.g., an envelope) as well as the type of surface such as the porosity or topography. Adapted from Rakowska et al. (2021) with permission <sup>169</sup>. 97

Figure 6.5 – **Antiviral assay of MUS coated surfaces against HSV-2.** Test were performed following a wet-to-wet protocol (120min incubation time). In green, results from a self-assembled monolayer (SAM) of MUS on a gold surface, compared to a pristine gold surface. In blue, results from a modified silane with undecane-sulfonate that modifies a silicon oxide wafer..... 98

Figure 6.6 – **SARS-CoV-2 inactivation by RGO-SDBS surfaces, at different time-points.** Complete inactivation can be detected after just 10 minutes. .... 98

Figure 6.7 – **SARS-CoV-2 and HSV-2 inactivation by different surfaces.** Results from wet-to-wet protocol (60 min incubation time) assessing the antiviral properties against SARS-CoV-2 (a) and HSV-2 (b) of PEEK samples covered by RGO and SDBS and different controls. In order the samples are as follow. Control: viral stock. PEEK: substrate. PEEK-SDBS-RT: substrate spray coated with a SDBS solution and annealed at room temperature. PEEK-SDBS-250°C: substrate spray coated with a SDBS solution and annealed at 250°C. PEEK-RGO: substrate spray coated with a GO solution and annealed at 250°C. PEEK-RGO-SDBS: substrate spray coated with a GO-SDBS solution and annealed at 250°C. PEEK-RGO-SDBS-washed: PEEK-RGO-SDBS rinsed with MilliQ before the test. Viral titers are shown ..... 99

Figure 6.8 – **Conductivity measurement for RGO-SDBS samples in MilliQ water.** SDBS is released in water within the first tens of seconds. After 3 minutes, a plateau is reached. .... 100

## List of tables

Table 2.1 – <b>Elemental analysis and molecular weight (Mn) of functionalized dPG.</b> * Mn is calculated based on the degree of functionalization of each dendritic polyglycerol which is determined by <sup>1</sup> H-NMR, considering the Mn of starting dPG core 10 kDa. ....	42
Table 2.2 – <b>Elemental analysis and molecular weight (Mn) of dPG-4.</b> * Mn is calculated based on the degree of functionalization of each dendritic polyglycerol which is determined by <sup>1</sup> H-NMR, considering the Mn of starting dPG core 10 kDa. ....	43
Table 2.3 – <b>Elemental analysis and molecular weight (Mn) of functionalized dPG-5.</b> * Mn is based on the functionalization degree of each dendritic polyglycerol, considering the Mn of starting dPG. Increase in the carbon and hydrogen contents of dPG6 (before sulfatio sulfation) compared to dPG is due to the functionalization with the eleven-carbon alkyl chain. Additionally, the decrease in carbon and hydrogen contents in dPG6 together with sulfur content is confirming the sulfation reaction.....	45
Table 2.4 - <b>Elemental analysis and molecular weight (Mn) of dPG-6 before and after sulfation.</b> * Mn is calculated based on the de-gree of functionalization of dPG-6 which is determined by <sup>1</sup> H-NMR, considering the Mn of starting dPG core 10 kDa. ....	47
Table 2.5 – <b>Elemental analysis and molecular weight (Mn) of dPG-7 and dPG-8 before and after sulfation.</b> * Mn is calculated based on the degree of functionalization of dPG-6 which is determined by <sup>1</sup> H-NMR, considering the Mn of starting dPG core 10 kDa.....	49
Table 3.1 – <b>Antiviral activities of MUS:OT NP and CD-MUS against HSPG-independent viruses</b> - EC50, 50% effective concentration (50% maximal effect); CI, confidence interval; CC50 cytotoxic concentration causing 50% cell death .....	63
Table 3.2 – <b>Antiviral activity of HS mimicking compounds against VSV-CoV-2 and SARS-CoV-2.</b> EC50 50% effective concentration, CC50 50% cytotoxic concentration .....	70
Table 3.3 – <b>Antiviral and virucidal activity of the CD-MXS against HSV-2.</b> All the dose-response are simplicate with technical duplicates. Virucidal assay performed at 300µg/ml for 1h incubation. For CD-M8S has been repeated also at 2000µg/ml, given the higher IC50, but no effect was detected.....	73
Table 3.4 – <b>Concentrations of CD-MUS in mouse plasma at different timepoints.</b> ....	74
Table 3.5 – <b>Concentrations of CD-MUS in different organs at different timepoints.</b> Underlined values were set as ½ LOQ for statistical purpose. Brain values were all <LOQ .....	75
Table 3.6 – <b>Pharmacokinetic parameters of each tissue/organ,</b> defined as follow:.....	75
Table 4.1 – <b>Structures of the ligands, charge density and the <i>in vitro</i> inhibitory efficacy of dendritic polymers against HSV-2.</b> * Degree of functionalization and number of ligands is measured by <sup>1</sup> H-NMR.† Ligand density (ligands/nm <sup>2</sup> ) was calculated on the basis of the assumption that the dPGs are spheres. The number of ligands is divided by the surface area of a dPG molecule. ‡ Effective concentration to have 50% antiviral inhibition. n.a. not assessable at tested concentrations. ....	81
Table 5.1 – <b>Antiviral activity of dPG-C10-COO and dPG-C11-SO3 against SARS-CoV-2.</b> Both compounds showed an inibhibtion against SARS-CoV-2, with the carboxylate dPG resulting more efficient than sulfonate one. Surprisingly, while dPG-C10-COO showed a virucidal inhibition mechanism, dPG-C11-SO3 showed a solely virustatic.....	87
Table 5.2 – <b>Antiviral activity of dPG-C10-COO and dPG-C11-SO3 against HSV-2.</b> Both the compounds showed an inibhibtion against HSV-2, with the sulfonate dPG more activity than the carboxylate one. However, both the compounds showed a virucidal mechanism of inhibition. ....	88
Table 5.3 – <b>Dose-response and virucidal assays against SARS-CoV-2 of different modified CD and AuNPs.</b> Results from gold nanoparticles covered by 11-mercapto-undecanoic acid (MUA) and a mixture of MUA and 11-mercapto-undecansulfonate (MUS) and beta-cyclodextrins modified in order to bear undecanoic acid. In	

the first row a dose-response curve is reported (N=1, technical duplicates), while in the second row virucidal assay are reported (1h incubation, 300µg/ml, N=1, technical duplicates)..... 89

# Introduction

2020 revealed to the public the existence of an extremely subtle threat in our world, that stays usually quiet and unnoticed: viruses. From January 2020 on, all the media started discussing the possibility of a novel pandemic coming from China threatening the lives of all of us. Such a small entity was so new that it did not even have a name and was initially identified as *Wuhan virus*, after the first city where it was detected or just *2019 novel coronavirus* referring to its family. We needed an official World Health Organization (WHO) committee to give it a name, with the virus that was finally called SARS-CoV-2 on the 11th of February 2020. Exactly one month later, on the 11th of March 2020, the WHO declared the pandemic emergency state.

After one and half years of pandemic, every human on the planet is aware of the threats that viruses can cause to humanity, not only in terms of diseases, and deaths, but also in terms of the disruption to social and economic activities. Our generation did not remember the 1918 H1N1 Flu pandemic, that caused over 100 million deaths around the world, but we have already experienced 3 to 4 major viral outbreaks during the last 20 years. Names as Zika, Dengue, Swine Flu, H1N1, H5N1, MERS, SARS, stayed in our memory for few months, depending on our geographic location at the time of the venue, only to be forgotten once the emergency was over.

In June 2020, out of curiosity, I read once again my Research Proposal, written in September 2018 by a naive researcher-to-be who was new to the field of virology. My first lines were a quote from Bill Gates, taken from a TedTalk he gave in March 2015 entitled: *The next outbreak? We're not ready*. He said: “when I was a kid, the disaster we worried about most was a nuclear war. (... But today) if anything kills over 10 million people in the next few decades, it's most likely to be a highly infectious virus, rather than a war. Not missiles, but microbes.”<sup>1</sup> At the moment of writing, the number of people who died of CoVID-19 has reached 4.5 millions<sup>2</sup>.

This talk became extremely popular during the last months, both among scientists and conspiracy theorists of all flavors. Bill Gates was not brilliant nor Machiavellian: he simply referred to solid scientific literature, that highlighted the threats our world could have to face.



Figure 0.1 – Cover of *Time Magazine*, May 2017

In my proposal, I continued referring to literature: “At the moment, vaccines represent the most powerful approach to prevent viral infections; however, every year 3-4 new viruses are discovered<sup>3</sup>. In addition, in case of an outbreak of pandemic, it would be difficult to take counteraction in time to prevent its spread.” Probably my proposal did not have the same number of readers of a slightly more popular magazine, Time, that in May 2017 warned the public with a scary cover: “We are not ready for the next pandemic”.

My words were sincere, but the deep understanding and belief in their meaning came just during the pandemic, when they became real with numbers and facts showing how endangered we were and what we could have done before. With hindsight, it is extremely simple to discuss and provide “old” suggestions. This pandemic was a terrific example of the importance of science in understanding, facing and solving a situation that the community had foreseen in large advance. This thesis hopes to be a small contribution to the scientific advancement in this direction.

The main focus of this thesis is to design and understand novel broad-spectrum antivirals.

Besides pandemics, viruses are a major harm for humans, causing a broad variety of diseases that target a plethora of organs with symptoms that range from mild to severe leading also to death.

Many strategies have been developed against viruses, the first and most efficient one being the vaccination. Vaccines are preventive drugs able to stimulate the immuno-response of the patient, thus preparing the body for a possible pathogen invasion. Vaccines were key to eradicate smallpox in 1979 and are crucial weapons in the battle against many diseases ranging from polio to influenza, from hepatitis B to diphtheria. Vaccines are strict prophylactics, so their downside is the need to be administered before the infection takes place, being of no use as therapies. In addition, the process of development is usually very long and expensive and, so far, vaccines against only 16 viruses have been approved<sup>4,5</sup>.

If a viral infection starts, vaccination will not help and the immune system of the patient will be the last barrier of defense. The only help in this fight can come from antivirals, *i.e.*, drugs designed to stop the viral replication thus helping the immune-system in clearing the infection. Such medications are usually developed to interfere with one step of the replication cycle of the virus. Since the replication of the virus is performed by the replication machinery of the host cell, the occurrence of side-effect is possible. Even though the development of antivirals has given a tremendous help in the fight against viral diseases, enormous work is still needed.

In fact, few viruses have been targeted and the development of antivirals is usually performed with a “one drug, one bug” approach, with a single drug developed for a single virus, which makes the process long and expensive. Conversely, against bacteria, many large-spectrum antibiotics have been developed, opening new routes. Recently, a new paradigm called “one drug, multiple bugs” has been postulated, with the idea of designing broad-spectrum antivirals, *i.e.*, drugs able to inhibit viral infections caused by different families of virus.

In the last decades, different entry inhibitors have shown broad-spectrum antiviral activity *in vitro*, but failed *in vivo*. Such compounds are designed mimicking the host cell receptors, so they interact with the virus extracellularly with a certain thermodynamic equilibrium that prevents the virus from infecting the cell. Upon dilution, a common situation in an *in vivo* setting, such interaction is lost and the virus regain its ability to infect.

Our research group has recently proposed a novel approach in designing antivirals. The key concept is to modify such entry inhibitors in order to render them virucidal: this makes the viral inhibition *irreversible* and unaffected by dilution. Our idea is realized based on three key structures that forms our virucidal compounds: a multivalent core, a hydrophobic linker and, a functional group. Such design proved to be effective as non-toxic broad-spectrum virucidal antivirals as we showed with binary coated gold nanoparticles (MUS:OT AuNPs) and modified beta-cyclodextrins (CD-MUS). Such compounds resulted to be effective in irreversibly inhibiting different families of viruses with low toxicity confirming their ability also *in vivo*.

Starting from these two seminal works, this thesis tries to go beyond in two different directions: on one hand, validating the results from the two compounds mentioned, on the other hand, proposing novel structures that confirms our approach and enlarge our understanding of the system. In addition, some other strategies in preventing viral spreading such as antiviral surfaces and filters will be tackled.

Chapter 1 is a broad introduction that gives the foundation of the work. Starting from the definition of a virus, it continues with a discussion on the interaction between virology and materials science, with historical hindsights. With a funnel approach, viral diseases and vaccines are introduced, before discussing the development of antivirals. Different approaches are presented such as entry inhibitors with a focus on multivalency. The concept of virustatic and virucidal is then deeply examined, leading to the two seminal works from our research group that are thoroughly discussed.

Chapter 2 describes all the materials and methods used in this thesis. First, the synthesis and characterization of all the compounds (nanoparticles, cyclodextrins and dendritic polyglycerols) are presented. Then, a more theoretical discussion introduces the biological assays used to test the antiviral properties of the proposed compounds. The results and discussions are presented in the chapters that follow.

Chapter 3 reports the new data that validated the broad-spectrum activity of gold nanoparticles and modified beta-cyclodextrins against other viruses, among which influenza and SARS-CoV-2. In addition, a study on some key features of cyclodextrins is reported, enhancing our understanding in the chemical design of virucidal antivirals. Finally, a first pharmacokinetics study on modified beta-cyclodextrins is reported.

In chapter 4, a novel class of compounds is proposed as antiviral: sulfated and sulfonated dendritic polyglycerols. Different chemical modifications are proposed and tested against HSV-2, leading to an optimization of the system and a deeper knowledge of the chemical design rules needed to have a virucidal antiviral. The most efficient compound shows broad-spectrum activity against HSV-2 and RSV at the nanomolar range with a virucidal mechanism. Such irreversible inhibition is further investigated and confirmed by DNA release assay. Indeed, the compound shows limited toxicity on different cell lines.

Chapter 5 reports the first results on a carboxylate dendritic polyglycerol as virucidal antiviral against SARS-CoV-2. These unexpected results are discussed and compared to other structures such as sulfonated dendritic polyglycerol or carboxylate nanoparticles and cyclodextrins. The activity of the compound is further validated *in vivo* on a hamster model.

Chapter 6 focuses on different strategies in limiting viral spreading and infection. In particular, antiviral surfaces are described along with filters.

Finally, chapter 7 briefly summarizes the thesis, reporting the main results achieved and conclusive remarks. In addition, outlook and future developments are proposed.



# Chapter 1 A journey into the viral world: from a virus to a novel paradigm

## 1.1 Virus: between virology and materials science

The word *virus* comes from classical Latin and originally meant *venom*, poisonous secretion of snakes, creatures or plants so in general it referred to a malignant quality. It started being used to refer to “agent that causes infectious diseases” by the 1790s out of its earlier use for venereal disease. The first to speculate about the existence of pathogens that are so small to be undetectable under a microscope was Louis Pasteur, during his studies on rabies<sup>6</sup>. Afterwards, multiple studies at the end of 1800s by Adolf Mayer, Dmitri Iwanowsky and Martinus Beijerinck brought to the discovery of tobacco mosaic virus: such virus was considered a new infectious agent initially called *contagium vivum fluidum*, for which the term virus was first re-introduced. The key definition was the ability to pass through filters that were capable of retaining bacteria. In the last century, decades of development of biology, physics and chemistry allowed for the discovery and understanding of bacterial, plant, animal, and human viruses, identifying their structures, biological roles and infection mechanisms.

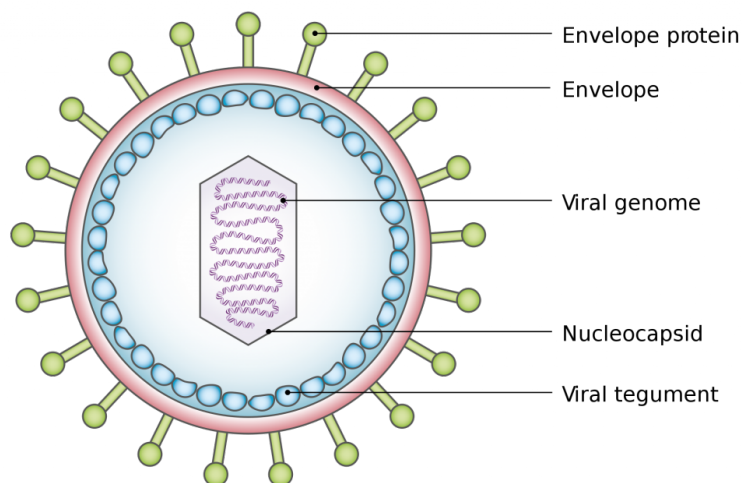


Figure 1.1 – **A scheme of the structure of an enveloped virus.** It is composed by an external lipid envelope, where specific proteins, needed for the recognition and the infection cycle, are located. Inside the envelope, a nucleocapsid, composed by proteins, contains the viral genome. Adapted from Bruslind (2015).

From a biological perspective a virus is an infectious agent, that can be defined as an inanimate parasite, since it does not consume energy and it does not have a real life-cycle. In fact, it cannot reproduce by itself but it can replicate only hijacking the replication machinery of its host. This feature puts the virus on the edge of life, in a gray area between living and non-living<sup>7</sup> opening philosophical questions on the definition of life. Recently, the discovery of « virophage », *i.e.* a virus that can infect other viruses, fueled the debate on the nature of viruses<sup>8-9</sup>. A virus can be seen as a protein cage, called capsid, that

protects the genetic material, sometimes surrounded by a lipid layer called envelop. Genomic material can be either DNA or RNA, both single or double stranded. The size of a virus ranges from 20 to 30 nm for some bacteriophages to over 500 nm for newly discovered Mimivirus<sup>9</sup>. In terms of structures, there are many possibilities that go from spherical to elongated, icosahedral to more intricate polyhedra. The last release from the International Committee on Taxonomy of Viruses (ICTV) on October 2020 reports 9110 species

discovered to date<sup>10</sup>. The ICTV is responsible for virus classification, even though many possibilities were proposed, given the range of differences. Viruses can be classified according to their host organism, the disease they cause, the virus particle morphology, the nucleic acids or the taxonomy. In 1971, David Baltimore proposed a classification based on the viral synthesis of mRNA, later named Baltimore classification<sup>11</sup>.

What can be seen as the life-cycle of a virus is basically the infection cycle, during which the virus can replicate. Fig. 1.2 shows the replication cycle of SARS-CoV-2. At first, the virus is released by an infected person through his breathing possibly contaminating air, water or surfaces. The virus can now encounter another human and once in his respiratory tract, recognize a host cell<sup>12</sup>. The recognition is due to the interaction between viral proteins and host cell receptors. Then, the virus injects its genetic material into the cell and, hijacking its replication machinery, the replication starts. Cellular ribosomes produce viral proteins that spontaneously self-assemble inside the cell, forming new virions, ready to be released and to start a new infection cycle. Such process usually causes the death of the cells that result in the disease's symptoms.

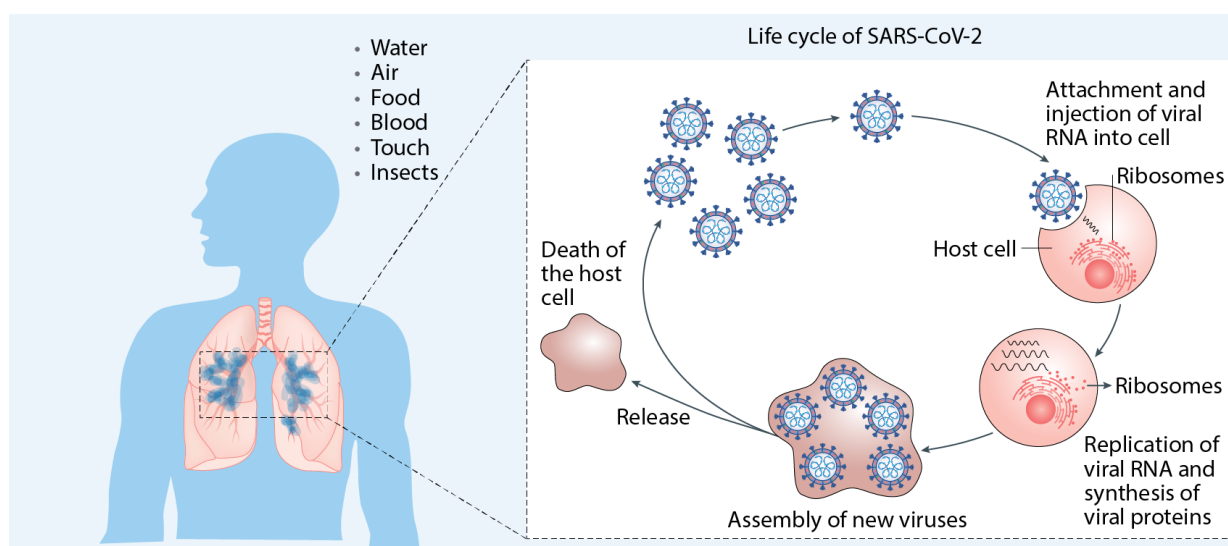


Figure 1.2 – **Replication cycle of SARS-CoV-2.** The virus infects the respiratory system of a person, coming from different possible sources such as air or surfaces. Once it attaches to a host cell, the virus starts the replication cycle, hijacking the replication machinery of the cell. New virions are assembled and then release, ready to infect other cells. Adapted with permission from Tang et al. (2020).

From a materials science or physical chemistry perspective a virus is a highly ordered supramolecular complex<sup>13</sup>. The fascinating features of viruses led to the birth of an entire research field called physical virology<sup>14</sup>. In fact, the absence of metabolic activity put the process of viral assembly as an ideal tool to investigate the basis of equilibrium thermodynamics. The first insight came in 1955, when Fraenkel-Conrat used an *in vitro* set-up, to demonstrate that proteins and nucleic acids of the tobacco mosaic virus (TMV) self-assemble spontaneously into infectious viral particles<sup>15</sup>. Later on, the whole thermodynamic phase diagram of TMV subunit assembly with respect to pH and ionic strength was established<sup>16</sup>. In addition, detailed studies on the mechanical properties of virions were carried out, in particular using atomic force microscopy (AFM)<sup>17</sup>.

Beyond its impact in the basic understanding on the structural features and the thermodynamics of the assembly and disassembly of a virus, materials science made a huge impact in many different aspects of virology.

Materials science produced some key discoveries and inventions that helped and influenced the development of virology during the last century. Fig. 1.4 shows a timeline starting from the “foundation” of virology, set in 1892 when the first virus was discovered until the release of the vaccines against SARS-CoV-2 in late 2020 with the contributions that materials science offered to virology and its evolution. As discussed by Tang et al., it is evident that techniques which were originally developed in materials science such as X-ray crystallography or electron microscopy become fundamental in the understanding of the viral world, opening the possibility for novel investigations. Microfluidics and microarrays revolutionized the whole field of bio-engineering, including virology. Furthermore, in the second half of the century, a branch of materials science, nanoscience, was crucial in the design of novel labeling both for basic science and for the manufacture of innovative rapid testing based on lateral flow. Finally, the surge of nanomedicine opened novel routes for drug delivery that were confirmed with the approval of the first nanodrug in 1995: Doxil. mRNA-based vaccines against SARS-CoV-2 are all based on lipid nanoparticles for encapsulation and stabilizations<sup>18</sup>.

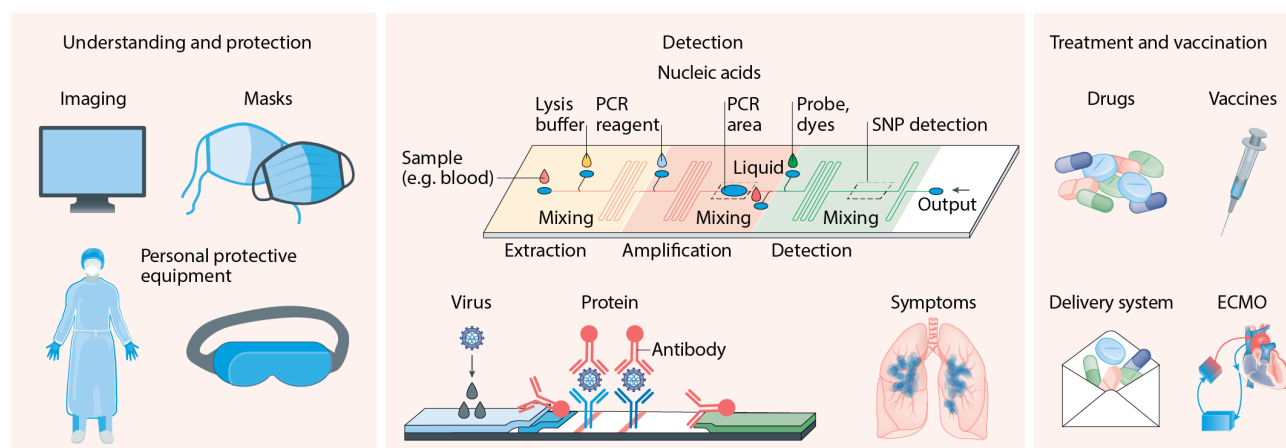


Figure 1.3 – **Contributions of materials science during the COVID-19 pandemic:** on the left, the development of materials for masks and protective equipment, in the center, the design and optimization of testing both for viral RNA, proteins or antibody, on the right, the advancements on drugs, vaccines and delivery systems. Adapted with permission from Tang et al. (2020).

As materials science strongly influenced virology, many materials scientists got interested in viruses due to their fascinating properties. Some of them, focused their efforts in designing novel drugs with approaches far from standard in traditional pharmaceutical science to treat different viral diseases.

During the pandemic, the contamination between materials science and virology have gone even further as brilliantly discussed by Tang et al. and showed in fig. 1.3. In particular, materials science was key in the development of appropriate materials in masks and protective equipment. Moreover, the rapid development of assays both for viral protein or genomic materials was key for fighting the pandemic. Finally, materials science has given crucial contributions in the drug delivery systems of approved mRNA vaccines and in the development of novel possible drugs.

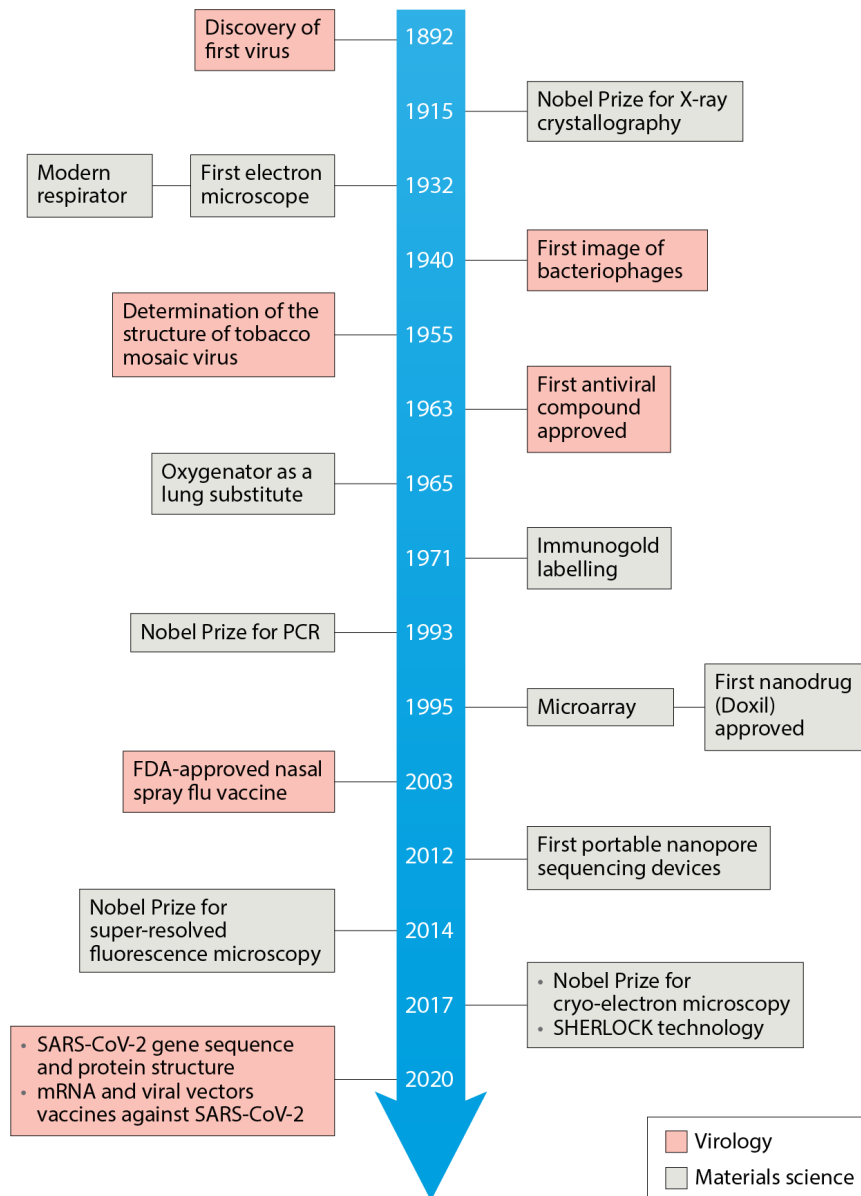


Figure 1.4 – Timeline of key contributions of materials science to virology. – Adapted with permission from Tang et al. (2020)

## 1.2 Viral diseases

A “romantic” quote says that “there are more viruses than stars in the universe.” More than a quadrillion quadrillion individual viruses exist on Earth, but luckily most do not see humans as possible hosts<sup>19</sup>. It is estimated that there are around 320.000 viruses in mammals waiting to be discovered<sup>20</sup> and each time a new species is identified hundreds of new viruses are found. All the organisms are affected by many viral diseases and humans are not exempted.

Estimations says that on and inside the body a single human being there around 380 trillion viruses<sup>21-22</sup>. Some of those species are able to infect us, while some others infect other different species that we host such as bacteria or microorganism, that compose our microbiota. Recently, the concept of human virome was postulated<sup>23-24</sup>, with the idea of sequencing the entire human viral population, having track of possible geographical changes and having the possibility of quickly identifying novel viruses. Until now, 220 viruses have been identified to be able to infect humans<sup>3</sup>. The variety of organs and tissues viruses can attack

is vast, as shown in fig. 1.5. However, our bodies have mechanisms to fight viral infections. Unfortunately, it is often not enough.

In fact, the human immune-system can cope with pathogens. Once a virus manages to enter the body, the innate immune system will start the battle, representing the first line of defense. Within several days, the adaptive immune system will become prominent, thanks to the activation of antigen-specific T-cells and B-cells. In particular, T-cells are able to recognize infected cells and cause their death to prevent the infection from spreading, while B-cells are able to detect and clear viral particles. Indeed, viruses can cause a large variety of symptoms and a viral infection can be as asymptomatic, with no manifestations, as having severe complications resulting even into death.

### 1.2.1 Vaccines

The best weapon we have developed so far to fight viral disease are vaccines. Vaccines are prophylactic drugs meant to stimulate the immunological bio-response of the organism against a certain pathogen. The first antiviral vaccine was produced in 1938 against yellow fever<sup>25</sup>, based on attenuated pathogens. Since then, many different strategies have been developed against a large number of viruses such as measles, polio, chickenpox and influenza saving millions of lives. Indeed, one of the biggest successes in medicine's history was achieved thanks to vaccines: the eradication of smallpox. In fact, in 1979, after a global vaccination plan, smallpox was officially declared eradicated.

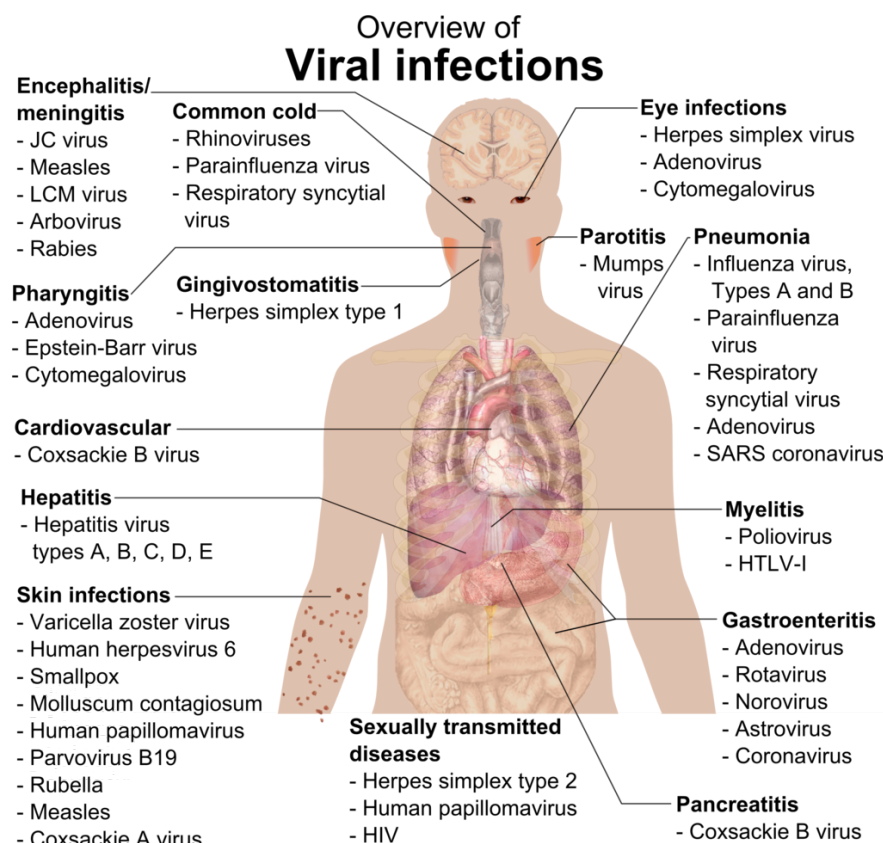


Figure 1.5 – **Overview of human viral infections.** All the organs or tissue can be infected by different families of viruses.

Vaccines are an extremely potent tool. In fact, from an individual perspective they are crucial to prevent diseases while from a public health point of view, they are key to control the spread of the pathogen

within the population, preventing epidemic or leading to elimination or eradication of the virus, as we have seen with smallpox. Key to achieve such goals are also operational and logistical hurdles, that go well beyond the mere effectiveness of a vaccine. In addition, social and political acceptance of the population, alongside with governments and organizations make even harder the large exploitation of vaccines. So far, vaccines against just 16 viruses have been produced<sup>4-5</sup>, mainly focusing on attenuated or inactivated pathogens. However, other promising routes were explored such as viral vectors or mRNA delivery as recently shown by Moderna<sup>26</sup> and BioNTech<sup>27</sup> in 2020.

As discussed above, vaccines are a preventive measure, and as such they are extremely useful when administered before a possible infection. In case a human is infected, its immune system should cope with the virus. If the immune system is not enough for the task, antivirals become the only therapeutic alternative.

### 1.3 Antivirals

Antivirals are medications designed to fight viral infections. The very first one was approved just in 1963, when idoxuridine was put in use<sup>28</sup>. The compound was initially synthesized by William Prusoff as an anticancer, and was lately used against Herpes Simplex 1. Since then, over 90 antiviral drugs have been approved against many different viruses<sup>28</sup>.

Antivirals are the homologue for virus of antibiotics for bacteria. Even so, the strategies to fight different infectious agents are largely different. In fact, bacteria are living entities, so, they have a whole metabolism that can be targeted. An example could be seen in bacterial protein synthesis, that is performed by bacterial ribosome. Such ribosomes are diverse enough from human ribosomes that make them a clear druggable target for an antibiotic that does not interfere with the host. In case of non-living entity, such as a virus, the possibilities to design an antiviral with low toxicity for the host are more limited. An antiviral is in fact designed to inhibit one step of the viral replication cycle, that is performed exploiting the host-cell replication machinery. The risk of also interfering with the host cell metabolism increases, resulting in side-effects. However, this is so far the only possible strategy in designing such medications.

As discussed above, the replication cycle of a virus can be divided in 5 steps: 1) Attachment to the host cell, 2) Penetration and release of viral genetic material (sometimes also enzymes), 3) Biosynthesis of viral components through the host-cell machinery, 4) Assembly of the new virions 5) Release of the new virions, ready to re-infect new cells. Each step can be exploited to design antivirals. During the last decades, many possibilities were explored but probably the most efficient ones involved the use of nucleoside analogues, that are briefly discussed below.

### 1.4 Broad-spectrum

The standard approach in antiviral design is the so called “one-drug, one-bug”, where a medication is specifically designed to target a single pathogen. Most antivirals target specific viral enzymes, in particular proteases and polymerases. However, this approach has intrinsic limitations. First, the cost of development of a new drug averages around 2 billion dollars, with a timeframe of 8 to 12 years<sup>29,30</sup>, which makes the design of a drug for each virus extremely expensive and slow. Then, the rapid emergence of resistance due to the error-prone replication system of the virus can compromise the efficacy of the drugs. Last, the presence of broad-spectrum therapeutics can enhance the control of viral infections, since it could be easily administered before an accurate diagnosis is in place, as normally done with broad-spectrum antibiotics.

The approach started shifting towards “one-drug, multiple-bugs” in the 1970s, with the discovery of ribavirin. Ribavirin is a prodrug, that, when metabolized, resembles guanosine, a nucleoside. It is then a nucleoside inhibitor, since it stops the viral RNA synthesis. In 1972 was reported to be active against a variety of DNA and RNA viruses <sup>31</sup>.

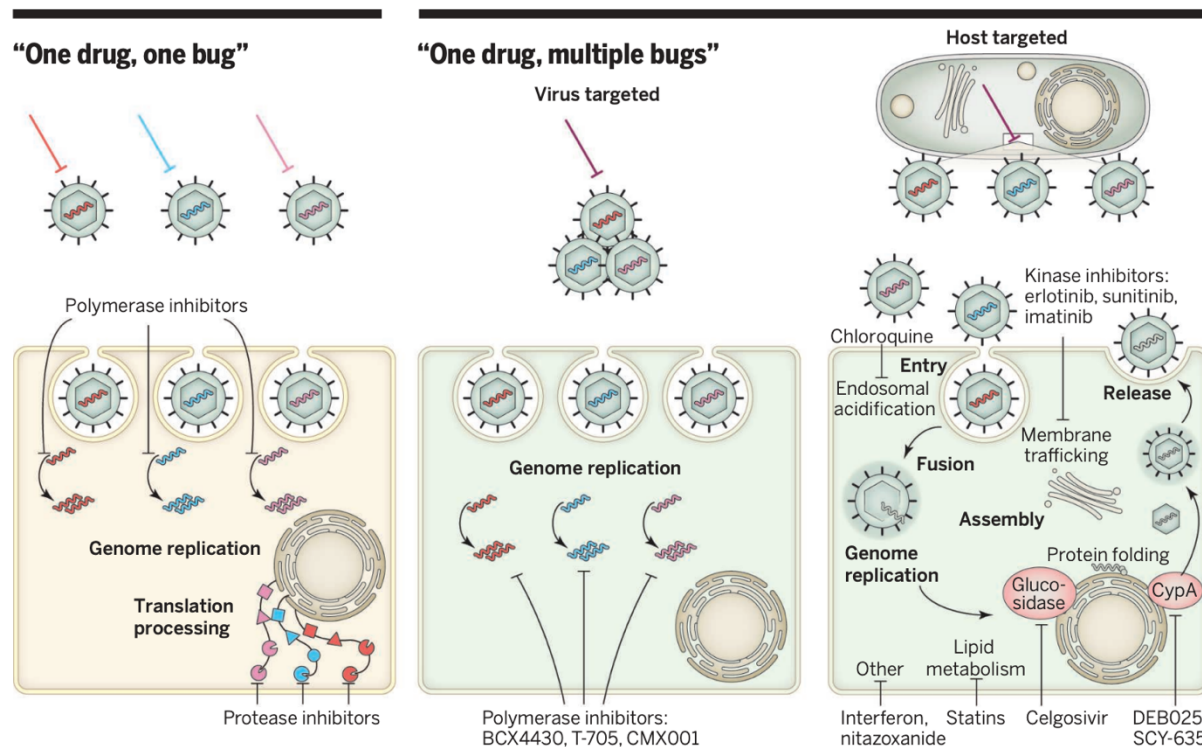


Figure 1.6 – **Different antiviral strategies.** On the left “one-drug, one-bug” with the development of solutions tailored for a single virus; on the right, “one-drug, multiple-bugs”. This strategy envisions the idea of having an antiviral that could eventually block the replication of multiple viruses. Such strategy can focus on the virus or on the host. Adapted from Bekerman e al. (2015) <sup>32</sup>.

Since then, other broad-spectrum antivirals have been proposed following different strategies. In general, as shown in fig. 1.6, a broad-spectrum antiviral can target either the virus itself or the host. Following the first approach, different nucleotide and nucleoside mimics have been developed and successfully tested. In some cases, the activity is narrow, and acts against a single type of virus or a family of viruses. An example is acyclovir, that is successfully employed against HSV-1 and -2 and other Herpes such as Varicella-Zoster virus. In other cases, the activity can be considered truly broad. This is the case for galidesivir (BCX4430), a synthetic adenosine nucleoside analog, which is a monophosphate nucleotide that is incorporated in the growing chain of viral RNA by viral RNA polymerases, causing premature chain termination.<sup>33</sup> Galidesivir has shown its efficacy against Ebola, Marburg, Rift Valley fever virus and Yellow Fever virus, demonstrating its broad-spectrum activity. Many other analogs are undergoing further investigations to prove their broad-spectrum potential<sup>34</sup>.

A key aspect to take into account in designing antivirals, and in particular broad-spectrum ones, is the balance between their efficacy and their toxicity. As discussed above, the fact that viruses employ the host cell machinery increases the complexity in affecting only pathogen replication; this is particularly true for all the approaches involving nucleotide or nucleoside analogs. An important parameter to determine the *in vitro* toxicity is the CC50, defined as the concentration at which 50% of cells are dead. CC50 should not be

analyzed by itself, but in relation to the IC<sub>50</sub>. IC<sub>50</sub>/EC<sub>50</sub> (Inhibitory Concentration or Effective Concentration) is defined as the concentration at which 50% of the viral infection is inhibited.

A parameter called Selectivity Index (SI) is usually employed to assess the possibility of employing a drug as an antiviral. Such parameter is defined as the ratio between the toxic concentration (CC<sub>50</sub>), and the active concentration, (IC<sub>50</sub>).

$$SI = \frac{CC_{50}}{IC_{50}}$$

SI defines the biological window in which a drug can be employed and if its further development can be envisioned. As reported from FDA in the report on Antiviral Product Development: “it is desirable to have a high therapeutic or selectivity index giving maximum antiviral activity with minimal cell toxicity”<sup>35</sup>. Of course, the higher is the SI, better is the therapeutic profile of the drug candidate. As an example, paracetamol has a SI around 10<sup>36</sup>.

Instead of targeting the virus, a broad-spectrum antiviral can target the host, thus the cell. An example is given by alisporivir, a cyclophilin inhibitor, now in phase II clinical trial for COVID-19, after being developed for HCV<sup>37</sup>.

Another approach that can be considered “broad-spectrum” is based on host immunomodulatory compounds, such as interferon. While conceptually this approach is correctly regarded as broad-spectrum, it does not target the virus directly or the host cell, but rather enhances the antiviral activity of the immune-system of the host.

## 1.5 Entry inhibitors

Entry inhibitors are a particular class of antivirals that targets the very first step of virus replication. Viruses recognize host-cells through glycoproteins, particular proteins present on the cell surface usually highly glycosylated. Different cells are decorated by different peculiar glycoproteins but some common features are present. Indeed, viral evolution brought viruses to exploit similar structures to recognize cells, due to their presence in a large part of cells in the host. For humans, heparan-sulfate proteoglycans (HSPGs) are one of the most present glycoproteins present on the cell surface and are a major component of the extra-cellular matrices.

Such moieties have a truly large number of functions in development and normal physiology. HSPGs structure is composed of a core protein, modified with one or more heparan sulfate (HS) glycosaminoglycan (GAG) chains<sup>38</sup>. Their key characteristic is the high negative charge, given by the presence of sulfate groups, as shown in fig. 1.7. Given the large presence of HSPGs in mammals and in humans in particular, many different pathogens have evolved to exploit such moieties to recognize the host cell, including different virus' family. Viruses such as HSV, Dengue, HPV, RSV, are known to first interact with HSPGs to recognize the host cell and start

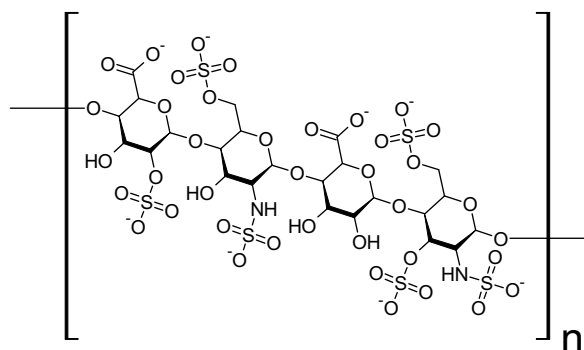


Figure 1.7 – **Generic structure of a subunit of heparan sulfate (HS).** The large number of sulfate groups gives rise to the high negative charge.

their infection cycle<sup>39</sup>. In particular, basic aminoacids present on the viral protein are responsible of this process.

Mimicking cell-receptors that are exploited by large class of viruses make such compounds intrinsically broad-spectrum. Therefore, mimicking HSPGs to inhibit the infectivity of different family of virus has been seen as a promising strategy since the 60s.

In fact, in 1964 two different papers from Nahmias<sup>40</sup> and Vaheiri<sup>41</sup> showed the capability of heparin of inhibiting HSV, both correlating the finding with the presence of sulfated groups. In the following years, other polyanionic compounds, both natural and synthetic, were proposed as possible entry inhibitors for different viruses<sup>42-43</sup>. In 1968, a seminal paper from DeSomer<sup>44</sup> showed the broad-spectrum capabilities of polyanionics as potential antivirals, with the first *in vivo* experiment. Since then, many different findings were made enlarging the chemical space of entry inhibitors<sup>45</sup>, along with a deeper knowledge of the biological interaction.

### 1.5.1 Multivalency

Multivalency is a key concept in nature: a large amount of weak non-covalent interactions between biomolecules make strong connections<sup>46</sup>. This interaction is the base of most of the signaling, regulation and recognition processes occurring in nature. Clearly, multivalent interaction is the base of the recognition process between viruses and cells, process mediated by viral proteins.

Entry inhibitors reverts the concept of multivalency against the virus: such compounds can expose multivalent ligands that can bind the viral proteins, preventing the viral attachment, thus the infection. Multivalency lower significantly the effective concentration respective to monovalent drug as shown in fig 1.8<sup>47</sup>.

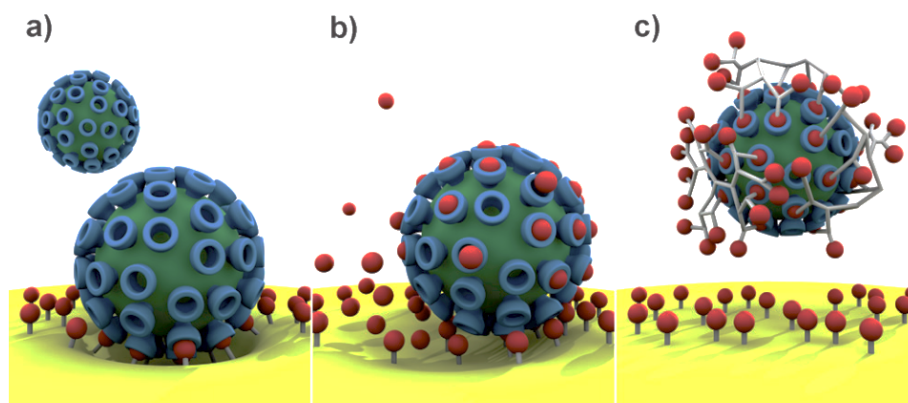


Figure 1.8 – **Multivalency in action: viruses, cells and drugs.** A) binding of a virus to cell surface. B) Monovalent drugs. C) Multivalent drug. Adapted with permission from Fasting et al (2012)<sup>47</sup>.

As shown by Papp *et al.*<sup>48</sup> and Kwon *et al.*<sup>49</sup>, the architecture has a crucial importance, since the ligands should match the size of the glycoproteins present on virus surface. In both works, the target is human Influenza A virus (IAV). This virus uses a glycoprotein, hemagglutinin (HA), to bind to carbohydrates present on the cell surface, in particular to sialic acid with alfa-2,6 linkage. While the monomeric sialic acid is not effective in preventing viral adhesion up to 4 mM<sup>48</sup>, the dendrimers, exploiting multivalency, prevent viral adhesion even at micromolar concentrations. Another crucial parameter to increase the binding affinity is the matching between the spacing of the ligands and the spacing of the receptors (fig. 1.9), as shown by Liese *et al.*<sup>50</sup>.

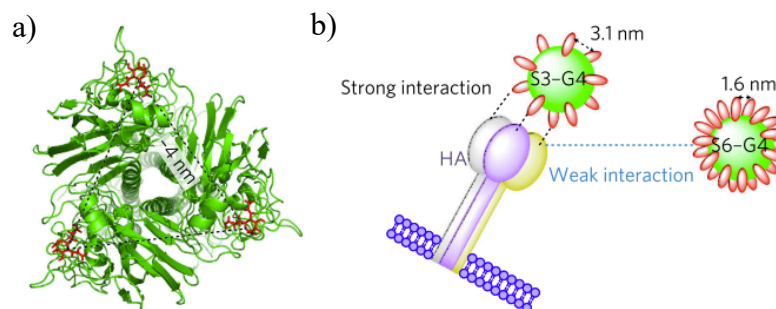


Figure 1.9 – **Hemagglutinin and multivalency**. On the left, a trimer of hemagglutinin (HA). On the right the binding dendrimers bearing sialic acid (SA) with different spacing, displaying the importance of the spacing in order to have a stronger interaction, so higher affinity. Adapted with permission from Kwon et al. (2017) <sup>51</sup>.

Similar nanogels based on dendritic polyglycerol but with sulfate terminal groups were proven to be broad-spectrum against HSPGs-dependent viruses<sup>52</sup>. The size of the nanogel is around 100 nm and the work shows the importance of the flexibility of the core to be effective at low concentration. More in general different structures have been successfully proposed ranging from dendrimers to liposomes, from polymeric and colloidal nanoparticles to inorganic ones, as discussed in detail by Szunerits <sup>53</sup> and shown in fig. 1.10.

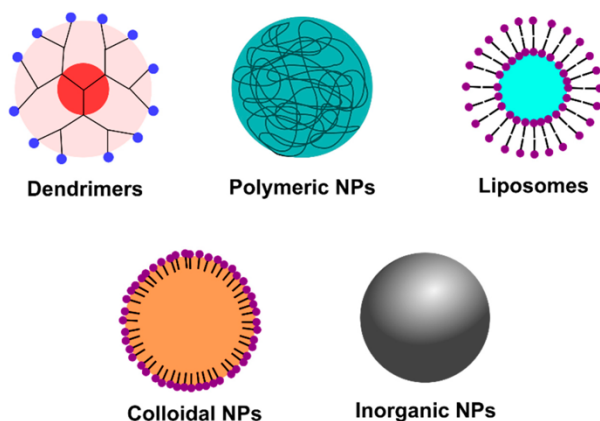


Figure 1.10 – **Different multivalent scaffold proposed as a viable candidate to design antiviral entry inhibitors**. Adapted from Szunerits et al. (2015) <sup>53</sup>.

### 1.5.2 Virustatic mechanism

An early report in 1964 by Vaheri<sup>41</sup> reported clearly the mechanism of action of heparin against HSV. “The anti-HSV action of heparin occurred during early interaction of HSV and cells and was reversible. Upon dilution of the heparin-HSV mixtures the inhibitory action of heparin was eliminated and HSV was quantitatively recovered. Heparin had no effect on the intracellular replication or the direct cell-to-cell spread of HSV. (...) To summarize, it appeared that the reversible effect of heparin on HSV may be characterized as an association-dissociation reaction in which electrostatic forces are determinative”. Later on, the report discusses the correlation of virucidal polyanion with toxicity.

The reversible action of heparin is likely common to all the entry inhibitors discussed above, even though dilution assays are usually not reported. Such reversible antiviral mechanism is called virustatic.

Virustatic compounds inhibit viral infection through a reversible mechanism, as sketched in fig. 1.11. Such materials bind to the viral attachment ligand, inhibiting virus-cell recognition. Since the interaction

is reversible, the inhibition is lost upon dilution (for instance in body fluids) and the virus re-gains its infectivity, making them medically irrelevant.

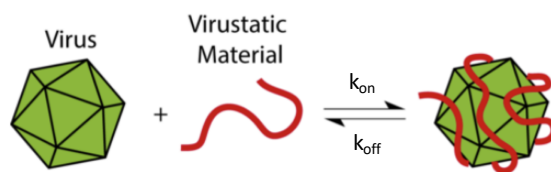


Figure 1.11 – **Sketch of virustatic mechanism.** There is an equilibrium between virus and virustatic nanomaterial, determined by kinetic constants  $k_{on}$  and  $k_{off}$ , that result in a thermodynamic constant  $K_D$ . Modified from <sup>54</sup>

Three clear cases of antiviral polyanions that failed in clinical trials support the poor translatability of reversible approach. The first case is given by PRO2000, a vaginal gel based on synthetic naphthalene sulphonate polymer to prevent HIV infection. Such compound showed extremely positive results *in vitro* as a potent antiviral entry inhibitor and safety profile in phase I. PRO2000 was so translated up to phase III clinical trial where it failed <sup>55</sup>, show no activity *in vivo*. A similar case is Carreguard, a polysulfated that, although safe, failed in phase III clinical trials in preventing HIV infection. <sup>56</sup>

An interesting case is given by cellulose sulfate, which was proven to be effective *in vitro* against HIV. Also in this case, a 6%-loaded gel was tested as preventive approach for HIV in a phase III clinical trial but it failed <sup>57</sup>. Moreover, the data reported an increase rate of HIV infection on the women that received the gel compared to the placebo group, even though with no statistical significance in a primary analysis. Such unexpected result can be explained with the reversible mechanism of action itself: the polyanions act as a sponge for the virus, but, in case of dermal lesion, the complex is easily diluted in body fluids, thus resulting in a detachment of the polymer from the virus and in the release of infective particles.

## 1.6 A superior approach : virucidal antivirals

A different mechanism is on the base of virucidal agents. Cleaning agents, disinfectants, bleach or strong acids are usually used to irreversibly inactivate viruses from surfaces or tools.

The definition of “virucidal” is in the norm EN 14476, where such agents are defined. These products alter the environment of the viruses, causing a physico-chemical damage that makes them unable to infect. Of notice, all those products are toxic. The reason is again intrinsic in the mechanism of action: cells are composed of the same bio-chemical structures of viruses, so, an alteration of the chemical environment of the virus, would cause a damage also to the host cells. This aspect makes this approach extremely powerful to disinfect surfaces or tools, but unusable as possible medicament, given the intrinsic toxicity.

Colacino in 2004 wrote: “Virucidal agents are those that are capable of inactivating a virus regardless of its replication state. Since metabolic activity is not required for maintenance of virion infectivity, it may be impossible to find non-toxic virucides, which, by definition, must be able to inactivate extracellular virus. [...] in the immediate future all antiviral drugs for clinical use are likely to be virustatic rather than virucidal.” <sup>58</sup>

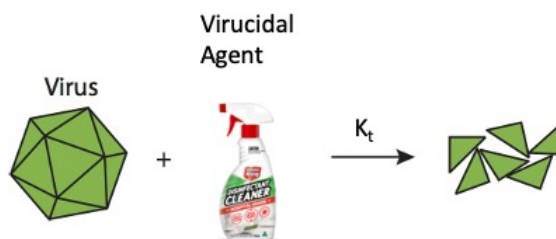


Figure 1.12 – **Sketch of virucidal mechanism.** Disinfectants, strong acids, detergents are common virucidal agents. Modified from <sup>54</sup>

In our lab, for the last years, we have been designing novel antiviral drugs with a virucidal mechanism aiming to be translated in clinical use. The key idea is to combine the two approaches just showed: a multivalent entry inhibitor designed to have a broad-spectrum activity modified in order to be virucidal, with a low-toxicity.

The starting point are entry inhibitors, that mimic host-cell receptor to inhibit virus recognition. The novelty in our approach is to modify them in a way that would render the interaction irreversible, causing a permanent damage to the virus so that, even upon dilution, could not retrieve its initial infectivity. This approach, in our view, greatly enhances the possibility of translating such novel compound in drugs.

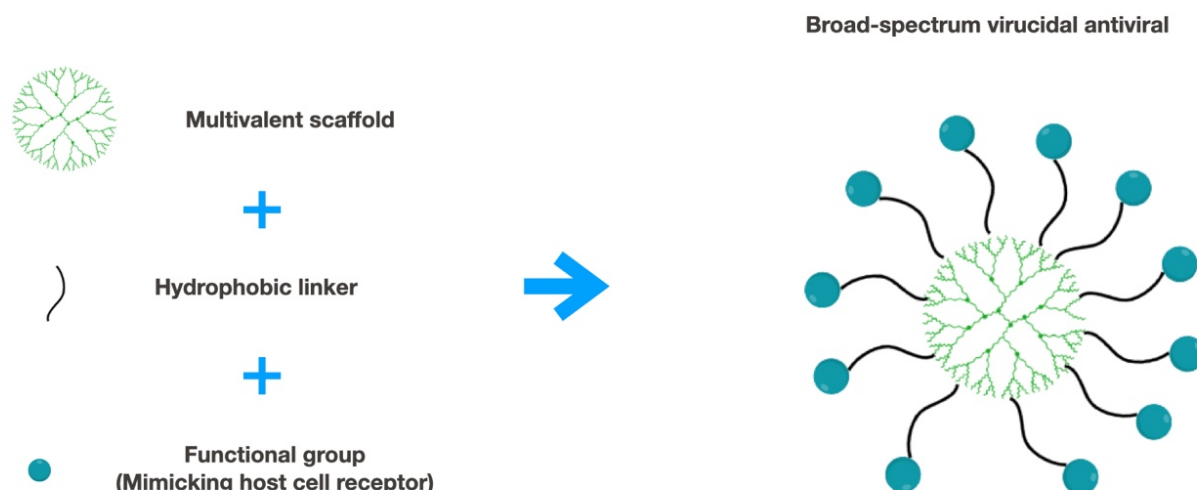


Figure 1.13 – **Design principle of our broad-spectrum virucidal antiviral.** We combine a multivalent scaffold, with a hydrophobic linker, and a functional group responsible of the recognition of the virus. In our vision, the hydrophobic linker is responsible of the virucidal activity.

Fig. 1.13 shows the building blocks of our flexible platform to design novel virucidal antivirals. Ideally there are three major components: a) a multivalent scaffold b) a hydrophobic linker c) a functional group. The multivalent scaffold could be of different nature (metallic, polymeric, small molecule) and is needed to have a large number of functionalization, giving rise to the multivalency. The functional group mimics the host cell receptor exploited by the virus to recognize it. This gives us the flexibility to modify them to target different viruses. In this thesis, the focus will be given to HSPGs, in order to have a broad-spectrum activity, but our group has shown that sialic acid can be targeted as well to target for instance influenza virus <sup>59</sup>, as discussed in detail in this review <sup>60</sup>. Lastly, the other component is the hydrophobic linker, placed in between the functional group and the multivalent scaffold. This moiety is the main difference with standard entry

inhibitors and, as it will be shown in the next paragraphs, is the key feature that render such antiviral virucidal.

The importance of hydrophobicity gained recently attention from different research groups that confirmed our hypothesis on different structure such as polymers<sup>61</sup>, dendritic polymer or modified 2D materials<sup>62</sup>. These compounds show structures similar to what discussed above and result to be virucidal against different viruses.

Fig 1.14 shows more in detail the mechanism of action of virucidal entry inhibitors. Initially, there is a first thermodynamic equilibrium between the virus and the material, determined by the kinetic constants  $k_{on}$  and  $k_{off}$ , that results in a dissociation constant  $K_D = k_{off}/k_{on}$ . The relationship between this equilibrium and the medically relevant IC50 of the drug has been deeply investigated and is summarized by the Cheng-Prusoff equation<sup>63-64</sup>. We hypothesize that once this equilibrium is established, in case of our virucidal entry inhibitor, there is a secondary irreversible chain of reactions that can be characterized by a kinetic constant  $k_v$ . This secondary chain of reactions leads to the permanent inhibition of the virus. Given the irreversibility of this second step, the viral inhibition is retained even upon dilution, conversely to standard entry inhibitors, making such compounds promising candidates for broad-spectrum antivirals.

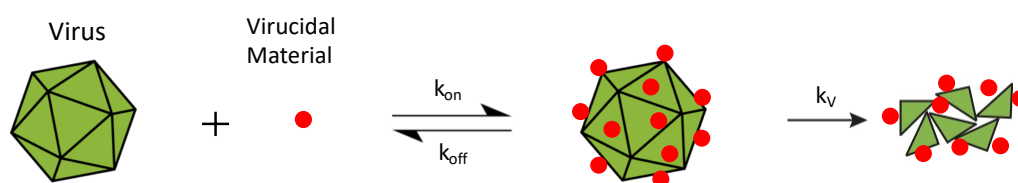


Figure 1.14 – **Sketch of virucidal mechanism for entry inhibitors.** Between the virus and the virucidal material, there is an equilibrium, determined by kinetic constants  $k_{on}$  and  $k_{off}$  that then evolves towards an irreversible inactivation (determined by a kinetic constants  $k_v$ ) of the virus that lose its infectivity. Modified from <sup>54</sup>

### 1.6.1 Gold Nanoparticles

As discussed above, probably the first HSPG-mimicking compound that has been proposed as antiviral was heparin. After that, many other heparin-like moieties were proposed employing different scaffold, among which metallic nanoparticles. In particular, a paper from Baram-Pinto, showed the capability of gold nanoparticles covered by mercapto-ethanesulfonate (MES) of inhibiting Herpes Simplex Virus 1 (HSV-1) <sup>65</sup>.

Starting from this approach, in our group, we synthesized gold nanoparticles with a core size of 2-3 nm, covered by a shell of two ligands: octanethiol (OT) and 11-mercaptoundecanesulfonate (MUS). Such ligands have the same functional group as MES (sulfonate group) but a much longer hydrophobic linker (11 carbon atoms vs 2). As can be seen in fig 1.15, heparin, MES AuNPs and MUS:OT AuNPs, shows similar inhibition against HSV-2, all with no toxicity in the range of interest. A striking difference comes when the three compounds are tested for their mechanism of inhibition. The graphs on the right of fig 1.16 shows the results of a virucidal assay<sup>66</sup>, (more technical detail are discussed in the next chapter). While heparin and MES AuNPs have a solely reversible inhibition (virustatic), MUS:OT AuNPs, thanks to their long hydrophobic linker are capable of irreversibly inhibit viral infection. In fact, if after mixing the virus and the compound above their active concentration, the mixture is diluted, for the two virustatic compounds, the viral infectivity is regained, while for the virucidal one, inactivation is maintained. Such virucidal inhibition was further confirmed on

different HSPG-dependent viruses, both enveloped such as Rhino Syncytial Virus (RSV) and non-enveloped such as Human Papilloma Virus (HPV).

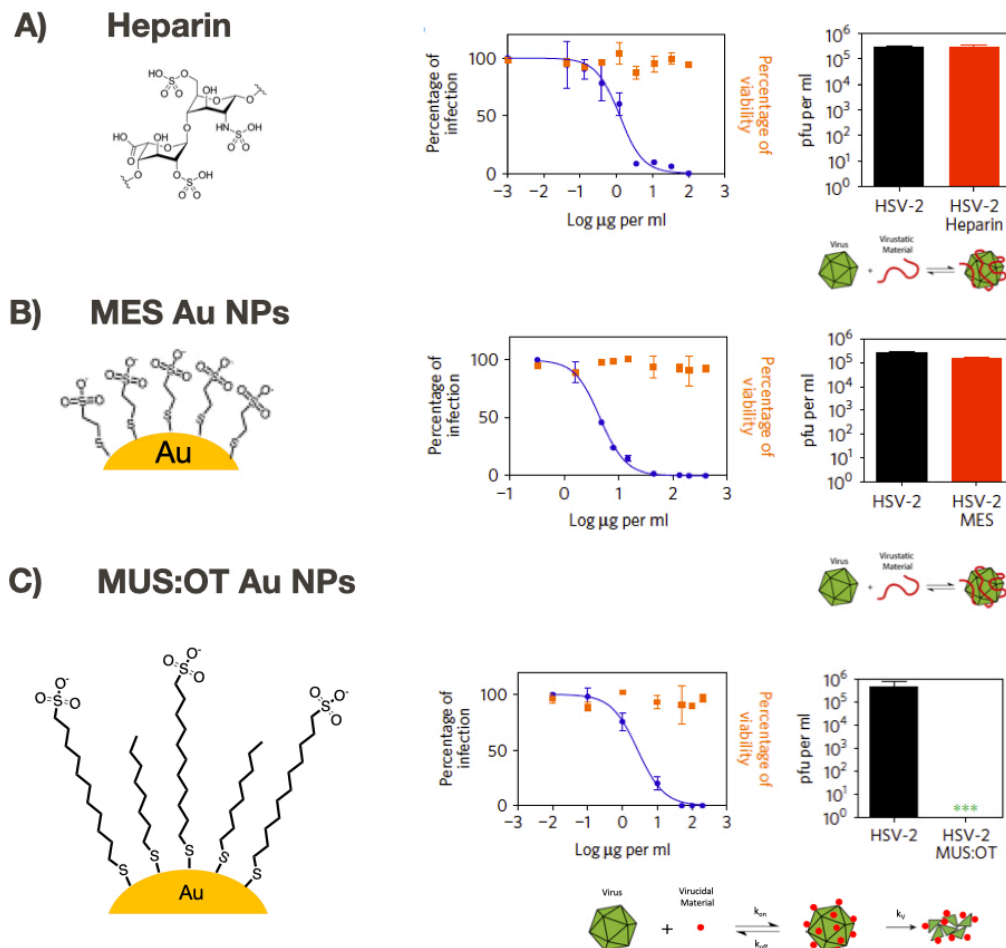


Figure 1.15 – Antiviral activity of heparin, MES AuNPs and MUS:OT AuNPs against HSV-2. From left to right: chemical structure, HSV-2 inhibition and cytotoxicity and virucidal assay for respectively a) heparin b) Mercapto-ethansulfonate (MES) gold nanoparticles (Au NPs) c) 11-Mercapto-undecansulfonate:octanthiol (MUS:OT) gold nanoparticles (Au NPs). Adapted with permission from Cagno et al. (2018)<sup>67</sup>.

The virucidal inactivation resulted to be time-dependent, with the complete inactivation happening after 30 minutes. The mechanism of action was further study via negative stain TEM, cryo-TEM and molecular dynamics (MD) simulation. Electron microscopy images of HSV-1 show that the interaction of MUS:OT NPs with the virus evolves over time, leading to a final disruption of the virus (fig 1.16). Such strong interaction between negatively charged sulfonate groups of MUS:OT AuNPs and positively charged aminoacids present on viral proteins was confirmed by MD, that proved the role of hydrophobic linker in the virucidal inhibition.

The antiviral activity of MUS:OT AuNPs was therefore tested in an *in vivo* setting, to prove their translatability. Indeed, the nanoparticles, administered to mice via intranasal injection, were able to significantly reduce the viral titer of RSV in the nose and to clear the infection from the lungs.

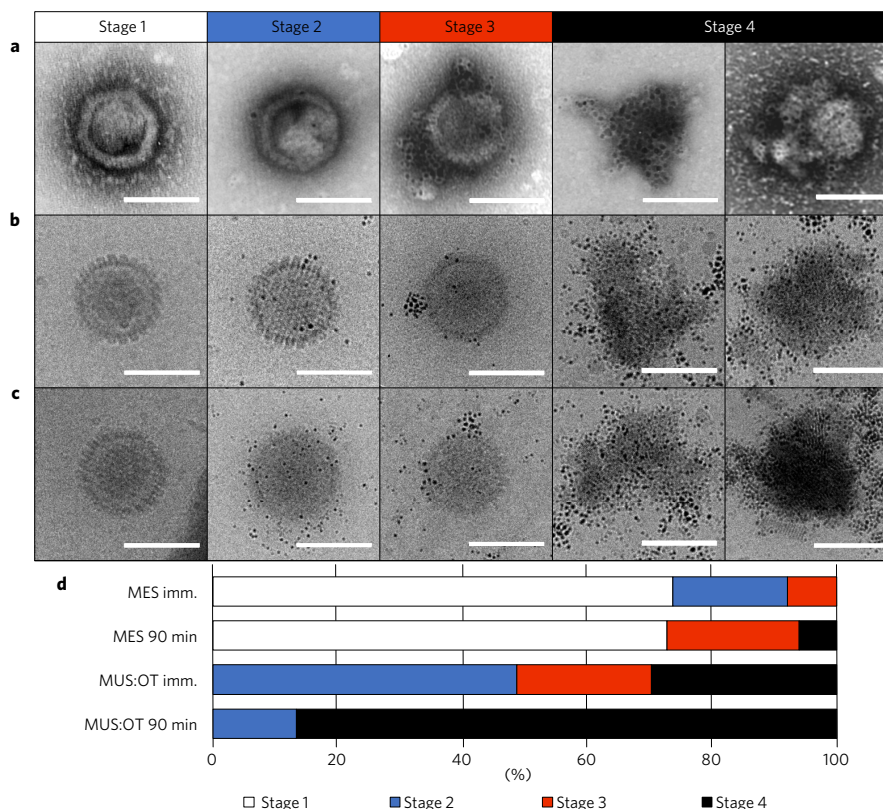


Figure 1.16 – **Association of MUS:OT NPs with HSV-2** a) using dry negatively stained TEM or b) and c) by cryo-TEM. D) shows the distribution of NPs associated with HSV-2 immediately or 90 min after the incubation. Stage 1: Virus with no NPs associated. Stage 2: virus with some NPs. Stage 3: virus with at least one local cluster of NPs. Stage 4: Deformed virus mostly covered by NPs. Scale bars are 100 nm. Adapted with permission from Cagno et al. (2020)<sup>67</sup>.

## 1.6.2 Cyclodextrins

With the previous work, we were able to demonstrate the validity of our approach in designing non-toxic virucidal antivirals. Indeed, it was important to translate such approach to other scaffold in order to prove its flexibility. In addition, for a medical application, the use of gold nanoparticles is not ideal. In fact, although the toxicity profile of AuNPs is practically safe, long-term accumulation raises concerns.

With this in mind, we have designed and synthesized modified beta-cyclodextrins (CD) bearing MUS, the same ligand that was used for AuNPs.

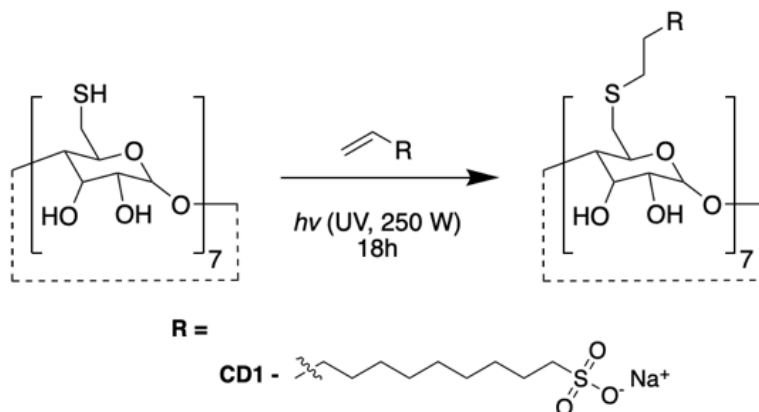


Figure 1.17 – **Synthesis of modified beta-cyclodextrins bearing MUS**. Adapted from Jones et al. (2020).<sup>68</sup>

CDs are an ideal platform for different reasons. First of all, they are widely used in many commercial applications such as cosmetics, food and air freshener<sup>69</sup> and already FDA-approved in drug delivery<sup>70</sup>. In addition, highly sulfated CD were already shown to be active against different viruses among which HIV<sup>71-72</sup>, but in a virustatic manner.

As shown in fig. 1.17, we started from thiolate CD and modified them to have 7-substituted CD, bearing 7 MUS groups (details in Chapter 2), so long aliphatic chain, terminated with a sulfonate group. Such compounds, called CD-MUS or CD-MUS, have been tested against different viruses and resulted to be virucidal *in vitro* against HSV-1, HSV-2, RSV, DENV-2, ZIKV, HCV, therefore with a broad-spectrum of activity. In addition, CD-MUS were tested in a drug-resistance assay against HSV-2, in comparison to the state-of-the-art drug, acyclovir (fig. 1.18). HSV-2 was passaged multiple times in presence of an increasing concentration of the drug: while the EC<sub>50</sub> for acyclovir increased by 87 times, for CD-MUS remained constant, showing its high barrier to resistance.

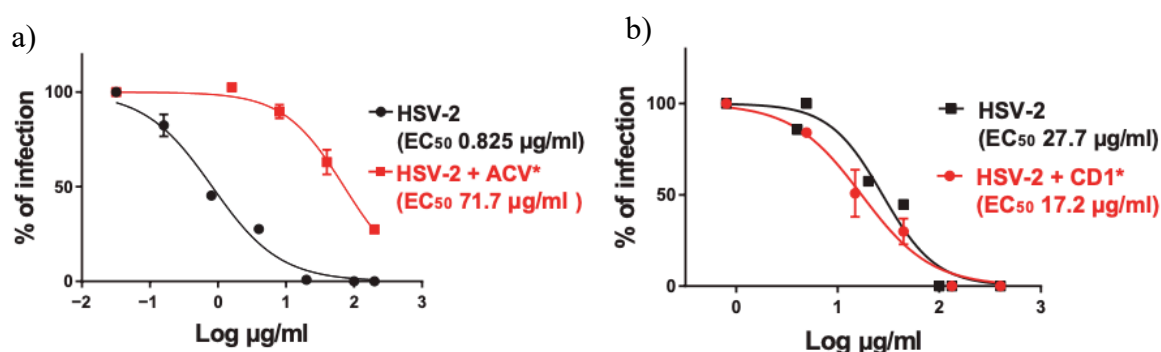


Figure 1.18 – **Drug resistance assay of CD-MUS and Acyclovir.** HSV-2 passaged eight times in the presence of increasing concentrations of (a) acyclovir or (b) CD-MUS, or no inhibitory compounds were subjected to a dose-response assay. The percentages of infection were calculated by comparing the number of plaques in treated and untreated wells. Results are mean and SEM of at least two independent experiments. Adapted from Jones et al. (2020).<sup>68</sup>

Finally, CD-MUS has been tested against *in vivo* in a murine model to prevent HSV-2 infection. In particular, the compound has been formulated in a vaginal gel (HEC). The results show a decrease of viral titer in vaginal mucosa and a higher survival rate, suggesting the potential use of CD-MUS as vaginal micro-bicide.

## Chapter 2 Materials and methods

This chapter is largely a re-arrangement of materials and methods and supplementary informations of different papers (postprint versions), all listed below:

- Z. P. Guven, P.H.J. Silva, Z. Luo, U. B. Cendrowska, M. Gasbarri, S. T. Jones, F. Stellacci "Synthesis and Characterization of Amphiphilic Gold Nanoparticles", *Journal of Visual Experiments* 149, e58872, (2019) DOI: 10.3791/58872
- V. Cagno, M. Gasbarri, C. Medaglia, D. Gomes, S. Clement, F. Stellacci, C. Tapparel, "Sulfonated nano-materials with broad-spectrum antiviral activity extending beyond heparan sulfate-dependent viruses", *Antimicrobial Agents and Chemotherapy* 64 (12) (2020) DOI: 10.1128/AAC.02001-20
- M. Gasbarri, P. V'kovski, G. Torriani, V. Thiel, F. Stellacci, C. Tapparel, V. Cagno, "SARS-CoV-2 inhibition by sulfonated compounds", *Microorganisms* 8 (12), 1894 (2020) DOI: 10.3390/microorganisms8121894
- S. T. Jones, V. Cagno, M. Janeček, D. Ortiz, N. Gasilova, J. Piret, M. Gasbarri, D. A. Constant, Y. Han, L. Vuković, P. Král, L. Kaiser, S. Huang, S. Constant, K. Kirkegaard, G. Boivin, F. Stellacci, C. Tapparel, "Modified cyclodextrins as broad-spectrum antivirals", *Science Advances* 6(5), eaax9381 (2020) DOI:10.1126/sciadv.aax931
- E. Mohammadifar<sup>+</sup>, M. Gasbarri<sup>+</sup>, V. Cagno, K. Achazi, C. Tapparel, R. Haag<sup>\*</sup>, F. Stellacci<sup>\*</sup>, "Polyanionic amphiphilic dendritic polyglycerols as broad-spectrum viral inhibitors with a virucidal mechanism", *submitted*, <sup>+</sup>EM and MG contributed equally.

The chapter is divided as follow. In a first part the different compounds are discussed, in particular gold nanoparticles, beta-cyclodextrins and dendritic polyglycerol. In a second part, the different biological assay are discussed, with a brief theoretical introduction to cytotoxicity, inhibition assay, virucidal assay and DNA release assay.

Regarding gold nanoparticles, I have performed synthesis and chemical characterizations of whole the batches used in the thesis, while the protocol reported here, were mainly prepared by Pelin Guven and Paulo H.J. Silva for <sup>73</sup>. Regarding beta-cyclodextrins, I have performed synthesis and chemical characterizations of the whole batches used in the thesis. Regarding dendritic polyglycerol, the synthesis and the characterization were performed by Ehsan Mohammadifar from Free University of Berlin. Most of the biological validations and assays reported on the thesis were performed by myself (if not, it is reported in the text).

## 2.1 Amphiphilic gold nanoparticles

### 2.1.1 Abstract

Gold nanoparticles covered with a mixture of 1-octanethiol (OT) and 11-mercapto-1-undecane sulfonic acid (MUS) have been extensively studied because of their interactions with cell membranes, lipid bilayers, and viruses. The hydrophilic ligands make these particles colloidally stable in aqueous solutions and the combination with hydrophobic ligands creates an amphiphilic particle that can be loaded with hydrophobic drugs, fuse with the lipid membranes, and resist nonspecific protein adsorption. Many of these properties depend on nanoparticle size and the composition of the ligand shell. It is, therefore, crucial to have a reproducible synthetic method and reliable characterization techniques that allow the determination of nanoparticle properties and the ligand shell composition. Here, a one-phase chemical reduction, followed by a thorough purification to synthesize these nanoparticles with diameters below 5 nm, is presented. The ratio between the two ligands on the surface of the nanoparticle can be tuned through their stoichiometric ratio used during synthesis. We demonstrate how various routine techniques, such as transmission electron microscopy (TEM), nuclear magnetic resonance (NMR), thermogravimetric analysis (TGA), and ultraviolet-visible (UV-Vis) spectrometry, are combined to comprehensively characterize the physicochemical parameters of the nanoparticles.

### 2.1.2 Introduction

The ligand shell of gold nanoparticles can be engineered to exhibit several different properties that can be applied to address challenges in biomedicine<sup>74–77</sup>. Such versatility allows for the control of the intermolecular interactions between nanoparticles and biomolecules<sup>78–80</sup>. Hydrophobicity and charge play a decisive role, as well as other surface parameters that affect how nanoparticles interact with biomolecules<sup>78,81,82</sup>.

To tune the nanoparticles' surface properties, the choice of thiolate molecules that make up the ligand shell offers a myriad of possibilities, according to the characteristics sought. For example, a mixture of ligand molecules with hydrophobic and hydrophilic (e.g., charged) end groups are often used to generate amphiphilic nanoparticles<sup>83,84</sup>.

One prominent example of this type of nanoparticles is protected by a mixture of OT and MUS (hereafter called MUS:OT nanoparticles) that has been shown to possess many relevant properties<sup>67,85,86</sup>. First, with a ligand shell composition of 66% MUS (hereafter 66:34 MUS:OT), the colloidal stability of the nanoparticles is high, reaching up to 33% in weight in deionized water, as well as in phosphate-buffered saline (1x, 4mM phosphate, 150 mM NaCl)<sup>87</sup>. Moreover, these particles do not precipitate at relatively low pH values: for example, at pH 2.3 and with salt concentrations of 1 M NaCl<sup>87</sup>, these nanoparticles remain colloidally stable for months. The stoichiometric ratio between the two molecules on the ligand shell is important because it dictates the colloidal stability in solutions with a high ionic strength<sup>88</sup>.

These particles have been shown to traverse the cell membrane without porating it, via an energy-independent pathway<sup>74,85</sup>. The spontaneous fusion between these particles and lipid bilayers underlies their diffusivity through cell membranes<sup>89</sup>. The mechanism behind this interaction is the minimization of contact between a hydrophobic solvent-accessible surface area and water molecules upon fusion with lipid bilayers<sup>18</sup>. Compared to all-MUS nanoparticles (nanoparticles having only the MUS ligand on their shell), the higher hydrophobicity on mixed MUS:OT nanoparticles (for example, at a 66:34 MUS:OT composition)

increases the span of the core diameter that can fuse with lipid bilayers<sup>90</sup>. Different self-assembly organizations of the ligand shell correlate to distinct binding modes of 66:34 MUS:OT nanoparticles with various proteins, such as albumin and ubiquitin, when compared to all-MUS particles<sup>91</sup>. Recently, it has been reported that 66:34 MUS:OT nanoparticles can be utilized as a broad-spectrum antiviral agent that irreversibly destroys the viruses because of multivalent electrostatic bindings of MUS ligands and nonlocal couplings of OT ligands to capsid proteins<sup>67</sup>. In all these cases, it has been found that the hydrophobic content, as well as the core size of the nanoparticles, determines how these bio-nano interactions take place. These diverse properties of MUS:OT nanoparticles have prompted many computer simulation studies that aimed to clarify the mechanisms underpinning the interactions between MUS:OT particles and various biological structures such as lipid bilayers<sup>92</sup>. The preparation of MUS:OT-protected Au nanoparticles poses a few challenges. First, the charged ligand (MUS) and the hydrophobic ligand (OT) are immiscible. Thus, the solubility of the nanoparticles and of the ligands needs to be taken into account throughout the synthesis, as well as during characterization. Additionally, the purity of the MUS ligand molecules—specifically, the content of inorganic salts in the starting material—influences the quality, reproducibility, as well as the short- and long-term colloidal stability of the nanoparticles. Here, a detailed synthesis and characterization of this class of amphiphilic gold nanoparticles protected by a mixture of MUS and OT are outlined. A protocol for the synthesis of the negatively charged MUS ligand is reported to ensure the purity and, hence, the reproducibility of different nanoparticle syntheses. Then, the procedure to generate these nanoparticles, based on a common one-phase synthesis, followed by thorough purification, is reported in detail. Various necessary characterization techniques<sup>93</sup>, such as TEM, UV-Vis, TGA, and NMR, have been combined to obtain all the necessary parameters for any further biological experiments.

### 2.1.3 Protocol

#### 2.1.3.1 Materials

Chemicals were reagent grade, were purchased from Sigma Aldrich, and used without further purification. All solvents were purchased from Sigma-Aldrich and used without further purification, if not reported explicitly.

#### 2.1.3.2 Synthesis of 11-mercapto-1-undecanesulfonate (MUS)

NOTE: This protocol can be used at any scale desired. Here, a 10 g scale-of-product is described.

##### A. Sodium undec-10-enesulfonate

1. Add 11-bromo-1-undecene (25 mL, 111.975 mmol), sodium sulfite (28.75 g, 227.92 mmol), and benzyltriethylammonium bromide (10

mg) to a mixture of 200 mL of methanol (MeOH) and 450 mL of deionized (DI) water (4:9 v/v MeOH:H<sub>2</sub>O ratio) in a 1 L round-bottom flask.

2. Reflux the reaction mixture at 102 °C for 48 h. Cap the system with a pressure relief mechanism—for example, a balloon with a needle, or simply a needle. This reaction is not sensitive to atmospheric gases.

NOTE: The solution becomes colorless when the reaction is complete.

3. Connect the reaction mixture to a rotary evaporator to evaporate MeOH and reduce the volume to approximately 300 mL.

4. Transfer the remaining solution to a 1 L addition funnel.

5. Extract the remaining aqueous solution 5x with diethyl ether, using the addition funnel. Unreacted 11-bromo-1-undecene stays in the

diethyl ether phase and the sulfonated product in H<sub>2</sub>O.

CAUTION: Release any pressure buildup frequently during the extraction, and consult the correct usage of addition funnels.

6. Collect the final extracted water solution into a 1 L single-neck round-bottom flask.

7. Connect the reaction flask to a rotary evaporator by putting a bit of grease (or Teflon ring strips or any other sealant) between the flask

and the trap.

8. Decrease the vacuum slowly to evaporate the aqueous phase in a rotary evaporator. Because the product is a surfactant, foaming will occur during the evaporation. To circumvent this problem, follow the instruction in the next step.

1. Add ethanol to the mixture to accelerate the evaporation of H<sub>2</sub>O and prevent foaming. When foaming restarts because of the decrease in ethanol content, stop the evaporation, remove the flask from the rotary evaporator, add more ethanol (about one-third of the total volume), and reconnect the flask to the rotary evaporator. Repeat this process until the solution mixture decreases significantly and does not form bubbles.

9. Dry the white powder directly by connecting the flask to a high vacuum. The drier the powder, the less inorganic salts will creep into the subsequent steps. NOTE: Heat can be used to dry the product—for example, by keeping the flask under vacuum in a 60 °C bath and left overnight.

10. Suspend the white powder in 400 mL of methanol in a flask. Sonicate to dissolve the maximum amount of product. NOTE: The goal of this step is to dissolve the product but not the inorganic byproducts, such as excess sodium sulfite and sodium bromide, that have limited solubility in methanol. Use methanol with the lowest water content possible, because water in the methanol will increase the solubility of the inorganic byproducts in the solvent.

11. To increase the solubility of the product, methanol can be gently heated close to its boiling point (~64 °C). CAUTION: Make sure to work under a fume hood during the heating of the flask. The fumes of the evaporated methanol are dangerous.

12. Filter the solution to remove the methanol insoluble inorganic byproducts. Use a filtering flask connected to a vacuum pump and a filtering funnel with quantitative filter paper, or a borosilicate filter. Both the product and the inorganic salts are white powders when dry: the product is soluble in methanol, while the salts are not.

13. Transfer the filtered solution from the filtering flask to a 1 L round-bottom flask.

14. Connect the flask to a rotary evaporator and evaporate the methanolic solution at 45 °C, redissolve the white powder in methanol, and filter the solution (protocol steps 1.1.7, 1.1.8, and 1.1.9). Repeat this process at least 2x, to decrease the amount of inorganic salt.

15. Collect the white, methanol soluble powder (approximately 30 g, at this scale).

16. Dissolve approximately 10 mg of product in 500 µL of D<sub>2</sub>O and transfer the solution to an NMR tube.

17. Perform  $^1\text{H}$  NMR spectrometry on the product in  $\text{D}_2\text{O}$  at 400 MHz with 32 scans. NOTE: The peak assignments for  $^1\text{H}$  NMR ( $\text{D}_2\text{O}$ ) are 5.97 (m, 1H), 5.09 (m, 2H), 2.95 (t, 2H), 2.10 (m, 2H), 1.77 (q, 2H), 1.44 (br s, 12H).

**B. Sodium 11-acetylthio-undecanesulfonate**

1. Dissolve the approximate 30 g of sodium undec-10-enesulfonate (the reaction product of section 1.1) in 500 mL of methanol inside a 1 L round-bottom flask. Add a 2.6x excess of thioacetic acid to the solution and stir it in front of a UV lamp (250 W) overnight (~12 h). In case a UV lamp is not available, the reaction can be performed by refluxing using a radical initiator, such as azobisisobutyronitrile (AIBN); however, the use of a UV lamp is strongly recommended. CAUTION: Make sure to work under the fume hood at all times. If the flask needs to be transported to another space where the UV lamp is located, seal the flask to avoid spreading the strong odor of thioacetic acid. Exercise care when operating a UV lamp: completely block the space where the lamp is located and consult the institution's safety guidelines on how to operate a UV lamp.

2. Monitor the reaction by taking ~2 mL aliquots from the reaction, evaporate solvent, and add deuterated water to check with  $^1\text{H}$ -NMR. Once the peaks corresponding to the double bond disappear, stop the reaction. NOTE: Usually, after 12 h in front of the UV lamp, the reaction is complete. If the reaction mixture becomes turbid, add more MeOH and continue the exposure to the UV light for six additional hours.

3. Evaporate all of MeOH in a rotary evaporator until the solid residue becomes orange-red. If left long enough, the product becomes brown to black. CAUTION: Work mindfully because of the strong odors from the thioacetic acid. The strong odors of any thiolate spills can be neutralized using an aqueous solution of bleach (sodium hypochlorite).

4. Using a filtering flask, wash the product with diethyl ether to remove any excess thioacetic acid, until no more colored (orange-yellow) substances appear in the diethyl ether supernatant. Dry the solid under high vacuum and, then, dissolve it in methanol, yielding a yellow to orange solution. NOTE: Add enough methanol to dissolve the product. NOTE: The color may vary at this step.

5. Add 3 g of carbon black to the solution, mix vigorously, and filter the mixture through filtration medium (see Table of Materials) covering two-thirds of a fluted filter paper. NOTE: The porous structure of carbon black captures the colored side-product material (and some of the product). The filtered solution should be clear. If the filtered solution is still colored (yellow), repeat this process.

6. Evaporate the solvent completely in a rotary evaporator and collect approximately 35 g of white powder.

7. Dissolve ~10 mg of the product in ~500  $\mu\text{L}$  of  $\text{D}_2\text{O}$  and transfer the solution to NMR tubes.

8. Perform  $^1\text{H}$ -NMR on the product in  $\text{D}_2\text{O}$  at 400 MHz with 32 scans. NOTE: The peak assignments for the  $^1\text{H}$ -NMR ( $\text{D}_2\text{O}$ ) are 2.93 (t, 4H), 2.40 (s, 3H), 1.77 (m, 2H), 1.62 (m, 2H), 1.45 (br s, 14H).

**C. 11-mercapto-1-undecanesulfonate (MUS)**

1. Reflux sodium 11-acetylthio-undecanesulfonate at 102  $^\circ\text{C}$  in 400 mL of 1 M HCl for 12 h to cleave the thioacetate group and obtain a thiol.

2. Transfer the product to a 1.5 L or 2 L round-bottom flask. Add 200 mL of 1 M NaOH to the final solution and top it with 400 mL of DI water to have a final volume of 1 L. This will keep the solution acidic and prevent the crystallization of inorganic salts as byproduct. NOTE: A complete neutralization of the solution to pH 7 will result in the crystallization of a product insoluble in methanol.

3. Keep the clear solution at 4 °C and it will crystallize overnight. The product crystallizes as fine crystals that are viscous when wet. NOTE: To accelerate the crystallization, add presynthesized MUS to the solution, if available.

4. Decant the clear supernatant and centrifuge down the viscous white product in 50 mL centrifuge tubes for 5 min at 4,000 x g.

5. Decant the supernatant into another flask and dry the white pellets under high vacuum—depending on the centrifuge available, this can be 2 - 16 tubes or more. NOTE: Filtering is not advised because of the surfactant nature of the product; excessive foaming will occur and most of the product will be lost.

6. Collect approximately 12 g (about 30% yield) of methanol-soluble MUS from this purification step. NOTE: Be mindful that the powder is fine and electrostatic—it tends to stick to spatulas and the surfaces of containers. Also, more material can be extracted from the supernatant of the centrifugation step by reducing the volume (to about a third of its original value) and keeping it at 4 °C. Decrease the volume even more (by 75%) to increase the yield at this step.

7. Dissolve ~10 mg of the product in ~500 µL of D<sub>2</sub>O and transfer the solution to NMR tubes.

8. Perform <sup>1</sup>H-NMR on the product in D<sub>2</sub>O at 400 MHz with 32 scans. NOTE: The peak assignments of <sup>1</sup>H-NMR (D<sub>2</sub>O) are 2.93 (t, 4H), 2.59 (t, 3H), 1.78 (m, 2H), 1.65 (m, 2H), 1.44 (br s, 14H). The calculated molar mass (including the sodium counterion) of the product is 290.42 g/mol.

#### **2.1.3.3 Nanoparticle Synthesis: Preparation of the Reagents**

1. Clean all glassware (one 250 mL and one 500 mL single-neck round-bottom flask, a 100 mL addition funnel, and a small funnel) with fresh aqua regia (three parts hydrochloric acid to one part nitric acid). Rinse the glassware with an excess amount of water inside a fume hood and remove all the fumes. Then, rinse the glassware with ethanol and dry it in a laboratory glassware oven (40 - 60 °C is recommended).

2. Weigh 177.2 mg (0.45 mmol) of gold (III) chloride trihydrate (HAuCl<sub>4</sub>·3H<sub>2</sub>O) in a small glass vial (10 or 20 mL clean glass vials, or on weighing paper).

3. Weigh 87 mg (0.3 mmol) MUS in a glass vial of 20 mL.

4. Add 10 mL of methanol to dissolve the MUS. Sonicate it in an ultrasonic bath until no solid material is visible, to ensure complete dissolution. NOTE: Alternatively, using a heat gun or a warm bath (~60 °C), heat the solution gently. When heated, run cold water through the outside of the flask to bring it back to room temperature.

5. Add 26 µL (0.15 mmol) of OT to the methanol solution and agitate it to mix the ligands.

6. Weigh 500 mg (13 mmol) of sodium borohydride (NaBH<sub>4</sub>) and add it to 100 mL of ethanol in the 250 mL round-bottom flask. Stir vigorously using magnetic stirring (600 - 800 rpm). (The NaBH<sub>4</sub> takes 10 to 20 min, depending on the grade, to form a clear solution in ethanol.)

#### **2.1.3.4 Synthesis of Gold Nanoparticles**

1. Dissolve gold salt in 100 mL of ethanol in the 500 mL round-bottom flask and start stirring at 800 rpm with a magnetic bar on a stirring plate. Make sure the gold salt dissolves completely.

2. Place a 100 mL addition funnel above the round-bottom flask. Put a funnel on the top of the addition funnel with a quantitative paper filter inside. When the NaBH<sub>4</sub> is dissolved in ethanol, start filtering the solution into the addition funnel through the filter paper in the funnel.

3. Add the ligand solution to the reaction mixture. Wait 15 min for the formation of gold-thiolate complex. The color change of the reaction mixture from translucent yellow to turbid yellow indicates the formation of gold-thiolate complex.

4. Start adding the filtered  $\text{NaBH}_4$  solution from the addition funnel dropwise. Adjust the interval time of the drops so that the addition of  $\text{NaBH}_4$  takes about 1 h.

5. After the complete addition of  $\text{NaBH}_4$ , remove the funnel. Keep stirring the reaction for another hour. At the end of the reaction, remove the magnetic stirring bar using a magnet placed on the outside of the flask.

6. Use a septum to close the flask and pierce a needle into the septum to release the  $\text{H}_2$  gas that will evolve after the reaction.

7. Keep the reaction mixture inside a laboratory refrigerator ( $4\text{ }^\circ\text{C}$ ) to precipitate the nanoparticles overnight.

#### **2.1.3.5 Workup of the Synthesis**

1. Decant the supernatant ethanol to reduce the volume.

2. Transfer the remaining precipitant to 50 mL centrifuge tubes and centrifuge for 3 min at  $4,000 \times g$ .

3. Decant the supernatant, disperse the nanoparticles again with ethanol by vortexing, and centrifuge them again. Repeat this washing process 4x.

4. Dry the nanoparticles under vacuum to remove the residual ethanol.

5. To clean the nanoparticles from free hydrophilic ligands/molecules, dissolve the precipitates in 15 mL of DI water and transfer them to the centrifuge tubes with a filtration membrane of 30 kDa cutoff molecular weight. Dialysis is also amenable for this procedure.

6. Centrifuge these tubes for 5 min at  $4,000 \times g$  to concentrate the nanoparticle solution.

7. Add 15 mL of DI water to this solution and centrifuge to concentrate again. Repeat this cleaning process at least 10x. NOTE: One indication that the water-soluble impurities have been removed is the absence of foaming when agitating the aqueous waste; after all, most of the impurities are disulfides of MUS with itself or with OT (this can be determined by collecting the material and performing  $^1\text{H-NMR}$ ).

8. After the centrifugation, transfer the concentrated nanoparticles to a 15 mL centrifuge tube. To turn the nanoparticles into a manageable powder, either precipitate them in a solvent such as acetone or freeze-dry the remaining aqueous solution. When freeze-dried, the nanoparticles tend to form a loose powder that sticks to surfaces and may be difficult to manipulate.

#### **2.1.3.6 Characterization of the Nanoparticles**

##### **A. Purity ( $^1\text{H-NMR}$ )**

1. To check whether the nanoparticles are free from unbound ligands, dissolve 5 mg of dry nanoparticles in 600  $\mu\text{L}$  of  $\text{D}_2\text{O}$  and perform a  $^1\text{H}$  NMR measurement of the particles. If there are no sharp peaks of the ligands, it means the nanoparticles are free from small organic molecules.

#### B. Ligand ratio (<sup>1</sup>H-NMR)

1. Prepare a 20 mg/mL methanol-d<sub>4</sub> solution of iodine. Add 600 µL of this solution to the ~5 mg of nanoparticles in a glass vial, to etch the nanoparticles.

2. Wrap the cap of the vial with paraffin film and sonicate it in an ultrasonic bath for 20 min. Transfer the solution to an NMR tube and acquire a <sup>1</sup>H-NMR (400 MHz) spectrum with 32 scans.

#### C. Ligand density (TGA)

1. Transfer 2 to 8 mg of nanoparticles to a TGA crucible. Choose a temperature range from 30 °C to 900 °C and a speed of 5 °C per minute under N<sub>2</sub> gas.

#### D. Size distribution (TEM)

1. Prepare 0.1 mg/mL nanoparticle solution in DI water. Drop 5 µL of the prepared solution onto the 400-mesh carbon-supported copper grid. Wait until it dries.

2. Transfer the grid in a TEM holder and insert it into the microscope. Acquire 5 - 10 images with a magnification of at least 64,000X, operated at 200 kV. NOTE: To increase the contrast, an objective aperture of 20 nm can be inserted.

#### E. Size distribution (UV-Vis)

1. Prepare a 0.2 mg/mL nanoparticle solution in DI water.

2. Put the required amount of this solution in the quartz cuvette and scan from 200 nm to 700 nm.

### 2.1.4 Representative results

The reaction steps to synthesize MUS are shown in fig 2.1. The <sup>1</sup>H-NMR spectra of the product of each step are represented in fig. 2.2. The synthesis workflow of the binary MUS:OT amphiphilic gold nanoparticles is described in fig. 2.3. Following the synthesis, the workup of the nanoparticles consisted of washing the particles several times with ethanol and DI water. Prior to any characterization of nanoparticles, the cleanliness of the nanoparticles from unbound free ligands was monitored by <sup>1</sup>H-NMR in D<sub>2</sub>O, as shown in fig. 2.4. The size distribution of the nanoparticles was characterized by TEM (fig. 2.5a,b). Localized surface plasmon resonance absorption was measured by acquiring UV-Vis spectra (fig. 2.5c).

The ratio of the two ligands was determined by etching the gold core using iodine, acquiring the <sup>1</sup>H NMR, and calculating the relative amounts of each ligand using the integrated values. Figure 6 shows the representative spectra, as well as the procedure of NMR peak assignments. To find the ligand ratio between MUS and OT, we calculated the integrals of the peaks between 0.8 - 1 (I<sub>1</sub>), 1.12 - 1.55 (I<sub>2</sub>), 1.6 - 1.9 (I<sub>3</sub>), and 2.6 - 3 (I<sub>4</sub>) ppm. The I<sub>1</sub> peak contains signal from three OT hydrogens, the I<sub>2</sub> peak from a combination of 14 MUS hydrogens and 10 OT hydrogens, and the I<sub>3</sub> and I<sub>4</sub> peaks from four MUS hydrogens and two OT hydrogens (for each peak). Therefore, to find the OT percentage, it is necessary to normalize I<sub>1</sub> to 3 and apply the following expressions.

For I<sub>2</sub>,

$$OT\% = \frac{1}{\left(\frac{I_2 - 10}{14}\right) + 1}$$

For I<sub>3</sub> and I<sub>4</sub>,

$$OT\% = \frac{1}{\left(\frac{I_{3,4} - 2}{4}\right) + 1}$$

These calculations indicate the ratio of OT to MUS, assuming there is one arbitrary unit of OT in the system. For fig. 2.6b, the three integrals gave similar values for OT percentage (i.e., 15.3, 15.9, and 15.9 from  $I_2$ ,  $I_3$ , and  $I_4$ , respectively). The surface coverage of the nanoparticles is examined by TGA as shown in fig. 2.7. TGA, NMR, and TEM data are combined to calculate the ligand density, which is the number of ligands on a unit of surface area, approximating the particles to a sphere. (This calculation assumes that Na boils as  $\text{NaHSO}_3$ .) TEM data shows that the average diameter of the nanoparticles is 2.4 nm, pointing to approximately  $18.08 \text{ nm}^2$  ( $A_{\text{par}} = 4\pi r^2$ ) of surface area ( $A_{\text{par}}$ ) and  $7.23 \text{ nm}^3$  ( $V_{\text{par}} = 4\pi r^3/3$ ) of volume per particle ( $V_{\text{par}}$ ). The density of gold is  $19.9 \text{ g/cm}^3$  and the mass of one particle is  $1.3969 \times 10^{-16} \text{ mg}$  ( $\text{Mass}_{\text{particle}} = V_{\text{par}} \times \text{the density of gold} = 7.23 \text{ nm}^3 \times 19.9 \text{ g/cm}^3 \times 10^{-18} \text{ mm}^3/\text{nm}^3$ ). The remaining mass around  $800^\circ\text{C}$  corresponds to the gold core, and there are approximately  $3.7 \times 10^{16}$  particles ( $N_{\text{par}}$ ) that are estimated using  $N_{\text{par}} = (\text{Mass}_{\text{gold}}/\text{Mass}_{\text{particle}}) = 5.17 \text{ mg} / 1.3969 \times 10^{-16} \text{ mg}$ . The total surface area ( $A_{\text{tot}}$ ) of the particles is  $6.69 \times 10^{17} \text{ nm}^2$  ( $A_{\text{tot}} = N_{\text{par}} \times A_{\text{par}} = 3.69 \times 10^{16} \times 18.08 \text{ nm}^2$ ). The NMR of iodine-etched nanoparticles showed that the MUS:OT ratio is 85:15 and the amount of organic content in TGA is  $0.00146 \text{ g}$ . Therefore, there are  $3.26 \times 10^{18}$  ligands ( $N_{\text{ligand}}$ ) following the formula of  $N_{\text{ligand}} = [\text{Mass}_{\text{organic}} / ((R_{\text{OT}} \times M_{\text{wOT}}) + (R_{\text{MUS}} \times M_{\text{wMUS}})) / (R_{\text{MUS}} + R_{\text{OT}})] \times N_{\text{Avogadro}} = [0.00146 \text{ g} / ((15 \times 146 \text{ g/mol}) + (85 \times 267.42 \text{ g/mol})) / (85 + 15)] \times (6.02 \times 10^{23}) = 3.26 \times 10^{18}$ . Finally, the ligand density is  $4.8 \text{ ligands/nm}^2$ , calculated by dividing the  $N_{\text{ligand}}$  by  $A_{\text{tot}}$  ( $4.8 = 3.26 \times 10^{18} / 6.69 \times 10^{17} \text{ nm}^2$ ). The stoichiometric ratios vs. the NMR ratios of the OT, resulting from various syntheses, are compared in fig. 2.8.

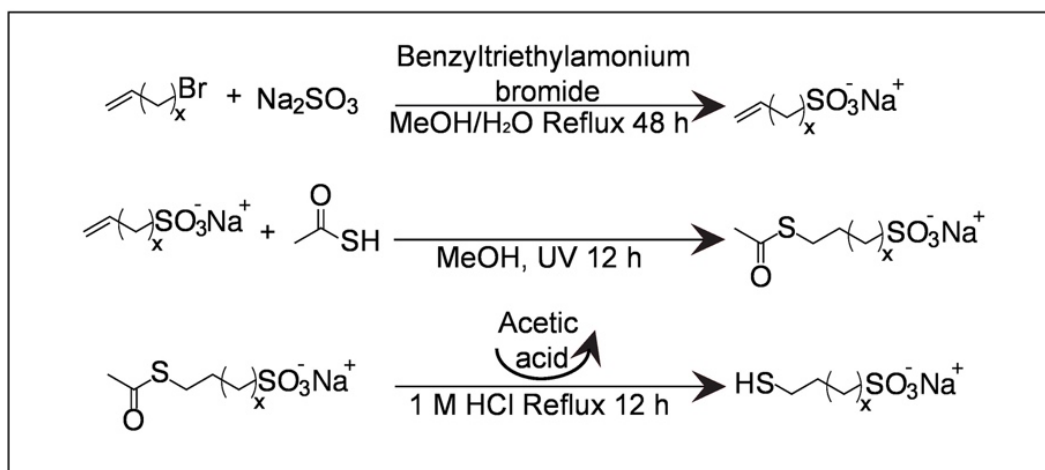


Figure.2.1 – **Schematic of MUS synthesis.** MUS synthesis is the key point for the reproducibility of amphiphilic nanoparticle synthesis. If MUS has a high salt content, the stoichiometric ratio of the ligands may deviate.  $X=9$ .

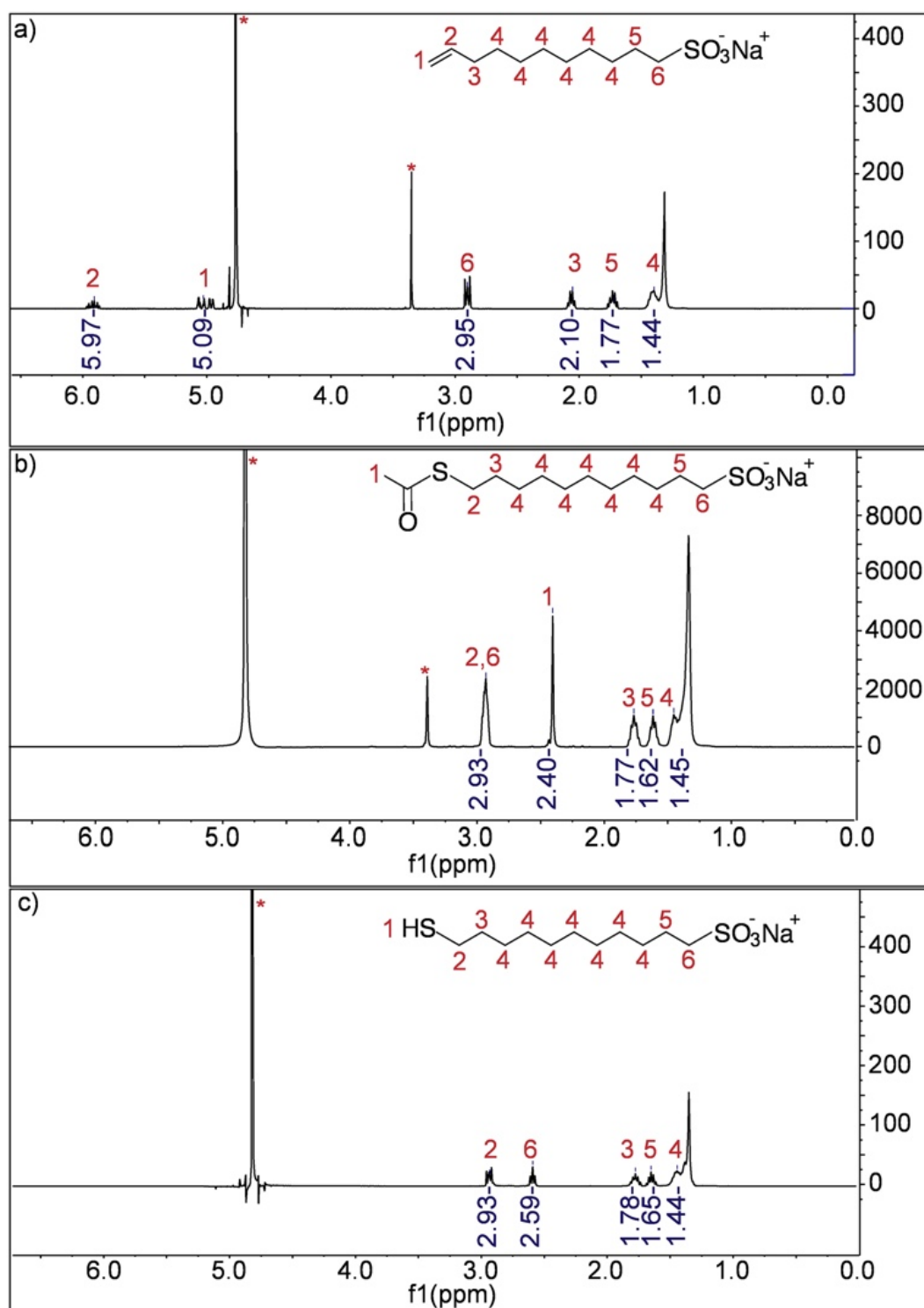


Figure 2.2 – **NMR spectra of the molecules after each step in the MUS synthesis** (400 MHz). (A) This panel shows the  $^1\text{H}$ -NMR spectrum of sodium undec-10-enesulfonate in  $\text{D}_2\text{O}$ . (B) This panel shows the  $^1\text{H}$ -NMR spectrum of sodium 11-acetylthio-undecanesulfonate in  $\text{D}_2\text{O}$ . (C) This panel shows the  $^1\text{H}$ -NMR spectrum of 11-mercapto-1-undecanesulfonate in  $\text{D}_2\text{O}$ . In all spectra, \* indicates the solvent peaks.

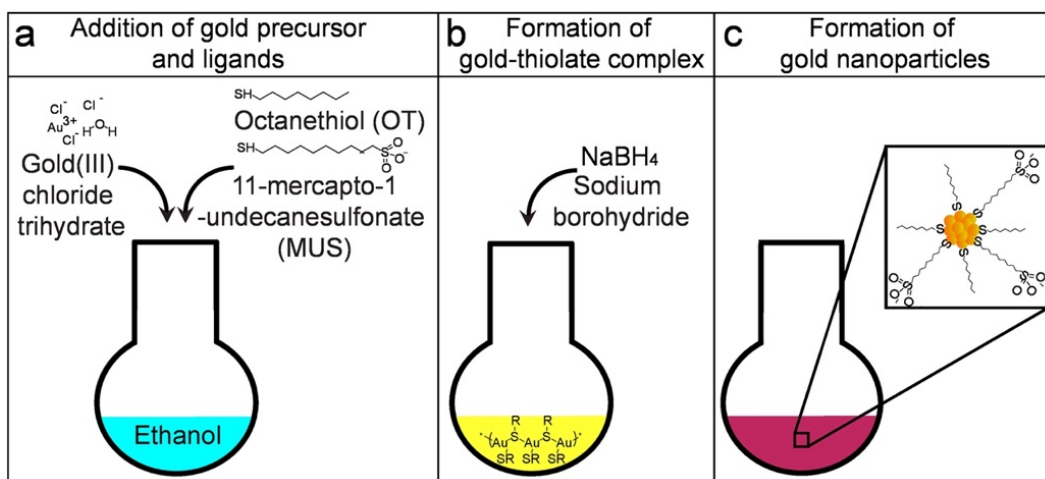


Figure 2.3 – **Schematic of the amphiphilic nanoparticle synthesis.** (A) This panel shows the preparation of the one-phase chemical reduction reaction using ethanol as solvent. (B) Gold-thiolate complex is allowed to form before the addition of a reducing agent. At this stage, the solution of gold salt became turbid. (C) During the dropwise addition of the reducing agent, gold nanoparticles are formed.

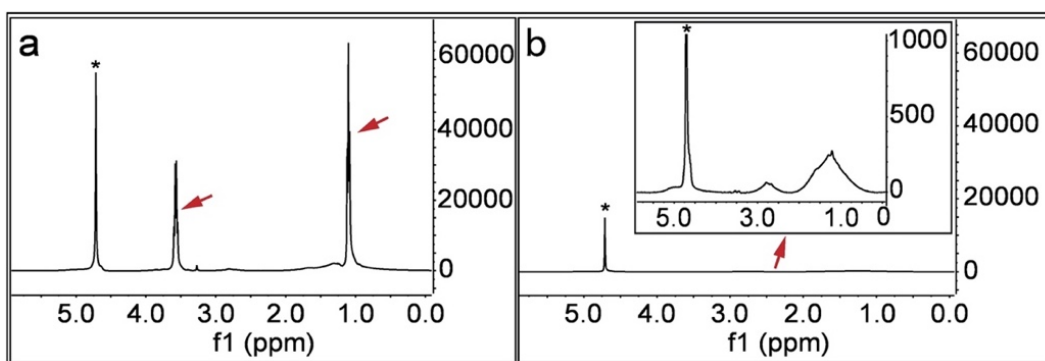


Figure 2.4 – **Cleanliness of the nanoparticles from unreacted free ligands.** (A) This panel shows the <sup>1</sup>H-NMR spectrum of the nanoparticles right after the synthesis and vacuum-drying. D<sub>2</sub>O is used as the solvent for the <sup>1</sup>H-NMR analysis. Sharp peaks shown by red arrows indicate the existence of free unbound ligands. (B) This panel shows the <sup>1</sup>H-NMR spectrum of the nanoparticles after a thorough purification (i.e., washes and centrifugation with ethanol and DI water). The red arrow points to the magnified part of the spectrum, in which the peaks are broad, not sharp as before indicating the absence of free ligands. In both spectra, \* indicates the solvent peaks.

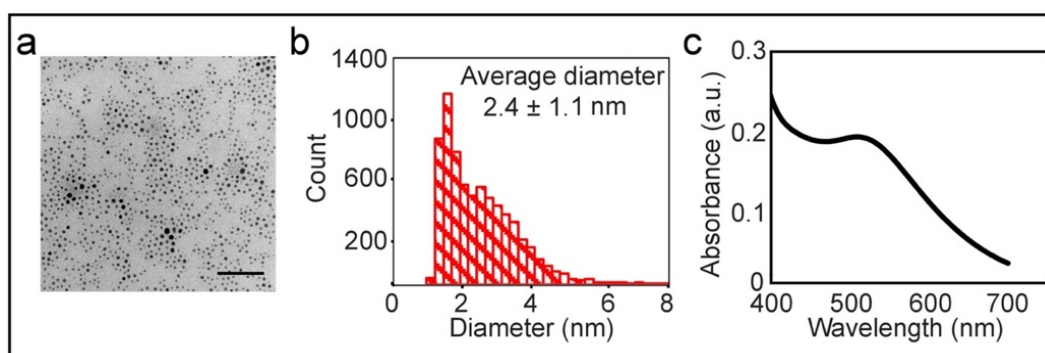


Figure 2.5 – **Size distribution of nanoparticles.** (A) This panel shows a representative TEM image of MUS:OT nanoparticles. The scale bar is 20 nm. (B) This panel shows a histogram of the core size of nanoparticles based on several TEM images. (C) UV-Vis spectra of the nanoparticles showed the characteristic surface plasmon resonance peak of the nanoparticles at around 520 nm.

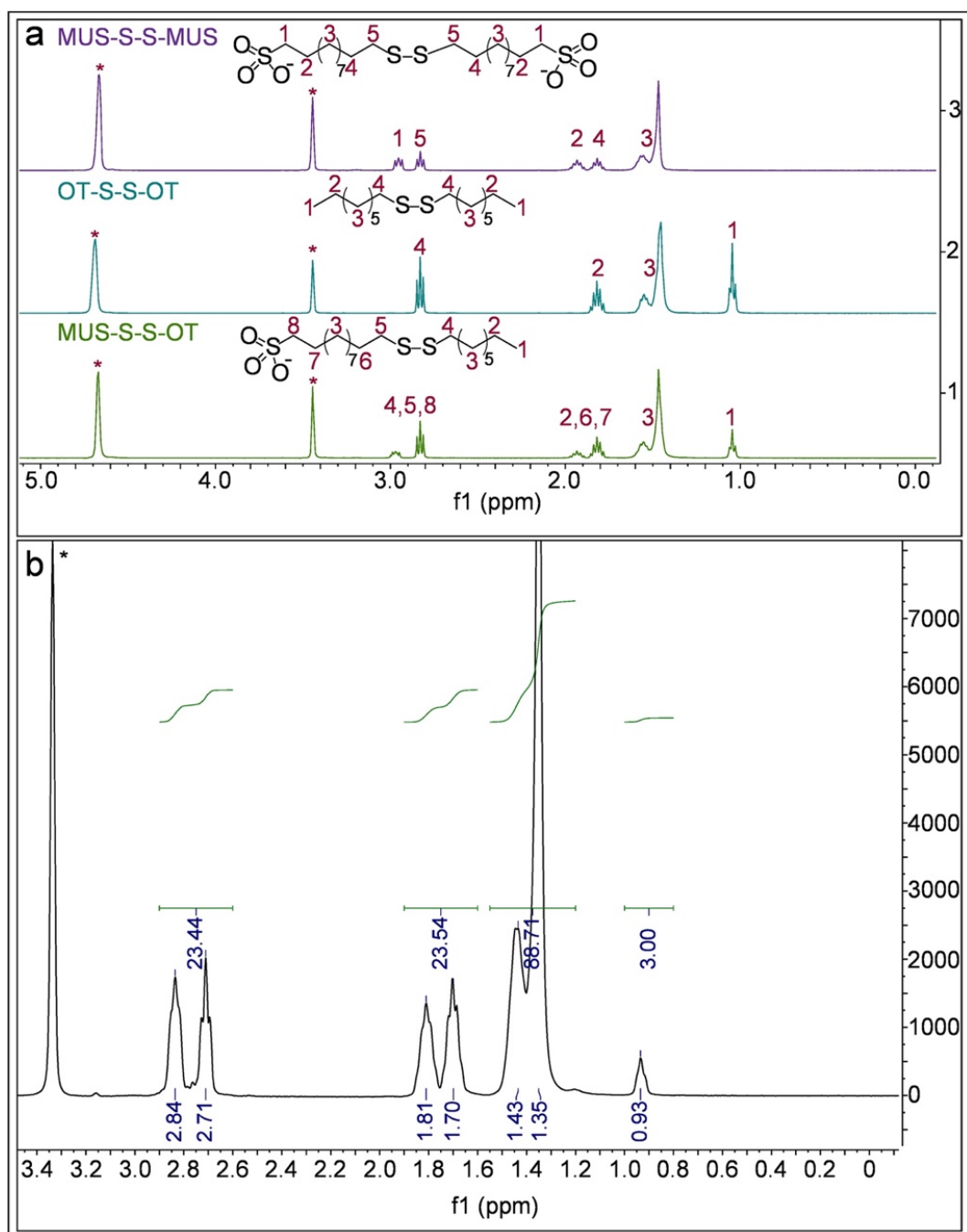


Figure 2.6 – **Ligand ratio calculation.** (A) This panel shows representative NMR spectra of combinations of disulfides (as references for ligands after core etching) and peak assignments for different protons in  $\text{MeOD-d}_4$ . (B) This panel shows  $^1\text{H}$ -NMR spectra of etched nanoparticles in  $\text{MeOD-d}_4$ . In all spectra, \* indicates the solvent peaks.

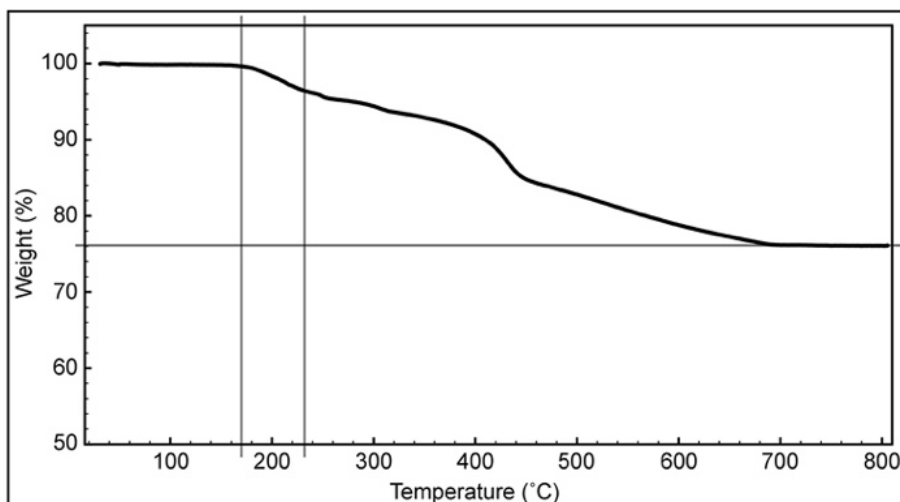


Figure 2.7 – **Ligand density analysis.** A TGA measurement of the nanoparticles was done to determine the ratio and density of organic material (ligands). The graph of the measurements is plotted as the weight percentage vs. the temperature. OT desorbs first, between 176 °C to 233 °C (vertical lines). MUS degrades to smaller molecules and is totally burned at around 800 °C. The remaining weight percentage corresponds to the gold core of the nanoparticles.

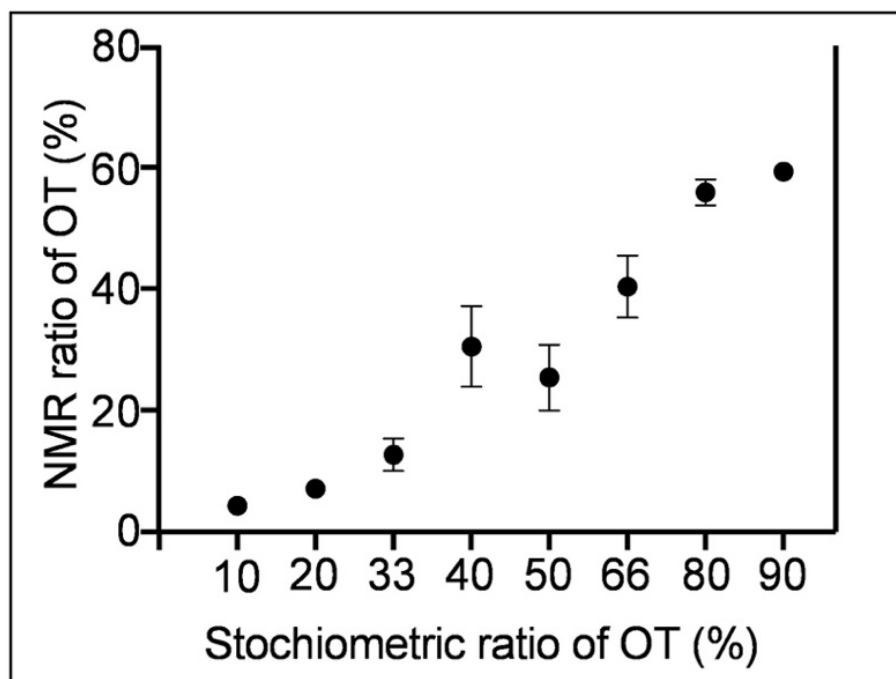


Figure 2.8 – **Comparison of stoichiometric and NMR ratios of OT on the particles.** It is possible to tune the amphiphilicity of the nanoparticles by changing the starting stoichiometric ratio between MUS and OT in the reaction. The error bars show the upper and lower limit of OT content acquired using the indicated stoichiometric ratios. Stoichiometric ratios of 10%, 20%, etc., up to 90% OT, were synthesized to observe the limits of OT content on the nanoparticle surfaces.

This protocol describes first the synthesis of MUS ligand and, then, the synthesis and characterization of amphiphilic MUS:OT gold nanoparticles. Synthesizing MUS with minimal salt content enables a better reliability of the stoichiometric ratio between the ligands during the nanoparticle synthesis, which is a key factor for the reproducible synthesis of MUS:OT nanoparticles with a target hydrophobic content (fig. 2.8). The use of methanol as a common solvent for MUS and OT, along with the synthesis of the particles in

ethanol, allows for a reliable synthesis of MUS:OT gold nanoparticles. The methods of characterization presented here make up a minimal list of experiments necessary to acquire sufficient information on the nanoparticles to verify the outcome of their synthesis. There are four critical steps in this protocol: (i) the synthesis of MUS with a low salt content along with the removal of colored impurities in the second step and a crystallization of pure MUS in the end; (ii) tuning and determining the stoichiometric ratio between MUS and OT; (iii) the workup of the nanoparticles; and (iv) the characterization of the nanoparticles. During the formation of nanoparticles, MUS preferentially binds to the nanoparticle surfaces, which might be related to the solubility of the resulting nanoparticles. For example, a 2:1 stoichiometric feed ratio between MUS and OT results in 15% of OT on the surface when calculated using the data from the  $^1\text{H}$ -NMR of etched gold nanoparticles. Therefore, a higher content of OT must be used during the synthesis of the particles (fig. 2.8) to obtain a nanoparticle with a lower MUS to OT ratio; in other words, a more hydrophobic particle. In order to assess the stoichiometric ratio between the ligands on the surface of the nanoparticles, it is necessary to ensure there are no unbound ligands in the solution. The presence of unbound ligands affects the determination of the ligand ratio on the nanoparticles and the density, along with subsequent tests and experiments that may lead to incorrect interpretations. Repetitive cleaning cycles with different solvents (such as ethanol and DI water) are required to eliminate all unbound ligands and other impurities (byproducts of sodium borohydride, gold ions, etc.).  $^1\text{H}$ -NMR is important to confirm the purity of the nanoparticles. The line-broadening effect of ligands owing to the complex chemical environment on the nanoparticles broaden the peaks corresponding to the ligands, while any sharp signal comes from unbound molecules<sup>94</sup>. Furthermore, due to restricted mobility, the NMR peaks corresponding to the methylene adjacent to the thiol groups cannot be detected, which is another signature of the nanoparticle when inspected using  $^1\text{H}$ -NMR. Once the nanoparticles are clean, then the metal core is etched with iodine. Iodine etching is a well-established method to quantify the ligand ratio on nanoparticles. For instance, two decades ago, Murray et al. reported the determination of monolayer composition on gold nanoparticles after iodine etching, in which the iodine decomposes the gold core and releases the thiolate ligands as disulfides<sup>95</sup>. The reliability of the iodine etching method has been established using other methods; for example, Harkness et al. reported that the ligand ratio obtained from NMR is within 1% deviation from mass spectroscopy measurements<sup>96</sup>. TGA is a straightforward method to calculate the organic content on the nanoparticles. The estimation of the surface ligand density assumes that all thiolate ligands bind to surface gold atoms and all free ligands have been removed during purification. To determine the ligand density, several assumptions are made, mainly that the particles are spherical, which is used to calculate the surface area, as well as the packing density, of the gold core. TEM provides a size distribution of the nanoparticle gold cores that can be used to calculate the approximate surface area of a nanoparticle. The nanoparticle synthesis described here produces a polydisperse population of particles with an average diameter of 2 - 3 nm and a size deviation of up to 30%. Also, the average radius, used to calculate the average volume of one particle (approximating the particles to spheres), combined with the density of gold, enables the calculation of the mass of one nanoparticle. Then, the mass measured by TGA over 800 °C enables the calculation of the number of particles initially present. By using this value and the average core size, the total surface area of the gold nanoparticles can be estimated. The ligand ratio calculated from the data acquired with  $^1\text{H}$ -NMR spectroscopy allows for the calculation of the number of moles of the ligands on the surface of the nanoparticles. The molar ratio between the ligands over the surface area of gold nanoparticles provides the ligand density (fig. 2.7). Clean nanoparticles have approximately 4 ligands per  $\text{nm}^2$ . TGA data can also be used to estimate the ligand ratio, if the temperature interval in which they desorb from the gold surface is known for each ligand, and desorption occurs at separate temperature ranges.

In summary, this protocol provides a straightforward way to synthesize the MUS ligand with a low salt content and MUS:OT amphiphilic gold nanoparticles. One of the key factors of the reproducibility of these nanoparticles is the low inorganic salt content in the MUS used. These nanoparticles are stable both as powder and in solution (e.g., H<sub>2</sub>O and physiologically-relevant ones), which should be emphasized as a prerequisite for many applications. Thorough characterization of the size and the surface properties of amphiphilic nanoparticles is essential for future applications in which the degree of amphiphilicity may play a key role.

## 2.2 Beta-cyclodextrins

The synthesis of beta-cyclodextrin was mainly developed by Dr. Sam Jones and Dr. Matej Janeczek as reported in Jones et al. The characterization techniques were developed and analyzed by Dr. Daniel Ortiz and Dr. Natalia Gasilova. The synthesis reported below is the one used for most of the experiments. In a second stage, CD-MUS synthesized by ProChimia were used, after being validated in our lab, as discussed below.

### 2.2.1 Materials

All solvents used were dry, and reactions were carried out under argon atmosphere. The starting materials were purchased from Sigma-Aldrich if not otherwise stated. Heptakis-(6-deoxy-6-mercapto)- $\beta$ -CD and hexakis-(6-deoxy-6-mercapto)- $\beta$ -CD were purchased from Cyclodextrin-Shop, Netherlands. Care was taken to use a freshly synthesized batch to minimize the presence of disulfides.

### 2.2.2 Synthesis

Heptakis-(6-deoxy-6-mercapto)- $\beta$ -CD (50 mg, 0.040 mmol), sodium undec-10-ene-1-sulfonate (108 mg, 0.421 mmol), and 2,2-dimethoxy-2-phenylacetophenone (22 mg, 0.084 mmol) were dissolved in DMSO (5 ml). The reaction mixture was placed under ultraviolet (UV) lamp (250 W) and stirred for 18 hours. Crude product was precipitated by the addition of Et<sub>2</sub>O (45 ml) and collected by centrifugation. The off-white solid was washed by MeOH (45 ml) and EtOH (45 ml) and collected by centrifugation. The product was purified by dialysis against Milli-Q H<sub>2</sub>O for 3 days, filtered through 0.2  $\mu$ m filter, and collected as a yellow solid (92 mg, 76%).

### 2.2.3 Characterization

#### 2.2.3.1 Mass Spectroscopy

Mass spectrometry analyses were performed on a LTQ Orbitrap Elite FTMS instrument (Thermo Scientific, Bremen, Germany) operated in the negative mode coupled to a modified HESI-II probe in an Ion Max ion Source able to perform Cold-spray ionization (CSI). Cold-spray ionization is an ESI-MS modification operated at very low temperature that can be used to prevent decomposition of labile molecules that are difficult to observe by conventional MS techniques. The experimental conditions for the ionization voltage were -1.2 kV. The temperature of ion transfer capillary was 60 °C, tube voltages. Sheath and auxiliary gases were 35 and 10 respectively to obtain a spray temperature around +5 °C. The infusion rate was 5  $\mu$ L/min. Spectra were obtained in the 80-1000 m/z range in the reduce profile mode with a resolution set to 120,000 and automatic gain control (AGC) value set at 10<sup>+6</sup>. A total of 100 scans each consisting in 10 mscans were acquired in reduced profile mode and averaged.

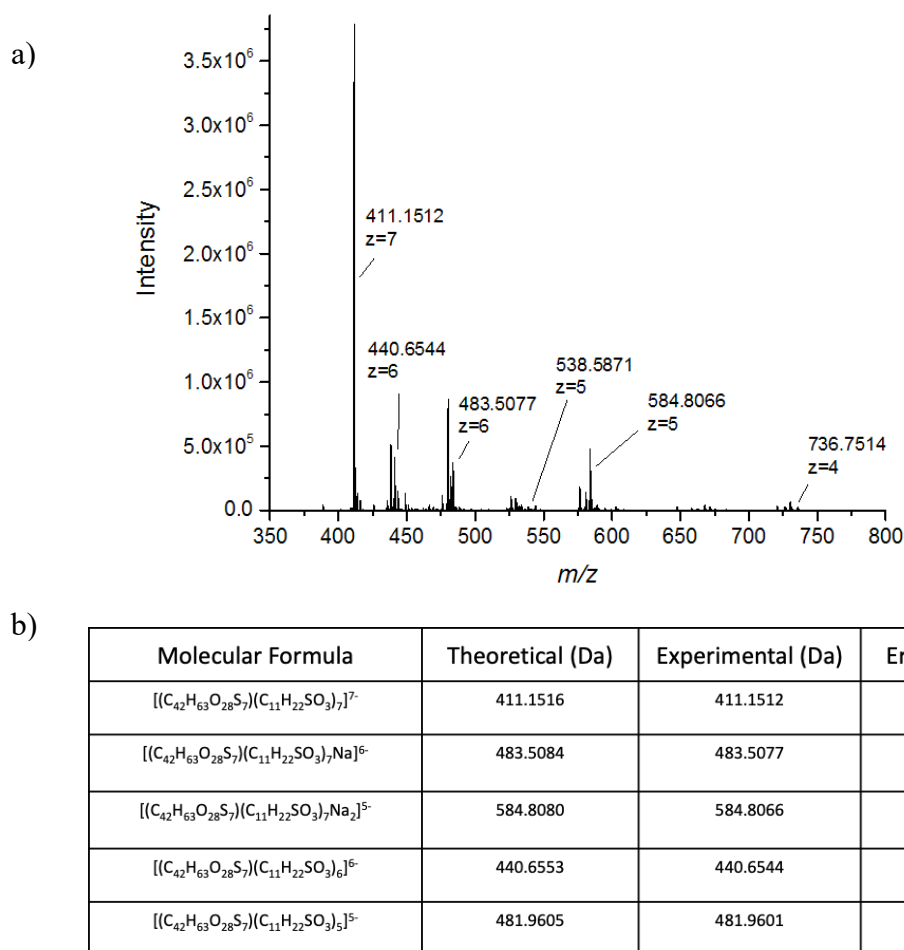


Figure 2.9 – **Mass spectrometry characterization of CD-MUS.** HRMS Cold-Spray Ionisation spectrum of CD-MUS in EtOH/H<sub>2</sub>O (50:50), b) HRMS Summary of CD-MUS in EtOH/H<sub>2</sub>O (50:50). Values correspond to the monoisotopic mass

### 2.2.3.2 Capillary electrophoresis with UV-detection (CE-UV)

Synthesised compounds were analysed by capillary electrophoresis (CE) with UV detection (CE-UV) following the protocol described by the United States Pharmacopeia (USP) and the National Formulary (NF) with minor modifications (Betadex Sulfobutyl Ether Sodium USP NF 33, Official Monograph, Betadex 6546-6550). CE-UV experiments were carried out using a 7100 A CE apparatus (Agilent, Waldbronn, Germany) and untreated fused silica separation capillary (BGB analytik AG, Bickten, Switzerland) of 50  $\mu$ m i.d., 40.5 and 49 cm of effective and total length, respectively. Background electrolyte (BGE) was 30 mM benzoic acid with pH 8 adjusted by addition of 100 mM Tris solution. Prior to sample analysis each new capillary was conditioned by flushing for 10 min with 1 M NaOH, followed by 5 min flushing with 0.1 M NaOH and then 5 min with milliQ H<sub>2</sub>O. CE-UV analysis program consisted of the following steps: a) flushing with 0.1MNaOH for 2 min; b) flushing with milliQ H<sub>2</sub>O for 2 min; c) flushing with BGE for 2 min; d) sample injection for 5 sec with 40 mbar pressure; e) application of 30 kV separation voltage for 10 min. UV signal was monitored at 230.0 nm wavelength. Peak assignment was performed with captisol as a reference compound taking into account capillary to capillary migration time variation.

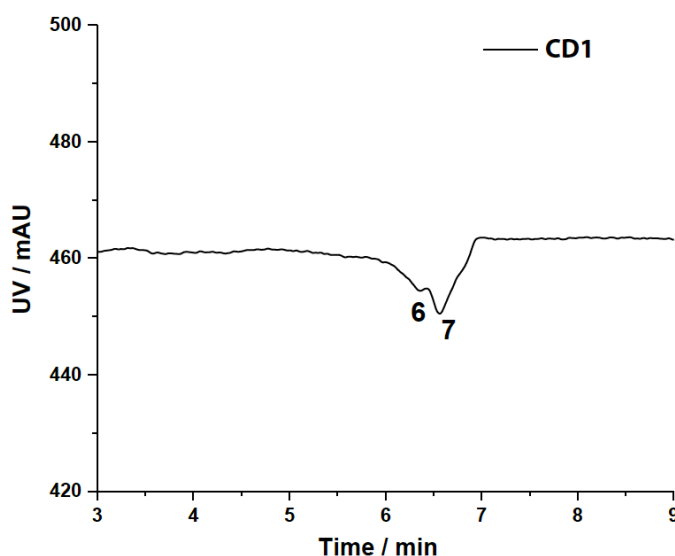


Figure 2.10 – **CE-UV electropherogram of CD-MUS.** Absorbance acquired at 230 nm with assigned CD species showing 31% of 6 and 69% of 7 sulfonates per CD.

#### 2.2.4 Further development

The synthesis has been then optimized and upscaled in collaboration with ProChimia (PL) and CycloLab (HU), in order to have a larger supply envisioning possible *in vivo* studies in larger animals. Such collaborations allow us to have now a stable and reliable method to have 7-substituted cyclodextrins relying on our external vendor with scale in order of the gram per batch.

### 2.3 Dendritic polyglycerol (dPG)

The synthesis of all the dPGs was developed and performed at Free University of Berlin by Dr. Ehsan Mohammadifar, under the supervision of prof. Rainer Haag, after joint discussions with the author and prof. Stellacci.

#### 2.3.1 Materials

Chemicals were reagent grade, were purchased from Acros Organics and Fischer Chemical, and used without further purification. All solvents were purchased from Sigma-Aldrich and used without further purification. Dialysis was performed in benzoylated cellulose tubing purchased from Sigma-Aldrich (MWCO 2000 g/mol). NMR spectra were recorded on a Jeol ECX 400 spectrometer. Proton and carbon NMR spectra were recorded in ppm and were referenced to the indicated solvents. Elemental analysis was performed with a VARIO EL III (Elementar). Dynamic light scattering (DLS) and  $\zeta$ -potential measurements were carried out with a Zetasizer Nano ZS equipped with a He-Ne laser (633 nm) in the backscattering mode (detector angle 173°) (Malvern Instruments Ltd.). Samples were dissolved in phosphate buffer (PB,  $10 \times 10^{-3}$  M, pH 7.4) at a concentration of 0.5 mg/mL. For the  $\zeta$ -potential measurements, the samples were dissolved in PB ( $10 \times 10^{-3}$  M, pH 7.4) at a concentration of 1 mg/mL. The solutions were measured by applying an electric field across at 25 °C in folded DTS 1060 capillary cells (Malvern Instruments Ltd.). An USHIO super high mercury lamp (USH 102d, 100 W) was used for UV assisted thiol-ene click reaction.

### 2.3.2 Synthesis of dPG core

The dPG core was synthesized through slow monomer addition for ring opening multi-branching polymerization of glycidol (fig. 2.11). In the first step, trimethylolpropane (TMP) (25 mmol) was deprotonated by potassium methoxide solution (10 mmol KOH in 10 mL methanol). The resulting methanol was evaporated at 60 °C under vacuum (3 mbar). The synthesis-reactor was then heated to 100 °C and glycidol was added slowly over a period of 24h. The resulting dPG, having an average molecular weight of 10 kDa ("dPG10kDa" or "C1"), was used for functionalization. Molecular weight was determined by GPC as shown in fig. 2.12b.

By varying the amount of glycidol and reducing the period of addition, the corresponding dPG, having a molecular weight of 5 kDa can be similarly obtained.

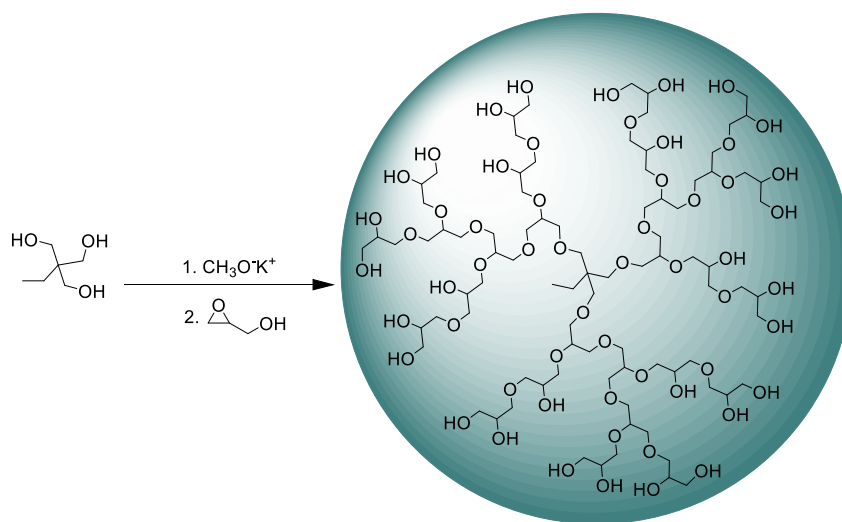


Figure 2.11 – Reaction scheme of dPG core

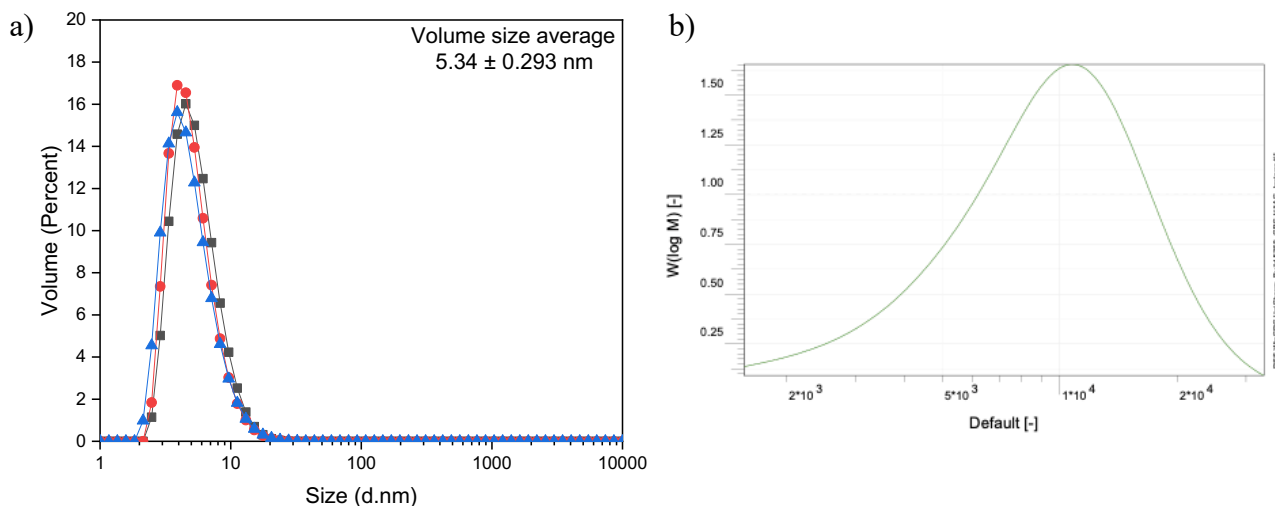


Figure 2.12 – DLS and GPC measurements of dPG core. A) Dynamic light scattering measurements shows the hydrodynamic diameter of dPG core in phosphate buffer at concentration of 1 mg/ml. Results are for three measurement series (indicated by triangles, circles and squares). B) Gel permeation chromatography (GPC) diagram of the non-functionalized core dPG (C1). (Mn: 7.2 kDa, Mw: 10 kDa, PDI: 1.4)

### 2.3.3 Synthesis of different dPG structures

#### 2.3.3.1 Synthesis of dPG-allyl

dPG (200 mg, 2.69 mmol OH to be functionalized) was dried at 60 °C overnight under high vacuum. Dried dPG was dissolved in dry DMF (20 mL) and cooled to 0 °C. To the stirred solution of dPG in dry DMF at 0 °C, NaH (129.12 mg, 5.38 mmol, 2 eq.) was added. After addition ice bath was removed and the temperature of the reaction mixture was allowed to reach room temperature. The reaction mixture was allowed to stir for 1 hours at room temperature and 1 hours at 40 °C and then cooled down again by using ice bath. The allyl bromide (465  $\mu$ L, 5.38 mmol, 2.0 eq.) in dry DMF (1 mL) was added dropwise to the reaction mixture using a syringe. The ice bath was removed and after stirring for 24 hours at 40 °C the reaction was quenched by addition of methanol and the resulting mixture was dialyzed in MeOH to afford dPG-allyl (DF = 100%). Degree of allylation was quantified by  $^1\text{H}$  NMR in  $\text{CD}_3\text{OD}$ . Only for the synthesis of precursor for dPG-1, the dPG-allyl with DF = 2% was synthesized.

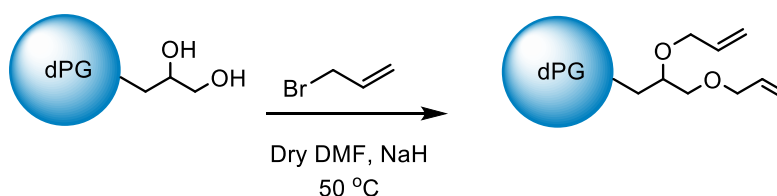


Figure 2.13 – Synthetic route for preparation the of dPG-allyl.

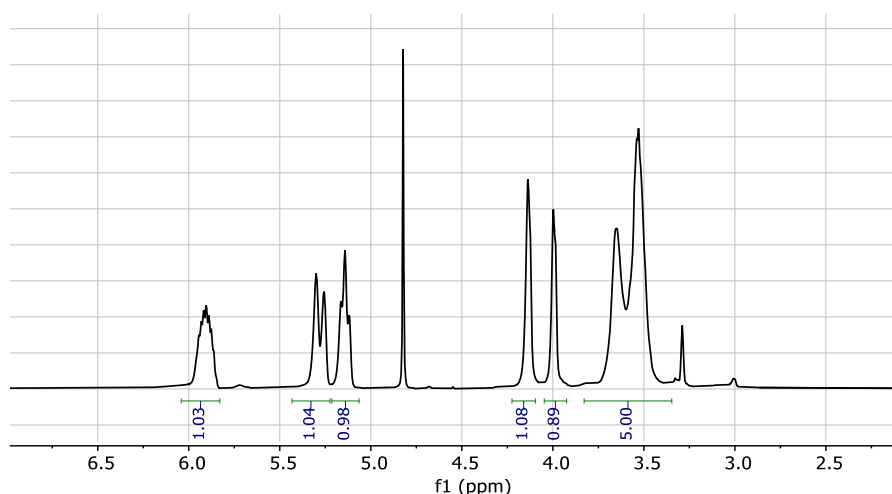


Figure 2.14 –  $^1\text{H}$ -NMR of dPG-allyl. The degrees of functionalization (DF) in the different reactions were confirmed by  $^1\text{H}$ -NMR of the pure product correlating the allyl protons at 5.9 -5.8 ppm with the polyglycerol backbone protons (3.7 - 3.4).

#### 2.3.3.2 Synthesis of dPG-1, dPG-2, dPG-3

dPG-allyl (DF=2) (50 mg, 0.01 mmol of allyl group) for dPG-1 and dPG-allyl (DF=100) (50 mg, 0.67 mmol of allyl group) for dPG-2 and dPG-3 have been used as precursor for the thiol-ene click reaction. Corresponding dPG-allyl and (11-mercapto-1-undecanesulfonate) with the determined molar ratio to the allyl groups were dissolved in methanol (5 mL). 2,2-dimethoxy-2-phenylacetophenone (DMPA) as radical initiator (50 mg, 0.19 mmol) and a catalytic amount of tris(2-carboxyethyl)phosphine hydrochloride (TCEP-HCl) was added to the reaction to avoid oxidation of the thiol intermediate. In the case precipitation, few drops of water were added to dissolve the precipitation and obtain a clear solution. The solution was degassed by

flushing argon through the reaction mixture for 10 minutes. The reaction mixture was stirred and irradiated with UV light using a high pressure UV lamp at room temperature for 5 hours. The reaction mixture was dialyzed (MWCO 2 kDa) against methanol/water mixture to remove the TCEP.HCl, DMPA and excess of unreacted thiol compound. The successful formation of product was confirmed by  $^1\text{H}$ -NMR of pure product by correlating the aliphatic protons of ligands at 1.5-1.00 ppm with the polyglycerol backbone protons at 3.7-3.2 ppm. In addition, elemental analysis was used for the sulfur content measurement confirming the click reaction.

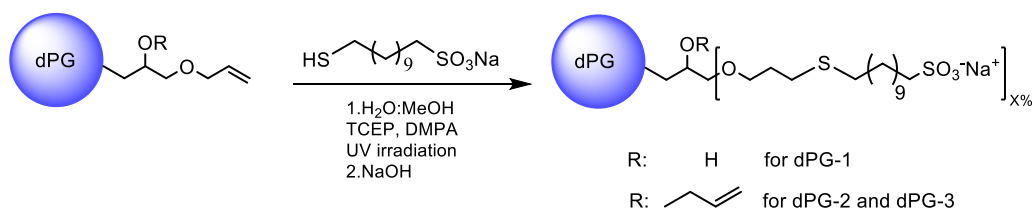


Figure 2.15 – Synthetic route for preparation of the dPG-1 (X = 2), dPG-2 (X = 50) and dPG-3 (X = 85).

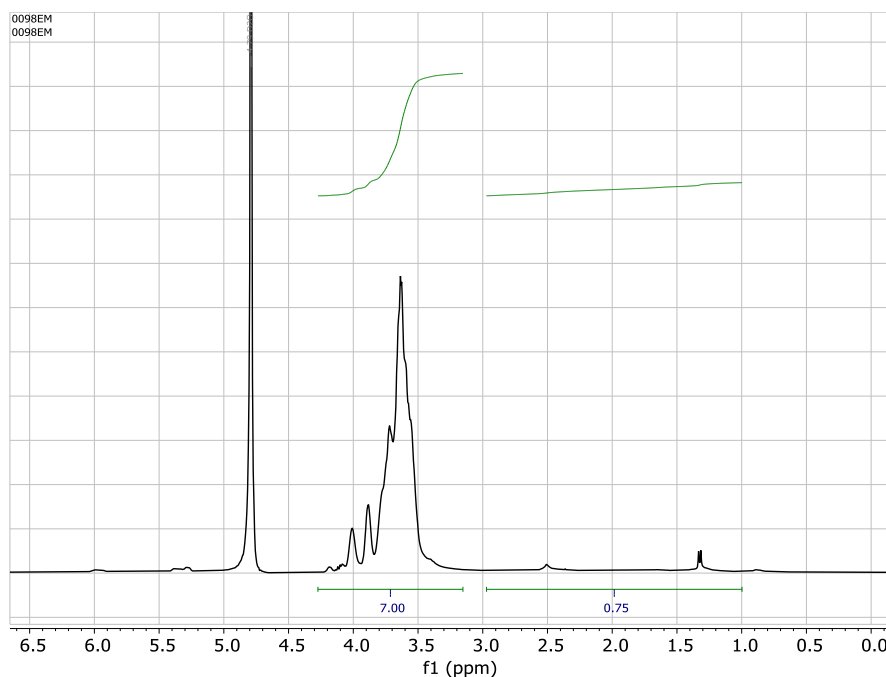


Figure 2.16 –  $^1\text{H}$ -NMR of dPG-1 in  $\text{D}_2\text{O}$ . dPG-1 was functionalized with 11-mercapto-1-undecanesulfonate (MUS) with degree of functionalization of 2%.

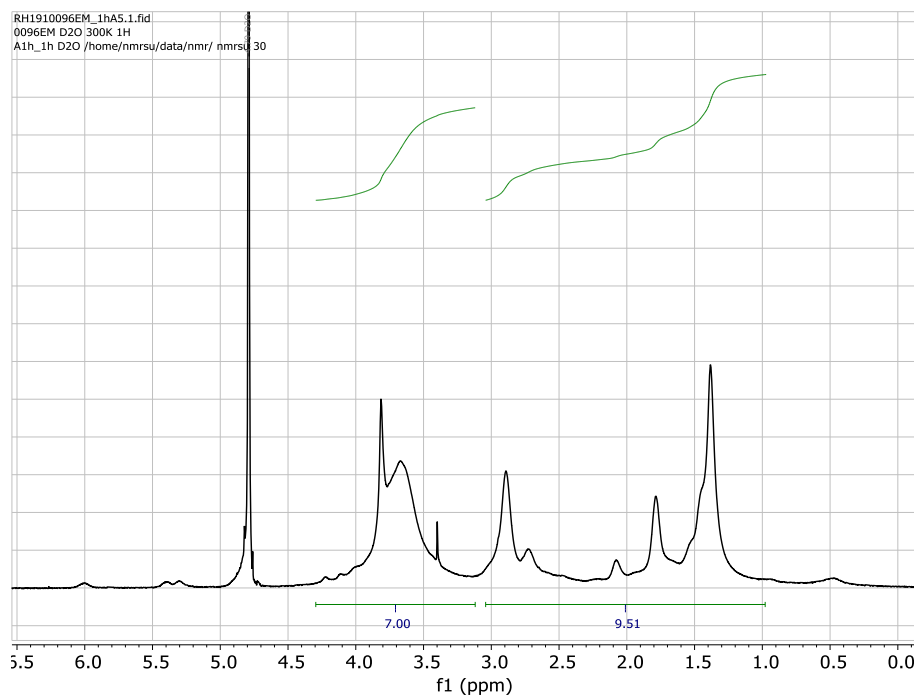


Figure 2.17 –  $^1\text{H}$ -NMR of dPG-2 in  $\text{D}_2\text{O}$ . dPG-2 was functionalized with 11-mercapto-1-undecanesulfonate (MUS) with degree of functionalization of 50%.

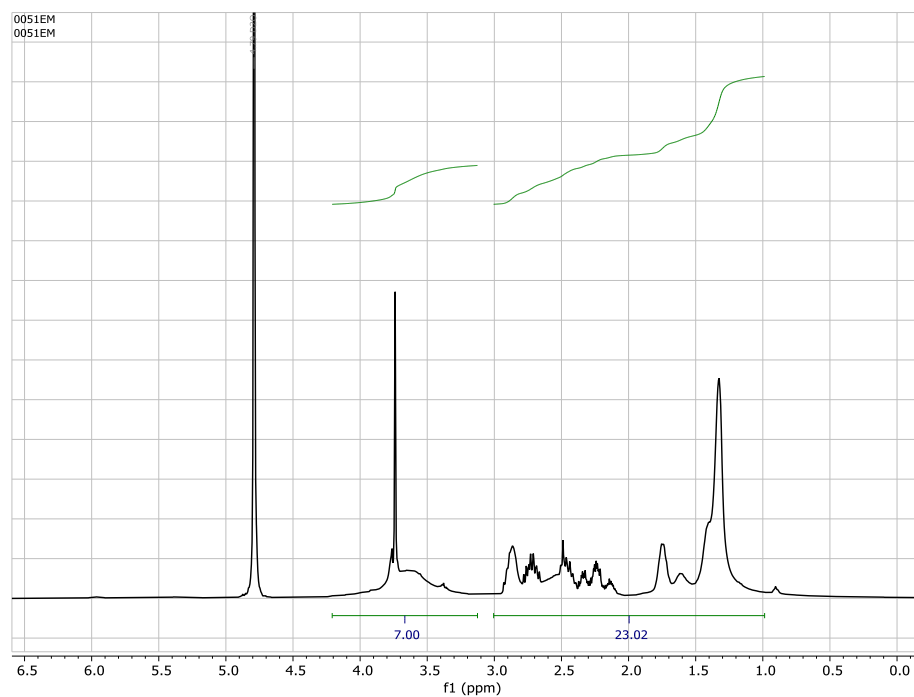


Figure 2.18 –  $^1\text{H}$ -NMR of dPG-3 in  $\text{D}_2\text{O}$ . dPG-3 was functionalized with 11-mercapto-1-undecanesulfonate (MUS) with degree of functionalization of 85%.

Table 2.1 – **Elemental analysis and molecular weight (Mn) of functionalized dPG.** \* Mn is calculated based on the degree of functionalization of each dendritic polyglycerol which is determined by  $^1\text{H}$ -NMR, considering the Mn of starting dPG core 10 kDa.

	dPG-1	dPG-2	dPG-3
C%	47.5	53.4	46.0
H%	7.5	7.9	7.4
N%	0.0	0.0	0.0
S%	1.0	6.6	9.6
Mn (kDa)*	11	29	40

### 2.3.3.3 Synthesis of dPG-4

dPG-allyl (DF=100) (50 mg, 0.67 mmol of allyl group) and the 11-Mercapto-1-undecanol (80 mg, 0.39 mmol) were dissolved in methanol (5 mL). 2,2-dimethoxy-2-phenylacetophenone (DMPA) as radical initiator (50 mg, 0.19 mmol) and a catalytic amount of tris(2-carboxyethyl)phosphine hydrochloride (TCEP-HCl) was added to the reaction to avoid oxidation of the 11-Mercapto-1-undecanol. The solution was degassed by flushing argon through the reaction mixture for 10 minutes. The reaction mixture was stirred and irradiated with UV light using a high-pressure UV lamp at room temperature for 4 hours. A small aliquot of the reaction solution was taken for characterization and the rest of allyl groups were quenched by addition of excess amount of 1-propanthiol. The reaction mixture was further stirred and irradiated with UV light for 4 more hours. At the end, the reaction mixture was dialyzed (MWCO 2 kDa) against methanol to remove the impurities and unreacted compounds. The degrees of functionalization were determined by  $^1\text{H}$  NMR of the pure product by correlating the aliphatic protons at 1.8-1.1 ppm with the polyglycerol backbone protons (4.0 - 3.2).

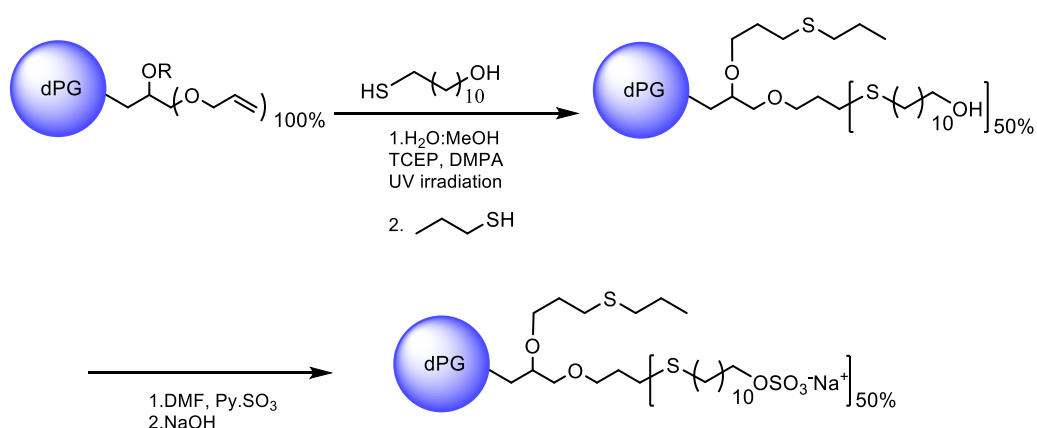
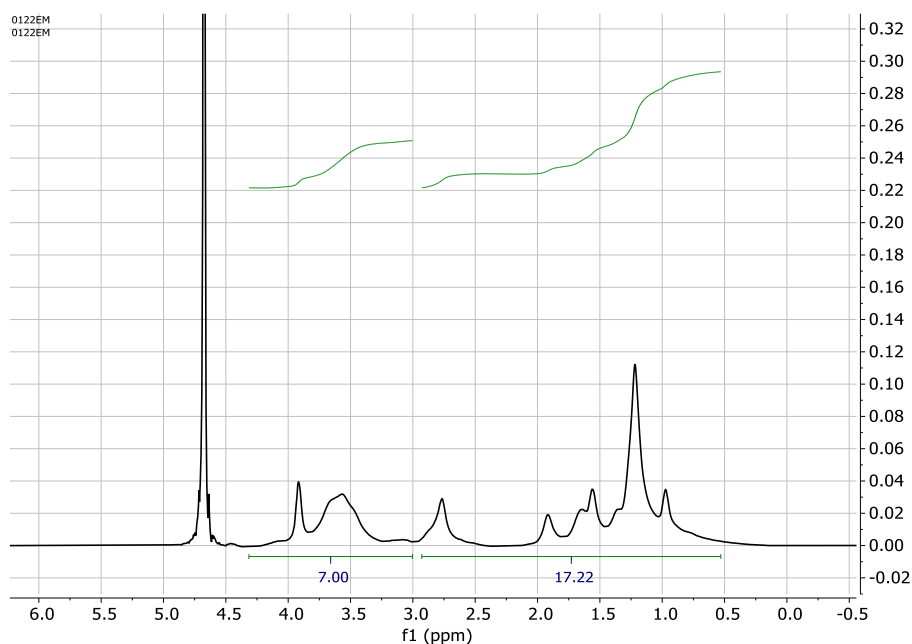


Figure 2.19 – **Synthetic route for preparation of the dPG-4.**

Figure 2.20 –  $^1\text{H}$ -NMR of dPG-4 in  $\text{D}_2\text{O}$ .Table 2.2 – **Elemental analysis and molecular weight (Mn) of dPG-4.** \* Mn is calculated based on the degree of functionalization of each dendritic polyglycerol which is determined by  $^1\text{H}$ -NMR, considering the Mn of starting dPG core 10 kDa.

	dPG-4
C%	40.6
H%	7.1
N%	0.0
S%	12.8
Mn (kDa)*	35

#### 2.3.3.4 Synthesis of dPG-5.

dPG (400 mg, 5.4 mmol OH to be functionalized) was dried at 60 °C overnight under high vacuum and dissolved in dry DMF (30 mL). To the stirred solution of dPG in dry DMF at room temperature, NaH (259.17 mg, 10.8 mmol, 2 eq.) was added. The reaction mixture was allowed to stir for 1 hour at room temperature and 1 hour at 40 °C and then cooled down by using an ice bath. 11-Bromo-1-undecanol (2 g, 8.1 mmol, 1.5 eq.) in dry DMF (5 mL) was added dropwise to the reaction mixture using a syringe. The ice bath was removed and the reaction was stirred 1h at room temperature and further 48 hours at 40 °C. The reaction was quenched by addition of methanol and the resulting mixture was dialyzed in methanol/chloroform mixture for 2 days to remove the unreacted compounds.

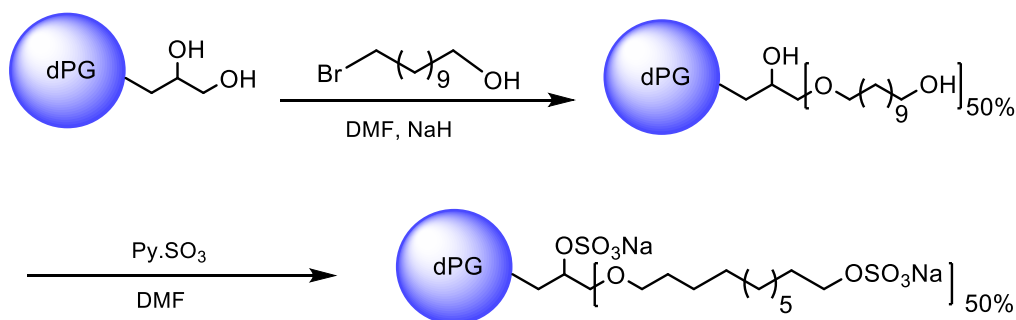


Figure 2.21 – Synthetic route for preparation of the dPG-5.

The product (dPG-C11-OH) was obtained as a white and highly viscose compound after evaporation of methanol by rotary evaporator. Degree of functionalization was quantified by  $^1\text{H}$ -NMR in  $\text{DMF-d}_6$ .

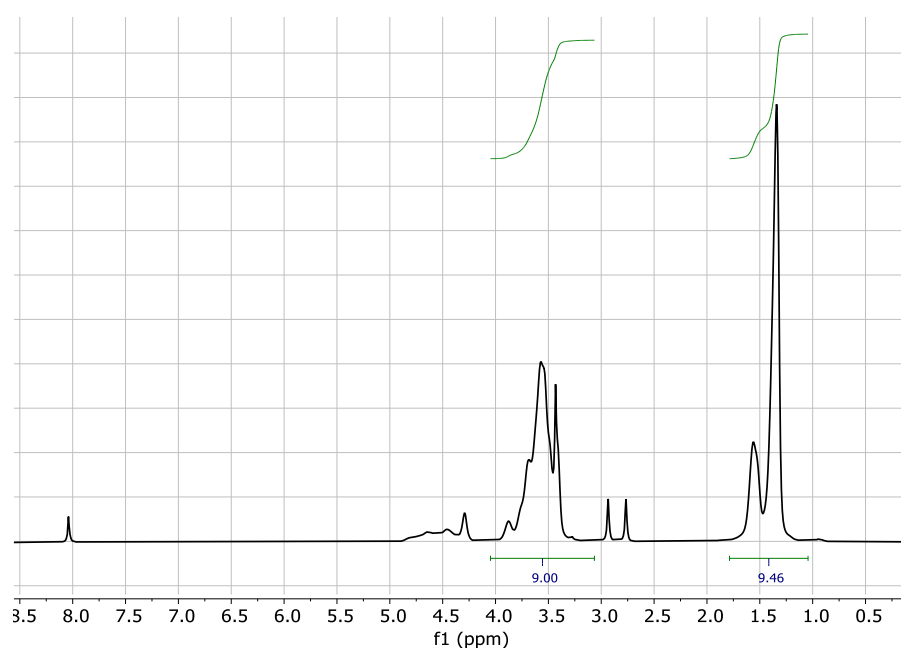


Figure 2.22 –  $^1\text{H}$ -NMR of dPG-1 (before sulfation reaction) in  $\text{DMF-d}_6$ .

In the next step both types of hydroxyl groups (on the dPG surface and at the end of alkyl chain) were sulfated through the reaction with pyridine sulfur trioxide ( $\text{Py.SO}_3$ ) complex. For this aim, dPG-C11-OH (700 mg, 5.4 mmol OH to be sulfated) was dried overnight at  $60^\circ\text{C}$  under vacuum and dissolved in dry DMF (30 mL) under inert atmosphere. To the stirred solution of dPG-C11-OH in dry DMF at  $60^\circ\text{C}$ ,  $\text{Py.SO}_3$  (1.289 g, 8.1 mmol, 1.5 eq.) in dry DMF (5 mL) was added dropwise. The reaction mixture was allowed to stir at  $60^\circ\text{C}$  overnight. The reaction was quenched with water, and the pH was adjusted to 8 by addition of NaOH solution. The mixture was then dialysed against brine using an ever-decreasing NaCl concentration for 2 days, until the medium was changed with distilled water and dialysis continued for 2 more days. The solvent was decreased under reduced pressure and the product was obtained as a white powder after lyophilisation.

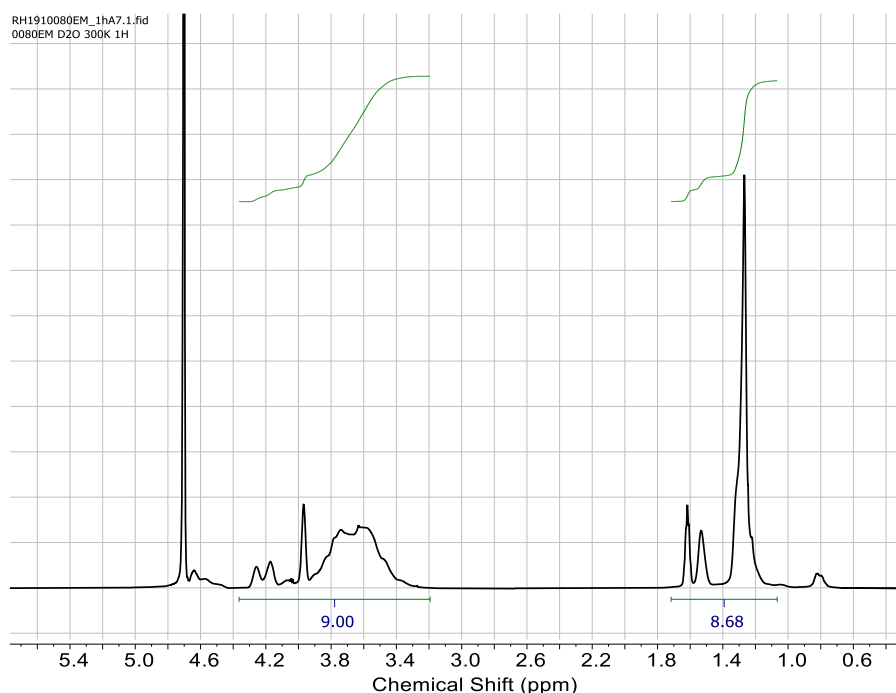
Figure 2.23 –  $^1\text{H}$ -NMR of dPG-5 in  $\text{D}_2\text{O}$ .

Table 2.3 – **Elemental analysis and molecular weight (Mn) of functionalized dPG-5.** \* Mn is based on the functionalization degree of each dendritic polyglycerol, considering the Mn of starting dPG. Increase in the carbon and hydrogen contents of dPG6 (before sulfatio sulfation) compared to dPG is due to the functionalization with the eleven-carbon alkyl chain. Additionally, the decrease in carbon and hydrogen contents in dPG6 together with sulfur content is confirming the sulfation reaction.

	dP5	dPG5 (before sulfation)	dPG5 (after sulfation)
C%	47.4	62.2	32.6
H%	7.8	10	5.7
N%	0	0	0
S%	0	0	12.1
Mn (kDa)*	9.6	23	36

### 2.3.3.5 Synthesis of dPG-6

dPG (400 mg, 5.4 mmol OH to be functionalized) was dried at 60 °C overnight under high vacuum. Dried dPG was dissolved in dry DMF (30 mL). To the stirred solution of dPG in dry DMF at room temperature, NaH (259.17 mg, 10.8 mmol, 2 eq.) was added. The reaction mixture was allowed to stir for 1 hours at room temperature and 1 hours at 40 °C and then cooled down by using an ice bath. 1-Bromoundecane (2 g, 8.5 mmol, 1.5 eq.) in dry DMF (5 mL) was added dropwise to the reaction mixture using a syringe. The ice bath was removed and the reaction was stirred 1h at room temperature and further 48 hours at 40 °C. The reaction was quenched by addition of methanol and the resulting mixture was dialyzed in methanol/chloroform mixture for 2 days to remove the unreacted compounds. The product (dPG-C<sub>11</sub>) was obtained as a white and highly viscous compound after evaporation of methanol by rotary evaporator. Degree of functionalization was determined by  $^1\text{H}$  NMR in  $\text{DMF-d}_6$ .

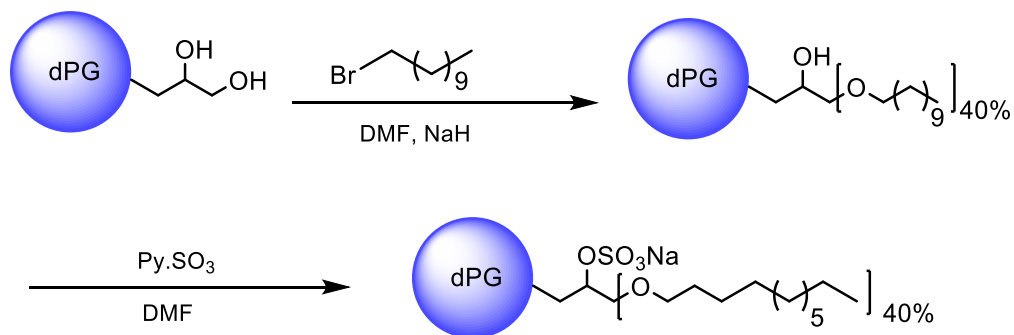
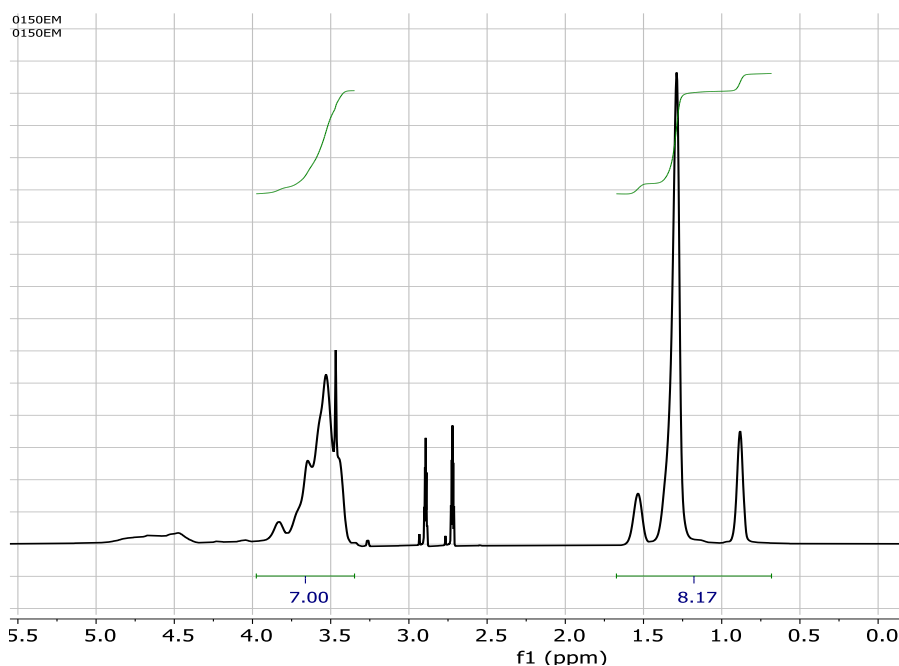


Figure 2.24 – Synthetic route for preparation of the dPG-6.

Figure 2.25 –  $^1\text{H}$ -NMR of dPG-6 in  $\text{DMF-d}_6$  before sulfation.

In the next the hydroxyl groups on the dPG surface have been sulfated through the reaction with pyridine sulfur trioxide ( $\text{Py}.\text{SO}_3$ ) complex. For this aim, dPG-C11 (700 mg, 5.4 mmol OH to be sulfated) was dried overnight at  $60^\circ\text{C}$  under vacuum. Dried dPG-C11 was dissolved in dry DMF (30 mL) under inert atmosphere. To the stirred solution of dPG-C11 in dry DMF at  $60^\circ\text{C}$ ,  $\text{Py}.\text{SO}_3$  (1.289 g, 8.1 mmol, 1.5 eq.) in dry DMF (5 mL) was added dropwise. The reaction mixture was allowed to stir at  $60^\circ\text{C}$  overnight. The reaction was quenched with water, and the pH was adjusted to 8 by addition of NaOH solution. The mixture was then dialysed against brine using an ever-decreasing NaCl concentration for 2 days, until the medium was changed with distilled water and dialysis continued for 2 more days. 4 The solvent was decreased under reduced pressure and the product was obtained as a white powder after lyophilisation. The degrees of functionalization (DF) in the different reactions were determined by  $^1\text{H}$  NMR of the pure product correlating the aliphatic protons at 1.7-0.6 ppm with the polyglycerol backbone protons (4.4 - 3.2).

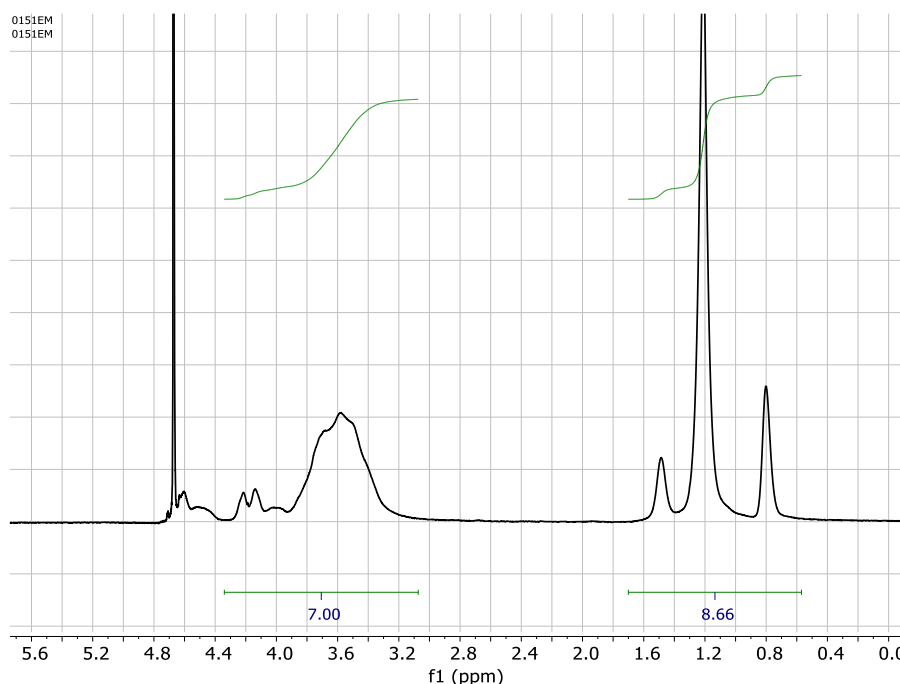


Figure 2.26 –  $^1\text{H}$ -NMR of dPG-6 in  $\text{D}_2\text{O}$  after sulfation.

Table 2.4 - **Elemental analysis and molecular weight (Mn) of dPG-6 before and after sulfation.** \* Mn is calculated based on the degree of functionalization of dPG-6 which is determined by  $^1\text{H}$ -NMR, considering the Mn of starting dPG core 10 kDa.

	dPG-6
C%	38.2
H%	6.5
N%	0.0
S%	6.5
Mn* (kDa)	29

### 2.3.3.6 Synthesis of dPG-7 and dPG-8

Through the one-step ring opening functionalization of dPG by using 1,4-Butane sultone and 1,3-Propanediol cyclic sulfate and 1,4-butane sultone dPG9 and dPG10 with short alkyl chain have been synthesized respectively. dPG (100 mg, 1.35 mmol OH to be functionalized) was dried at 60 °C overnight under high vacuum. Dried dPG was dissolved in dry DMF (5 mL). To the stirred solution of dPG in dry DMF at room temperature, NaH (65 mg, 2.7 mmol, 2 eq.) was added. The reaction mixture was allowed to stir for 1 hours at room temperature. At this step for the synthesis of dPG9 1,3-propanediol cyclic sulfate (373.3 mg, 2.7 mmol, 2 eq.) and for dPG10, 1,4-butane sultone (276  $\mu\text{L}$ , 2.7 mmol, 2 eq.) were added to the reaction and the reaction was stirred overnight at room temperature. The mixture was then dialysed against brine using an ever-decreasing NaCl concentration for 2 days, until the medium was changed with distilled water and dialysis continued for 2 more days. The solvent was decreased under reduced pressure and the product was obtained as crystalline powder after lyophilisation. The degrees of functionalization (DF) in the different

reactions were determined by  $^1\text{H}$ -NMR of the pure product correlating the aliphatic protons at 1.9-1.5 ppm with the polyglycerol backbone protons (4.2 - 3.2).

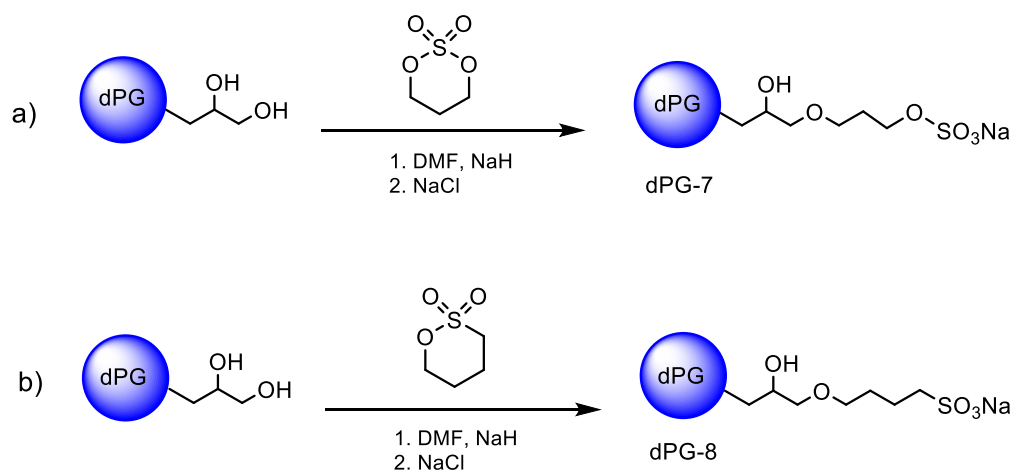


Figure 2.27 – One-pot approach for the synthesis of the a) dPG-7 b) dPG-8.

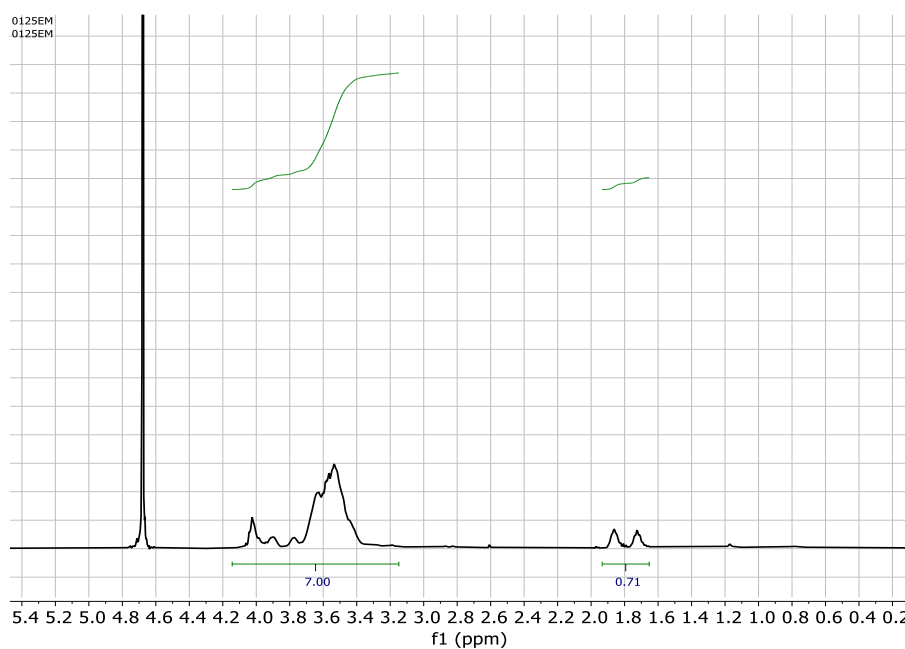
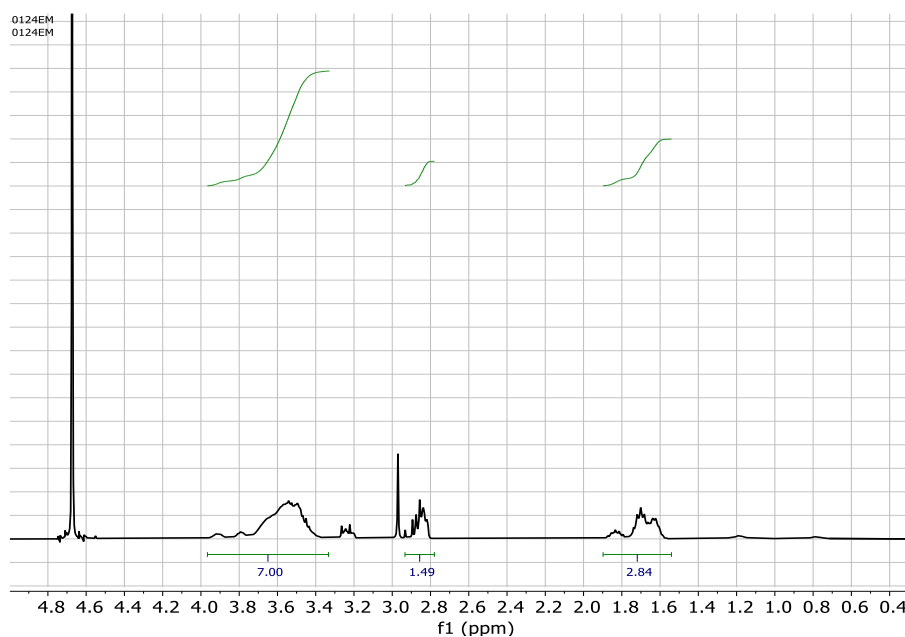


Figure 2.28 –  $^1\text{H}$ -NMR of dPG-7 in  $\text{D}_2\text{O}$ .

Figure 2.29 –  $^1\text{H}$ -NMR of dPG-8 in  $\text{D}_2\text{O}$ .Table 2.5 – Elemental analysis and molecular weight ( $M_n$ ) of dPG-7 and dPG-8 before and after sulfation. \*  $M_n$  is calculated based on the degree of functionalization of dPG-6 which is determined by  $^1\text{H}$ -NMR, considering the  $M_n$  of starting dPG core 10 kDa.

	dPG-7	dPG-8
C%	35.7	38.1
H%	6.8	6.2
N%	0.0	0.0
S%	8.0	11.8
$M_n^*$ (kDa)	20	25

### 2.3.3.7 Synthesis of dPG-C10-COO

As illustrated in fig. 2.30, dPG-allyl and about 2 eq. of 11-mercaptoundecanoic acid are dissolved in suitable methanol. To this solution are added 2,2-dimethoxy-2-phenylacetophenone (DMPA) as radical initiator and a catalytic amount of tris(2-carboxyethyl)phosphine hydrochloride (TCEP-HCl) (to avoid oxidation of the thiol intermediate).

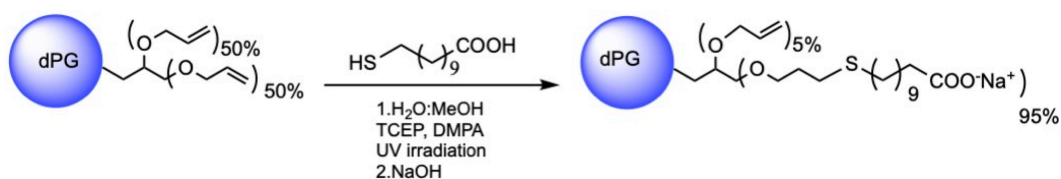


Figure 2.30 – Synthetic route for preparation of the dPG-C10-COO.

A few drops of water can be added to dissolve any precipitation and obtain a clear solution. The solution is degassed by flushing argon through the reaction mixture for about 10 minutes. The reaction mixture is then stirred and irradiated with UV light using a high-pressure UV lamp at room temperature for about 5 hours. The product(s) from the reaction mixture can be conventionally isolated and purified, for example being dialyzed (MWCO 2 kDa), e.g., against methanol/water mixture, to remove the TCEP.HCl, DMPA and any excess of unreacted thiol compound. The product(s) will have a DF of about 85-95%. The product can be analyzed by  $^1\text{H}$ -NMR and the pure product can be identified by correlating the aliphatic protons of ligands at 1.5-1.00 ppm with the polyglycerol backbone protons at 3.7-3.2 ppm.

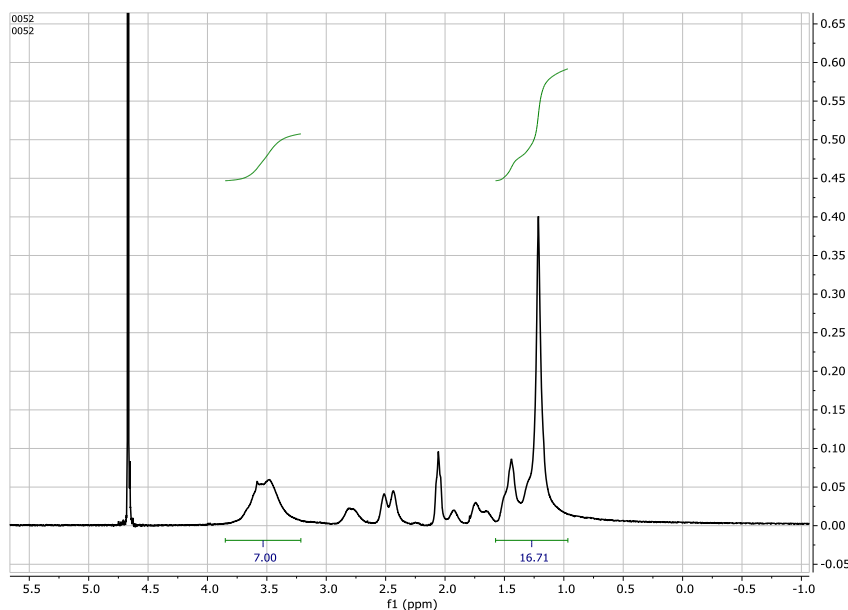


Figure 2.31 –  $^1\text{H}$ -NMR of dPG-C10-COO in  $\text{D}_2\text{O}$ .

## 2.4 Biological assays

In this paragraph the various biological assays shown in the thesis are reported. Experimental details of each assay are discussed in each paragraph. A brief theoretical introduction is discussed hereafter.

### 2.4.1 Cytotoxicity

As the swiss physician Paracelsus used to say “sola dosis facit venenum”, meaning that “the dose makes the poison”. Indeed, as discussed in Chapter 1, toxicity is the major hurdle in designing antivirals, but the important value to look at, is the selective index, where both toxicity and efficacy are taken in account. An easy and reliable method to assess *in vitro* cell toxicity is to measure their viability upon interaction with the compound of interest. In particular, different concentration of the compound of interest are incubated with the cell for a fixed time (i.e. 24 hours) and the difference in cell viability is measured against a control where the cells are untreated. Fitting the data with non-linear regression analysis using a four-parameter logistic curve will provide parameter such as the  $\text{CC}_{50}$ , so the concentration at which 50% of cells are dead (similar to the  $\text{IC}_{50}$  showed in fig 2.33).

#### 2.4.1.1 Cell viability assay MTS

Cell viability was measured by a colorimetric assay, employing MTS assay (Promega). For VERO cell, 14.500 cells per well were seeded 24h before the experiment in a 96-well plate, supplemented with DMEM+10%FBS+1%P/S. Media is replaced with DMEM+2%FBS+1%P/S and different concentration of the compound of interest are incubated in duplicates or triplicates. Cells are incubated for 24h at 37°C and 5% CO<sub>2</sub>. Cells are washed twice with same media to remove the compound and are supplemented with 100µl of DMEM+2%FBS+1%P/S. Then, 20µl of MTS solution are added on each well and cells are incubated for 2-4hours at 37°C and 5% CO<sub>2</sub>. Absorbance is then measured by a plate reader ( $\lambda$  = 490 µm). Intensity of absorbance is then normalized by the blank and divided by the untreated (multiply by 100) in order to have cell viability expressed in percentage.

#### 2.4.1.2 Cell viability assay CCK-8

The cytotoxicity of the compounds was analyzed by the cell viability assay Cell Counting Kit 8 (CCK-8) from Sigma-Aldrich Chemie GmbH (Taufkirchen, Germany) according to the manufactures' instructions. For the assays, three cell lines were used: A549 human lung carcinoma cells (DSMZ ACC 107), 16HBE14o- human bronchial epithelial cells (Millipore SCC150) and Vero E6 African green monkey kidney epithelial cells (ATCC CRL-1586). A549 and Vero E6 cells were cultured in Dulbecco's Modified Eagle Medium (DMEM) and the 16HBE14o- cells in Minimum Essential Media (MEM) supplemented with 10% fetal bovine serum, penicillin/streptomycin and GlutaMAX or Glutamine (all from Gibco BRL, Eggenstein, Germany). The cells were passaged every 3 to 4 days after reaching 70% to 90% confluency. For the assay, cells were seeded in a 96 well plate (4.000 cells/well) and incubated over night at 37°C and 5% CO<sub>2</sub>. Then, compounds were added in serial dilutions in triplicates. SDS (1%) and non-treated cells served as a control. For background subtraction, wells without cells were used. Cells were incubated for another day at 37 °C before CCK-8 solution was added. After approximately 2 hours absorbance was measured at a measurement wavelength of 450 nm and a reference wavelength of 650 nm with a plate reader (Infinite pro200, TECAN-reader Tecan Group Ltd., Männedorf, Switzerland). The assay was repeated three times. The cell viability was calculated by setting the non-treated control with cells to 100% after subtracting the background using the GraphPad Prism software (GraphPad Prism 6 for Windows, Version 6.01).

#### 2.4.1.3 Data Analysis

The CC<sub>50</sub> (half-maximal cytotoxic concentration) are calculated by non-linear regression analysis using a four-parameter logistic curve by GraphPad Prism 8.0 or superior. All the data are from at least 2 independent experiments performed in duplicate.

#### 2.4.2 Dose-response

The capability of an antiviral drug of inhibiting viral replication is usually assessed in a so-called inhibition assay. Such assay is based on testing different concentration of the drug with the same amount of virus, in order to develop a dose-dependent response of the virus to the drug.

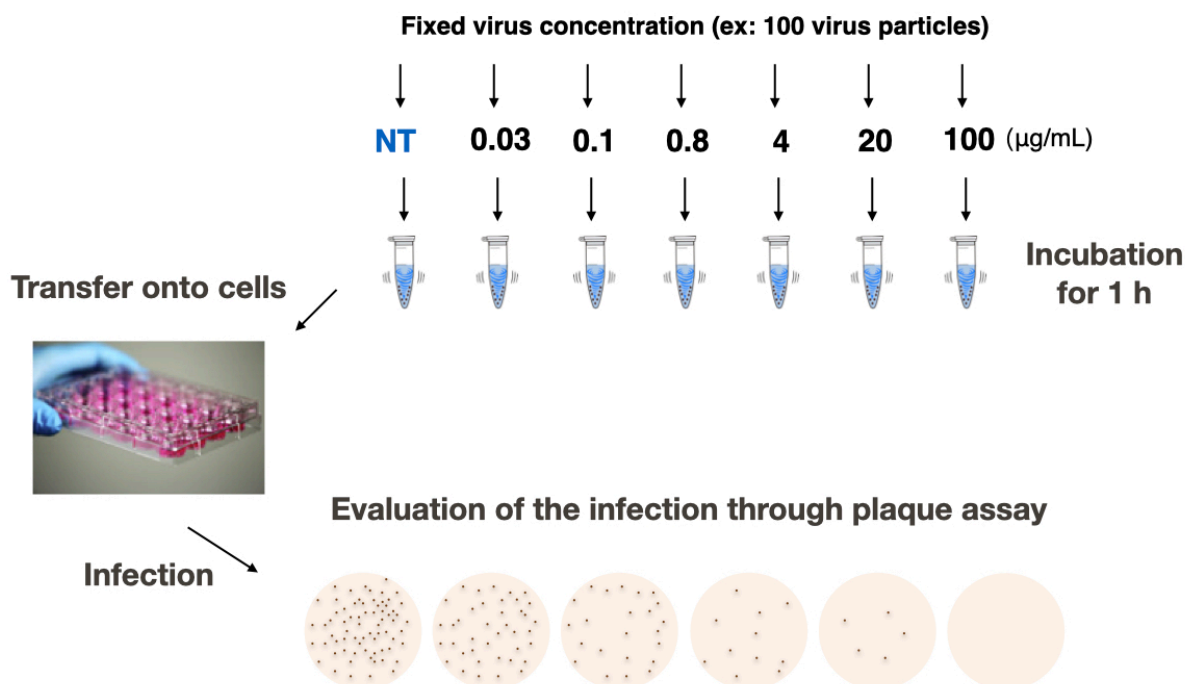


Figure 2.32 – **Sketch of a dose-response inhibition assay for HSV-2.** A fixed amount of virus is incubated for a certain amount of time with an increasing concentration of the compound of interest. Then, the mixtures are added onto cells and the virus is let infect. After a given time, the cells are stained and the infection state measured via a plaque assay. Percentage of infection is compared to a non treated control.

In particular, in this thesis, mostly a pre-treatment is performed, as shown in fig. 2.32. In fact, virus and antiviral are pre-incubated for 1h, before transferring the solution onto the cells, in order to quantify the viral inhibition. Such approach is particularly valid for extra-cellular entry inhibitors, for which the mechanism of action happens outside the cell and the interaction of virus and antiviral is needed. In this way, the interaction can build up in the pre-mixing step, before transferring the mixture onto cells. At this stage just a certain amount of virus will be able to infect. Different methods to quantify viruses are possible : for viruses such as HSV-2 that develops cytopathic effect, the easier option is to form viral plaques, so to determine the units of virus capable of forming a plaque. Such units are called plaque forming units (PFU). A classical method to form plaques is to add media containing highly viscous polymers such as methylcellulose, in order to limit the infectivity of a virus to the neighboring cells. After a certain amount of time, needed for the virus to create a detectable plaque, cells are stained and plaques counted. The infectivity at each concentration is then normalized to an untreated control and data plotted in a classical log vs inhibition curve. A fitting to determine the curve can be performed, usually based on four-parameter logistic curve using non-linear regression analysis. From such curve the IC<sub>50</sub>, so the concentration at which the compound can inhibit 50% of the virus can be determined, as shown in fig. 2.33. Such assay cannot predict whether a compound is virucidal or virustatic but can just reveal whether it has some antiviral effect and the concentration at which it is effective.

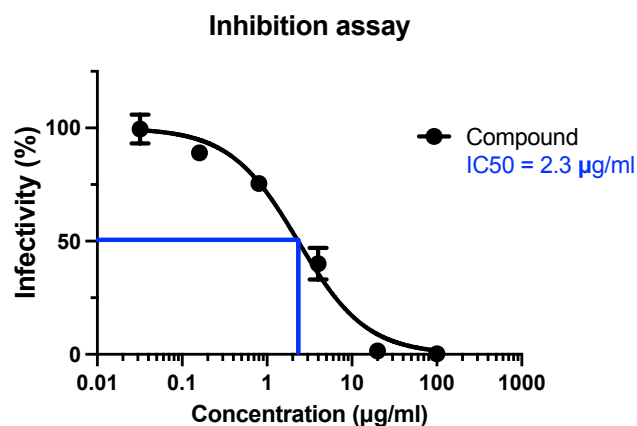


Figure 2.33 – **Example of an inhibition assay curve.** On the y-axis the infectivity (or percentage of infection) is reported, while on the x-axis the concentration of the compound in log scale. A fitting with a four-parameter dose-response curve is performed, in order to identify the IC<sub>50</sub>, i.e. the concentration at which the infection is reduced by 50%.

#### 2.4.2.1 Inhibition assay against HSV-2

HSV-2 was provided by M. Pistello (University of Pisa, Italy) and it was propagated and titrated on Vero cells with plaque assays. Antiviral effect of dendritic polymer against HSV-2 was tested by plaque reduction assays on Vero cells. Vero cells were plated 24h before the experiment in 24-well plates at a density of  $10^5$  cells. A fixed amount of virus (MOI = 0.0005) was pre-incubated for 1 hour with serial dilutions of the compound of interest. The solution was then transferred onto the cells and incubated for 1 hour. Afterwards, the solution was removed and the cells incubated for 24h in DMEM w2% FBS with 0.45w% Methyl-Cellulose. The cells were then stained with crystal violet and the plaques counted.

#### 2.4.2.2 Inhibition assay against RSV

The antiviral effect of dendritic polymer against RSV was tested by plaque reduction assays on A549 cells. A549 cells were plated 24h before the experiment in 96-well plates at a density of  $10^4$  cells. A fixed amount of virus expressing GFP (MOI = 0.05) was pre-incubated for 1 hour with serial dilutions of the compound of interest. The solution was then transferred onto the cells and incubated for 2 hours. The following day cells were fixed with paraformaldehyde 4%, stained with DAPI and visualized using an ImageXpress Micro XL (Molecular Devices) microplate reader and a 10× S Fluor objective. The percentage of infected cells was estimated by counting the number of cells expressing GFP and the total number of cells (DAPI-positive cells) from four different fields per well using MetaXpress software (Molecular Devices).

#### 2.4.2.3 VSV-CoV-2 inhibition assays

VSV-based SARS-CoV-2 pseudotypes (VSV-CoV-2) generated according to <sup>97</sup> and <sup>98</sup> expressing a 19 amino acids C-terminal truncated spike protein (NCBI Reference sequence: NC\_045512.2) were produced in HEK293F and titrated in Vero-E6.

Vero-E6 cells (13000 cells per well) were seeded in a 96-well plate. Compounds were serially diluted in DMEM and incubated with VSV-CoV-2 (MOI, 0.001 ffu/cell) for 1h at 37°C. The mixture was added on cells for 1h at 37°C. The monolayers were then washed and overlaid with medium containing 2% FBS for 18h. The following day cells were fixed with paraformaldehyde 4%, stained with DAPI and visualized using an ImageXpress Micro XL (Molecular Devices) microplate reader and a 10× S Fluor objective. The percentage of infected cells was estimated by counting the number of cells expressing GFP and the total number of cells (DAPI-positive cells) from four different fields per sample using MetaXpress software (Molecular Devices).

#### 2.4.2.4 Inhibition assay against SARS-CoV-2

Vero C1008 (clone E6) (ATCC CRL-1586) was a kind gift from Prof Gary Kobinger, and were propagated in DMEM High Glucose + Glutamax supplemented with 10% fetal bovine serum (FBS) and 1% penicillin/streptavidin (pen/strep).

SARS-CoV2/Switzerland/GE9586/2020 was isolated from a clinical specimen in the University Hospital in Geneva in Vero-E6 and passaged twice before the experiments (this was used for all the experiment at EPFL). SARS-CoV-2/München-1.1/2020/929 (kindly provided by M. Müller and C. Drosten; Charité, Berlin, Germany) was propagated on Vero-E6 cells cultured in Dulbecco's modified minimal essential medium supplemented with 10% heat inactivated fetal bovine serum, 1% non-essential amino acids, 100 µg/mL of streptomycin, 100 IU/mL of penicillin, and 15 mM of HEPES. Supernatant of infected cells were collected 3 days post infection, clarified, aliquoted and frozen at -80°C and subsequently titrated by plaque assay in Vero-E6.

Vero-E6 cells (100000 cells per well) were seeded in a 24-well plate. Compounds were serially diluted in DMEM and incubated with SARS-CoV-2 (MOI, 0.005 PFU/cell) for 1 hour at 37°C. The mixture was added on cells for 1h at 37°C. The monolayers were then washed and overlaid with 0.8% avicel rc581 in DMEM supplemented with 5% FBS. For the experiments described in Figure S1 the protocol is the same as described with two modifications: the number of cells seeded is 83000 cells per well and the overlay contained 1.2% avicel. Two days after infection, cells were fixed with paraformaldehyde 4% and stained with crystal violet solution containing ethanol. Plaques were counted, and the percent inhibition of virus infectivity was determined by comparing the number of plaques in treated wells with the number in untreated control wells. 50% effective concentration (EC50) was calculated with Prism 8 (GraphPad, USA). Serial dilutions of hydroxychloroquine were added on cells 1h before infection and readed during infection.

#### 2.4.2.5 Data Analysis

The EC50/IC50 (half-maximal antiviral effective/inhibition concentration) were calculated by non-linear regression analysis using a four-parameter logistic curve by GraphPad Prism 8.0 or superior. All the data are from at least 2 independent experiments performed in duplicate.

### 2.4.3 Virucidal assay

In Chapter 1, the difference between virucidal and virustatic antivirals is thoroughly discussed as the importance that is envisioned of such property for translating entry inhibitors. Indeed, so far, few publications report studies on the mechanism of action of such antivirals, not providing data on such crucial feature.

Virucidal assay is reported in detail by Shogan<sup>66</sup>. The reasoning behind this assay is to determine whether the antiviral activity is irreversible or not. Fig. 1.11 and 1.14 clearly show the difference in the thermodynamics of a virustatic and a virucidal inhibition: while the first is a solely thermodynamic equilibrium, that can be reverted upon dilution, the second presents a further irreversible inactivation step, that is so maintained even upon dilution.

The assays are conceived as follow. Virus and the compound of interest are co-incubated at a fixed concentration (c) for a fixed amount of time (t). The concentration of compound should be in a range at which is known to be effective, so above the IC99 (concentration at which 99% of the virus is inhibited, previously determined through a dose-response assay). The time of incubation is also a key parameter since the virucidal

effect has a kinetic curve, as already shown both in Cagno et al. and in Jones et al. So far, 1h has resulted to be sufficient to have a complete virucidal effect.

Once the interaction has taken place and the effect is completed, the mixture of virus and compound should be diluted in order to verify if the mechanism of action is reversible (virustatic) or irreversible (virucidal), so if the inhibition can be reverted or not. Indeed, the “amount” of dilution is important, since to revert the equilibrium, one should dilute the virus-compound mixture below the concentration at which the compound is effective, namely below the IC<sub>50</sub>. To obtain such an effect and being able to quantify the viral titer, serial dilutions are performed and then transferred onto cells. Viral titer can be quantified using plaque assay or TCID<sub>50</sub>. The viral titer is then compared to an untreated control in order to measure the reduction caused by the compound, usually expressed in logarithmic scale.

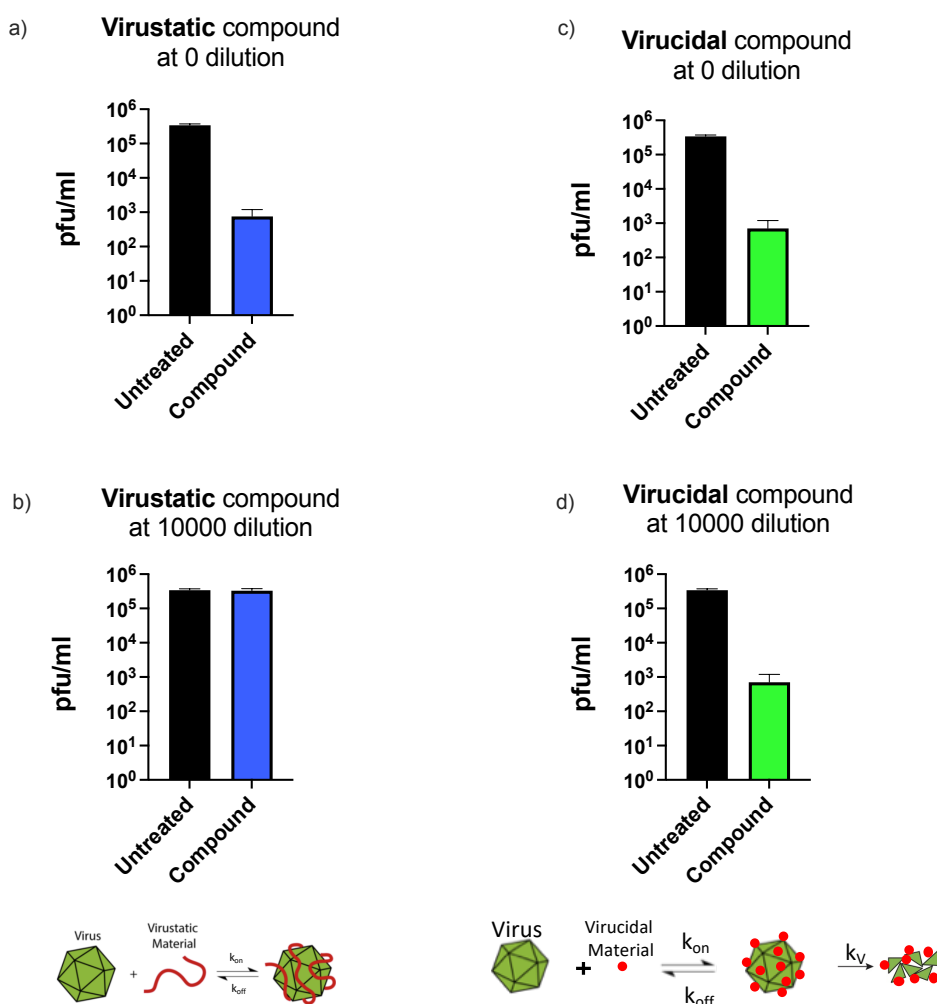


Figure 2.34 – **Sketch of virucidal assay graphs for virustatic and virucidal drugs.** On top, the effect of virucidal and virustatic drug at the incubation concentration. Both are able to inhibit the viral infection. On the bottom, the viral titer of both cases is reported upon dilution: a clear difference can be detected. For the virustatic drug, the inhibition is lost upon dilution, while there is an irreversible viral inhibition in case of a virucidal compound.

Fig. 2.34 shows the results of a theoretical experiment to better understand and visualize the different behavior of virustatic vs virucidal antivirals. In particular the viral titer, expressed in plaque forming unit per milliliter (pfu/ml) is reported. On the left, the results for a virustatic compound are shown, while on the right for a virucidal one. On the top, the viral titer is reported at the initial concentration of incubation,

while on the bottom, the viral titer measured after diluting the mixture is displayed. As can be seen, a virustatic and a virucidal compound do not show any difference at the initial concentration. Indeed, if both show a similar dose-response curve for a given virus, once they are incubated at a concentration above the IC<sub>99</sub>, a decrease of infectivity above 2 logs is expected. On the other side, a strike difference appears after diluting the virus-compound mixture. In fact, a virustatic compound loses its capability of inhibiting viral infection if diluted below its IC<sub>50</sub>. The thermodynamic equilibrium, that was initially installed at the IC<sub>99</sub>, is reverted and the interaction causing the inhibition lost. The virus is so released, capable of start its infective cycle, as shown in fig. 2.34.b : the viral titer of the mixture with the compound is the same as the untreated control. Conversely, a virucidal compound causes a permanent viral inhibition, due to a further irreversible step. As such, the inhibition installed during the incubation above the IC<sub>99</sub> is kept upon dilution since it caused permanent damages to the virions. Indeed, the decrease of the viral titer of at least 2 logs is maintained, as shown in fig. 2.34.d.

#### 2.4.3.1 *Virucidal assay against HSV-2*

Vero cells were plated 24h before the experiment in 96-well plates in order to have a confluent layer. An effective amount of dendritic polymer (100 or 300 µg/mL) were incubated with a fixed amount of viruses (10<sup>5</sup> pfu/ml) for 1 hour at 37°C in DMEM – 2%FBS. A serial dilution of this solution was added in each well and incubated for 1 hour at 37°C. Afterwards, the solution was removed and the cells incubated for 24h in DMEM w2% FBS with 0.45w% Methyl-Cellulose. The cells were then stained with crystal violet and the plaques counted. The viral titer was evaluated and compared with a reference with no compound.

#### 2.4.3.2 *Virucidal assay against RSV*

A549 cells were plated 24h before the experiment in 96-well plates in order to have a confluent layer. An effective amount of dendritic polymer (300 µg/mL) were incubated with a fixed amount of viruses (10<sup>5</sup> pfu) for 1 hour at 37°C in DMEM – 2%FBS. A serial dilution of this solution was added in each well and incubated for 2 hour at 37°C. Afterwards, the solution was removed and the cells incubated for 48h in DMEM w2% FBS. The viral titer was evaluated from the percentage of infected cells obtained by counting the number of cells expressing GFP and the total number of cells (DAPI-positive cells) from four different fields per well using MetaXpress software (Molecular Devices) by and compared with a reference with no compound.

#### 2.4.3.3 *Virucidal assay against SARS-CoV-2*

Viruses (10<sup>5</sup> pfu of SARS-CoV-2) and or MUS:OT NPs or CD-MUSs (300 µg/ml) were incubated for 1 h at room temperature and then the virucidal effect was investigated by adding serial dilutions of the mixtures on Vero-E6 for 1h, followed by addition of medium containing avicel as described above. Viral titers were determined at dilutions at which the material was not effective.

#### 2.4.3.4 *Data Analysis*

The EC<sub>50</sub> (half-maximal antiviral effective concentration) were calculated by non-linear regression analysis using a four-parameter logistic curve by GraphPad Prism 8.0 or superior. All the data are from at least 2 independent experiments performed in duplicate.

#### 2.4.4 DNA release assay

Virucidal assay discussed in paragraph 2.4.3 gives key information on the mechanism of action of an entry inhibitor, but other experiments can be designed to gain further insights. In particular, cryo-TEM was utilized in Cagno et al. to visualize the disruption of viruses upon contact with AuNPs confirming the

hypothesis of having such irreversible inhibition. Such technique is extremely powerful to visualize single events, but it becomes not suitable when trying to get collective or statistically relevant information, since it requires a very large dataset becoming costly and time-intensive. Conversely, biological assays can give information on the whole viral population. Virucidal assay, in fact, measures the decrease in titer caused by the virucidal compound, without saying much about the fate of the virions.

DNA release assay can instead quantify the amount of viruses disrupted by the interaction with virucidal compound. Such assay measures in fact the DNA released by virions incubated with a compound meaning that, in case of an enveloped virus, both the envelop and the capsid have been disrupted.

A sketch of the steps of the assay is drawn in fig. 2.35. The assay starts with a pre-incubation of the compound and the virus for a fixed amount of time (i.e. 1h) at a concentration above IC<sub>99</sub>, as for the virucidal assay discussed above. If the compound is virucidal and has disrupted the virus, DNA can be released and is present in solution unprotected by the protein cage composed by the capsid. At this stage, a dilution step is required in order to have the optimum milieu for next step, where DNase is added. DNase is an enzyme that cleaves DNA. At this step there are two populations of DNA : one is free in solution, accessible to DNase, the other one inside the intact virus, where is inaccessible to DNase ; the first will be cleaved, the second will remain intact. After that, a lysate buffer is added, with two different roles : first it inactivates the DNase, second will disrupt the viruses that were still intact, releasing the DNA. The solution is then washed (by a column or other techniques such as magnetic beads), collected and quantified by qPCR by the Ct (threshold cycle). Different controls are designed : 1) the quantification of the DNA present without virucidal material, so relative to the actual amount of intact virus present 2) the quantification of DNA released by the virus upon contact with virucidal material, without addition of DNAase in the third step.

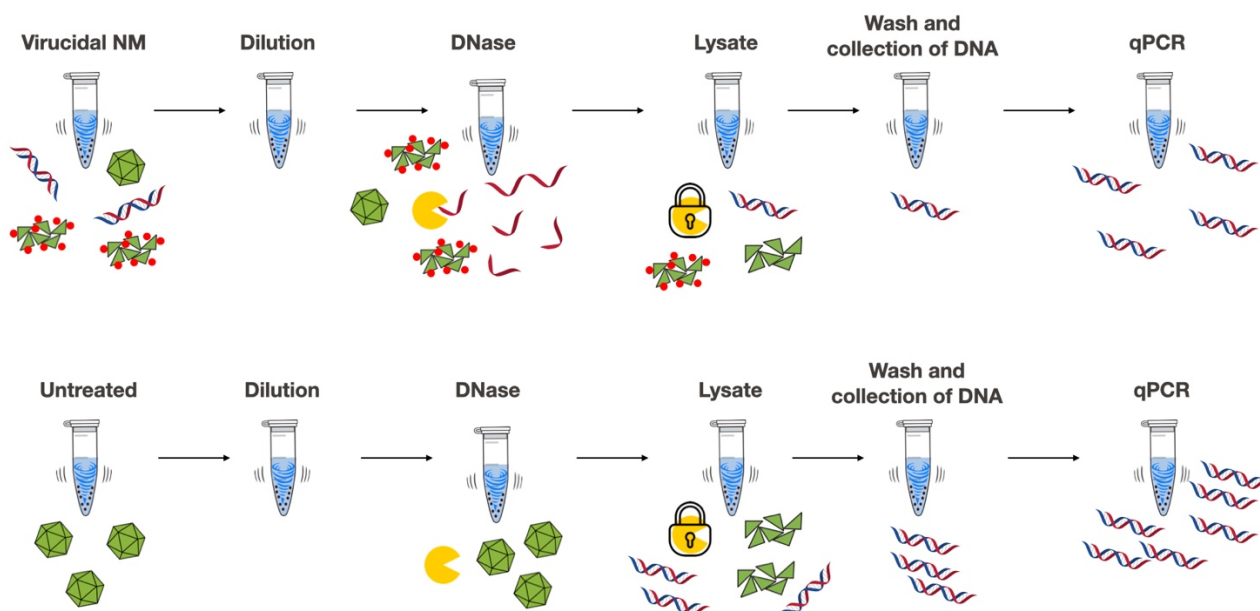


Figure 2.35 – **Sketch of DNA release assay.** The assay consists of multiple step: a) incubation of virus and virucidal drug b) dilution and addition of DNase with relative buffer c) addition of lysate buffer to stop the activity of DNase and disrupt the virus d) washing and collection of DNA e) quantification of DNA via qPCR. The Ct are the compared to an untreated control.

The difference in Ct between DNase treated and untreated is then calculated, obtaining a value per a virucidal compound that relates to its capability of disrupting the virions.

Such assay can be clearly utilized also for RNA viruses, tailoring the enzyme and the qPCR protocol accordingly.

#### **2.4.4.1 DNA release assay HSV-2**

HSV-2 ( $1 \times 10^5$  PFU) was incubated for 1 hour at 37°C with DMEM or with DMEM and 30 µg of dPG. Subsequently, the mixture was diluted in 1:20 in DMEM, and 100 µl of mixtures was either exposed to 8 units of Turbo DNase (Thermo Fisher Scientific) or only incubated with Turbo DNase buffer for 30 min at 37°C. At the end of the incubation, cells were lysed and subjected to DNA extraction through Nuclisens EasyMag and qPCR amplification with TaqMan Universal PCR Master Mix (primers: 5'-CCGTCAGCACCTTCATCGA-3' and 5'-CGCTGGACCTCCGTGTAGTC-3'; probe, 5'-FAM-CCACGAGATCAAGGACAGCGGCC-TAMRA). Fold change was calculated with the Delta Ct method.

#### **2.4.5 Antiviral surfaces testing**

The tests of antiviral surfaces were designed based on a seminal protocol paper by Klibanov<sup>99</sup> and on the ISO protocol 21702:2019 ("Measurement of antiviral activity on plastics and other non-porous surfaces"). The assays were further developed and optimized together with Dr. Nicolò Razza.

The idea is to study the inactivation capability of a given surface on a certain virus after an incubation of a certain time. The experimental conditions could be very different depending on the effect or the mechanism of activation proposed. In particular we focused on two approaches, that we named wet-to-wet and wet-to-dry. The main difference is in the state of the virus over the incubation period, with the first one remaining wet, with a system to prevent the evaporation of the liquid, while the second exposing the viral solution to evaporation and letting drying the solution on the substrate. We have tested surfaces both on HSV-2

##### **2.4.5.1 Wet-to-wet protocol**

With this assay, we aim to evaluate the antiviral activity of a surface in a scenario in which the inoculum does not evaporate but remains hydrated during the time it is in contact with the surface. The assay can be divided in four steps: 1) deposition of the virus inoculum on the surface 2) limiting the evaporation of the inoculum (coverage of the inoculum with a glass cover and putting the sample in a closed Petri dish) 3) Recovering of the inoculum from the surface 4) titration of the inoculum onto cells.

Standardizing the protocol, we decided to use samples with a size of 20x20mm with a total area of 400mm<sup>2</sup>. During the first step, we usually use 80 µl of inoculum (both for HSV-2 or SARS-CoV-2) with an initial concentration of  $10^{5-6}$  pfu/ml. The inoculum is homogeneously spread onto the surface to have a complete coverage. The surface is then covered with standard glass slide (18x18mm) and the sample placed in a closed Petri dish. The sample is then incubated at room temperature for given time (i.e., 0, 30, 60 or 120 min) and the inoculum is recovered carefully washing the surface and the glass slide with 920 µl of media (DMEM with 2vol% FBS and 1% P/S). The recovered inoculum is then serially diluted and titrated with a protocol similar to what discussed above in the virucidal assay for each virus. Relevant internal controls are usually run such as an untreated surface and the initial viral stock.

##### **2.4.5.2 Wet-to-dry protocol**

With this assay, we aim to evaluate a more realistic scenario, in which the inoculum undergoes to evaporation onto the surface of interest and it is then recovered and quantified. Similarly to the wet-to-wet protocol, the wet-to-dry protocol can be divided in four steps: 1) deposition of the virus inoculum on the

surface 2) evaporation of the inoculum (performed at R.T. inside a biosafety cabinet for 15min) and incubation for a certain time 3) Recovering of the inoculum from the surface 4) titration of the inoculum onto cells.

Similarly to wet-to-wet protocol, we decided to use samples with a size of 20x20mm with a total area of 400mm<sup>2</sup>. During the first step, we usually use 80 µl of inoculum (both for HSV-2 or SARS-CoV-2) with an initial concentration of 10<sup>5-6</sup> pfu/ml. The inoculum is homogeneously spread onto the surface to have a complete coverage. The sample is then allowed to dry in a biosafety cabinet at room temperature for 15 min. The samples are then incubated at room temperature for a given time (i.e., 0, 30, 60 or 120 min) and the inoculum is recovered. In this case, the recovery is performed by intensively swabbing the surface using a cotton-tipped swab (VWR, 115-1881) pre-dipped in (DMEM with 2vol% FBS and 1% P/S or in 5-fold diluted Dey-Engley Neutralizing broth (Condalab, 5169) in PBS at pH 7.4 (Gibco, 10010023)). The swab is then transferred in an Eppendorf tube containing 1000 µl of media or neutralizing broth. The plastic handle of the swab is cut in order to close the tube and vortex it vigorously to release the virus. The recovered inoculum is then serially diluted and titrated with a protocol similar to what discussed above in the virucidal assay for each virus. Relevant internal controls are usually run such as an untreated surface and the initial viral stock.



# Chapter 3 Gold nanoparticles and beta-cyclodextrins: beyond the state of the art

Our group has designed and validated two virucidal compounds capable of irreversibly inactivating HSPG-dependent viruses, MUS:OT AuNPs and CD-MUS, as thoroughly discussed in Chapter 1. In this chapter, the main advances on these two compounds are reported. In particular, the first paragraph focuses on the activity of MUS:OT AuNPs and CD-MUS against other families of virus that do not depend on HSPGs to infect cells, such as influenza and VSV. The main results are exposed and discussed. The second paragraph is focused on the activity of both the compounds against SARS-CoV-2, against which the two antivirals were tested at the beginning of the pandemic as viable candidates. In the third paragraph, a study on the role of the hydrophobic chain of CD-MUS on the antiviral activity against HSV-2 is reported. Last, a preliminary pharmacokinetic (PK) study on the use of CD-MUS via intranasal administration is discussed.

In addition to unpublished data, this chapter summarizes the core of results presented in two papers (postprint version):

- V. Cagno, M. Gasbarri, C. Medaglia, D. Gomes, S. Clement, F. Stellacci, C. Tapparel, "Sulfonated nanomaterials with broad-spectrum antiviral activity extending beyond heparan sulfate-dependent viruses", *Antimicrobial Agents and Chemotherapy* 64 (12) (2020) DOI: 10.1128/AAC.02001-20

- M. Gasbarri, P. V'kovski, G. Torriani, V. Thiel, F. Stellacci, C. Tapparel, V. Cagno, "SARS-CoV-2 inhibition by sulfonated compounds", *Microorganisms* 8 (12), 1894 (2020) DOI: 10.3390/microorganisms8121894

In the first paper, I was responsible for the synthesis and chemical characterization of all the compounds used (both gold nanoparticles and beta-cyclodextrins), while Valeria Cagno and Chiara Medaglia performed most of the biological validations.

In the second paper, I was responsible for the synthesis and chemical characterization of all the compounds used (both gold nanoparticles and beta-cyclodextrins), while most of the biological characterizations were performed in collaboration between myself and Valeria Cagno.

## 3.1 Broad-spectrum activity beyond HSPGs viruses

### 3.1.1 Abstract

Viral infections are among the main causes of death worldwide, and we lack antivirals for the majority of viruses. Heparin-like sulfated or sulfonated compounds have been known for decades for their ability to prevent infection by heparan sulfate proteoglycan (HSPG)-dependent viruses but only in a reversible way. We have previously shown that gold nanoparticles and -cyclodextrins coated with mercapto-undecane sulfonic acid (MUS) inhibit HSPG-dependent viruses irreversibly while retaining the low-toxicity profile of most

heparin-like compounds. In this work, we show that, in stark contrast to heparin, these compounds also inhibit different strains of influenza virus and vesicular stomatitis virus (VSV), which do not bind HSPG. The antiviral action is virucidal and irreversible for influenza A virus (H1N1), while for VSV, there is a reversible inhibition of viral attachment to the cell. These results further broaden the spectrum of activity of MUS-coated gold nanoparticles and -cyclodextrins.

### 3.1.2 Introduction

In the absence of vaccines, antivirals represent a major line of defense against viruses. However, currently available antivirals are virus specific, and they have been developed against only a limited number of viruses. The recent pandemic of COVID-19 calls our attention to the major benefit of identifying broad-spectrum antivirals, ready to use when a new epidemic starts. In the past years, we worked on developing broad-spectrum antiviral compounds. To potentially maximize their efficacy *in vivo*, we sought to develop compounds that had an irreversible inhibition mechanism (i.e., virucidal compounds). Irreversible inhibition is insensitive to dilution, for instance, in body fluids, and thus does not require a constant concentration of the inhibitors *in vivo*. To achieve a broad-spectrum response, we designed compounds mimicking heparan sulfate proteoglycan (HSPG), a receptor broadly present on eukaryotic cells and used by a wide variety of viruses (here called HSPG-dependent viruses) to attach to host cells and subsequently find a more specific entry receptor<sup>39</sup>. This approach, which began with seminal studies on heparin, is known to lead to efficient *in vitro* inhibition of many viral strains although with a reversible mechanism of action. To achieve irreversible inhibition, we added to the design long hydrophobic linkers conferring to the compounds the ability to permanently inhibit a large number of HSPG-dependent viruses<sup>67-68</sup>. The key chemical moiety used was a long hydrophobic chain terminating with a sulfonic acid (undecyl sodium sulfonate) presented in a multivalent way, in order to achieve a good inhibitory concentration and strong hydrophobic contact (required to render the interaction irreversible). In the first designed compound (named MUS:OT NP) (fig. 3.1a), such a moiety was fixed on gold nanoparticles (4-nm gold nanoparticles [NPs] coated with a mixture of octane thiol [OT] and mercapto-undecane sulfonic acid [MUS])<sup>67</sup>. In the second compound (named CD-MUS), the moiety was linked to the primary face of -cyclodextrins (CD)<sup>68</sup> (fig. 3.1b).

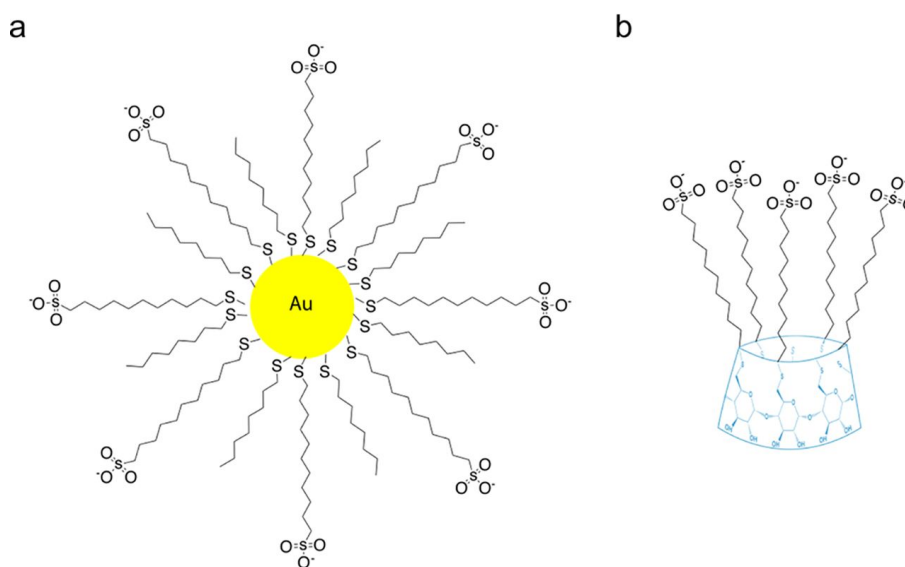


Figure 3.1 – **Chemical structure of MUS:OT AuNPs and CD-MUS.** (a) MUS:OT AuNPs, composed of a gold (Au) core covered by the ligands mercaptoundecansulfonate (MUS) and 1-octanethiol (OT). (b) CD-MUS, composed of a cyclodextrin (in blue) conjugated with MUS.

Both compounds achieved virucidal action against viruses binding to HSPG, such as herpes simplex virus 1 (HSV-1), HSV-2, respiratory syncytial virus (RSV), dengue virus, and many other viruses. Both compounds also exhibited good *ex vivo* and *in vivo* efficacy<sup>67-68</sup>. We have thus shown that the use of undecyl sodium sulfonate (multivalently presented) generates compounds that display the same broad-spectrum antiviral and low-toxicity profile of heparin but, unlike heparin, can exert irreversible and virucidal activity. In this study, we investigate the interaction of our previously reported compounds (MUS:OT NP and CD-MUS) with viruses that do not use HSPGs as attachment receptors (here called HSPG-independent viruses), such as different strains of influenza virus<sup>100</sup> and vesicular stomatitis virus (VSV)<sup>101-102</sup>. We highlight the virucidal activity of both compounds against influenza virus and virustatic activity against VSV. We further show that the activity against VSV is partially cell mediated but mostly caused by interference with viral attachment.

### 3.1.3 Results

#### 3.1.3.1 Antiviral activities of MUS:OT NP and CD-MUS against HSPG-independent viruses.

Antiviral assays were carried out by incubating different strains of influenza virus or VSV with a dose range of MUS:OT NP or CD-MUS, whose structure is shown in fig. 3.1, for 1 h at 37°C before infection of appropriate cell lines. The results are presented in Table 3.1. Both compounds display inhibitory activity in the absence of toxicity, with 50% effective concentrations (EC50s) generally lower for MUS:OT NP than for CD-MUS, in line with our previous publications<sup>67-68</sup>. Importantly, we also verified that MUS:OT NP inhibits the same viruses as CD-MUS, which were not tested with this compound in our previous works (see Table S1 in the supplemental material), confirming the same spectrum of activity of both materials.

Table 3.1 – Antiviral activities of MUS:OT NP and CD-MUS against HSPG-independent viruses - EC50, 50% effective concentration (50% maximal effect); CI, confidence interval; CC50 cytotoxic concentration causing 50% cell death

Compound	Virus	EC50 (µg/ml) (95% CI)	EC50 (µM)	CC50 (µg/ml)
MUS:OT-NP	VSV	0.053 (0.032–0.084)	0.00024	>300
	A/Netherlands/602/2009 (H1N1)	1.38 (1.17–1.62)	0.0068	>300
	A/Singapore/37/2004 (H3N2)	12.0 (8.59–16.7)	0.055	>300
	A/Vietnam/1203/2004 (H5N1)	4.01 (3.15–5.02)	0.018	>300
	B/Wisconsin/01/2010	7.08 (3.73–12.8)	0.032	>300
CD-MUS	VSV	45.4 (35.8–57.6)	15.8	>300
	A/Netherlands/602/2009 (H1N1)	6.28 (4.58–8.39)	2.2	>300
	A/Singapore/37/2004 (H3N2)	17.3 (13.7–22.0)	6.0	>300
	A/Vietnam/1203/2004 (H5N1)	53.2 (28.2–149)	18.5	>300
	B/Wisconsin/01/2010	13.1 (10.0–17.5)	4.6	>300

#### 3.1.3.2 Antiviral activities of other heparan sulfate-mimicking compounds against HSPG-independent viruses.

To confirm the HSPG dependence of VSV and influenza, we further investigated the inhibitory activity of heparin, -carrageenan, and K5NOS(H)<sup>39</sup>, other heparan sulfate analogues previously shown to inhibit HSPG-dependent viruses. To this end, we used the same protocol as the one described above, i.e.,

preincubation of viruses and the compound for 1 h at 37°C before addition to cells. The results, presented in fig. 3.2a and b, show different inhibition profiles of the two viruses. H1N1 is inhibited by -carrageenan and K5NOS(H) but very weakly inhibited by heparin and only at the highest concentration tested (Fig. 2a). Conversely, VSV is not inhibited by any of the sulfate analogues tested (fig. 3.2b).

### 3.1.3.3 Virucidal activities of MUS:OT NP and CD-MUS against VSV and influenza virus.

Next, we investigated if the compounds show virucidal activity, i.e., irreversible inhibition, against VSV and H1N1. This property was previously reported to be exerted by the nanomaterials against HSPG-dependent viruses<sup>39-67-68</sup>. The virucidal assay was performed as previously reported<sup>67</sup>, by incubating the virus with the inhibitory concentration of the compound, followed by serial dilutions of the complex and evaluation of residual viral infectivity at concentrations at which the compound is not active. The results revealed the virucidal activities of both compounds against influenza virus, with reductions of 2.4 logs at 300 µg/ml and 1.6 logs at 100 µg/ml for MUS:OT NP and of 1.0 log at 300 µg/ml for CD-MUS (fig. 3.2c). The extent of virucidal inhibition is comparable to that observed for RSV previously<sup>67-68</sup>.

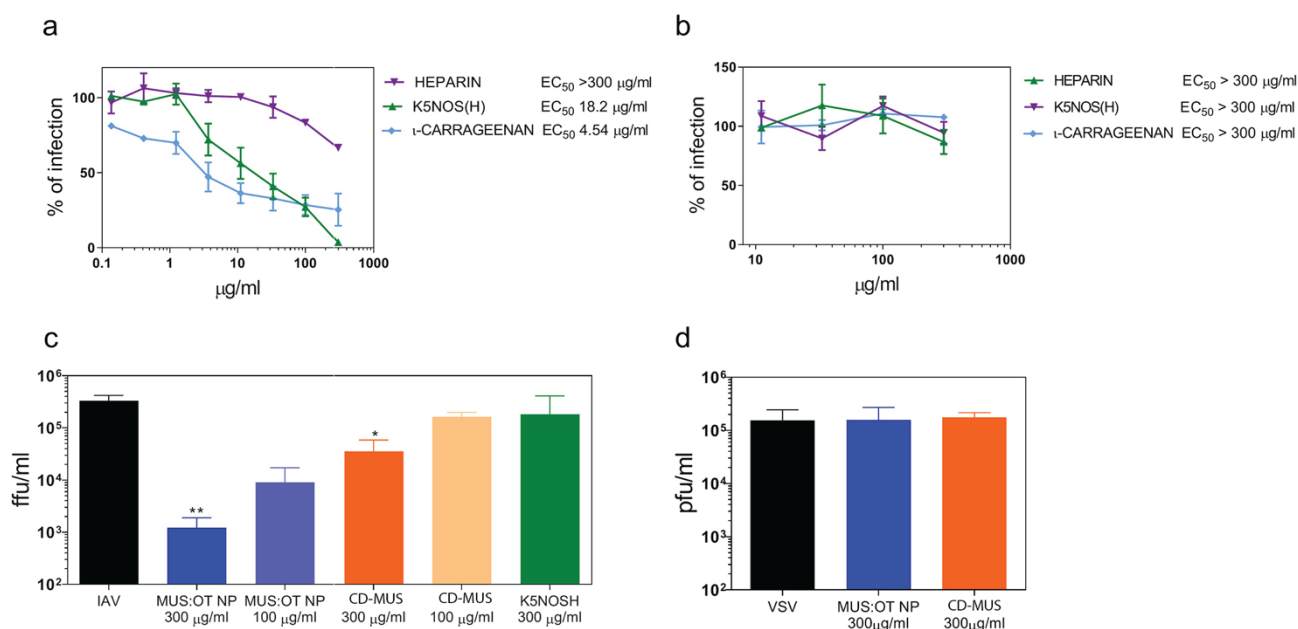


**Figure 3.2 – Antiviral and virucidal activity of heparan sulfate analogues and MUS:OT NPs and CD-MUS against H1N1 A/Netherlands/602/2009 (a) and VSV (b).** Viruses and compounds were incubated for 1 h at 37°C and subsequently added to cells. Infectivity was evaluated at 24 hpi for both viruses. The percentage of infection was calculated by comparing the number of infected cells for H1N1 or plaques for VSV to those for the untreated controls. (c and d) Virucidal activities of MUS:OT NP, CD-MUS, and K5NOS(H) against H1N1 (c) and MUS:OT NP and CD-MUS against VSV (d). Approximately 10<sup>5</sup> focus-forming units (ffu) (H1N1) or 10<sup>5</sup> PFU (VSV) were incubated for 1 h at 37°C with the indicated concentrations of the compound and subsequently serially diluted in cells. Infectious titers were evaluated under each treatment condition at dilutions at which the concentration of compound is not active. Results are expressed as means and standard errors of the means (SEM) from three independent experiments performed in duplicate. Statistical significance relative to the untreated control was calculated using one-way ANOVA (\*\*,  $P < 0.01$ ; \*,  $P < 0.05$ ). EC<sub>50</sub>, 50% effective inhibitory concentration.

Importantly, we also included in the virucidal assay a highly sulfated polysaccharide, K5NOS(H), previously reported to exert antiviral activity against multiple HSPG-dependent viruses<sup>103</sup>. As shown in fig. 3.2c, K5NOS(H) is not virucidal against influenza virus despite displaying good antiviral activity (fig. 3.2a). These results confirm that the presence of the long alkylic chains is a key factor in the virucidal mechanism of action<sup>68</sup>. Conversely, the two compounds do not display virucidal activity against VSV (fig. 3.2d) despite the low EC<sub>50</sub> measured in inhibitory assays (Table 3.1).

### 3.1.3.4 Mechanisms of action of MUS:OT NP and CD-MUS against VSV

As the two compounds show different activity profiles against VSV and influenza virus, i.e., virustatic versus virucidal activity, we carried out time-of-addition experiments, flow cytometry, and immunofluorescence analyses to elucidate the antiviral mechanism of action against this virus. CD-MUS (Fig. 3a) or MUS:OT NP (Fig. 3b) was either (i) preincubated for 1 h at 37°C with the virus (pretreatment with virus plus infection at 37°C), (ii) preincubated for 2 h at 37°C with the cells and then washed out before infection (pretreatment of cells), (iii) directly added to the cells together with the virus at 37°C (cotreatment), or (iv) preincubated with the virus for 1 h at 37°C followed by the addition of the mixture of the virus and compound on prechilled cells for 1 h at 4°C to prevent viral entry (pretreatment with virus plus infection at 4°C). Under all conditions, after washing out the viral inoculum, the cells were overlaid with medium containing methylcellulose and incubated at 37°C for 24 h.

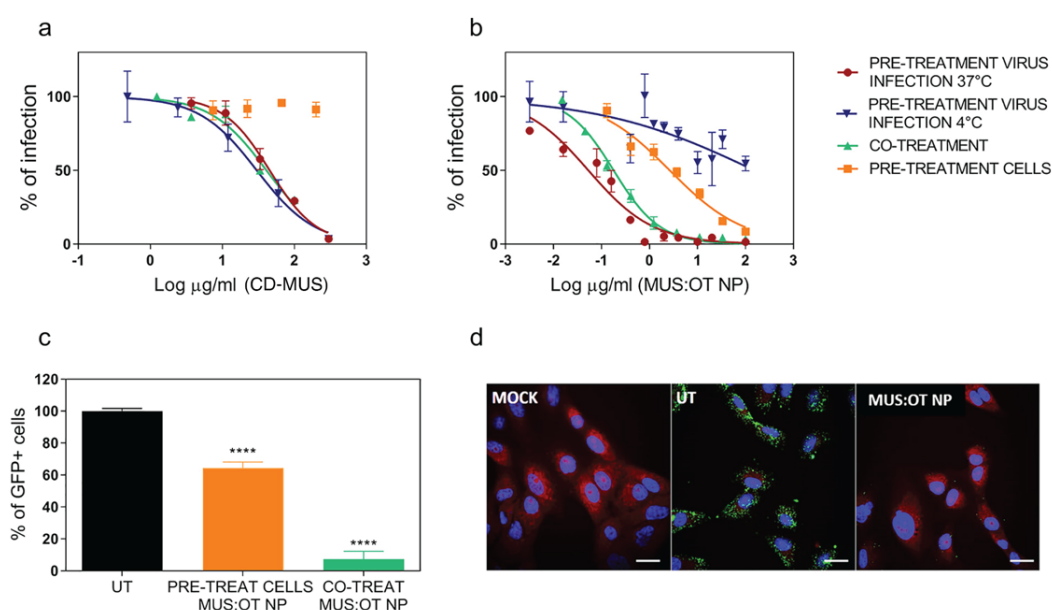


**Figure 3.3 – Mechanisms of action of CD-MUS (a) and MUS:OT NP (b) against VSV.** The compounds were either added to cells for 2 h before infection (pretreatment of cells), incubated with the virus for 1 h and then added to cells at 37°C (pretreatment with virus infection at 37°C), added with the virus to the cells (cotreatment), or preincubated with the virus for 1 h and then added to cells at 4°C for 1 h before shifting to 37°C (pretreatment with virus infection at 4°C). Infectivity was evaluated at 24 hpi. (c) Flow cytometry was performed at 3 hpi with Vero cells infected with VSV expressing GFP (MOI of 5) after pretreatment with MUS:OT NP for 2 h (pretreated cells) or in the presence of MUS:OT NP (cotreatment). Percentages of infection are normalized according to the untreated (UT) conditions. (d) Vero cells that were uninfected (mock) or infected with VSV (MOI of 20) in the absence (UT) or presence of MUS:OT NP (100 g/ml) were fixed at 1 hpi and subjected to immunostaining with an anti-VSV polyclonal antibody. Green, VSV; red, Evans blue; blue, DAPI. Bars, 10 µm. Results are expressed as means and SEM from two independent experiments performed in duplicate. Statistical significance relative to the untreated control was calculated using one-way ANOVA (\*\*\*\*,  $P < 0.001$ ).

Dose-response curves and EC50s were not significantly different under all conditions for CD-MUS, except when the cells were pretreated with the compound, where no activity was observed (fig. 3.3a). Similarly, inhibitory activities under pre- and cotreatment conditions were comparable for MUS:OT NP (fig. 3.3b). Interestingly, pretreatment of cells with MUS:OT NP also inhibited VSV infection but with an EC50 significantly higher than that reported upon pre- or cotreatment with the virus (2.6 versus 0.053 g/ml). Of note, a similar assay performed with HSV-2, which binds HSPG moieties, showed no inhibition. The partial cell-mediated inhibition observed against VSV is thus virus specific. To further dissect the contribution of cell-mediated inhibition versus direct virus inhibition, we infected Vero cells with green fluorescent protein (GFP)-expressing VSV (multiplicity of infection [MOI] of 5) and measured GFP expression by flow cytometry at early

times postinfection, in the presence or absence of MUS:OT NP added for pretreatment of cells or cotreatment. The results revealed significantly greater inhibition with cotreatment (fig. 3.3c), confirming that the major component of inhibition is a direct interaction with the virus. To highlight the step of the viral life cycle inhibited by the compound, we performed a cotreatment assay (MOI of 20) and fixed the cells 1 h after incubation at 37°C for immunostaining with an anti-VSV antibody. In contrast to the untreated virus, almost no signal was observed in the presence of the compound, indicating that MUS:OT NP prevents the virus from binding and/or entering the cell (fig. 3.3d). Finally, the inhibitory activity was lost if infection was preceded by a 1-h incubation at 4°C (fig. 3.3b), in contrast to what was observed for HSV-2. This confirms that the association of the virus with the NP is reversible and likely lost at 4°C.

### 3.1.4 Discussion

Influenza viruses are known to attach to sialic acid to infect cells<sup>100</sup>. However, we show that recently developed HSPG-mimicking compounds (MUS:OT NP and CD-MUS<sup>67-68</sup>) are able to inhibit several influenza A (H1N1, H3N2, and H5N1) and B virus strains. Our results are supported by glycan array studies that highlight interactions between the influenza virus hemagglutinin protein and sulfated glycans (particularly with a sulfation on N-acetylglucosamine, linked to galactose and sialic acid)<sup>104</sup>. In line with the glycan array data, the lowest EC<sub>50</sub>s achieved with our HSPG-mimicking compounds were obtained against the H1N1 strain, which was also reported to have the highest affinity for sulfated glycans<sup>104</sup>. In addition, we demonstrate that H1N1 is also inhibited by highly sulfated molecules, such as -carrageenan, in line with previous literature<sup>105</sup>, and by K5NOS(H), due to the affinity of hemagglutinin for sulfated and sulfonated molecules. Our results also provide evidence of full or partial virucidal activity against influenza virus of MUS:OT NPs or CD-MUS, respectively. Altogether, these data suggest a direct interaction between the virus and the compound and subsequent virucidal activity mediated by the hydrophobic portion of both MUS:OT NPs and CD-MUS. Importantly, despite good inhibitory activity, K5NOS(H) did not exert any virucidal effect, further supporting the importance of a long hydrophobic linker to mediate virucidal activity<sup>67-68</sup>. Of note, in contrast to our previous observations<sup>68</sup>, in the present study, we report that CD-MUS inhibits the infectivity of H3N2. An optimized synthesis protocol as well as a different number of ligands per -cyclodextrin likely account for the broader activity of the recently synthesized CD-MUS molecules. VSV is also inhibited by MUS:OT NPs and CD-MUS (fig. 3.3b) but only in a reversible way, as shown by the lack of inhibition when the compound-virus complex is diluted out before infection (fig. 3.2d). Unlike influenza virus, VSV is not inhibited by any of the heparin analogues. Importantly, these results clearly show that the virucidal activity is a feature independent of the EC<sub>50</sub> value since the EC<sub>50</sub> of MUS:OT NP against VSV is lower than that measured against H1N1 (table 3.1), but the interaction is irreversible only against the latter. Interestingly, both CD-MUS and MUS:OT NP show maximal inhibition upon direct interaction with VSV, as observed for HSV-2. This suggests that the types of interaction in both cases must be similar, although the action on HSV-2 is stronger and irreversible due to the natural dependence of the virus on HSPG<sup>67</sup>. Of note, CD-MUS and MUS:OT NP do not show comparable activity profiles against VSV. CD-MUS activity is maintained under all experimental conditions (pretreatment, cotreatment, and pretreatment plus 1 h at 4°C) except cell pretreatment. These results suggest an electrostatic interaction that does not play a role when CD-MUS is preincubated with the cell and washed out before the addition of the virus. Our interpretation is that viral inhibition depends on a rather quick interaction of CD-MUS with the virus that is sufficient to prevent viral attachment. Interestingly, under the same experimental conditions, part of the inhibition is maintained for MUS:OT NP, indicating a partial cell-mediated effect for this compound. This effect is not observed with HSV-2 and is thus virus specific. In contrast to CD-based molecules, NPs are able to interact with or cross cellular membranes<sup>85</sup>. This cell-mediated inhibition

observed in the case of VSV is probably due to interactions with specific domains of the cellular membranes or internalization of the particles during pretreatment of the cells and subsequent colocalization with the virus in cytosolic compartments, as previously described for other compounds<sup>106</sup>. Finally, we demonstrate that the nanoparticles lose their inhibitory ability when added to the cells together with the virus and incubated at 4°C for 1 h. In line with their virustatic effect, we assume that at this temperature, the nanoparticle-virus complex dissociates.

### 3.1.5 Conclusions

We previously demonstrated that irreversible inhibition of viral infectivity of HSPG-dependent viruses is possible with heparin-mimicking compounds presenting undecyl sulfonic acids in a multivalent fashion. Here, we show that these molecules also exert the same effect also against several sialic acid-dependent influenza virus strains. In line with glycan array results<sup>104</sup>, we propose that this interaction is due to the ability of hemagglutinin of influenza virus to bind sulfated sugars. We further demonstrate that the same compounds can achieve reversible inhibition of other HSPG-independent viruses such as VSV. In this context, we highlight complex interaction profiles that are consistent with a weak electrostatic interaction. In light of these results, further investigations will be directed to an even broader panel of viruses in order to define structural commonalities and better understand the mechanism of action of our sulfonated nanomaterials against HSPG-independent viruses.

## 3.2 SARS-CoV-2 inhibition by sulfonated compounds

### 3.2.1 Abstract

SARS-CoV-2 depends on ACE2 for cellular entry, but it might rely as well on attachment receptors such as heparan sulfates. Several groups have recently demonstrated an affinity of the SARS-CoV2 spike protein for heparan sulfates and a reduced binding to cells in presence of heparin or heparinase treatment. Here, we investigated the inhibitory activity of several sulfated and sulfonated molecules, which prevent the interaction with heparan sulfates, against VSV-pseudotyped-SARS-CoV-2 and the authentic SARS-CoV-2. Sulfonated cyclodextrins and nanoparticles that have recently shown broad-spectrum non-toxic virucidal activity against many heparan sulfates binding viruses showed inhibitory activity in the micromolar and nanomolar range, respectively. In stark contrast with the mechanisms that these compounds present for these other viruses, the inhibition against SARS-CoV-2 was found to be simply reversible.

### 3.2.2 Introduction

SARS-CoV-2 is causing an unprecedented pandemic and a better understanding of its biology and pathogenesis is required to identify effective antiviral strategies.

Presently, the only approved antiviral drug is remdesivir, a nucleoside analogue that inhibits viral RNA synthesis of several coronaviruses<sup>107</sup>. However, the results of randomized double-blind clinical trials showed only a reduction in hospitalization time (from 15 to 11 days) while mortality was not significantly reduced compared to placebo<sup>108-109</sup>. Hydroxychloroquine, despite being widely used, did not show any activity in human respiratory cell lines<sup>110</sup>, animal models<sup>111</sup>, and *in vivo* clinical trials<sup>112-109</sup>. Conversely, dexamethasone, a corticosteroid, significantly reduced mortality in patients with severe COVID-19<sup>113</sup>, the efficacy of tocilizumab, a monoclonal antibody directed against interleukin-6 receptor, is being evaluated in clinical

trials<sup>114</sup>, and anticoagulant treatments have proven to be beneficial<sup>115</sup>. Demonstrating that targeting the excessive activation of the immune response is a promising strategy.

However, inhibiting viral replication during the initial stages of infection rather than treating the symptoms resulting from immune activation and inflammation will be largely more beneficial in preventing hospitalization and long-term sequelae of infection. For this reason, development of direct-acting antiviral compounds should be a research priority. One class of antiviral compounds in study are attachment inhibitors, with a strategy that is intrinsically broad-spectrum, since many different viruses use similar attachment receptors.

The two major classes of attachment receptors used by viruses are heparan sulfates (HS)<sup>39</sup> and sialic acid<sup>116</sup>. These receptors are widely expressed on eukaryotic cells and used by a wide range of viruses to adhere to the cell surface before interacting with a more specific entry receptor, which triggers uptake and entry<sup>39</sup>. This strategy is used as well by coronaviruses (CoVs). Middle East Respiratory Syndrome (MERS) – CoV uses sialic acid (with a preference for  $\alpha$ 2,3-linked SAs)<sup>117</sup> while NL63<sup>118</sup>, and Severe Acute Respiratory Syndrome (SARS) CoV<sup>119</sup> were reported to use HS. In addition to adhesion receptors, NL63, SARS and SARS-CoV-2 use Angiotensin Converting Enzyme 2 (ACE2), as entry receptor<sup>120-121</sup>. For SARS-CoV-2 has been further shown that HS act as co-receptor, inducing a conformational change on the spike that enhances the interaction with ACE2<sup>122-123</sup>.

Sialic acid dependency of SARS-CoV-2 has so far only been investigated with computational methods<sup>124-125</sup>, and no biological confirmation is available to date. In contrast, given the sequence similarity between SARS-CoV-2 and SARS-CoV, the dependence on HS has already been investigated by many groups with different approaches. In the work of Kim et al, the interaction of the receptor binding domain of the spike (S) protein of SARS-CoV-2 with heparin and HS was shown by surface plasmon resonance (SPR)<sup>126</sup>. Recombinant S protein was also used in glycan array studies to evaluate the interaction with different glycans, and highlighted a higher binding for highly sulfated glycans<sup>122</sup>. In two recent studies<sup>127-128</sup>, the ability of heparin or heparinase treatment to inhibit the binding of SARS-CoV-2 was shown both with pseudotyped or wild-type viruses. In addition, docking studies<sup>123</sup> suggest that the interaction between S and HS is mediated by a site in proximity but independent from the ACE2 binding domain. Interestingly Clausen et al<sup>123</sup> also pointed out that the virus is less dependent on HS on Vero E6, due to a high expression of ACE2.

The proposition of using heparin and heparin analogues is extensively discussed by Tiwari et al.<sup>128</sup> as the repurposing of clinical stage anti-cancer that mimic HS such as Pixatimod (PG454)<sup>129</sup> or mitoxantronea drug used for acute nonlymphocytic leukemia, prostate cancer, and multiple sclerosis<sup>130</sup>.

Additionally, unfractionated heparin (UFH) or low molecular weight heparin (LMWH) are being tested in clinical trials. Heparin is known to have anti-clotting, anti-coagulant, anti-thrombotic and anti-inflammatory properties and could therefore be effective in treating the coagulopathy and hyper inflammatory response characteristic of critically ill COVID-19 patients. However, this use is unrelated to the direct antiviral activity exerted on viral attachment.<sup>131</sup>

Based on these published studies, we tested sulfonated compounds which were previously shown to be active against HS-dependent viruses. In the past years we synthesized gold nanoparticles<sup>67</sup>, and  $\beta$ -cyclodextrins<sup>68</sup> coated with mercapto-undecan-sulfonates. In contrast to heparin and other molecules, in which a long alkyl moiety is not present, our compounds are endowed with an irreversible mechanism of

action in absence of toxicity. Upon interaction with HS-dependent viruses, the multivalent binding coupled to structural features of our compounds lead to structural damage of the viruses, i.e. the compounds display a virucidal activity.

Here we show that sulfonated materials with a hydrophobic component show inhibitory activity in the same concentration range reported for HS-dependent viruses, however, differently than what observed for a number of other viruses, the inhibition for SARS-CoV-2 is virustatic (reversible) and not virucidal (irreversible).

### 3.2.3 Results

In order to evaluate the ability of sulfonated compounds to inhibit the attachment of SARS-CoV-2, we pre-incubated VSV pseudo-viruses expressing the spike protein of SARS-CoV-2 (VSV-CoV-2) or SARS-CoV-2 wild-type viruses and the compounds for 1h at 37°C, followed by addition on cells. After 1h, cells were washed and the infection was quantified 48 hpi by plaque assay for the wild-type virus or 24 hpi through GFP positive cells quantification for VSV-CoV-2. The results (fig. 3.4) show that our nanoparticles (MUS:OT NP) and cyclodextrins (CD-MUS) showed inhibitory activity in both cases.

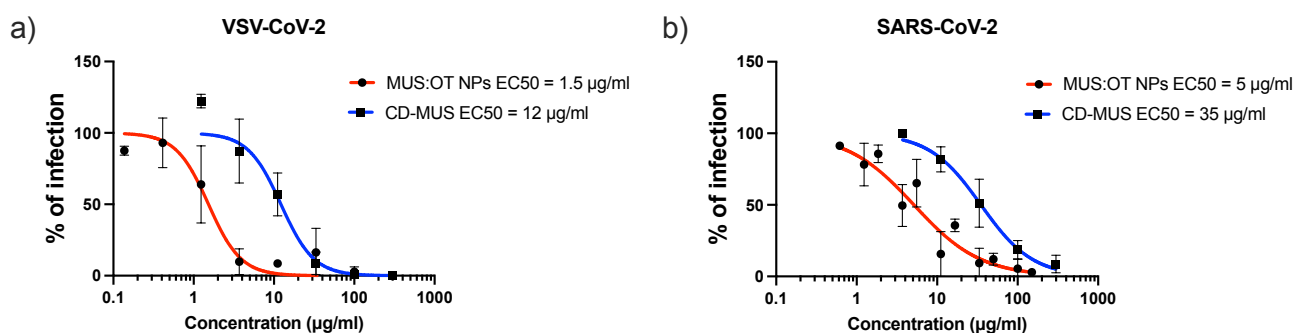


Figure 3.4 – **Inhibitory activity of sulfonated nanomaterials against SARS-CoV-2.** a) VSV-CoV-2 or b) SARS-CoV-2 were incubated for 1h at 37°C with different doses of MUS:OT NP or CD-MUS and subsequently serially added on cells. In a), the number of GFP positive cells was evaluated 24hpi while in b) the number of plaques was determined 48hpi. Results are expressed as mean and SEM of three independent experiments.

Importantly, the results on SARS-CoV-2 with MUS:OT NP and CD-MUS were confirmed in two independent labs with two different strains of SARS-CoV-2 (SARS-CoV-2/München-1.1/2020/929 and SARS-CoV2/Switzerland/GE9586/2020). In both cases MUS:OT NP showed higher potency when compared to CD-MUS (fig. 3.4b).

The two compounds previously showed virucidal activity against different HS-dependent viruses, i.e. the ability to permanently impair viral infectivity. Therefore, we assessed whether they also display virucidal activity against SARS-CoV-2. SARS-CoV-2 ( $10^5$  pfu) was incubated for 1h with 300 μg/ml of the nanomaterials and the mixture was subsequently diluted on cells. The residual infectivity was evaluated at concentrations of molecules known to be non-inhibitory. The results (fig. 3.5) evidence a lack of virucidal activity of both materials.

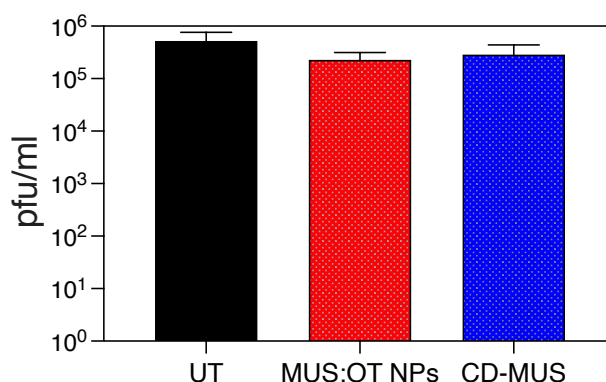


Figure 3.5 – **Virucidal activity of sulfonated nanomaterials against SARS-CoV-2.** 10<sup>5</sup> pfu of SARS-CoV-2 were incubated for 1h at 37°C with 300 µg/ml and subsequently serially diluted on cells. Infectious titers were evaluated for each treatment condition at dilutions at which the concentration of compound was not active. Results are expressed as mean and SEM of three independent experiments.

To address the HS-dependency of our SARS-CoV-2 strains, we tested, with the same protocol described for MUS:OT NP and CD-MUS, the antiviral effect of heparins from different sources, of another sulfated polymer (K5N,OSH) and of commercially available sulfated beta-cyclodextrins against VSV-CoV-2 and SARS-CoV-2. All of these molecules failed to show antiviral activity up to 1000 µg/ml, while a sulfated polymer, carrageenan, showed very weak antiviral activity but only against wild-type SARS-CoV-2 (Table 3.1).

Table 3.2 – **Antiviral activity of HS mimicking compounds against VSV-CoV-2 and SARS-CoV-2.** EC50 50% effective concentration, CC50 50% cytotoxic concentration

	Compound	EC50 (µg/ml)	EC50 µM	CC50 (µg/ml)
VSV-CoV-2	Carrageenan	> 300	>317	> 300
	K5N,OS(H)	> 300	>20	> 300
	Sulfated beta-CD	> 300	>145	> 300
	Resonium A	> 300	>300	> 300
	MUS:OT NP	1.5	0.005	> 300
	CD-MUS	12.2	4	> 300
	Hydroxychloroquine		3.9	-
SARS-CoV-2	Carrageenan	267	282	> 300
	K5N,OS(H)	> 300	>20	> 300
	Sulfated beta-CD	>1000	>485	> 300
	MUS:OT NP	5.38	0.017	> 300
	CD-MUS	35	11.5	> 300
	Heparin sodium salt (Tocris)	> 1000	>40	-
	Heparin Sodium Salt (Porcine)	>1000	>55	> 300
	Enoxaparin Sodium Salt	>1000	>200	
	Hydroxychloroquine		2.92	-

### 3.2.4 Discussion

Here we show the antiviral activity of sulfonated compounds against SARS-CoV-2. These compounds (MUS:OT NP and CD-MUS) were previously reported to exert a virucidal (*i.e. irreversible*) activity against HS-dependent viruses such as Herpes Simplex Virus 2, respiratory syncytial virus, papillomavirus and dengue virus<sup>67-68</sup> and a virustatic (*i.e. reversible*) activity against vesicular stomatitis virus (VSV), a HS-independent virus. The results displayed in fig. 3.4 and fig. 3.5 show a reversible inhibition for both compounds against SARS-CoV-2, similarly to what we previously reported for VSV. In addition, we show that other HS-mimicking compounds are inactive against SARS-CoV2 as also reported for VSV.

Two different scenarios could account for the lack of virucidal activity of MUS:OT NP and CD-MUS against SARS-CoV-2. The restricted virustatic effect may be explained by the peculiar shape of CoVs, whose receptor binding domain (RBD) is approximately ten nanometers away from the viral envelope. We suggested that the virucidal activity of our compound results from a pressure exerted on the RBD of the viral glycoprotein that is then transmitted to the whole virion<sup>67</sup>. This mechanism may then not be applicable to CoVs due to the distance between the RBD and the envelope. Alternatively, and as previously described for VSV<sup>132</sup>, the absence of virucidal activity of MUS:OT NP and CD-MUS could be due to the poor affinity of the SARS-CoV-2 spike protein for HS. This second scenario is supported by the absence of inhibitory activity of other sulfated compounds. Of note, the observed virustatic effect of our compound compared to the absence of activity of various types of sulfated compounds could be explained by the presence of long hydrophobic linkers that may enhance binding to the basic amino-acid residues of the spike protein.

We acknowledge that our results suggest that HS is not used by SARS-CoV2 for infection, and there is abundant literature showing the opposite<sup>123-122-127-130-131-133</sup>. However, also in the current literature, discrepancies in the antiviral potencies of the heparins and heparin analogues are present<sup>133</sup>. For instance, Tandon et al. report IC50 of 5.99 µg/L, 1.08 mg/L, for UFH and enoxaparin, respectively, while Tree et al.<sup>131</sup> report values of 41 µg/mL and 7800 µg/mL, respectively. In our experimental setting, both UFH and LMWH do not show efficacy up to 1000 µg/mL.

The discrepancy of our data with the existing literature could be explained by different hypotheses: (i) differences in the clinical isolate used: point mutations in the spike protein might result in different binding of the virus to HS, as reported for other viruses<sup>134</sup>; moreover, it is well known that multiple passaging in cell culture could lead to cell adaptation and the acquisition of the ability to bind heparan sulfates<sup>39</sup>. In order to prevent this from happening, our clinical isolates were passaged only twice in cells before the experiment, and there is no information about viral passage number in some of the published reports<sup>123-122</sup>. (ii) The secondary role of HS in SARS-CoV-2 entry and the presence of distinct putative domains of interaction on the spike protein of SARS-CoV-2 for HS and ACE2. Indeed, Clausen et al. showed that SARS-CoV-2 exploits ACE2 as primary receptor for cell recognition, using heparan sulfate (HS) only as a binding enhancer. They also reported that in Vero-E6, the cell line used in our study, the abundance of ACE2 decreases the dependency of the virus on HS.

### 3.2.5 Conclusions

In conclusion, here we show that sulfonated cyclodextrin and nanoparticle show respectively micromolar and nanomolar inhibitory activity against SARS-CoV-2, further broadening the number of viruses inhibited by these compounds. However, the reversible nature of the inhibition points to a lesser clinical

relevance. The lack of irreversible activity could be due to the peculiar shape of coronaviruses or to the low dependency of SARS-CoV-2 on HS for viral attachment.

### 3.3 Modified cyclodextrins : a study on the influence of the lenght of the linkers

As discussed in details in Chapter 1, our strategy in designing novel virucidal antivirals is based on three main structural components: a multivalent core, a hydrophobic linker and a functional group. In this chapter, we have validated the capability of two cores, gold nanoparticles and beta-cyclodextrin, covered by the same linker, MUS, of permanently inactivating different classed of virused. In Cagno et al. and in Jones et al., different modifications of the hydrophobic linker were proposed. Indeed, a complete systematic investigation was missing.

In collaboration with Camilla Servidio and Dr. Paulo H. J. Silva, that developed and performed the synthesis of the precursors and the final compounds, we focused on the investigation of the role of the hydrophobic linker on the antiviral effect of beta-cyclodextrins. In particular the length of the aliphatic chain was studied, as shown in fig. 3.6. A series of modified cyclodextrins have been synthesized keeping the same structure of the core, beta-CD, and the same functionality, sulfonate group. The only modification is in the length of the hydrophobic linker that ranged from 4 to 18 carbon atoms. Such study allowed us to investigate how the length of the hydrophobic linker affects the antiviral activity.

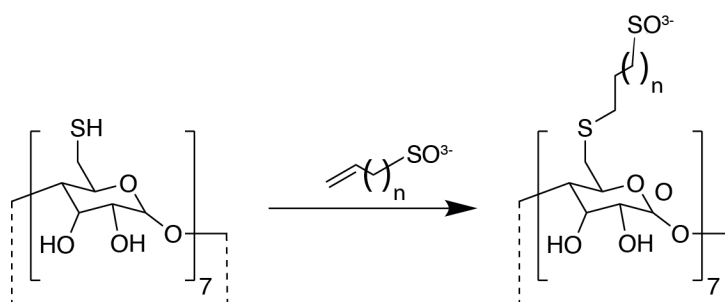


Figure 3.6 – **Reaction scheme used to synthesis different CD-MXS.** X represents the number of carbon atoms present on the aliphatic chain. N ranged from 2 to 16 resultin in X ranging between 4 and 18.

All the compounds were then tested against HSV-2, both in a dose-response assay, in order to evaluate the IC<sub>50</sub>, and in a virucidal assay, in order to evaluate the nature of the process of inactivation (reversible or irreversible). The results are reported in Table 3.3.

As can be seen, the compounds with a chain shorter then 7 carbons, do not show any inhibition up to 2000µg/ml. Increasing the length, the IC<sub>50</sub> decreases very quickly going from 290 µg/ml for CD-M8S, to 29 µg/ml for CD-M9S to 10 µg/ml for CD-M10S. Above 10 carbons, the IC<sub>50</sub> is stable in a range between 1-10 µg/ml within experimental error until the longest chian tested, being CD-M18S.

The virucidal behaviour has a similar trend: while for a length between 4 to 7 carbons there is no inhibiton in the range of interest, for CD-M8S an IC<sub>50</sub> value can be detected. However, the mechanism of inhibition is solely virustatic. Given the high IC<sub>50</sub>, the compound has been tested at different concentration (300 and 2000 µg/ml) but still no irreverisble inhibiton could be detected.

On the other hand, all compounds with an aliphatic chain longer than 9 (from CD-M9S upwards) showed a virucidal mechanism with a complete irreverisble inhibition against HSV-2.

Table 3.3 – **Antiviral and virucidal activity of the CD-MXS against HSV-2.** All the dose-response are simplicate with technical duplicates. Virucidal assay performed at 300µg/ml for 1h incubation. For CD-M8S has been repeated also at 2000µg/ml, given the higher IC50, but no effect was detected.

Compound	IC50 (µg/ml)	Virucidal
CD-M4S	>2000	No
CD-M5S	>2000	No
CD-M6S	>2000	No
CD-M7S	>2000	No
CD-M8S	290	No
CD-M9S	29	Yes
CD-M10S	10	Yes
CD-M11S	7	Yes
CD-M12S	8	Yes
CD-M13S	2.5	Yes
CD-M14S	8.5	Yes
CD-M15S	0.7	Yes
CD-M16S	27	Yes
CD-M17S	5	Yes
CD-M18S	6	Yes

Such results need to be further investigated but a possible explanation could be the difference in solubility of the various compounds. In fact, shorter is the hydrophobic chain, higher is the solubility of the compound in water/media. If the compound is more soluble in media, the free energy of the bound state to the virus is higher, meaning that the compound is less likely to stay bounded to the viral proteins, resulting in a higher IC50. Our results show that between 4 to 7 carbons, the compound does not interact with the virus up to 2000 µg/ml, given the extremely high solubility of the compounds. In fact, even though the overall negative charge is the same, the extremely hydrophilic nature of the compound favours its unbound state in solution. For compounds with chain linkers between 8 and 9, the IC50 drops. For these compounds the ratio between hydrophilicity and hydrophobicity decreases and in our hypothesis at this stage the entropic energy lost by the sulfonate group (highly hydrophilic) is balanced by the enthalpic energy gained by the hydrophobic linker interacting with the viral protein. Increasing the length such effect is not enhanced, but we reach a plateau, at least in terms of IC50.

A similar rationale applies to the mechanism of action: the long hydrophobic linkers decrease the solubility in aqueous media, thus enhancing the retention time on the viral protein. Since we envision the virucidal mechanism as a two-step process, this would let the compound to permanently damage the virus.

These results confirm our hypothesis on the design of a virucidal antiviral: the requirement of a long hydrophobic chain to reach a virucidal mechanism of action. In addition, we prove that a certain amount of hydrophobicity is required in order to induce the interaction and promote the virucidal inhibition.

This experimental approach could be supported by molecular dynamic simulations that could confirm our hypothesis and shed lights on the mechanism of action of our virucidal antivirals.

### 3.4 Pharmacokinetic study (PK)

Envisioning a possible use of CD-MUS as a therapeutic agent against respiratory viruses such as RSV or SARS-CoV-2, we have performed a study in collaboration with Aphad to establish the pharmacokinetic and organ distributions in mice, after intranasal administration. The study was designed as follow: 4 mice per group were administered with 10mg/kg dose (15µl in H<sub>2</sub>) of CD-MUS via intranasal administration. Each group was euthanized at different time-points, 15, 30, 60, 120, 240, 360 and 1440 min and different organs (lung, liver, kidney, pancreas, spleen and brain) and blood were collected. Samples were then analyzed after purification via LC-MS/MS.

#### 3.4.1 Results

All the data are reported in tables 3.4 through 3.7. No mice showed any signs of toxicity during the treatment, confirming the low toxicity of our treatment. Data for the lungs are probably underestimated, because repeated freeze-thaw cycles for such samples during the analysis causes degradation of the compound. Such instability was later confirmed in a different study (not reported here), where CD-MUS were tested in different conditions. Indeed, as expected, the lung is the organ that retained the highest concentration of the compound.

CD-MUS was found in plasma with a T<sub>max</sub> after 4hrs from the administration and was still quantifiable up to 24hrs. CD-MUS was not detected in the brain and was found at low amounts in the liver (detectable only after 15min), in the spleen and at higher concentrations in the pancreas where some variability was present, possibly due to the difficulty to excise this organ from the fat tissue. CD-MUS was present from 2 h on in the kidney suggesting a possible renal excretion mechanism.

Table 3.4 – Concentrations of CD-MUS in mouse plasma at different timepoints.

Time (min)	Plasma (ng/mL)	SD
15	173.2	53.3
30	266.1	189.5
60	170.5	57.2
120	324.2	121.4
240	420.9	177.2
360	335.3	106.1
1440	50.2	31.8

Table 3.5 – **Concentrations of CD-MUS in different organs at different timepoints.** Underlined values were set as ½ LOQ for statistical purpose. Brain values were all <LOQ

Time (min)	ng/g tissue									
	Liver	SD	Lung	SD	Kidney	SD	Pancreas	SD	Spleen	SD
15	10.9	6.9	141	123.5	<LOQ		99.2	122.4	<u>12.5</u>	-
30	<LOQ		63.5	36.2	<LOQ		248.8	414.6	23.4	13.4
60	<LOQ		100.1	114.9	<LOQ		234.8	321.6	27.6	11.4
120	<LOQ		25.4	13.7	14.2	8.2	<LOQ	-	28.5	17.8
240	<LOQ		40.9	41.1	13.1	7.1	<LOQ	-	37	18.5
360	<LOQ		<LOQ	-	15.7	10.6	<LOQ	-	18.3	5.7
1440	<LOQ		<LOQ	-	12.7	3.9	<LOQ	-	72.9	50.7

Table 3.6 – **Pharmacokinetic parameters of each tissue/organ**, defined as follow:

$C_{max}$  Maximum plasma concentration

$C_{last}$  Plasma concentration at last timepoint

$t_{max}$  Time of maximum plasma concentration

$AUC_{0-last}$  AUC from time zero to the time of the last quantifiable plasma concentration

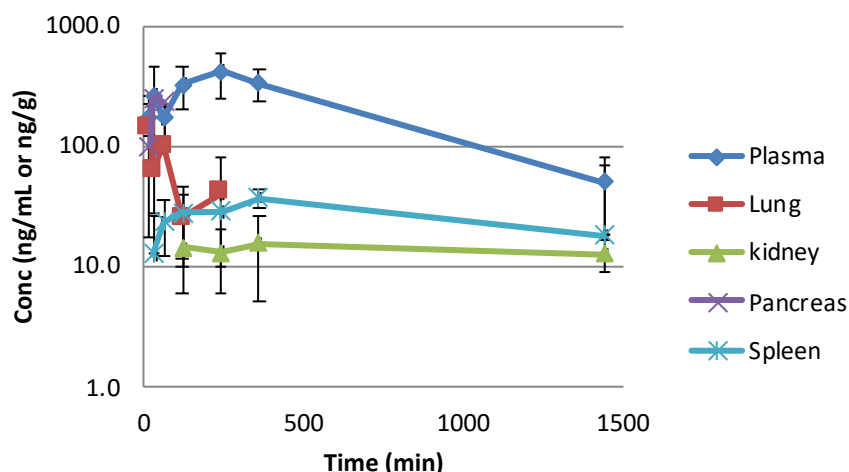
$AUC_{inf}$  AUC from time zero extrapolated to infinity  $= \int_0^{\infty} C dt$

$MRT$  Mean Residence Time  $MRT = \frac{1}{N} \sum_{i=1}^m t_i n_i$

$T_{1/2}$  Half life  $= \frac{\ln(2)}{k_e}$

		Plasma	Lung	Kidney	Pancreas	Spleen
$t_{1/2}$	min	393	-	-	-	-
$T_{max}$	min	240	15	360	30	1440
$C_{max}$	ng/ml	421	141	16	249	73
$T_{last}$	min	1440	240	1440	60	1440
$C_{last\_obs}$	ng/ml	50	41	13	235	73
$AUC_{0-t}$	ng/ml*min	324254	12786	19518	10607	59294
$AUC_{0-inf\_obs}$	ng/ml*min	352704	21002	-	-	-
$MRT_{0-t}$	min	394	94	708	38	1048
$MRT_{0-inf\_obs}$	min	524	-	-	-	-

Figure 3.7 – Kinetic profiles of the CD-MUS concentrations in plasma and organs



### 3.5 Summary

This chapter discusses the new results obtained studying gold nanoparticles and beta-cyclodextrins as antivirals, going beyond our published works shown in Cagno et al. and Jones et al. Three main topics were discussed.

First, the two antivirals have been tested against other viruses, not directly dependent on HSPGs. We have proved that both AuNPs and CD act as virucidal antivirals inhibiting viral infection also in other viral families, such as Influenza. In case of VSV, the inhibition is solely virustatic. With the emergence of the COVID-19 pandemic, we have tested our two compounds against SARS-CoV-2, but, as for VSV, both AuNPs and CD showed an inhibition yet just virustatic.

Second, we have focused on beta-cyclodextrins and investigated the importance of the length of the hydrophobic linker respect to the antiviral activity. We have shown that a chain of at least 8 carbon atoms is required in order to have a virucidal mechanism of action. Indeed, at least in case of CDs, even in the presence of a sulfonate group, shorter hydrophobic chain (between 4 and 7 carbon atoms) did not show any inhibition.

Thirs and last, envisioning the possible translation of CD-MUS as drug, we have run a pharmacokinetic study. In particular, we have administered the drug intranasally (potential application against respiratory diseases) and we have quantified the distribution in different organs at different time-points. CD-MUS has been found mainly in the lung in the first 30min, and then, more and more in plasma, kidney and spleen, suggesting a renal clearance mechanism.

# Chapter 4 Polyanionic dendritic polyglycerol as novel broad-spectrum virucidal antivirals

This chapter focuses on a novel class of virucidal agents: polyanionic dendritic polyglycerols. The findings result in the following paper, from which most of the chapter is taken from.

E. Mohammadifar+, M. Gasbarri+, V. Cagno, K. Achazi, C. Tapparel, R. Haag\*, F. Stellacci\*, “Polyanionic amphiphilic dendritic polyglycerols as broad-spectrum viral inhibitors with a virucidal mechanism”, *submitted*.

+ EM and MG contributed equally to this work.

In addition, the invention is part of the patent application PCT/EP2021/071188 filed 28 July 2021, claiming the priority of EP20 188 654.6, filed 30 July 2020 entitled “Sulfated and sulfonated dendritic polyglycerols and use thereof as broad-spectrum virucidal agents”. The inventors of this patent are Matteo Gasbarri, Ehsan Mohammadifar, Francesco Stellacci and Rainer Haag, and the patent is co-owned by EPFL and FUB (Free University of Berlin).

The whole work was conceived by Ehsan Mohammadifar and prof. Rainer Haag from FUB and prof. Francesco Stellacci and myself from EPFL. FUB was responsible of the synthesis and chemical characterization of the compounds while the biological assays were performed at EPFL by myself. DNA assays were performed at University of Geneva with a collaboration between myself and Valeria Cagno under the supervision of prof. Carolin Tapparel.

## 4.1 Abstract

Heparin has been known to be a broad-spectrum inhibitor of viral infection for close to 70 years. This non-toxic biocompatible polymer efficiently binds to many types of viruses and prevents their attachment to cell membranes. Many heparin-like compounds have been developed through the years; however, the reversible nature of the virus inhibition mechanism has prevented their translation to the clinic. *In vivo* such mechanism requires the unrealistic maintenance of the concentration above the binding constant. Recently, we have shown that the addition of long hydrophobic linkers to heparin-like compounds renders the interaction irreversible while maintaining the low-toxicity and broad-spectrum activity. To date, such hydrophobic linkers have been used to create heparin-like gold nanoparticles and beta-cyclodextrins. The former achieves nanomolar inhibition concentration on a non-biodegradable scaffold. The latter, on a fully biodegradable scaffold, show only micromolar inhibition concentration. Here we show that the addition of hydrophobic linkers to a new type of scaffold (dendritic polyglycerols) creates biocompatible compounds endowed with nanomolar activity. Furthermore, we present an in-depth analysis of the molecular design rules needed to achieve irreversible virus inhibition. The most active compound (dPG-5) shows activity against HSV-2 and RSV (a proof-of-principle for broad-spectrum) while keeping low-toxicity. In addition, we demonstrate that

the virucidal activity is leading to the release of viral DNA upon interaction between the virus and our polyanionic dendritic polymers. We believe that this paper will be a stepping stone towards the design of a new class of irreversible non-toxic broad-spectrum antivirals.

## 4.2 Introduction

COVID-19 pandemic has clearly evidenced the need of the world for effective antivirals, especially broad-spectrum ones. In fact, only the latter will have a reasonable probability to show efficacy against the next emerging (pandemic) virus. Indeed, new viruses can emerge or re-emerge every 3-5 years<sup>3</sup>. As recently shown by SARS-CoV-2 and previously by Influenza H1N1 and H5N1, Ebola and Zika new or re-emerging viruses are very different, thus a first line of defense can only be a broad-spectrum antiviral.

Approved antivirals are designed to interfere with one of the viral replication steps mostly intracellular. By design, these drugs are virus specific. Already in the 50's approaches to identify broad-spectrum antiviral were developed<sup>135</sup>. They started by the discovery that heparin was able to inhibit a large number of viruses,<sup>136-137-118</sup> because of its ability to mimic heparan sulfates, a key moiety of the cell-membrane glycans bound by a truly large number of viruses<sup>138-139-39</sup>. Heparin binds to the virus, it prevents viral attachment to the cell membrane hence it stops the first step in the replication mechanism<sup>140-116-47</sup>. Since the initial discovery, a large number of heparin-like compounds has been developed. They show broad-spectrum efficacy and very limited toxicity<sup>48-141</sup>. The variety in terms of chemical motifs is truly large, ranging from polymers, to dendrimers, nanoparticles, liposomes, monoclonal antibodies, and small molecules<sup>142-52-65-143-144-145-146-147-147-148</sup>. Yet, none of them has been translated into a drug and many of them show high anticoagulant activity as heparin itself<sup>55</sup>. The main limitation lies in the mechanism itself. Their mechanism is virustatic, *i.e.* it is based on reversible binding between the virus and the compound. Virustatic compounds are competitive binding inhibitors meaning that the inhibition of the infectivity is lost upon dilution in body fluids when the virus-compound complex is dissociated and, consequently, infective viruses are released. Such a dilution effect, however, is a common event, especially *in vivo*. Recognizing such limitations, some virustatic compounds have been tried in clinical trials as topical drugs, but have failed<sup>149</sup>. To the best of our knowledge the only commercial product based on similar concept is VivaGel from Starpharma<sup>150</sup>.

We have recently reported two novel classes of heparin-like compounds that, as expected, are broad-spectrum entry inhibitors with low-toxicity profiles, but importantly due to their molecular architecture are capable of irreversibly inhibiting viral infection, *i.e.*, virucidal. Specifically, we showed that that virucidal non-toxic broad-spectrum antivirals could be achieved by adding multiple 11-mercapto undecan-sulfonate (MUS) moieties to gold nanoparticles (AuNPs)<sup>67</sup> as well as to  $\beta$ -cyclodextrins (CDs)<sup>68</sup>. AuNPs showed virucidal activity against a broad range of viruses at nanomolar concentration but they raise concerns about gold bio-accumulations. Conversely CD overcame this issue having an organic core that should be biodegradable, but they showed activity only in the micromolar range. By changing the core from Au NPs to CDs there was a loss of 3 orders of magnitude in affinity *in vitro* as well as less efficacy *in vivo*, probably due to a lower number of ligands present on the single macromolecule (7 vs  $\sim 100$ ). Therefore, a biocompatible core with a higher number of ligands presented on the surface would be a suitable alternative to gold nanoparticles.

Dendritic polyglycerols (dPG) with a flexible and globular architecture offer multiple hydroxyl groups on the surface for further functionalization to present ligands multivalently<sup>47-151-152</sup>. We have established dPG as a highly biocompatible polymer platform for multivalent presentation of ligands that can

adhere to pathogen surfaces<sup>153-154</sup>. In addition, we have recently designed multivalent nano-systems that are highly potent but yet reversible<sup>52-152-155-156</sup>.

Here we report on a novel class of broad-spectrum antiviral compounds based on biocompatible cores that are virucidal (irreversible) with nanomolar affinity against HSV-2 and RSV. Thus, we show the possibility to achieve high affinity while retaining irreversible inhibition on a fully organic core.

Herein, we hypothesize that dPG-sulfate has a virustatic mechanism of multivalent virus inhibition, while functionalization of dPG with C<sub>11</sub> alkyl chain having sulfate/sulfonate end groups makes the compounds virucidal against different viruses. The virucidal activity was confirmed measuring the release of viral DNA upon interaction with dPGs, proving the disruption of viral membrane and capsid thus proving the irreversibility of the inhibition. This new antiviral strategy combines potent multivalent inhibitors with the membrane disrupting hydrophobic segments on a soft (not-shape persistent) and biocompatible dendritic platform.

### 4.3 Result and discussion

A library of antiviral multivalent dendritic polymers has been synthesized through the chemical modification of dendritic polyglycerols (dPGs) as a soft globular core to compare with the previously presented shape persistent virucidal compounds having a rigid nanogold core<sup>67</sup>. In Table 1 we present the chemical structure and the physicochemical characterization (ligand density and surface charge) of the dPG conjugates that we have prepared and that we will discuss in the paper.

The syntheses were performed starting from dPG synthesis through slow monomer addition for ring opening multi-branching polymerization of glycidol (fig. 2.11)<sup>157-60</sup>. In the next step, functionalization of dPG was carried out based on three synthetic methods including thiol-ene click reaction, nucleophilic substitution or ring opening functionalization. dPG with molecular weight of 10 kDa and 5 nm of hydrodynamic diameter, comparable with Au NPs of our recent study<sup>67</sup>, has been used for further functionalization. First, the hydroxyl groups of dPG were functionalized by allyl bromide resulting in a platform (dPG-allyl) that can be further modified by thiol-terminated ligands via UV initiated thiol-ene click chemistry (fig. 2.13). In order to compare the effects of end-functional groups and ligand density, dPG was modified with 11-mercapto-1-undecanesulfonate with three different functionalization degrees (dPG-1, dPG-2 and dPG-3) (fig. 2.15). In a similar method 11-mercapto-1-undecanol was reacted to 50 % of allyl groups on the dPG-allyl and the remaining allyl groups were quenched by adding 1-propanethiol. The end hydroxyl groups were then converted to sulfate groups through the reaction with sulfur trioxide pyridine complex to obtain dPG-4 (fig. 2.19). Moreover, in a simple and gram-scale synthetic method the dPG with molecular weight of 10 kDa was modified with 11-Bromo-1-undecanol through the nucleophilic substitution of bromine followed by sulfation of both types of hydroxyl groups located directly on dPG or at the end of C<sub>11</sub> alkyl chain (dPG-5) (fig. 2.21). By reaction of dPG and 1-bromoundecane, dPG-6 was synthesized as a control for dPG-5 to understand the importance of sulfate groups located on the end of the C<sub>11</sub> alkyl chain (fig. 2.24). Finally, dPG-7 and dPG-8 with a short carbon chain through the ring opening reaction with 1,3-propanediol cyclic sulfate and 1,4-butane sultone, respectively (fig. 2.27). For the detailed synthesis and characterization methods see the supporting information.

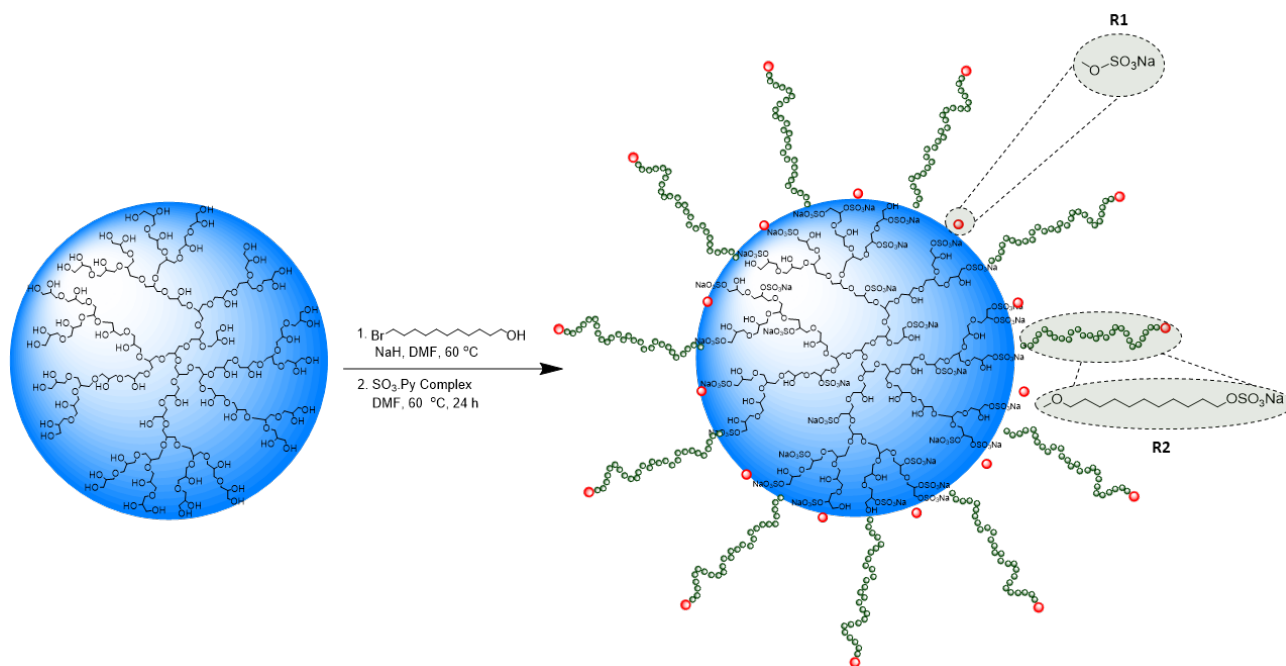
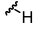
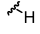
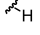
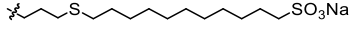
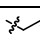
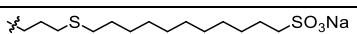
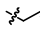
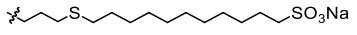
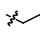
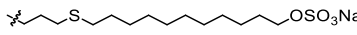
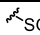
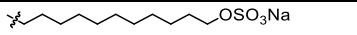
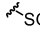
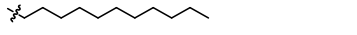
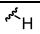
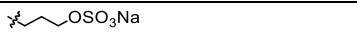
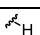
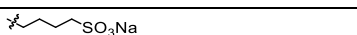


Figure 4.1 – **Schematic structure of functionalized dendritic polyglycerols (dPGs).** In the scheme the ligands shown are for the most active compound (dPG-5). The ligands structures (R1 and R2) for other compounds are shown at Table 1.

Initially, the inhibitory effect of surface functional groups of dPG on the antiviral and virucidal activity against HSV-2 were studied. The antiviral activity was evaluated via a standard *in vitro* dose-response assay pre-incubating the compound with a fixed concentration of HSV-2 for 1 hour and then infecting Vero cells to determine the inhibition of infectivity compared to an untreated control. Virucidal activity was evaluated pre-incubating the compound at a fixed concentration with the virus and then diluting the solution. We then calculated the viral titer and compared it to an untreated control. As commonly done in literature,<sup>67-68</sup> when the inhibition was retained upon dilution, the compound was defined virucidal (irreversible inhibition), otherwise it was defined as virustatic (reversible inhibition). We investigate the different structural designs of dPG attempting to reveal structure-activity correlations both for antiviral inhibition (EC<sub>50</sub>, the effective concentration at which we have a 50% inhibition) and for the mechanism of action (reversible/virustatic or irreversible/virucidal).

The ample chemical variability that the dPG backbone allows was used to address fundamental questions that were left open in previous works in virucidal heparin-like compounds. First, we started by investigating the relationship between the compound's terminal group and their ability to have an irreversible inhibition on the viruses. We designed two compounds that differed solely in the terminal groups placed after the alkyl chains, one was a sulfonate (dPG-2) and the other a sulfate (dPG-4). The basic idea was that all two groups would lead to negatively charged dPG that could electrostatically interact with the virus, but while the sulfate of dPG-4 would be a great mimic of heparan sulfate proteoglycan (HSPG) the sulfonate of dPG-2 would be a less optimal mimic. First, we compared the effective inhibitory concentration (EC<sub>50</sub>), that is related to the binding affinity<sup>63-64</sup>. The sulfate and sulfonate functionalized-dPGs showed strong inhibition of cell infection against HSV-2 (EC<sub>50</sub> between 1 and 10 µg/mL) but without a major difference. Both showed a strong virucidal effect. Thus, we concluded that a strong HSPG mimic is not needed in these types of compounds.

Table 4.1 – Structures of the ligands, charge density and the *in vitro* inhibitory efficacy of dendritic polymers against HSV-2. \* Degree of functionalization and number of ligands is measured by <sup>1</sup>H-NMR. † Ligand density (ligands/nm<sup>2</sup>) was calculated on the basis of the assumption that the dPGs are spheres. The number of ligands is divided by the surface area of a dPG molecule. ‡ Effective concentration to have 50% antiviral inhibition. n.a. not assessable at tested concentrations.

Compound	R1	R2 (Functionalization %)	Ligand density <sup>†</sup>	charge density (mV)	EC50 <sup>‡</sup> (μg/ml)	EC50 (nM)	Mechanism
dPG			0	-7	n.a.	n.a.	n.a.
dPG-1		 (2%)	0.05	-10	n.a.	n.a.	n.a.
dPG-2		 (50%)	0.86	-25	8.9	307	Virucidal
dPG-3		 (85%)	1.45	-27	22	550	Virucidal
dPG-4		 (50%)	0.86	-24	1.2	34	Virucidal
dPG-5		 (50%)	0.86	-42	0.16	4.5	Virucidal
dPG-6		 (40%)	0.69	-21	0.6	28	Virucidal
dPG-7		 (30%)	0.51	-29	58	2900	Virustatic
dPG-8		 (70%)	1.20	-27	37	1480	Virustatic

Once we established the need for alkyl sulfate/sulfonates to achieve a virucidal effect we tried to determine the other design parameters in the molecules needed to achieve optimal inhibition concentration as well as good virucidal activity. First, we studied the effect of the ligand density. We synthesized sulfonated hyperbranched polyglycerol (dPG-1, dPG-2, dPG-3) bearing a C<sub>11</sub> sulfonated alkyl chain with different ligand density and tested against HSV-2. We determined the number of ligands through <sup>1</sup>H NMR measurements and assumed a spherical shape for dPG with ~ 5 nm diameter. The average ligand density was calculated by dividing the number of ligands by surface area. As shown in Table 1, the bare dPG and the dPG-1 with 0.05 ligand/nm<sup>2</sup> (~4 ligand per one dPG) do not show any antiviral activity in the range tested. However, the strong viral inhibition and virucidal activity of compounds dPG-2 and dPG-3 with higher ligand density (0.86 and 1.45 ligands/nm<sup>2</sup> respectively) illustrates the importance of the density of binding groups to achieve a good inhibitory activity.

The effect of decoration of sulfate groups on the dPG was tested. We placed the sulfate groups at the end of the alkyl chain (dPG-4) or directly on dPG surface (dPG-6) or a combination of both cases (dPG-5). The results showed that in all cases the compounds had good inhibitory concentration and were virucidal. However, dPG-5 showed a very potent activity compared to dPG-4 and dPG-6 which could be due to the high negative surface charge originating from the large number of sulfate groups the dPG-5. To test whether the hydrophobic feature and the recognition functional group could be decoupled we designed a dPG having a short sulfate group and a long alkyl chain (dPG-6). Importantly, dPG-6 showed antiviral and virucidal activity against HSV-2 revealing that both functionalities are necessary to achieve irreversible inhibition but they do not necessarily need to be on the same ligands. This finding allows for a drastic simplification in the chemical approaches to achieve non-toxic virucidal anti-viral compounds.

Finally, we investigated the effect of alkyl chain length on inhibitory activity and mechanism. We synthesized dPG-7 and dPG-8 with three-carbon sulfated and four-carbon sulfonated alkyl chains with a simple synthetic approach. In stark contrast with what observed on AuNPs, we observed a strong effect of chain length on the inhibitory concentration that was lowered to the micromolar range when using shorter alkyl chains. As previously observed on nanoparticles and cyclodextrins, the compounds with shorter alkyl chains had solely a reversible inhibition of the viral infectivity. Indeed, infectivity regained its original value upon dilution. These results are consistent with our previous publications,<sup>67-68</sup> showing the necessity of a longer hydrophobic alkyl chain for achieve a virucidal (irreversible) inhibition mechanism.

To examine the broad-spectrum inhibition activity of our best antiviral candidate, dPG-5 was tested against HSV-2 and RSV. The compound showed a very potent antiviral activity, with an EC<sub>50</sub> in the nanomolar range for both viruses. Anticipating a potential topical respiratory use, the toxicity of the compound was evaluated on different mammalian cell lines (VERO, HBE, A549). The CC<sub>50</sub> was found to be between 190 and 900 µg/ml, thus resulting in a remarkable selectivity index (SI) in the range of 1200 and 5920 for RSV considering using three cell lines for toxicity tests.

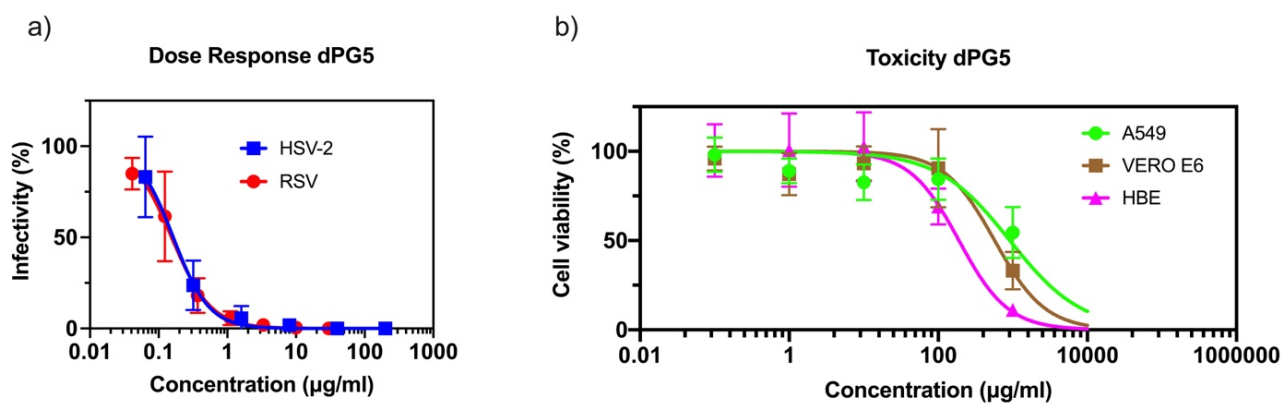


Figure 4.2 – **Antiviral activity and toxicity profile of dPG5.** a) *In vitro* activity of dPG-5 against HSV-2 (blue) and RSV (red). dPG-5 shows an antiviral activity with an EC<sub>50</sub> respectively of 0.16 µg/ml and 0.15 µg/ml. b) , the cell viability of dPG-5 against three different cell lines. Data from 2 independent experiments performed in duplicates.

As shown in fig. 4.2.a-b, dPG-5 has a virucidal mechanism against both RSV and HSV-2. In the case of RSV, 1.2 log reduction were detected, while for HSV-2 a complete inhibition was kept upon dilution (5.5 log reduction), in line with what we have previously shown for CD and AuNPs.

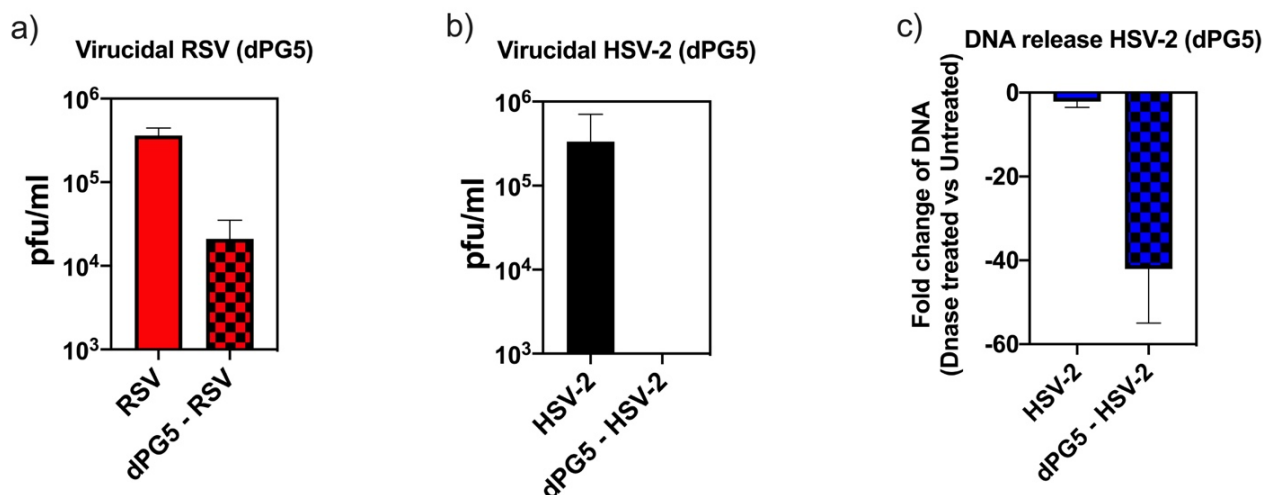


Figure 4.3 – **Virucidal activity and DNA release assay for dPG-5.** Virucidal activity of dPG-5 against RSV (a) and HSV-2 (b). In both cases we show the viral titer after 1h incubation with 300 µg/ml of dPG-5. Graph c) show DNA release assay: HSV-2 was incubated in the presence or absence of dPG-5 (µg/ml) for 1 hour at 37°C and then incubated for 30 min with Turbo DNase or only buffer and subsequently subjected to qPCR. Results are expressed in fold change of DNase treated versus untreated. Data from 2 independent experiments performed in duplicates. Shown mean + SD.

The real nature of the interaction that leads to an irreversible inhibition mechanism is still under investigation. Clearly the hydrophobic linkers damage the membrane of the virus they interact with, but they do so quite slowly<sup>26</sup> thus a simple effect due to the amphiphilic nature of the ligands is hard to justify. In the case of modified beta-cyclodextrin,<sup>27</sup> we used a DNA release assay to show that the viral capsid also loses its integrity because DNA is released upon interaction of the compounds with the HSV-2 virus. To prove that this effect is common to this class of compounds, we performed the same DNA test for dPG-5. Briefly, after incubation of HSV-2 with or without dPG-5, the solution is treated with DNase to digest accessible DNA. qPCR is then performed to quantify the difference in undigested viral DNA between the solution with and the one without antiviral compound. In fig. 3c we show the difference in fold-reduction between DNase-treated or untreated solution. In case of dPG-5, a 40-fold reduction is detected, meaning that the dPG-5 is able to lead to the loss of integrity of the capsid, making the viral DNA accessible for enzymatic degradation. This data confirms the ability of virucidal dPG-5 to irreversibly inactivate the virus and shows that the results previously found for modified beta-cyclodextrins are of broader significance.

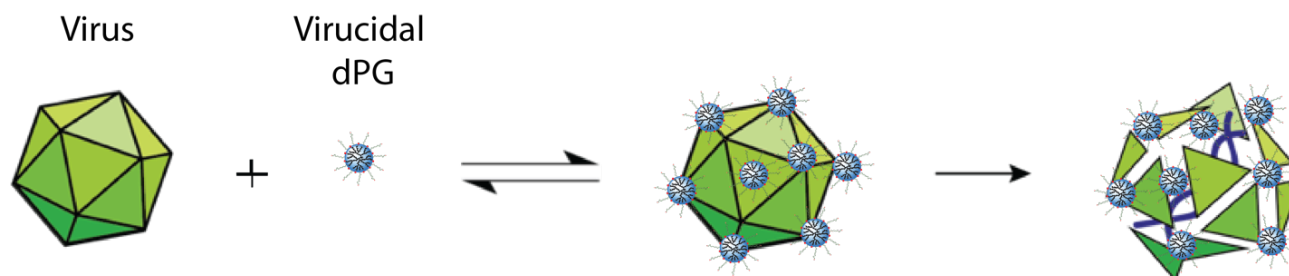


Figure 4.4 – **Schematic representation of the virucidal mechanism of action** (envelope is not represented for clarity). dPG first interacts with the virion and then leads to an irreversible step that disrupts the capsid causing the release of viral DNA.

#### 4.4 Conclusion

We have shown a novel class of compounds based on biocompatible dendritic polyglycerol that combine a nanomolar activity against HSV-2 and RSV, with a virucidal (irreversible) mechanism of action without significant cell-toxicity. Specifically, in this paper we present the most potent heparin-like antiviral with a virucidal effect published to date (dPG-5). Importantly we show that the chemical moiety need to bind to the virus (sulfate or sulfonate in this case) can be decoupled to the one needed to have a virucidal inhibition (alkyl chains). The versatility of our chemical design has allowed us to synthesize a library of branched polymer structures and establish that in order to have a strong and irreversible inhibition it is necessary to have a sulfate or sulfonate groups, in order to mimic the attachment receptor of viruses. The combination of a long hydrophobic chain and sulfate/sulfonate group leads to a virucidal mechanism. The irreversibility on the inhibition, conferred by the alkyl chain, was shown to result into the accessibility of viral DNA to enzymatic degradation, hence it is due to permanent damage not only to the envelope but also to the capsid. Finally, we have presented systematic studies on a new amphiphilic dendritic polyglycerol.

# Chapter 5 Novel virucidal candidate against SARS-CoV-2

This chapter discusses a different functionalized dendritic polyglycerol respect to chapter 4, able to irreversibly inhibit SARS-CoV-2.

This invention is part of the patent application PCT/EP2021/070990 filed on the 27<sup>th</sup> of July 2021, claiming the priority of EP20 188 654.6, filed on the 30<sup>th</sup> of July 2020 entitled “Virucidal compositions and use thereof”. The inventors of this patent are Matteo Gasbarri, Ehsan Mohammadifar, Francesco Stellacci and Rainer Haag, and the patent is co-owned by EPFL and FUB.

The whole work was conceived by Ehsan Mohammadifar and prof. Rainer Haag from FUB and prof. Francesco Stellacci and myself from EPFL. FUB was responsible of the synthesis, chemical and physico-chemical characterization of the compounds while I performed the the biological assays and optimised the use of the compounds as an antiviral at EPFL.

## 5.1 Abstract

The development of new vaccines against SARS-CoV-2 has given a tremendous help in the fight against COVID-19 pandemic. Yet, herd immunity is far from being achieved and the circulation of new variants has risen concerns given the lower efficacy of the current vaccines on the novel strains. Currently, no specific drug for the treatment of SARS-CoV-2 is available. Different candidates are undergoing clinical trials, with a focus on repurposed drugs. Entry inhibitors are valid candidates to develop broad-spectrum antivirals. Here, we report a preliminary study on a carboxylate dendritic polyglycerol as virucidal antiviral against SARS-CoV-2 and HSV-2. Such compound shows antiviral activity at the nanomolar range combined with an irreversible mechanism of action. Other structures are also investigated, in order to better understand the key features of such compound. So far, no carboxylated compounds showed such results against SARS-CoV-2, and this unexpected result is discussed. A preliminary *in vivo* study is also presented, supporting the antiviral activity of the carboxylate dendritic polyglycerol.

## 5.2 Introduction

As already discussed in section 3.1.2, in the search for possible antivirals against SARS-CoV-2, entry inhibitors were investigated. Different classes of compounds were proposed, with a strong focus on antibodies, nanobodies or peptides<sup>158–160</sup>. Little attention was given to nano/supramolecular entry inhibitors, from which possible candidates were proposed<sup>62,161</sup>. In particular, HSPG mimicking compounds have been foreseen as possible antivirals given the interaction of SARS-CoV-2 with these receptors<sup>123</sup> (of notice, in our own experiments, heparin did not inhibit viral entry). Different sulfonated and sulfated compounds were proposed against SARS-CoV-2, among which MUS:OT AuNPs and CD-MUS, as already largely discussed in Chapter

3. None of the compounds of interest showed a virucidal activity, with MUS:OT AuNPs and CD-MUS showing only a virustatic activity against SARS-CoV-2.

To deepen our understanding of this lack of virucidal activity, we have investigated other structures such as the sulfated and sulfonated dendritic polyglycerols discussed in Chapter 4. These compounds were able to inhibit SARS-CoV-2, but, similarly to AuNPs and CD-MUS, none of them were virucidal.

Because the driving force for such inhibition is an electrostatic interaction between the sulfate/sulfonate group of the compounds and the virus, we have challenged this idea, testing a different functionalized dendritic polyglycerol. The compound, later called dPG-C-10-COO, is composed of the same dPG core, but modified with a long aliphatic chain terminated with a carboxylic acid. Such functional group has a higher pKa compared to the sulfate and sulfonate groups, so the compound has a higher zeta potential. Ideally, such compound would be an adequate negative control to show that the charge present on the other compounds was key to determine the inhibition, yet not sufficient to determine the virucidal inhibition in case of SARS-CoV-2.

Surprisingly, dPG-C-10-COO (fig. 5.1) showed an inhibition activity at the nanomolar range, with a virucidal activity (2log viral titer reduction) against SARS-CoV-2, resulting, so far, the only virucidal antiviral against SARS-CoV-2.

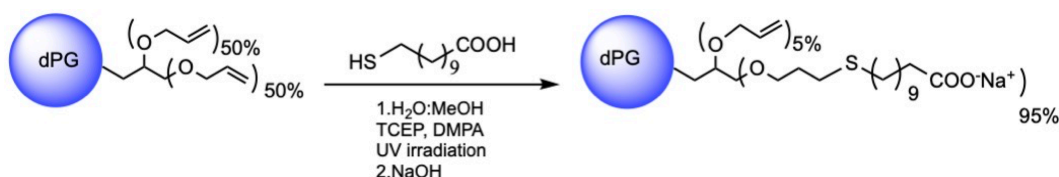


Figure 5.1 – **Reaction scheme of dPG-C10-COO.** Starting from a dPG-allyl, a 11-mercapto-undecanoic acid react via click reaction catalyzed via UV in order to obtain a fully functionalized dPG.

### 5.3 In vitro results

Here, we present a compound composed by a dendritic polyglycerol core, modified to expose long hydrophobic chain that terminates with a carboxylic acid functionality (fig. 5.1). The compound is structurally similar to dPG-2 (Chapter 4), with the only difference being the functionalization with a carboxylate terminal group instead of a sulfonate terminal group. The core is the same as the dPG discussed throughout chapter 4 and the functionalization route very similar.

First, we tested its possible cytotoxic effect, given its lower solubility compared to its sulfonate analogue. However, dPG-C10-COO, showed no cytotoxicity on Vero cells in the range of interest, as reported in fig. 5.2.

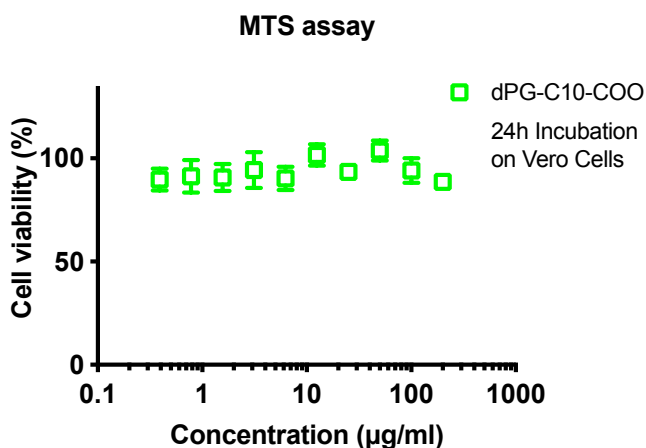
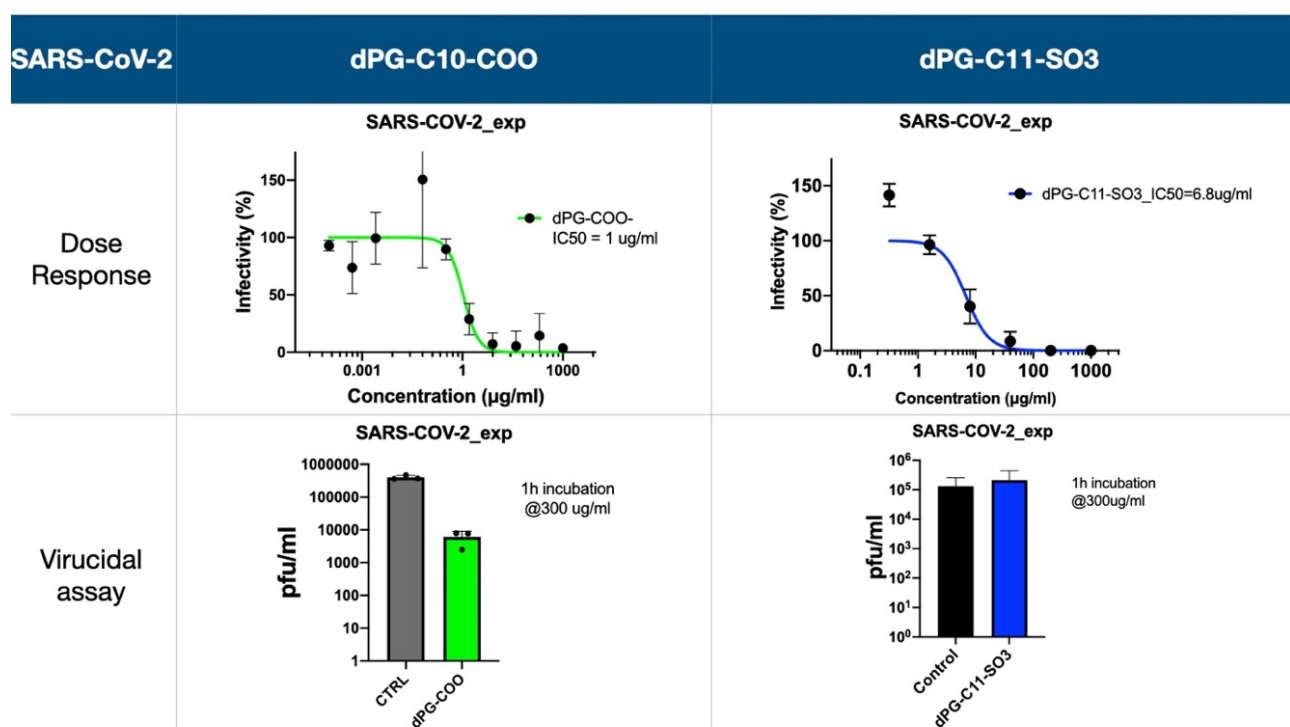


Figure 5.2 – **Cell viability assay of dPG-C10-COO.** MTS assay is performed on Vero cells. (24h incubation). Cell viability expressed as percentage relative to the untreated control.

dPG-C10-COO was then tested *in vitro* for its capability of inhibiting SARS-CoV-2 and compared to dPG-2, its sulfonated analogue. dPG-C10-COO showed a very similar IC<sub>50</sub> compared to dPG-2. In fact, as reported in table 5.2, dPG-C10-COO has an IC<sub>50</sub> of 1 µg/ml that converts to a value of 33nM, against 6.8µg/ml for its sulfonated counterpart. Such result was surprising since, in our knowledge, there are no report showing entry inhibitors against SARS-CoV-2 in the nanomolar range.

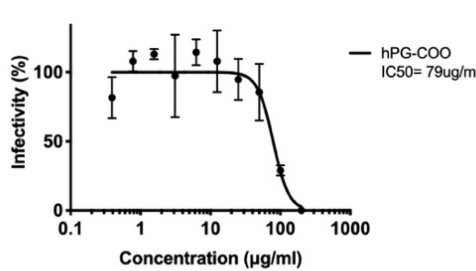
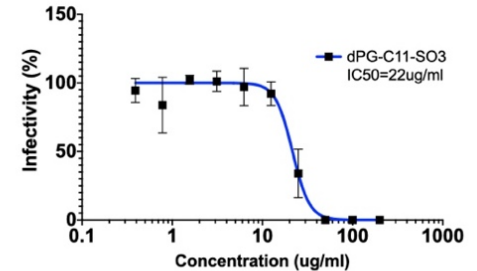
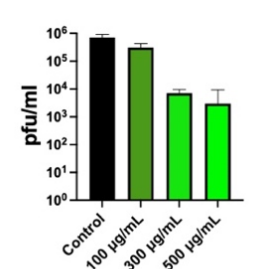
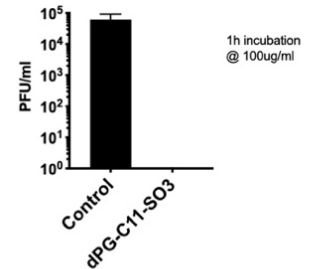
Furthermore, while all the other sulfated/sulfonated compounds failed to show virucidal activity, as already thoroughly discussed in chapter 3, dPG-C10-COO showed a clear irreversible viral inhibition. In fact, when SARS-CoV-2 was incubated with 300µg/ml of dPG-C10-COO, 2 log reductions were detected compared to the untreated control. In case of dPG-2, no irreversible inactivation could be measured.

Table 5.1 – **Antiviral activity of dPG-C10-COO and dPG-C11-SO<sub>3</sub> against SARS-CoV-2.** Both compounds showed an inhibition against SARS-CoV-2, with the carboxylate dPG resulting more efficient than sulfonate one. Surprisingly, while dPG-C10-COO showed a virucidal inhibition mechanism, dPG-C11-SO<sub>3</sub> showed a solely virustatic.



In order to further assess the antiviral activity of dPG-C10-COO, the compound was tested against HSV-2 and compared to dPG-2 (data from all the other dPG are reported in table 4.1). The compound was able to inhibit HSV-2 with a virucidal mechanism but at higher concentration compared to dPG-2, so less efficiently, as reported in table 5.2. Such behavior could be probably due to the different dissociation constant (K<sub>d</sub>) between the carboxylic groups of the dPG and the viral proteins, that was yet lower but still present, resulting in a higher IC<sub>50</sub> compared to the sulfonated counterpart (4 times higher). Such results validate dPG-C10-COO as valid broad-spectrum virucidal antiviral.

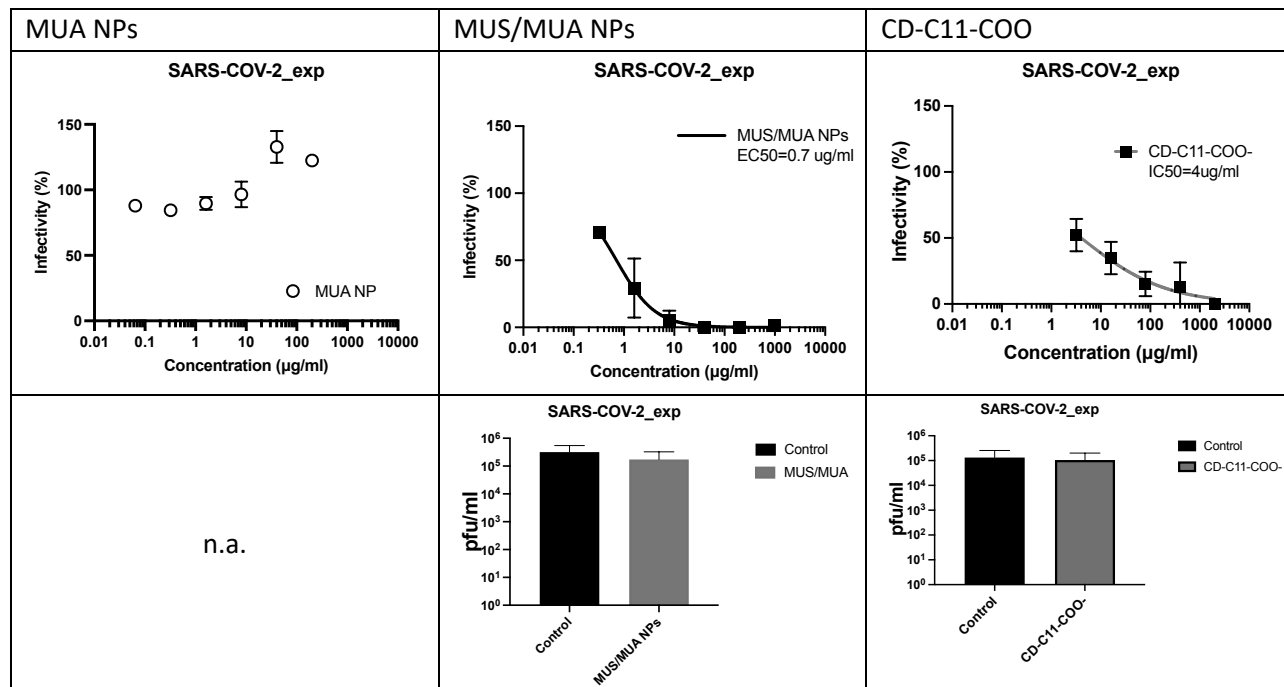
Table 5.2 – **Antiviral activity of dPG-C10-COO and dPG-C11-SO<sub>3</sub> against HSV-2.** Both the compounds showed an inhibition against HSV-2, with the sulfonate dPG more activity than the carboxylate one. However, both the compounds showed a virucidal mechanism of inhibition.

HSV-2	dPG-C10-COO	dPG-C11-SO <sub>3</sub>
Dose Response	<p>HSV-2 exp</p>  <p>hPG-COO IC<sub>50</sub>= 79µg/ml</p>	<p>HSV-2_exp</p>  <p>dPG-C11-SO<sub>3</sub> IC<sub>50</sub>=22ug/ml</p>
Virucidal assay	<p>Virucidal HSV-2</p>  <p>pfu/ml</p> <p>Control 100 µg/mL 300 µg/mL 500 µg/mL</p>	<p>HSV-2_exp</p>  <p>PFU/ml</p> <p>Control dPG-C11-SO<sub>3</sub></p> <p>1h incubation @ 100ug/ml</p>

Trying to better elucidate the role of carboxylic acid in the virucidal behavior, we have synthesized and tested different compounds bearing the same functionality. In particular, we assessed the antiviral properties of AuNPs bearing mercapto-undecanoic acid (MUA) or a mix MUA/MUS (synthesized by Francesca Olgati and Heyun Wang) and cyclodextrins, modified in similar manner, so exposing a hydrophobic chain of 11 carbon atoms, terminating with carboxylic acid (synthesized by Paulo J. H. Silva). In table 5.3 all the results are reported.

MUA NPs did not show any inhibition in the concentration tested. Conversely, as shown in chapter 3, the addition of MUS rendered them antiviral, but with a virustatic mechanism. This is in agreement with our data on MUS:OT AuNPs. Last, CD-C11-COO displayed an antiviral behavior but in a reversible manner.

Table 5.3 – **Dose-response and virucidal assays against SARS-CoV-2 of different modified CD and AuNPs.** Results from gold nanoparticles covered by 11-mercapto-undecanoic acid (MUA) and a mixture of MUA and 11-mercapto-undecansulfonate (MUS) and beta-cyclodextrins modified in order to bear undecanoic acid. In the first row a dose-response curve is reported (N=1, technical duplicates), while in the second row virucidal assay are reported (1h incubation, 300µg/ml, N=1, technical duplicates).



In addition, different other structures of dPG were investigated. In fig. 5.4, two dendritic structures are reported: Z2 and Z9. Z2 is a dPG modified with a shorter hydrophobic chain (3 carbon atoms) terminated with a carboxylic acid. Z2 do not show any inhibition against SARS-CoV-2. Such result is in agreement with our previous results reported in chapter 4, where shorter linker result in a lower affinity probably due to a higher water solubility. Z9 has instead a slightly different core, synthesized reacting 2-hydroxypropane-1,2,3-tricarboxylic acid with glycerol. Such dendritic structure exposes different carboxylic groups, but did not show any inhibition against SARS-CoV-2.

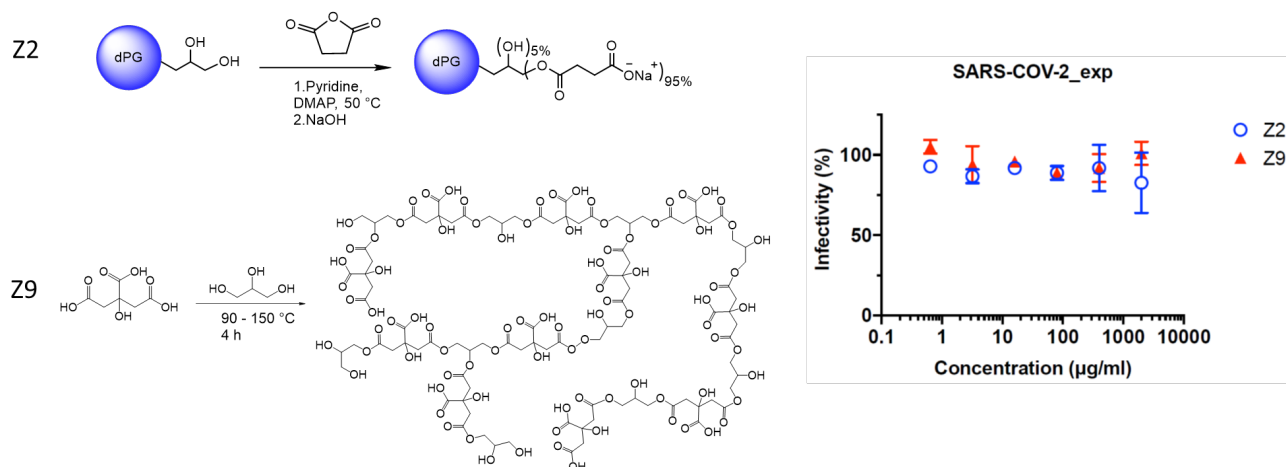


Figure 5.3 – **Structures and antiviral activity of two different carboxylate dendritic polymers.** On the left, chemical structure of Z2 and Z9, two different dendritic structures. Z2 is a dPG modified with a short 3 carbon atoms linker terminated with a carboxylic acid. Z9 is a dendritic structure synthesized reacting 2-hydroxypropane-1,2,3-tricarboxylic acid with glycerol. On the right, viral inhibition against SARS-CoV-2 is reported. No inhibition has been detected up to 2mg/ml.

dPG-C10-COO is therefore the only compound that, so far, showed a nanomolar inhibition and virucidal behavior against SARS-CoV-2. Such antiviral properties were further confirmed in a post-treatment setting. In such experiment, no pre-incubation between the virus and the compound is performed, but the compound is directly added onto pre-infected cells. The viral titer of the supernatant of treated cells is then quantified and compared to an untreated control. Ideally, an effective antiviral would diminish the viral titer compared to the control. The results for dPG-C10-COO against SARS-CoV-2 are reported in fig. 5.3. The incubation of the infected cells over 2 days with 100 µg/ml of dPG-C10-COO resulted in a titer reduction over 3 logs, confirming its antiviral activity.

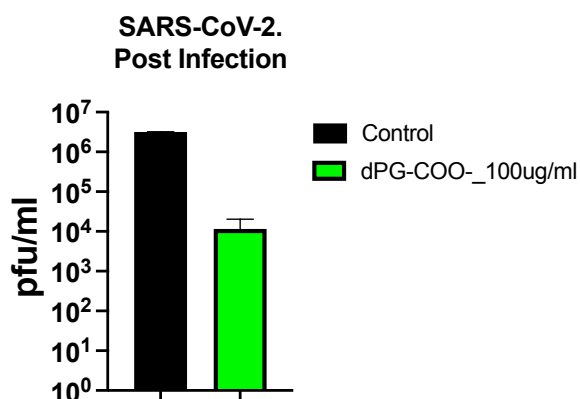


Figure 5.4 – Post-infection assay of dPG-C10-COO against SARS-COV-2. More than 2 log in viral titer reduction can be detected compared to an untreated control.

## 5.4 In vivo results

Given the results obtained *in vitro*, we designed a first *in vivo* study to confirm the feasibility of such compound as valid antiviral against SARS-CoV-2. In collaboration with prof. Desmecht from University of Liege, we used hamster as animal model, on the basis of previous publication<sup>162</sup>. The rationale of the study was to challenge the compound as possible treatment via intranasal administration. In particular, the study was designed as follow.

5 groups of 5 mice were formed. First group was daily inoculated with PBS for 5 days via intranasal route, with no infection. Second group (Placebo) was infected with SARS-CoV-2 at day 0 and then, 12h post-infection, treated daily for 5 days with PBS via intranasal route. Third group was infected with SARS-CoV-2 at day 0 and then, 12h post-infection, treated daily for 5 days with dPG-C10-COO via intranasal route with 1.5mg/kg/day dose (low dose). Forth group was infected with SARS-CoV-2 at day 0 and then, 12h post-infection, treated daily for 5 days with dPG-C10-COO via intranasal route with 4.5mg/kg/day dose (medium dose). Last group was our positive control for which we used MK-4482 (molnupiravir), formulated as reported in Rosenke et al. with a dose of 250mg/kg/day. In this case, hamsters were treated via oral administration once a day.

As can be seen in fig. 5.4, the control group increased its weight during the 15 days, showing no effect due to neither the anesthesia nor the intranasal administration of PBS. The placebo group, that was infected but received just PBS for 5 days, had instead a strong body weight loss up to day 6, after which it recovered, regaining its original weight at day 12. The body weight loss averaged around 20% at day 6. The positive control group, that received MK-4482, had a much less evident body weight loss, reaching a maximum of 10% at day 6, and steadily regaining weight from day 7 on. For what concern the two groups that received dPG-C10-COO, we detected a dose-response behavior. In fact, the low dose shows no antiviral effect, with the body weight curve basically overlapping with the placebo group. The medium dose group, that received 3 times the dose of the low-dose group, showed a significant difference compared to the placebo. In fact, while the weight loss up to day 6 is similar to the placebo group, the recover seems to be accelerated

by the administration of dPG-C10-COO. In fact, between day 6 and day 10, the body weight loss is significantly lower than the placebo group, indicating a possible positive effect due to the compound.

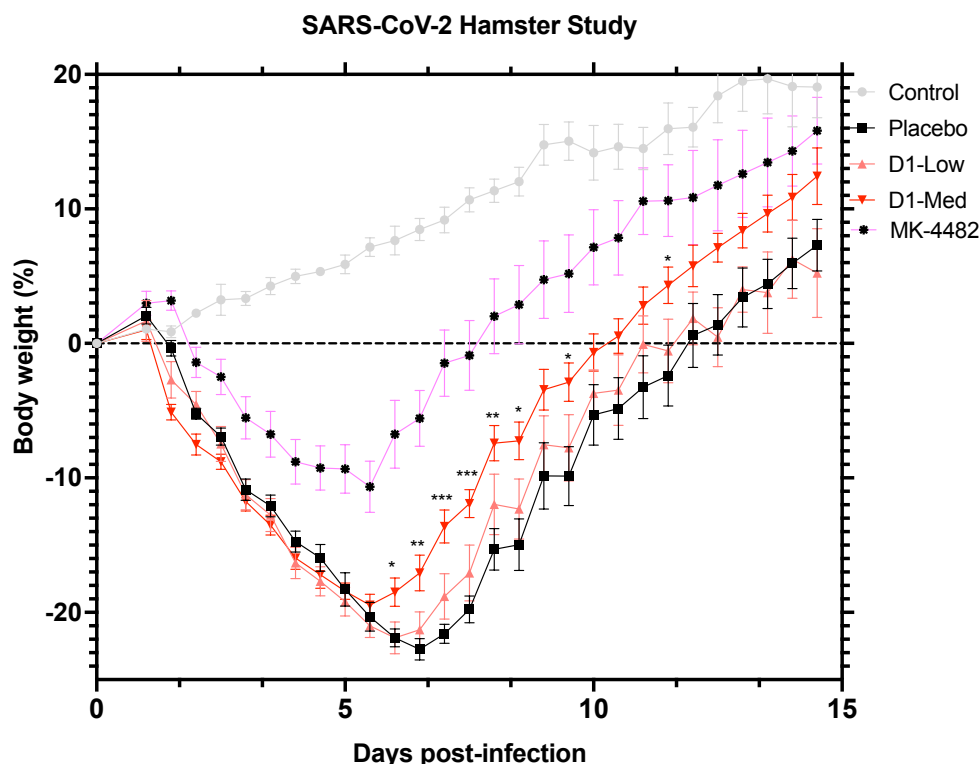


Figure 5.5 – Results of the *in vivo* experiments against SARS-CoV-2 in hamster. On the y-axis is reported the relative change in body weight (%) every twelve hours, while on the x-axis the days post-infection.

Other histopathology studies have been performed at the end of the study on the animals, but on day 14, no significant differences were possible to be detected since all the animals completely recovered from the infection. For example, no viral genomic loads nor viral infection loads could be detected in any animal of the study. Of notice, no detrimental effects given by possible toxicity were detected, supporting the safeness of the compound.

## 5.5 Conclusions

The data reported in this chapter supports the possibility of employing dPG-C10-COO as possible virucidal antiviral against SARS-CoV-2. Different possibilities were explored to determine the factors playing a key-role in such features, but yet no clear explanation has been formulated. More investigations need to be performed in this direction in order to have a better understanding of the system. Identifying the chemical design features that made such compound virucidal compared to the other virustatic ones, would enable us to improve our design and get a deeper knowledge of the system. Molecular dynamic simulations may help to determine the actual interaction between the compound and the virus and what makes the carboxylate different compared to the sulfate/sulfonate modifications. Such crucial information may enable us to improve the antiviral efficacy of this compound.

Indeed, the results from the *in vivo* experiments are a first step in its translation, but higher doses need to be tested in order to determine its maximum efficacy and tolerability.



# Chapter 6 Other antiviral strategies: from filters to surfaces

This chapter focuses on antiviral strategies different from drugs that would prevent the spreading of viral infections. Paragraph 6.2 of this chapter is partly taken from:

- A. Palika, A. Armanious, A. Rahimi, C. Medaglia, M. Gasbarri, S. Handschin, A. Rossi, M. Pohl, I. Busnadi-ego, C. Gübeli, R. Anjanappa, S. Bolisetty, M. Peydayesh, S. Stertz, B. Hale, C. Tapparel, F. Stellacci, R. Mezzenga, “An anti-viral trap made of protein nanofibrils and iron oxyhydroxide nanoparticles”, *Nature Nanotechnology* (2021) DOI: 10.1038/s41565-021-00920-5

The project was led by the group of prof. R. Mezzenga, in particular by Archana Palika and Antonius Armanious. My contribution was focused on the characterization of the filter against SARS-CoV-2.

## 6.1 Abstract

Minimizing the spread of viruses in the environment is the first defence line when fighting outbreaks and pandemics, but the current COVID-19 pandemic demonstrates how difficult this is on a global scale, particularly in a sustainable and environmentally friendly way. Here, we report two different technological solutions that could play a role in diminishing viral spreading. First, we introduce and develop a sustainable and biodegradable antiviral filtration membrane composed of amyloid nanofibrils made from food-grade milk proteins and iron oxyhydroxide nanoparticles synthesized in situ from iron salts by simple pH tuning. Thus, all the membrane components are made of environmentally friendly, non-toxic and widely available materials. The membrane has outstanding efficacy against a broad range of viruses, which include enveloped, non-enveloped, airborne and waterborne viruses, such as SARS-CoV-2, H1N1 (the influenza A virus strain responsible for the swine flu pandemic in 2009) and enterovirus 71 (a non-enveloped virus resistant to harsh conditions, such as highly acidic pH), which highlights a possible role in fighting the current and future viral outbreaks and pandemics. Second, we report an initial study on the design and testing of antiviral surfaces. The idea is to translate our concept of broad-spectrum antivirals from compounds to surfaces, having surface modification that render them capable of inactivating viruses. Different strategies are explored and discussed, going from self-assembled monolayers (SAMs) to graphene coatings. The results were not successful but let us refine and optimize both the testing system and the future developments.

## Introduction

This thesis focuses on novel broad-spectrum antivirals, with the idea of designing possible novel drugs. The aim is to develop on the long-term medications, so preventive or curative formulations that would be used in humans to prevent or cure certain diseases.

As briefly discussed in Chapter 1, viruses use very different routes to spread from an infected person to uninfected ones going from droplets<sup>163</sup> to fomites<sup>164</sup>, from wastewater<sup>165</sup> to direct contact. The prevention

of the transmission would be therefore a key defense strategy against viral diseases. This was particularly clear during the pandemic during which the use of masks, gloves, barriers or hand-hygiene were the first measures to counter-act the spreading of the virus.

In this chapter we propose two technological solutions that would be beneficial in reducing the spread of viral disease: antiviral filters and antiviral surfaces. The antiviral filter proposed, discussed in paragraph 6.2, is designed to filter bulk water and it would be extremely beneficial in the treatment of wastewater or to eliminate pathogens from water in an easy and efficient way. The antiviral surfaces studied could be instead surface treatment to reduce infectivity from fomites in highly-touched surfaces such as touchscreens, doorknob, etc. Our approach is discussed in paragraph 6.3.

## 6.2 Anti-viral filter

The group of prof. Mezzenga at ETH developed an antiviral membrane trap composed of amyloid nano-fibrils obtained from a food-grade milk protein,  $\beta$ -lactoglobulin (BLG), modified in situ with iron oxyhydroxide nanoparticles (NPs). The resulting membrane is thus composed of food-grade components and shows no toxicity on experimentally treated cell lines, as demonstrated by cytotoxicity tests.

The filtration membrane trap was tested by filtering water that contained respectively three different types of enveloped viruses: (1)  $\Phi 6$ , an enveloped bacteriophage that infects *Pseudomonas syringae* bacteria and is often used as a surrogate of human enveloped viruses, (2) H1N1, an influenza A virus strain responsible for the swine flu pandemic in 2009 and (3) SARS-CoV-2, the coronavirus strain responsible for the ongoing COVID-19 pandemic. The infectious virus concentrations went from  $\sim 10^6$  PFU ml<sup>-1</sup> before filtration to below the detection limit after filtration for all three viruses. No remarkable effect on the infectivity of the viruses was observed when filtering the viruses through the cellulose support or the BLG AF alone, which suggests a unique synergetic effect of the BLG AF-Fe membranes. By quantifying the viral genomes, which indicate the total number of viruses (both infectious and non-infectious), before and after filtration (Fig. 6.2), we observed that most of the viruses were retained on the membrane material. Still, for H1N1 and SARS-CoV-2, a detectable amount of genomes passed through the filter. It is, however, important to reiterate that the infective viruses in the filtrate were below the detection limit for both viruses.

Further assessment of the virucidal effect of the membrane was conducted by attempting to recover the  $\Phi 6$  viruses retained on the membrane filter. This was done by incubating the membrane material used for  $\Phi 6$  filtration in a beef buffer of pH 9.3—beef buffer has often been used to recover viruses adsorbed to iron oxides.

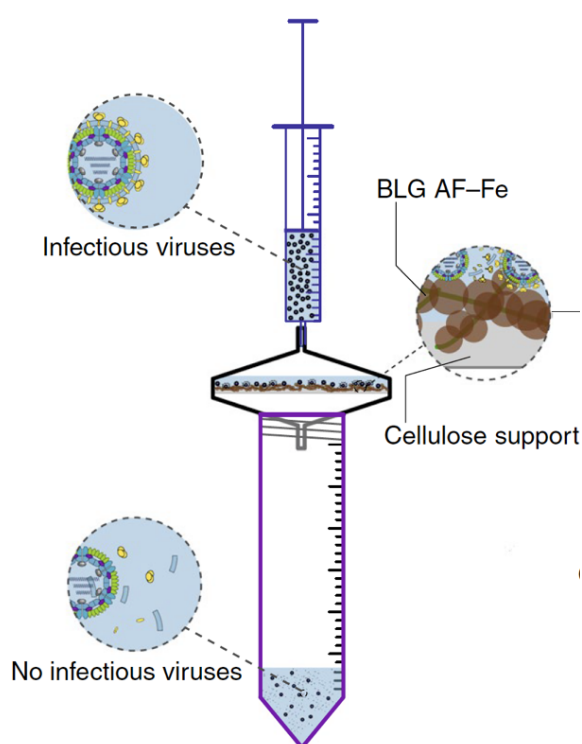


Figure 6.1 – Schematic of the experimental filtration set-up.

Keeping in mind the challenges of an efficient recovery of adsorbed viruses and potential damage to the virus in that process, we still observed a pronounced decrease in the ratio of infective to total viruses from 0.05 for the filtered solution to as low as  $8.8 \times 10^{-4}$  of the recovered viruses. This observation provides additional evidence that the viruses not only adsorb to the membrane but also are mostly inactivated.

In order to better elucidate the mechanism of inactivation, different experiments were run. In particular,  $\Phi 6$  viruses were incubated with a suspension of BLG AF–Fe hybrids in PBS buffer for one hour followed by assessing the infectivity of the viruses. No infective  $\Phi 6$  viruses were detected in the solution at the end of the incubation time. These results show that virus elimination during filtration cannot be attributed to simple retention on the filter material due to small pore sizes, that is, by size exclusion: indeed, no change in the  $\Phi 6$  infectivity was observed in control experiments when the viruses were incubated with BLG AF or Fe NPs alone. The reduction in infective viruses in solution started to become noticeable when the viruses were incubated with BLG monomer–Fe; still it was neither as effective nor as reproducible as incubation with BLG AF–Fe hybrids.

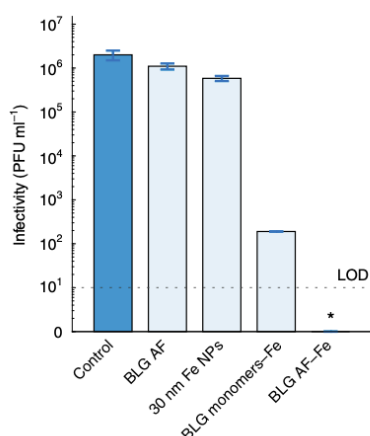
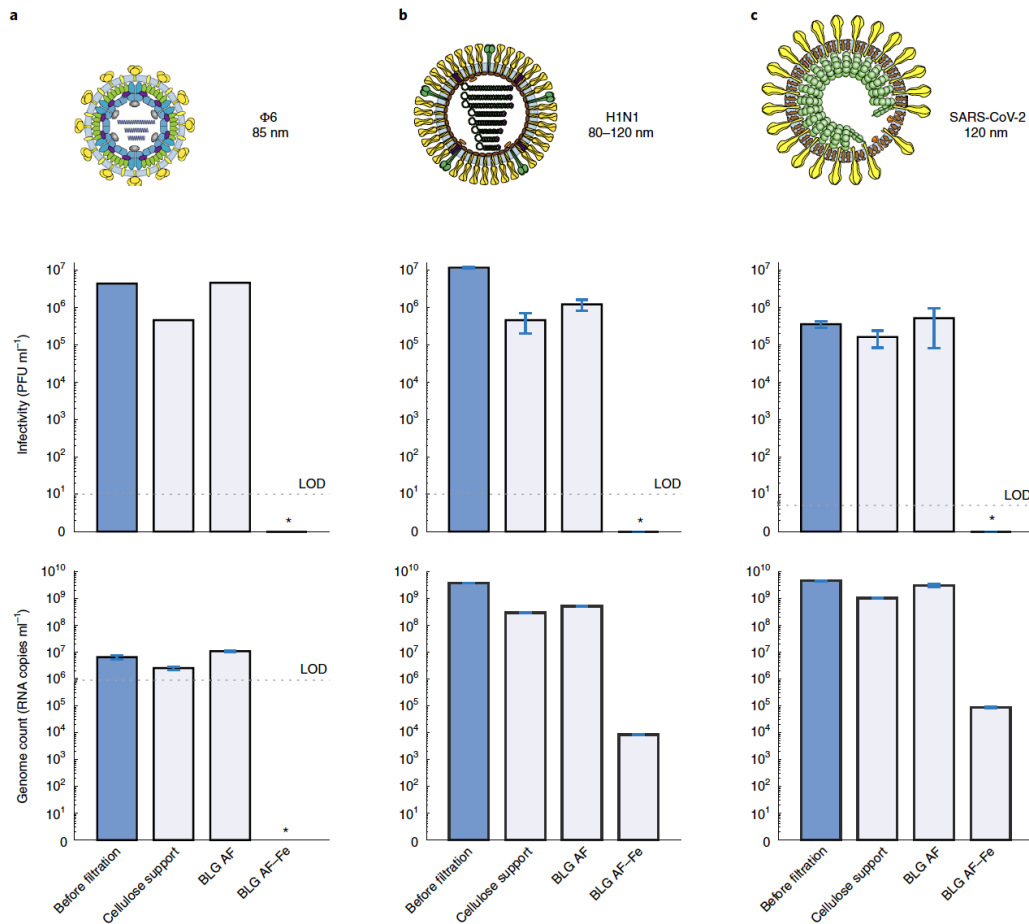


Figure 6.2 – Infectivity of  $\Phi 6$  after 1 h of incubation with BLG AF, 30 nm Fe NPs, BLG

Our results, indeed, confirm that the Fe NPs, the BLG monomer–Fe and BLG AF–Fe are all positively charged at physiological pH values, whereas literature values show that H1N1 and the spike protein of SARS-CoV-2 are both negatively charged at physiological pH values. What is critically important, however, is the surface-to-volume ratio at which these surfaces become available: the 30nm Fe NP control had no virucidal effect on  $\Phi 6$ , the BLG monomer Fe had a noticeable, partial effect and only BLG AF–Fe had an outstanding effect. The BLG AF provide an intricate network template that supports the formation of an Fe coating a few nanometers thick onto their elongated surface, that is, at a remarkably higher surface-to-volume ratio than that offered by the spherical geometry of Fe NPs and BLG monomer–Fe NPs.

In summary, we have shown the general and broad efficacy of AF–Fe membranes against both enveloped and non-enveloped viruses, which include key viruses such as SARS-CoV-2, H1N1 and EV71. The membrane introduced in this work is made by combining two widely available, food-grade components: AFs obtained by fibrillization of the milk protein BLG on which iron oxyhydroxide NPs are synthesized in situ from iron salts by simple pH changes, in a straightforward fabrication procedure. This is an antiviral filtration membrane made entirely by biosourced and biodegradable components. When combined with the outstanding virucidal properties of the membrane and the inactivation of the virus within it, these characteristics may allow a disposal of used membranes that is safe for both humans and the environment. Taken together, these results make this technology of immediate importance to mitigate current and future viral pandemics, as well as to address worldwide clean water challenges associated with pathogens.



**Figure 6.3 – Elimination of infectious enveloped viruses for water filtered through BLG AF-Fe membranes.** a–c, Complete elimination of infectious viruses and the corresponding reduction in the genome count for Φ6 (a), H1N1 (b) and SARS-CoV-2 (c) when filtered through BLG AF-Fe membranes (blue, before filtration; grey, after filtration). A limited or no elimination was observed when filtering the same viruses through the cellulose support or the BLG AFs alone. The lower value of the genome count of Φ6 than that of the other two viruses is probably due to both a higher ratio of infectious viruses to genome count than those of the other two viruses and also the low efficiency of the genome extraction from these phages (Supplementary Table 2). Φ6 infectivity represents the plaque count from one plate of a series of dilutions that consist of at least three plates. A replicate of the Φ6 filtration experiment for which the infectivity was calculated using three technical replicas is shown in Supplementary Fig. 3. The genome count for Φ6 represents the average of four technical replicas and the error bars represent the standard deviation (s.d.). The infectivity and genome count of H1N1 as well as the genome count of SARS-CoV-2 represent the average of two technical replicas and the error bars represent the range. The infectivity of SARS-CoV-2 represents the average of four technical replicas and the error bars represent the s.d. LOD, limit of detection; \*below the LOD. Representations of the virions are reproduced from pictures on ViralZone

### 6.3 Anti-viral surfaces

The role of fomites in spreading viral disease is very well known<sup>164</sup>. During COVID-19 pandemic an extremely large sets of measures such as the use of gloves, the continuous disinfection of the surfaces or the hand disinfections were in place to limit the contagiousness of highly-touch surfaces such as doorknobs, cash, public transportation handles, touchscreens etc. In case of SARS-CoV-2, such measures resulted to be of limited impact<sup>166-167</sup>, with CDC confirming these hypothesis in April 2021 “...because of the many factors affecting the efficiency of environmental transmission, the relative risk of fomite transmission of SARS-CoV-2 is considered low compared with direct contact, droplet transmission, or airborne transmission”<sup>168</sup>. Indeed, for other viruses, such as enteric viruses, the role of fomites in the transmission is still major.

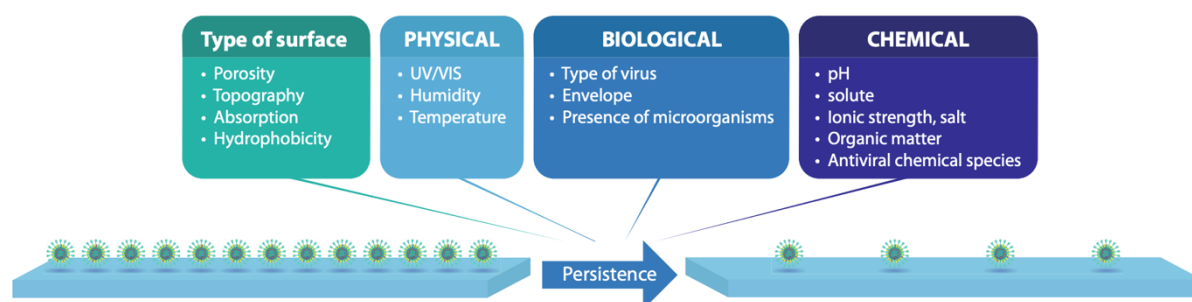


Figure 6.4 – **Surface properties influencing the persistence of viruses.** These include physical properties (including light exposure, temperature and humidity), chemical properties (such as pH or antiviral coatings) and biological properties (depending on the virus vulnerabilities, e.g., an envelope) as well as the type of surface such as the porosity or topography. Adapted from Rakowska et al. (2021) with permission<sup>169</sup>.

However, during the last year, different reviews and papers were published investigating different strategies and technologies that could be exploited in the design of novel antiviral strategies<sup>170-169</sup>. A very comprehensive and complete work from Rakowska et al. discusses the different parameters influencing the viral inactivation and the different properties of a surface that could reduce the viral persistence on fomites, as shown in fig. 6.4. Before the pandemic, little research has been devoted to the design and understanding of antiviral surfaces, while more interest has been placed in antimicrobial surfaces, surfaces with treatments or agents that inhibit the growth of microorganisms. In early 2000, some seminal works on antiviral surfaces from Klibanov group were published, employing polymers as antiviral coatings and discussing the role of charges and hydrophobic moieties. In addition, different testing protocols were thoroughly discussed<sup>171-99</sup>.

In our group, during the last year, we have started a whole new project on antiviral surfaces. The idea was to translate our concept of designing novel broad-spectrum antivirals from compounds to surfaces. Following the same route, we envisioned a surface modification based on hydrophobic plus sulfate/sulfonate groups that would act as a sponge for the virus leading to an irreversible de-activation. To assess the antiviral properties of the surface/coating, we have optimized different assays, starting from<sup>99</sup>. More details can be found in Chapter 2, but the key idea is to incubate a certain viral inoculum on the surface for a certain amount of time and with certain conditions and later quantify its viral titer compared to an appropriate control. We have performed all preliminar tests with HSV-2 due to its easy access in the lab (BSL2, compared to BSL3 for SARS-CoV-2) and its extensive use in our study with HSPG mimics. Indeed, it can be used as a model for enveloped viruses. After a preliminar screening, we have assessed its efficacy also against SARS-CoV-2.

First, we have produced self-assembled monolayers (SAMs) on gold substrate, employing the same molecule we used to cover gold nanoparticles, 11-mercapto-undecansulfonate (MUS). In fig. 6.5, in green, the results of its viral de-activation against HSV-2 after 2h incubation are shown. No activity was detected compared to bare gold substrate. Given the results on MUS SAMs, we decided to test a silane, modified to expose a similar structure as MUS, so undecansulfonate (US). In such a way, the silane would be covalently bonded to the silicon oxide wafer. Indeed, as shown in fig. 6.5, in blue, the Silane-US, did not reduce the viral titer of HSV-2 compared to the bare silicon wafer, thus showing no antiviral activity.

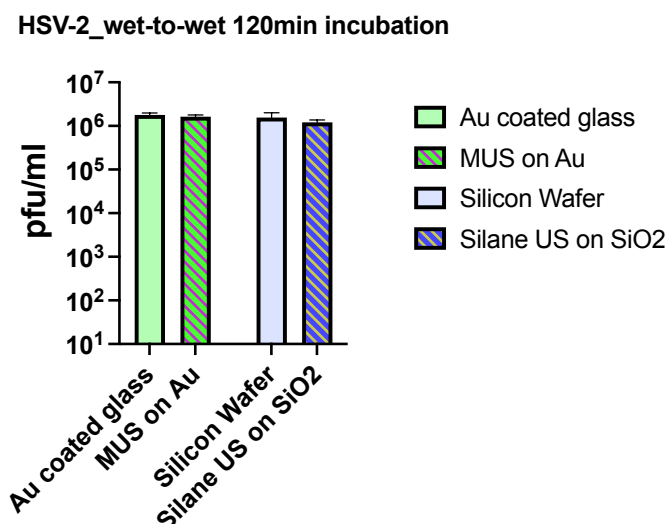


Figure 6.5 – **Antiviral assay of MUS coated surfaces against HSV-2.** Test were performed following a wet-to-wet protocol (120min incubation time). In green, results from a self-assembled monolayer (SAM) of MUS on a gold surface, compared to a pristine gold surface. In blue, results from a modified silane with undecane-sulfonate that modifies a silicon oxide wafer.

### 6.3.1 Graphene-based surfaces

In collaboration with prof. Ferrari, at University of Cambridge, we have tested the capability of graphene to inactivate viruses on surfaces. The hypothesis was to produce coatings made of functionalized-graphene. In particular, the graphene should have been functionalized with hydrophobic, sulfonate/sulfate moieties. In our vision, such structure could capture and eventually inactivate viruses on the surface. Graphene would be an ideal platform given its outstanding properties among which the electrical conductivity, a key feature envisioning applications on conductive surfaces such as touch-screens.

The production of the graphene coating, performed by Jeremiah Marcellino in University of Cambridge, was based on spray-coating. A graphene oxide solution was in fact directly sprayed on the substrate of interest and subsequently annealed on a hot plate at 250°C. The low-temperature of the annealing lead us to explore both hard substrate such as glass or plastic substrate such as PEEK.

The graphene oxide solution contains also sodium-dodecyl benzenesulfonate (SDBS), a surfactant composed of a long hydrophobic chain and a terminal sulfonate

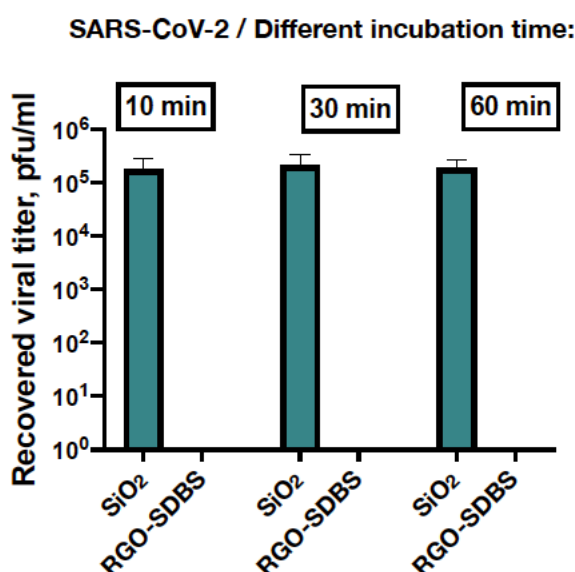


Figure 6.6 – **SARS-CoV-2 inactivation by RGO-SDBS surfaces, at different time-points.** Complete inactivation can be detected after just 10 minutes.

group. In our vision, SDBS should covalently bond to graphene oxide during the annealing step, during which the graphene undergoes to a reduction, becoming reduced graphene oxide (RGO). Such coating will be later called RGO-SDBS. Raman spectroscopy confirmed the oxidation state of graphene, but further XPS studies should confirm the SDBS reaction. The surfaces were then tested against SARS-CoV-2 in a wet-to-wet protocol, assessing the ability of the coating to inactivate the virus at different time point. The results were striking. After just 10 minutes of incubation, the viral titer was below the limit of detection, 5 log reduction compared to a pristine silicon oxide wafer. Same results were produced for HSV-2 (not shown here). However, two important facts were noticed during the experiments: a) during the incubation with the inoculum, the coating released some particles b) when this happened, the cells on which the virus was then titrated showed some toxicity. Starting from this, we have designed further controls to better understand our initial results. The idea so to evaluate the role of SDBS alone and the effect of the annealing on its properties and the role of RGO alone. Indeed, we have rinsed RGO-SDBS with MilliQ water before the test to remove eventual residues present on the coating. We have then prepared and compared for their antiviral activity against both SARS-CoV-2 and HSV-2: PEEK substrate alone, PEEK substrate coated with just SDBS and annealed at RT, PEEK substrate coated with just SDBS and annealed at 250°C, PEEK substrate coated with just RGO, PEEK substrate coated with RGO-SDBS and last, PEEK substrate coated with just RGO-SDBS rinsed with MilliQ.

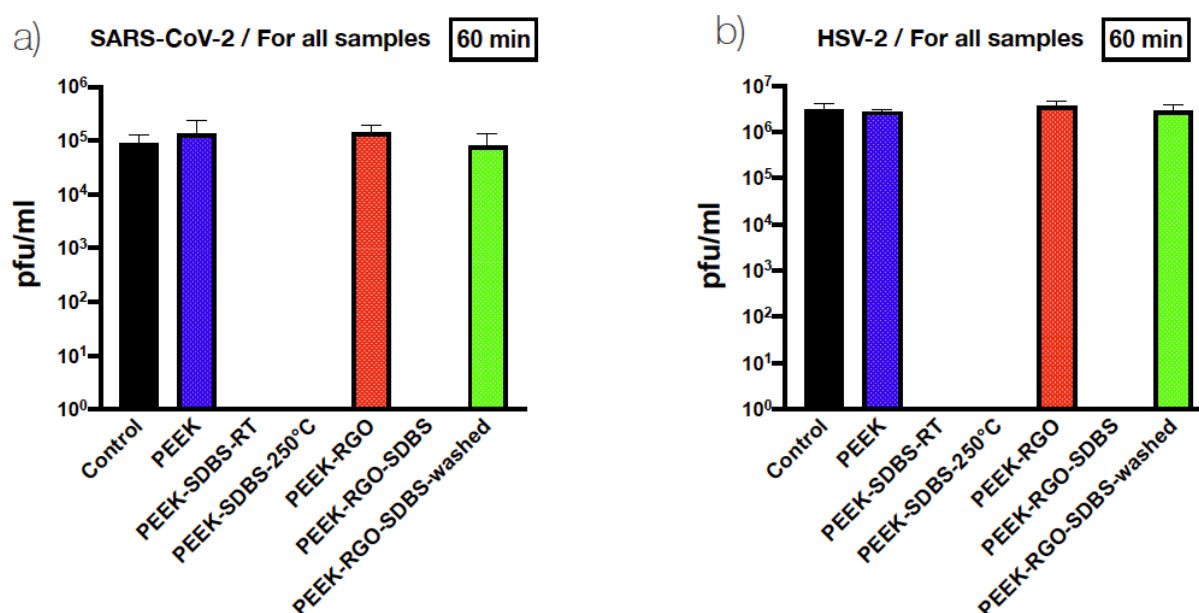


Figure 6.7 – **SARS-CoV-2 and HSV-2 inactivation by different surfaces.** Results from wet-to-wet protocol (60 min incubation time) assessing the antiviral properties against SARS-CoV-2 (a) and HSV-2 (b) of PEEK samples covered by RGO and SDBS and different controls. In order the samples are as follow. Control: viral stock. PEEK: substrate. PEEK-SDBS-RT: substrate spray coated with a SDBS solution and annealed at room temperature. PEEK-SDBS-250°C: substrate spray coated with a SDBS solution and annealed at 250°C. PEEK-RGO: substrate spray coated with a GO solution and annealed at 250°C. PEEK-RGO-SDBS: substrate spray coated with a GO-SDBS solution and annealed at 250°C. PEEK-RGO-SDBS-washed: PEEK-RGO-SDBS rinsed with MilliQ before the test. Viral titers are shown

The overall results are presented in fig. 6.7. First of all, there is no difference between SARS-CoV-2 and HSV-2, showing an activity independent from the virus. Second of all, it is clear that there is no effect given by RGO, but it is all due to SDBS alone, independently from the annealing temperature. In addition, and this last control explains the mechanism of inactivation we were measuring, if we first wash the RGO-SDBS before the test, the antiviral activity is completely lost. This result proves that the activity we were assessing was due just to the release of unreacted SDBS, that we recall it is a surfactant, that was inactivating the viral inoculum. To further challenge this hypothesis, we have measured the conductivity of the water in which the RGO-SDBS substrate was immersed: if SDBS was released from the coating, being charged would increase the conductivity. In fig.

6.8 the results are shown: a clear increase in conductivity is detected during the first minutes, reaching a plateau soon after. This data confirms our hypothesis that the inactivation of the virus was just given by release of SDBS in the inoculum and not by the coating itself.

This project was clearly not a success but helped us to design and optimize the different testing protocols to assess the efficacy of antiviral surfaces to deactivate viral inoculum. In addition, the process of understanding our mistakes and misjudgments helped us to clarify the key features and properties to address in designing an antiviral surface with our approach. These developments were the basis for the next steps of the project that are currently developed in our research group.

## 6.4 Conclusions

In this chapter, we have presented other strategies and technological solutions that could help in the prevention and control of viral spreading. The first approach is based on a filter made of amyloid fibers and iron nanoparticles that is able to reduce the viral titer of liquids of more than 4 log. The antiviral filter shows efficacy against different viruses such as SARS-CoV-2, Influenza, EV71. Such device could be used to treat water and wastewater reducing the spreading of different diseases caused by waterborne viruses. The second part of the chapter is focused on antiviral surfaces, so surfaces capable of inactivating viruses upon contact. This approach could be of extreme help in limiting the role of fomites, such as highly-touch surfaces, in the spreading of viral disease. We report different strategies and approaches that lead us to define and refine our routes towards the design of efficient antiviral surfaces.

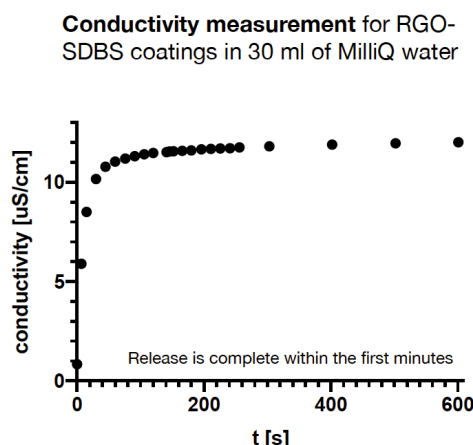


Figure 6.8 – **Conductivity measurement for RGO-SDBS samples in MilliQ water.** SDBS is released in water within the first tens of seconds. After 3 minutes, a plateau is reached.

# Chapter 7 Conclusions and outlook

This final chapter summarizes the results discussed throughout the thesis, providing concluding remarks and proposing possible future developments.

## 7.1 Achieved results

This thesis can be divided in three main areas: further assessing the antiviral capabilities of gold nanoparticles and modified beta-cyclodextrins; development of novel virucidal compounds such as dendritic polyglycerol; investigating other novel antiviral strategies.

Gold nanoparticles covered by a binary shell of MUS:OT were the first system that proved our hypothesis on the design of broad-spectrum virucidal antiviral. Such system was very important to demonstrate both *in vitro* and *in vivo* the feasibility of our strategy. However, since we did not foresee its use as a drug given the presence of the gold core, we have developed a completely organic analogue: CD-MUS. Indeed, in this thesis we further expanded the broad-spectrum activity of both compounds beyond HSPGs-dependent viruses, proving that MUS:OT AuNPs and CD-MUS can irreversibly inhibit influenza and reversibly inhibit VSV and SARS-CoV-2. We have further shown, for CD-MUS, the importance of the hydrophobic linker in the antiviral activity. In addition, we have performed a first pharmacokinetic study, envisioning an intranasal administration of CD-MUS.

In the second part of the thesis, we have shown a novel class of broad-spectrum virucidal antivirals: sulfated/sulfonated dendritic polyglycerol. In this case, we were able to translate on a different core our initial design principle. The core of these compounds is a dendritic polyglycerol, that can be further functionalized with different modifications. The ease in the modification, allowed us to investigate different parameters involved in the antiviral activity such as the degree of functionalization, the length of the linker or the size of the core. Such optimization process allowed us to design the most efficient compound that proved to be effective at the nanomolar range against RSV and HSV-2 with an irreversible mechanism of action. In addition, we proved that such permanent inhibition led to the release of DNA of the virus upon contact with dendritic polyglycerol.

In the search for antivirals against SARS-CoV-2, we have tested sulfated/sulfonated dendritic polyglycerols but all of them show a solely virustatic inhibition, as CD-MUS and MUS:OT AuNPs. Thus, we have modified dendritic polyglycerol with linkers bearing carboxylic acid. Surprisingly, such dPG result to be effective against SARS-CoV-2 at the nanomolar range with a virucidal mechanism of action. Such compound was further assessed for its antiviral activity in a hamster model showing promising preliminary results.

In addition to the development of novel broad-spectrum virucidal antivirals, we have worked on different technological solutions that could prevent and control viral spreading. In particular we have shown the outstanding properties of a filter composed of amyloid fibers and iron nanoparticles in inactivating different viruses such as influenza, EV71, SARS-CoV-2. Moreover, we have shown initial study on the development and testing of antiviral surfaces.

---

## 7.2 Future development

This thesis is part of a much larger project started in our research group almost 10 years ago that has advanced thanks to many researchers and many successful collaborations. In order to better identify future developments, it is important to place this thesis in such context.

The key idea has been thoroughly discussed in Chapter 1 and it is what gives the title to the thesis: developing novel broad-spectrum virucidal antivirals. Starting from virustatic entry inhibitors, we proposed to modify them in such way to render the viral inhibition irreversible, thus making viable drug candidates.

First, we have managed to prove our idea showing the ability of MUS:OT NPs in irreversibly inhibiting different classes of viruses. Such first proof-of-concept confirmed the feasibility of our approach. We were able to identify three key components, required to synthesis a broad-spectrum virucidal antiviral: a multivalent scaffold, a hydrophobic linker and a specific functional group. In this first work, we have further investigated the mechanism of action of our compounds, showing by CryoEM that the interaction of NPs with the virus causes an irreversible disruption of the envelop.

With the aim of further translating such approach to viable drug candidate, we moved from a metallic multivalent scaffold to a fully organic one: beta-cyclodextrins. CD-MUS showed similar results as AuNPs, with the non-trivial result that our approach was confirmed and could be translated to other multivalent cores. In addition, we show that CD-MUS can not only disrupt the envelop, but also the capsid of the virus, having measured the DNA released upon interaction. CD-MUS proved to be a broad-spectrum virucidal antiviral with efficacy *in vivo* against HSV-2.

Being beta-cyclodextrin a valid scaffold, we have modified them with a different functional group respect to sulfate/sulfonate. In fact, in this thesis we focused on viruses that rely on HSPGs, but other families of virus rely on sialic acid. Thus, we modified CD in order to bear a long hydrophobic chain terminating with a sialic acid, that could be simple (SA) or with a more complex architecture (6'SLN). This strategy allowed us to synthesis CD-6'SLN, an extremely potent virucidal antiviral against different strains of influenza, and CD-SA, a similar compound that could enlarge its broad-spectrum capability beyond CD-6'SLN. Such compound confirmed its capability of inhibiting viral infection also in *in vivo* setting<sup>59</sup>.

As shown above, in this thesis we explored a novel core, composed of dendritic polyglycerol. Such sulfated/sulfonate dPGs outperformed CD-MUS *in vitro* resulting to be a viable candidate to perform further study *in vivo*. Indeed, we have investigated more in detail different chemical features crucial to have a virucidal inhibition.

The overall project can now proceed in two different directions. On one hand, we can further investigate the process of irreversible viral Inhibition, on the other hand, we can focus on the translation of the compounds discussed into viable drugs.

The virucidal mechanism of inhibition is the key novelty of our approach. Such irreversible inhibition could allow the translation of broad-spectrum entry-inhibitors into drugs. In fact, as discussed in Chapter 1, the major reason that prevented the translation of virustatic entry inhibitors into efficient drugs, has been the reversible nature of the inhibition process. Our modifications show a clear difference in the inhibition process and provided promising results *in vivo*. However, a head-to-head comparison between similar virustatic and virucidal compounds *in vivo* is missing. Such key experiment could further confirm our hypothesis

---

and validate the approach we are currently developing. Ideally, we could compare in vivo the activity against HSV-2 or RSV of CD-M8S and CD-M9S, the two sulfonated beta-cyclodextrins for which we see the transition from virustatic to virucidal regime. The importance of the virucidal inhibition would be eventually confirmed from such experiment that would also justify the failure in vivo of the previously proposed virustatic drugs.

Regarding the mechanism of inactivation of the virus, we have shown by CryoEM the capability of MUS:OT NPs of disrupting the viral envelop. However, CryoEM can represent just snapshots of the process taken at different timepoints of different virions. Currently, in collaboration with prof. Battaglia at UCL, we are trying to follow the whole process in real time via in situ liquid STEM. Preliminary results show that it is possible to image in real time the disassembly of the virus upon contact with our virucidal compounds, thus providing further information on the kinetics of the process and insights on the mechanism. Molecular dynamic simulation could also provide information on the recognition and disruption mechanism. The actual process of viral disruption, key in the irreversible inhibition, needs to be addressed both experimentally and via simulation. The possibilities to explore are few, but safety limitations due to the use of infective virus are present. Furthermore, a thermodynamic investigation of the process of disassembly of the virus could be of extreme interest in the field of physical virology.

The recognition process between the virucidal compounds and the viral proteins occurs via electrostatic interaction. First insights were proposed via molecular dynamic simulations for AuNPs, but newly developed compounds deserve further investigations, even though the nature of the ligands is similar. Experimentally, such interaction could be studied more in detail by surface plasmon resonance (SPR), identifying the specific interaction of our compounds with each specific membrane protein of each virus.

Apart from more fundamental understanding of the inhibition process, our compounds are ideally drug candidates. The process of translating a drug from a research lab to a clinical trial, and then eventually to the market, is long and with many pitfalls. In fact, after a first validation in vitro, many key steps need to be addressed. At first, the administration route needs to be chosen. For instance, in case of CD-MUS and dPG-5, we have shown activity against, among others, RSV, a respiratory virus, and HSV-2, a genital virus. The application routes are completely different in the two cases: for the first, intranasal administration could be envisioned, being instillation, nebulization or aerosol, while for the second one, a cream or paste needs to be formulated. Even though we postulated a broad-spectrum of activity, one virus needs to be prioritized to further proceed in the development. In fact, such studies are extremely expensive and time-consuming, requiring specific development for each case. Furthermore, in vivo studies in larger animals will require larger amount of compound. Such upscaling of the production will need further optimization of the synthesis and a higher control on each compound. Part of this work has already been performed for CD-MUS, for which large quantity (up to gram-scale) can be reproducibly produced, such as for dPG-5. However, in order to comply to GxP condition (Good X Practices), the synthesis of the compounds need to be contracted out to contract research organizations (CROs) that would produce them in GMP conditions. At this stage, animal experiments would also be run in GLP conditions, in order to be validated as pre-clinical studies. In particular toxicity and pharmacokinetic studies should go along with efficacy study in relevant animal model for the virus of choice. Toxicity will be important to identify the maximum tolerated dose (MTD), crucial to determine the doses relevant in the efficacy study. Of relevance, what can be seen as a “simple” PK study, will require the development of the detection mode for such supramolecular compounds we proposed, that are not small molecules nor proteins. In addition, another toll of complexity comes from the intrinsic polydispersity of structures as dPG, where a spectrum of masses and structures form the mixture of the active compound. In

---

this regard, other molecularly defined structures are being investigated, given their simpler chemical structure that would allow more precise quantifications.

In brief, the journey towards the translation of such virucidal antiviral compounds into drugs is long, complex and demanding, but also challenging and stimulating, with many open questions and lots of work ahead.

## References

1. Bill Gates. The next outbreak? We're not ready. *TedTalk*  
[https://www.ted.com/talks/bill\\_gates\\_the\\_next\\_outbreak\\_we\\_re\\_not\\_ready?language=it](https://www.ted.com/talks/bill_gates_the_next_outbreak_we_re_not_ready?language=it).
2. WHO Covid-19. <https://covid19.who.int/>.
3. Woolhouse, M., Scott, F., Hudson, Z., Howey, R. & Chase-Topping, M. Human viruses: Discovery and emergence. *Philos. Trans. R. Soc. B Biol. Sci.* **367**, 2864–2871 (2012).
4. Graham, B. S. Advances in antiviral vaccine development. *Immunol. Rev.* **255**, 230–242 (2013).
5. Ellebedy, A. H. & Ahmed, R. Antiviral Vaccines: Challenges and Advances. in *The Vaccine Book* 283–310 (Elsevier, 2016). doi:10.1016/B978-0-12-802174-3.00015-1.
6. Pasteur, L. Review: on the shoulders of giants. *Microbes Infect.* **8** (2003).
7. Luis P. Villarreal. Are viruses alive? *Scientific American*.
8. Pearson, H. 'Virophage' suggests viruses are alive. *Nature* **454**, 677–677 (2008).
9. La Scola, B. *et al.* The virophage as a unique parasite of the giant mimivirus. *Nature* **455**, 100–104 (2008).
10. ICTV October 2020 Report. <https://talk.ictvonline.org/taxonomy/>.
11. Baltimore, D. Expression of Animal Virus Genomes. *BACTERIOL REV* **35**, 7 (1971).
12. Sungnak, W. *et al.* SARS-CoV-2 entry factors are highly expressed in nasal epithelial cells together with innate immune genes. *Nat. Med.* **26**, 681–687 (2020).
13. Buzón, P., Maity, S. & Roos, W. H. Physical virology: From virus self-assembly to particle mechanics. *WIREs Nanomedicine Nanobiotechnology* **12**, (2020).
14. Roos, W. H., Bruinsma, R. & Wuite, G. J. L. Physical virology. *Nat. Phys.* **6**, 733–743 (2010).
15. H. Fraenkel-Cornat & Robley C. Williams. Reconstitution of active tobacco mosaic virus from its inactive protein and nucleic acid components. *PNAS* 690–698 (1955).
16. Klug, A. The tobacco mosaic virus particle: structure and assembly. *Philos. Trans. R. Soc. Lond. B. Biol. Sci.* **354**, 531–535 (1999).

17. Mateu, M. G. Mechanical properties of viruses analyzed by atomic force microscopy: A virological perspective. *Virus Res.* **168**, 1–22 (2012).
18. Tang, Z. *et al.* A materials-science perspective on tackling COVID-19. *Nat. Rev. Mater.* **5**, 847–860 (2020).
19. Katherine J. Wu. There are more viruses than stars in the universe. Why do only some infect us? *National Geographic* (2020).
20. Anthony, S. J. *et al.* A Strategy To Estimate Unknown Viral Diversity in Mammals. *mBio* **4**, (2013).
21. David Pride. Viruses Can Help Us as Well as Harm Us. *Scientific American* (2020).
22. Mokili, J. L., Rohwer, F. & Dutilh, B. E. Metagenomics and future perspectives in virus discovery. *Curr. Opin. Virol.* **2**, 63–77 (2012).
23. Anderson, N. G., Gerin, J. L. & Anderson, N. L. Global Screening for Human Viral Pathogens. *Emerg. Infect. Dis.* **9**, 768–773 (2003).
24. Delwart, E. A Roadmap to the Human Virome. *PLoS Pathog.* **9**, e1003146 (2013).
25. Frierson, J. G. The Yellow Fever Vaccine: A History. **9**.
26. Baden, L. R. *et al.* Efficacy and Safety of the mRNA-1273 SARS-CoV-2 Vaccine. *N. Engl. J. Med.* **384**, 403–416 (2021).
27. Polack, F. P. *et al.* Safety and Efficacy of the BNT162b2 mRNA Covid-19 Vaccine. *N. Engl. J. Med.* **383**, 2603–2615 (2020).
28. De Clercq, E. & Li, G. Approved Antiviral Drugs over the Past 50 Years. *Clin. Microbiol. Rev.* **29**, 695–747 (2016).
29. DiMasi, J. A., Grabowski, H. G. & Hansen, R. W. Innovation in the pharmaceutical industry: New estimates of R&D costs. *J. Health Econ.* **47**, 20–33 (2016).
30. Wouters, O. J., McKee, M. & Luyten, J. Estimated Research and Development Investment Needed to Bring a New Medicine to Market, 2009–2018. *JAMA* **323**, 844–853 (2020).
31. Sidwell, R. W. *et al.* Broad-Spectrum Antiviral Activity of Virazole: 1-f8- D-Ribofuranosyl- 1,2,4-triazole-3-carboxamide. *Science* **177**, 705–706 (1972).
32. Bekerman, E. & Einav, S. Combating emerging viral threats. *Science* **348**, 282–283 (2015).

33. Taylor, R. *et al.* BCX4430 - A broad-spectrum antiviral adenosine nucleoside analog under development for the treatment of Ebola virus disease. *J. Infect. Public Health* **9**, 220–226 (2016).
34. Geraghty, R. J., Aliota, M. T. & Bonnac, L. F. Broad-Spectrum Antiviral Strategies and Nucleoside Analogues. *Viruses* **13**, 667 (2021).
35. FDA. Antiviral Product Development — Conducting and Submitting Virology Studies to the Agency. 17 (2006).
36. Bertolini, A. *et al.* Paracetamol: New Vistas of an Old Drug. *CNS Drug Rev.* **12**, 250–275 (2006).
37. Watashi, K. Alisporivir, a cyclosporin derivative that selectively inhibits cyclophilin, for the treatment of HCV infection. *Curr. Opin. Investig. Drugs Lond. Engl.* **2000** **11**, 213–224 (2010).
38. Bishop, J. R., Schuksz, M. & Esko, J. D. Heparan sulphate proteoglycans fine-tune mammalian physiology. *Nature* **446**, 1030–1037 (2007).
39. Cagno, V., Tseligka, E. D., Jones, S. T. & Tapparel, C. Heparan Sulfate Proteoglycans and Viral Attachment: True Receptors or Adaptation Bias? *Viruses* **11**, E596 (2019).
40. Nahmias, A. J. & Kibrick, S. Inhibitory effect of heparin on herpes simplex virus. *J. Bacteriol.* **87**, 1060–6 (1964).
41. Vaheri, A. Heparin and Related Polyonic Substances as Virus Inhibitors. *Acta Pathol. Microbiol. Scand.* (1964).
42. Nahmias, A. J., Kibrick, S. & Bernfeld, P. Effect of Synthetic and Biological Polyanions on Herpes Simplex Virus. *Proc. Soc. Exp. Biol. Med.* **115**, 993–996 (1964).
43. Bianculli, R. H., Mase, J. D. & Schulz, M. D. Antiviral Polymers: Past Approaches and Future Possibilities. *Macromolecules* **53**, 9158–9186 (2020).
44. De Somer, P., De Clercq, E., Billiau, A., Schonne, E. & Claesen, M. Antiviral Activity of Polyacrylic and Polymethacrylic Acids. *J. Virol.* **2**, 878–885 (1968).
45. Smith, A. A. A. *et al.* Macromolecular (pro)drugs in antiviral research. *Polym. Chem.* **5**, 6407–6425 (2014).

46. Mammen, M., Choi, S. K. & Whitesides, G. M. Polyvalent interactions in biological systems: Implications for design and use of multivalent ligands and inhibitors. *Angew. Chem. - Int. Ed.* **37**, 2754–2794 (1998).
47. Fasting, C. *et al.* Multivalency as a chemical organization and action principle. *Angew. Chem. - Int. Ed.* **51**, 10472–10498 (2012).
48. Papp, I. *et al.* Inhibition of Influenza Virus Activity by Multivalent Glycoarchitectures with Matched Sizes. *ChemBioChem* **12**, 887–895 (2011).
49. Kwon, S. J. *et al.* Nanostructured glycan architecture is important in the inhibition of influenza A virus infection. *Nat. Nanotechnol.* **12**, 48–54 (2017).
50. Liese, S. & Netz, R. R. Quantitative Prediction of Multivalent Ligand–Receptor Binding Affinities for Influenza, Cholera, and Anthrax Inhibition. *ACS Nano* **12**, 4140–4147 (2018).
51. Kwon, S. J. *et al.* Nanostructured glycan architecture is important in the inhibition of influenza A virus infection. *Nat. Nanotechnol.* **12**, 48–54 (2017).
52. Dey, P. *et al.* Multivalent Flexible-Nanogels Exhibit Broad-Spectrum Antiviral Activity by Blocking Virus Entry. *ACS Nano* **12**, 6429–6442 (2018).
53. Szunerits, S., Barras, A., Khanal, M., Pagneux, Q. & Boukherroub, R. Nanostructures for the inhibition of viral infections. *Molecules* **20**, 14051–14081 (2015).
54. Jones, S. Jones Lab. <https://broadpectrumantivirals.com/research/>.
55. McCormack, S. *et al.* PRO2000 vaginal gel for prevention of HIV-1 infection (Microbicides Development Programme 301): a phase 3, randomised, double-blind, parallel-group trial. *The Lancet* **376**, 1329–1337 (2010).
56. Statement on carraguard phase III clinical trial findings | Microbicide Trials Network. <https://www.mtnstopshiv.org/news/statement-carraguard-phase-iii-clinical-trial-findings>.
57. Guédou, F., Pradeep, B. S., Ramjee, G. & Taylor, D. Lack of Effectiveness of Cellulose Sulfate Gel for the Prevention of Vaginal HIV Transmission. *N. Engl. J. Med.* **10** (2008).
58. Colacino, J. M. & Heinz, B. A. *Hepatitis prevention and treatment*. (2004).

59. Kocabiyik, O. *et al.* Non-Toxic Virucidal Macromolecules Show High Efficacy Against Influenza Virus Ex Vivo and In Vivo. *Adv. Sci.* 2001012 (2020) doi:10.1002/advs.202001012.
60. Heida, R. *et al.* Advances in the development of entry inhibitors for sialic-acid-targeting viruses. *Drug Discov. Today* (2020) doi:10.1016/j.drudis.2020.10.009.
61. Schandock, F. *et al.* Macromolecular Antiviral Agents against Zika, Ebola, SARS, and Other Pathogenic Viruses. *Adv. Healthc. Mater.* **6**, 1700748 (2017).
62. Donskyi, I. S. *et al.* Graphene Sheets with Defined Dual Functionalities for the Strong SARS-CoV-2 Interactions. *Small* **17**, 2007091 (2021).
63. Cheng, Y.-C. & Prusoff, William H. Relationship between the inhibition constant ( $K_i$ ) and the concentration of inhibitor which causes 50 per cent inhibition ( $I_{50}$ ) of an enzymatic reaction. **22**, 3099–3108 (1973).
64. Cheng, H. C. The power issue: determination of  $K_B$  or  $K_i$  from  $IC_{50}$ . A closer look at the Cheng-Prusoff equation, the Schild plot and related power equations. *J. Pharmacol. Toxicol. Methods* **46**, 61–71 (2001).
65. Baram-Pinto, D., Shukla, S., Perkas, N., Gedanken, A. & Sarid, R. Inhibition of Herpes Simplex Virus Type 1 Infection by Silver Nanoparticles Capped with Mercaptoethane Sulfonate. *Bioconjug. Chem.* **20**, 1497–1502 (2009).
66. Shogan, B., Kruse, L., Mulamba, G. B., Hu, A. & Coen, D. M. Virucidal Activity of a GT-Rich Oligonucleotide against Herpes Simplex Virus Mediated by Glycoprotein B. *J. Virol.* **80**, 4740–4747 (2006).
67. Cagno, V. *et al.* Broad-spectrum non-toxic antiviral nanoparticles with a virucidal inhibition mechanism. *Nat. Mater.* **17**, 195–203 (2018).
68. Jones, S. T. *et al.* Modified cyclodextrins as broad-spectrum antivirals. *Sci. Adv.* **6**, eaax9318 (2020).
69. Del Valle, E. M. M. Cyclodextrins and their uses: a review. *Process Biochem.* **39**, 1033–1046 (2004).
70. Davis, M. E. & Brewster, M. E. Cyclodextrin-based pharmaceuticals: past, present and future. *Nat. Rev. Drug Discov.* **3**, 1023–1035 (2004).

71. Anand, R., Nayyar, S., Pitha, J. & Merrill, C. R. Sulphated Sugar Alpha-Cyclodextrin Sulphate, a Uniquely Potent Anti-HIV Agent, Also Exhibits Marked Synergism with AZT, and Lymphoproliferative Activity. *Antivir. Chem. Chemother.* **1**, 41–46 (1990).
72. Moriya, T. *et al.* A new candidate for an anti-HIV-1 agent: modified cyclodextrin sulfate (mCDS71). *J. Med. Chem.* **36**, 1674–1677 (1993).
73. Guven, Z. P. *et al.* Synthesis and Characterization of Amphiphilic Gold Nanoparticles. *J. Vis. Exp.* (2019) doi:10.3791/58872.
74. Verma, A. & Stellacci, F. Effect of surface properties on nanoparticle-cell interactions. *Small* **6**, 12–21 (2010).
75. Yeh, Y.-C., Creran, B. & Rotello, V. M. Gold nanoparticles: preparation, properties, and applications in bionanotechnology. *Nanoscale* **4**, 1871–1880 (2012).
76. Mirza, A. Z. A novel drug delivery system of gold nanorods with doxorubicin and study of drug release by single molecule spectroscopy. *J. Drug Target.* **23**, 52–58 (2015).
77. Mirza, A. Z. & Shamshad, H. Fabrication and characterization of doxorubicin functionalized PSS coated gold nanorod. *Arab. J. Chem.* **12**, 146–150 (2019).
78. Nel, A. E. *et al.* Understanding biophysicochemical interactions at the nano–bio interface. *Nat. Mater.* **8**, 543–557 (2009).
79. Yeo, E. L. L. *et al.* Protein Corona around Gold Nanorods as a Drug Carrier for Multimodal Cancer Therapy. *ACS Biomater. Sci. Eng.* **3**, 1039–1050 (2017).
80. Lin, J. & Alexander-Katz, A. Cell Membranes Open “Doors” for Cationic Nanoparticles/Biomolecules: Insights into Uptake Kinetics. *ACS Nano* **7**, 10799–10808 (2013).
81. Saha, K. *et al.* Regulation of Macrophage Recognition through the Interplay of Nanoparticle Surface Functionality and Protein Corona. *ACS Nano* **10**, 4421–4430 (2016).
82. Fabrication of Corona-Free Nanoparticles with Tunable Hydrophobicity | ACS Nano. <https://pubs.acs.org/doi/10.1021/nn5006478>.

83. Pengo, P. *et al.* Gold nanoparticles with patterned surface monolayers for nanomedicine: current perspectives. *Eur. Biophys. J.* **46**, 749–771 (2017).
84. Kuna, J. J. *et al.* The effect of nanometre-scale structure on interfacial energy. *Nat. Mater.* **8**, 837–842 (2009).
85. Verma, A. *et al.* Surface-structure-regulated cell-membrane penetration by monolayer-protected nanoparticles. *Nat. Mater.* **7**, 588–595 (2008).
86. Van Lehn, R. C. *et al.* Lipid tail protrusions mediate the insertion of nanoparticles into model cell membranes. *Nat. Commun.* **5**, 4482 (2014).
87. Uzun, O. *et al.* Water-soluble amphiphilic gold nanoparticles with structured ligand shells. *Chem. Commun.* 196–198 (2008) doi:10.1039/b713143g.
88. Huang, R., Carney, R. P., Stellacci, F. & Lau, B. L. T. Colloidal Stability of Self-Assembled Monolayer-Coated Gold Nanoparticles: The Effects of Surface Compositional and Structural Heterogeneity. *Langmuir* **29**, 11560–11566 (2013).
89. Carney, R. P. *et al.* Electrical method to quantify nanoparticle interaction with lipid bilayers. *ACS Nano* **7**, 932–942 (2013).
90. Van Lehn, R. C. *et al.* Effect of particle diameter and surface composition on the spontaneous fusion of monolayer-protected gold nanoparticles with lipid bilayers. *Nano Lett.* **13**, 4060–4067 (2013).
91. Huang, R., Carney, R. P., Ikuma, K., Stellacci, F. & Lau, B. L. T. Effects of surface compositional and structural heterogeneity on nanoparticle-protein interactions: Different protein configurations. *ACS Nano* **8**, 5402–5412 (2014).
92. Lehn, R. C. V. & Alexander-Katz, A. Free energy change for insertion of charged, monolayer-protected nanoparticles into lipid bilayers. *Soft Matter* **10**, 648–658 (2013).
93. Ong, Q., Luo, Z. & Stellacci, F. Characterization of Ligand Shell for Mixed-Ligand Coated Gold Nanoparticles. *Acc. Chem. Res.* **50**, 1911–1919 (2017).
94. Marbella, L. E. & Millstone, J. E. NMR Techniques for Noble Metal Nanoparticles. *Chem. Mater.* **27**, 2721–2739 (2015).

95. Templeton, A. C., Hostetler, M. J., Kraft, C. T. & Murray, R. W. Reactivity of Monolayer-Protected Gold Cluster Molecules: Steric Effects. *J. Am. Chem. Soc.* **120**, 1906–1911 (1998).
96. Harkness, K. M. *et al.* A Structural Mass Spectrometry Strategy for the Relative Quantitation of Ligands on Mixed Monolayer-Protected Gold Nanoparticles. *Anal. Chem.* **82**, 9268–9274 (2010).
97. Rentsch, M. B. & Zimmer, G. A Vesicular Stomatitis Virus Replicon-Based Bioassay for the Rapid and Sensitive Determination of Multi-Species Type I Interferon. *PLOS ONE* **6**, e25858 (2011).
98. Fukushi, S. *et al.* Vesicular stomatitis virus pseudotyped with severe acute respiratory syndrome coronavirus spike protein. *J. Gen. Virol.* **86**, 2269–2274.
99. Haldar, J., Weight, A. K. & Klibanov, A. M. Preparation, application and testing of permanent antibacterial and antiviral coatings. *Nat. Protoc.* **2**, 2412–2417 (2007).
100. Weis, W. *et al.* Structure of the influenza virus haemagglutinin complexed with its receptor, sialic acid. *Nature* **333**, 426–431 (1988).
101. Kim, I. S. *et al.* Mechanism of membrane fusion induced by vesicular stomatitis virus G protein. *Proc. Natl. Acad. Sci.* **114**, E28–E36 (2017).
102. Nikolic, J. *et al.* Structural basis for the recognition of LDL-receptor family members by VSV glycoprotein. *Nat. Commun.* **9**, 1029 (2018).
103. Cagno, V. *et al.* Highly Sulfated K5 Escherichia coli Polysaccharide Derivatives Inhibit Respiratory Syncytial Virus Infectivity in Cell Lines and Human Tracheal-Bronchial Histocultures. *Antimicrob. Agents Chemother.* **58**, 4782–4794 (2014).
104. Stevens, J., Blixt, O., Paulson, J. C. & Wilson, I. A. Glycan microarray technologies: tools to survey host specificity of influenza viruses. *Nat. Rev. Microbiol.* **4**, 857–864 (2006).
105. Leibbrandt, A. *et al.* Iota-Carrageenan Is a Potent Inhibitor of Influenza A Virus Infection. *PLOS ONE* **5**, e14320 (2010).
106. Covés-Datson, E. M. *et al.* A molecularly engineered antiviral banana lectin inhibits fusion and is efficacious against influenza virus infection in vivo. *Proc. Natl. Acad. Sci.* **117**, 2122–2132 (2020).

107. Pruijssers, A. J. *et al.* Remdesivir Inhibits SARS-CoV-2 in Human Lung Cells and Chimeric SARS-CoV Expressing the SARS-CoV-2 RNA Polymerase in Mice. *Cell Rep.* **32**, 107940 (2020).
108. Beigel, J. H. *et al.* Remdesivir for the Treatment of Covid-19 — Final Report. *N. Engl. J. Med.* (2020) doi:10.1056/NEJMoa2007764.
109. Consortium, W. S. trial *et al.* Repurposed antiviral drugs for COVID-19 –interim WHO SOLIDARITY trial results. *medRxiv* 2020.10.15.20209817 (2020) doi:10.1101/2020.10.15.20209817.
110. Hoffmann, M. *et al.* Chloroquine does not inhibit infection of human lung cells with SARS-CoV-2. *Nature* **585**, 588–590 (2020).
111. Maisonnasse, P. *et al.* Hydroxychloroquine use against SARS-CoV-2 infection in non-human primates. *Nature* **585**, 584–587 (2020).
112. NIH halts clinical trial of hydroxychloroquine. *National Institutes of Health (NIH)* <https://www.nih.gov/news-events/news-releases/nih-halts-clinical-trial-hydroxychloroquine> (2020).
113. Group, T. R. C. Dexamethasone in Hospitalized Patients with Covid-19. *N. Engl. J. Med.* (2020) doi:10.1056/NEJMoa2021436.
114. Xu, X. *et al.* Effective treatment of severe COVID-19 patients with tocilizumab. *Proc. Natl. Acad. Sci. U. S. A.* **117**, 10970–10975 (2020).
115. Srivastava, S., Garg, I., Bansal, A. & Kumar, B. COVID-19 infection and thrombosis. *Clin. Chim. Acta Int. J. Clin. Chem.* **510**, 344–346 (2020).
116. Stencel-Baerenwald, J. E., Reiss, K., Reiter, D. M., Stehle, T. & Dermody, T. S. The sweet spot: defining virus–sialic acid interactions. *Nat. Rev. Microbiol.* **12**, 739–749 (2014).
117. Li, W. *et al.* Identification of sialic acid-binding function for the Middle East respiratory syndrome coronavirus spike glycoprotein. *Proc. Natl. Acad. Sci. U. S. A.* **114**, E8508–E8517 (2017).
118. Milewska, A. *et al.* Human coronavirus NL63 utilizes heparan sulfate proteoglycans for attachment to target cells. *J. Virol.* **88**, 13221–13230 (2014).
119. Lang, J. *et al.* Inhibition of SARS Pseudovirus Cell Entry by Lactoferrin Binding to Heparan Sulfate Proteoglycans. *PLOS ONE* **6**, e23710 (2011).

120. Mathewson, A. C. *et al.* Interaction of severe acute respiratory syndrome-coronavirus and NL63 coronavirus spike proteins with angiotensin converting enzyme-2. *J. Gen. Virol.* **89**, 2741–2745.
121. Zhou, P. *et al.* A pneumonia outbreak associated with a new coronavirus of probable bat origin. *Nature* **579**, 270–273 (2020).
122. Mycroft-West, C. J. *et al.* Heparin inhibits cellular invasion by SARS-CoV-2: structural dependence of the interaction of the surface protein (spike) S1 receptor binding domain with heparin. *bioRxiv* 2020.04.28.066761 (2020) doi:10.1101/2020.04.28.066761.
123. Clausen, T. M. *et al.* SARS-CoV-2 Infection Depends on Cellular Heparan Sulfate and ACE2. *Cell* **183**, 1043-1057.e15 (2020).
124. Milanetti, E. *et al.* In-Silico evidence for two receptors based strategy of SARS-CoV-2. *bioRxiv* 2020.03.24.006197 (2020) doi:10.1101/2020.03.24.006197.
125. Robson, B. Bioinformatics studies on a function of the SARS-CoV-2 spike glycoprotein as the binding of host sialic acid glycans. *Comput. Biol. Med.* **122**, 103849 (2020).
126. Kim, S. Y. *et al.* Characterization of heparin and severe acute respiratory syndrome-related coronavirus 2 (SARS-CoV-2) spike glycoprotein binding interactions. *Antiviral Res.* **181**, 104873 (2020).
127. Wolfert, M. SARS-CoV-2 spike protein binds heparan sulfate in a length- and sequence-dependent manner. 15.
128. Tiwari, V., Beer, J. C., Sankaranarayanan, N. V., Swanson-Mungerson, M. & Desai, U. R. Discovering small-molecule therapeutics against SARS-CoV-2. *Drug Discov. Today* **25**, 1535–1544 (2020).
129. Guimond, S. E. *et al.* Synthetic Heparan Sulfate Mimetic Pixatimod (PG545) Potently Inhibits SARS-CoV-2 By Disrupting The Spike-ACE2 interaction. *bioRxiv* 2020.06.24.169334 (2021) doi:10.1101/2020.06.24.169334.
130. Zhang, Q. Heparan sulfate assists SARS-CoV-2 in cell entry and can be targeted by approved drugs in vitro. 14 (2020).
131. Tree, J. A. *et al.* Unfractionated heparin inhibits live wild type SARS-CoV-2 cell infectivity at therapeutically relevant concentrations. *Br. J. Pharmacol.* **178**, 626–635 (2021).

132. Cagno, V. *et al.* Sulfonated Nanomaterials with Broad-Spectrum Antiviral Activity Extending beyond Heparan Sulfate-Dependent Viruses. *Antimicrob. Agents Chemother.* **64**, (2020).
133. Tandon, R. Effective Inhibition of SARS-CoV-2 Entry by Heparin and Enoxaparin Derivatives. 20.
134. Tseligka, E. D. *et al.* A VP1 mutation acquired during an enterovirus 71 disseminated infection confers heparan sulfate binding ability and modulates ex vivo tropism. *PLoS Pathog.* **14**, e1007190 (2018).
135. WuDunn, D. & Spear, P. G. Initial interaction of herpes simplex virus with cells is binding to heparan sulfate. *J. Virol.* **63**, 52–58 (1989).
136. Ghezzi, S. *et al.* Heparin prevents Zika virus induced-cytopathic effects in human neural progenitor cells. *Antiviral Res.* **140**, 13–17 (2017).
137. Vicenzi, E. *et al.* Coronaviridae and SARS-associated Coronavirus Strain HSR1. *Emerg. Infect. Dis.* **10**, 413–418 (2004).
138. Skidmore, M. A. *et al.* Inhibition of influenza H5N1 invasion by modified heparin derivatives. *MedChemComm* **6**, 640–646 (2015).
139. Vaillant, A. Nucleic acid polymers: Broad spectrum antiviral activity, antiviral mechanisms and optimization for the treatment of hepatitis B and hepatitis D infection. *Antiviral Res.* **133**, 32–40 (2016).
140. Sarrazin, S., Lamanna, W. C. & Esko, J. D. Heparan Sulfate Proteoglycans. *Cold Spring Harb. Perspect. Biol.* **3**, a004952–a004952 (2011).
141. Rusnati, M. *et al.* Sulfated K5 Escherichia coli polysaccharide derivatives: A novel class of candidate antiviral microbicides. *Pharmacol. Ther.* **123**, 310–322 (2009).
142. Tang, S. *et al.* Antiviral Agents from Multivalent Presentation of Sialyl Oligosaccharides on Brush Polymers. *ACS Macro Lett.* **5**, 413–418 (2016).
143. Cheng, H.-W. *et al.* Synthesis of S-linked NeuAc- $\alpha$ (2-6)-di-LacNAc bearing liposomes for H1N1 influenza virus inhibition assays. *Bioorg. Med. Chem.* **26**, 2262–2270 (2018).
144. Abela, I. A. *et al.* Cell-Cell Transmission Enables HIV-1 to Evade Inhibition by Potent CD4bs Directed Antibodies. *PLoS Pathog.* **8**, e1002634 (2012).

145. van Dongen, M. J. P. *et al.* A small-molecule fusion inhibitor of influenza virus is orally active in mice. *Science* **363**, eaar6221 (2019).
146. Ziem, B. *et al.* Polyvalent 2D Entry Inhibitors for Pseudorabies and African Swine Fever Virus. *Macromol. Biosci.* **17**, (2017).
147. Ziem, B. *et al.* Size-dependent inhibition of herpesvirus cellular entry by polyvalent nanoarchitectures. *Nanoscale* **9**, 3774–3783 (2017).
148. Donskyi, I. S. *et al.* Functionalized nanographene sheets with high antiviral activity through synergistic electrostatic and hydrophobic interactions. *Nanoscale* **11**, 15804–15809 (2019).
149. Tao, W., Richards, C. & Hamer, D. *Short Communication*: Enhancement of HIV Infection by Cellulose Sulfate. *AIDS Res. Hum. Retroviruses* **24**, 925–929 (2008).
150. Starpharma. <https://www.starpharma.com/vivagel>.
151. Weinhart, M., Gröger, D., Enders, S., Dervede, J. & Haag, R. Synthesis of dendritic polyglycerol anions and their efficiency toward L-selectin inhibition. *Biomacromolecules* **12**, 2502–2511 (2011).
152. Bhatia, S., Camacho, L. C. & Haag, R. Pathogen Inhibition by Multivalent Ligand Architectures. *J. Am. Chem. Soc.* **138**, 8654–8666 (2016).
153. Donskyi, I. *et al.* Interactions of Fullerene-Polyglycerol Sulfates at Viral and Cellular Interfaces. *Small Wein. Bergstr. Ger.* **14**, e1800189 (2018).
154. Ziem, B. *et al.* Highly Efficient Multivalent 2D Nanosystems for Inhibition of Orthopoxvirus Particles. *Adv. Healthc. Mater.* **5**, 2922–2930 (2016).
155. Bhatia, S. *et al.* Adaptive Flexible Sialylated Nanogels as Highly Potent Influenza A Virus Inhibitors. *Angew. Chem. Int. Ed Engl.* **59**, 12417–12422 (2020).
156. Bhatia, S. *et al.* Linear polysialoside outperforms dendritic analogs for inhibition of influenza virus infection in vitro and in vivo. *Biomaterials* **138**, 22–34 (2017).
157. Abbina, S. *et al.* Hyperbranched polyglycerols: recent advances in synthesis, biocompatibility and biomedical applications. *J. Mater. Chem. B* **5**, 9249–9277 (2017).

158. Cannalire, R. *et al.* SARS-CoV-2 Entry Inhibitors: Small Molecules and Peptides Targeting Virus or Host Cells. *Int. J. Mol. Sci.* **21**, 5707 (2020).
159. Chen, Z., Du, R., Galvan Achi, J. M., Rong, L. & Cui, Q. SARS-CoV-2 cell entry and targeted antiviral development. *Acta Pharm. Sin. B* (2021) doi:10.1016/j.apsb.2021.05.007.
160. Chitsike, L. & Duerksen-Hughes, P. Keep out! SARS-CoV-2 entry inhibitors: their role and utility as COVID-19 therapeutics. *Viol. J.* **18**, 154 (2021).
161. Nie, C. *et al.* Polysulfates Block SARS-CoV-2 Uptake through Electrostatic Interactions\*\*. *Angew. Chem. Int. Ed.* **60**, 15870–15878 (2021).
162. Rosenke, K. *et al.* Orally delivered MK-4482 inhibits SARS-CoV-2 replication in the Syrian hamster model. *Nat. Commun.* **12**, 2295 (2021).
163. Morawska, L. & Cao, J. Airborne transmission of SARS-CoV-2: The world should face the reality. *Environ. Int.* **139**, 105730 (2020).
164. Boone, S. A. & Gerba, C. P. Significance of Fomites in the Spread of Respiratory and Enteric Viral Disease. *Appl. Environ. Microbiol.* **73**, 1687–1696 (2007).
165. Gall, A. M., Mariñas, B. J., Lu, Y. & Shisler, J. L. Waterborne Viruses: A Barrier to Safe Drinking Water. *PLOS Pathog.* **11**, e1004867 (2015).
166. Goldman, E. Exaggerated risk of transmission of COVID-19 by fomites. *Lancet Infect. Dis.* **20**, 892–893 (2020).
167. Coronavirus is in the air — there’s too much focus on surfaces. *Nature* **590**, 7–7 (2021).
168. CDC. Coronavirus Disease 2019 (COVID-19). *Centers for Disease Control and Prevention* <https://www.cdc.gov/coronavirus/2019-ncov/more/science-and-research/surface-transmission.html> (2020).
169. Rakowska, P. D. *et al.* Antiviral surfaces and coatings and their mechanisms of action. *Commun. Mater.* **2**, 1–19 (2021).
170. Sun, Z. & Ostrikov, K. (Ken). Future antiviral surfaces: Lessons from COVID-19 pandemic. *Sustain. Mater. Technol.* **25**, e00203 (2020).

171. Hsu, B. B., Yinn Wong, S., Hammond, P. T., Chen, J. & Klibanov, A. M. Mechanism of inactivation of influenza viruses by immobilized hydrophobic polycations. *Proc. Natl. Acad. Sci.* **108**, 61–66 (2011).

## List of publications

E. Mohammadifar<sup>+</sup>, **M. Gasbarri**<sup>+</sup>, V. Cagno, K. Achazi, C. Tapparel, R. Haag<sup>\*</sup>, F. Stellacci<sup>\*</sup>, “Polyanionic amphiphilic dendritic polyglycerols as broad-spectrum viral inhibitors with a virucidal mechanism”, *submitted*.  
<sup>+</sup> EM and MG contributed equally to this work.

Ł. Richter, K. Paszkowska, U. Cendrowska, F. Olgiati, P. Silva, **M. Gasbarri**, P. Guven, J. Paczesny and F. Stellacci “Broad-spectrum nanoparticles against bacteriophage infections”, *Nanoscale* (2021)

E. Canepa, D. Bochicchio, **M. Gasbarri**, D. Odino, C. Canale, R. Ferrando, F. Canepa, F. Stellacci, G. Rossi, S. Dante, A. Relini, “Cholesterol hinders passive uptake of amphiphilic nanoparticles into fluid lipid membranes”, *The Journal of Physical Chemistry Letters* (2021) 12 (35), 8583-8590

A. Palika, A. Armanious, A. Rahimi, C. Medaglia, **M. Gasbarri**, S. Handschin, A. Rossi, M. Pohl, I. Busnadiego, C. Gübeli, R. Anjanappa, S. Bolisetty, M. Peydayesh, S. Stertz, B. Hale, C. Tapparel, F. Stellacci, R. Mezzenga, “An anti-viral trap made of protein nanofibrils and iron oxyhydroxide nanoparticles”, *Nature Nanotechnology* 16, 918–925 (2021)

**M. Gasbarri**, P. V'kovski, G. Torriani, V. Thiel, F. Stellacci, C. Tapparel, V. Cagno, “SARS-CoV-2 inhibition by sulfonated compounds”, *Microorganisms* 8 (12), 1894 (2020)

V. Cagno, **M. Gasbarri**, C. Medaglia, D. Gomes, S. Clement, F. Stellacci, C. Tapparel, “Sulfonated nanomaterials with broad-spectrum antiviral activity extending beyond heparan sulfate-dependent viruses”, *Antimicrobial Agents and Chemotherapy* 64 (12) (2020)

R. Heida, Y. C. Bhide<sup>\*</sup>, **M. Gasbarri**<sup>\*</sup>, Ö. Kocabiyik, F. Stellacci, A.L.W. Huckriede, W.L.J. Hinrichs, H.W. Frijlink, “Advances in the development of entry inhibitors for sialic-acid-targeting viruses”, *Drug Discovery Today* 26(1), 122-137 (2020)

S. T. Jones, V. Cagno, M. Janeček, D. Ortiz, N. Gasilova, J. Piret, **M. Gasbarri**, D. A. Constant, Y. Han, L. Vuković, P. Král, L. Kaiser, S. Huang, S. Constant, K. Kirkegaard, G. Boivin, F. Stellacci, C. Tapparel, “Modified cyclodextrins as broad-spectrum antivirals”, *Science Advances* 6(5), eaax9381 (2020)

Z. P. Guven, P.H.J. Silva, Z. Luo, U. B. Cendrowska, **M. Gasbarri**, S. T. Jones, F. Stellacci “Synthesis and Characterization of Amphiphilic Gold Nanoparticles”, *Journal of Visual Experiments* 149, e58872, (2019)

## List of patents

“Sulfated and sulfonated dendritic polyglycerols and use thereof as broad-spectrum virucidal agents”, **M. Gasbarri**, E. Mohammadifar, R. Haag, F. Stellacci, PCT/EP2021/071188, filed 28 July 2021, claiming the priority of EP 20 188 654. 6 filed 30.07.20.

“Virucidal compositions and use thereof”, **M. Gasbarri**, E. Mohammadifar, R. Haag, F. Stellacci, PCT/EP2021/07990, filed 27 July 2021, claiming the priority of EP 20 188 654. 6 filed 30.07.20.



# Curriculum Vitae

## Matteo Gasbarri

Rue Jean-Louis-De-Bons, 2

Lausanne (CH) 1006

+41 77 917 38 76

[gasbarri.matteo@gmail.com](mailto:gasbarri.matteo@gmail.com)

[www.linkedin.com/in/matteo-gasbarri](http://www.linkedin.com/in/matteo-gasbarri)

### Strengths:

- Academic and industrial experience in 4 countries
- Strong analytical mindset
- Team-player attitude
- Passionate about innovation



### EDUCATION

---

2017 – to date	<b>Ph.D. in Materials Science and Engineering</b> Swiss Federal Institute of Technology (EPFL), Switzerland
2014 – 2016	<b>M.Sc. in Science and Technology of Materials</b> University of Rome "Tor Vergata", Italy - 110/110 cum laude - GPA: 29.4/30 Erasmus+ Exchange at University of Technology of Eindhoven (TU/e), the Netherlands
2010 – 2014	<b>B.Sc. in Materials Science</b> University of Rome "Tor Vergata", Italy - 110/110 cum laude - GPA: 28.4/30

### ADDITIONAL EDUCATION

---

2021	Business Concept Training (InnoSuisse)
2020	Prince 2 Project Management Foundation Certification Training (Axelos)
2020	Management of Innovation and Technology Transfer (TTO-EPLF)
2019	Drug and Device Product Development and Regulation in Europe and the United States (EPFL and San Diego University)

**EXPERIENCE**

---

- 2017-2021      **Doctoral Assistant**, EPFL, Switzerland  
Design of novel antivirals with broad-spectrum and virucidal activity:
- Synthesis and characterization of nanoparticles, cyclodextrins and dendrimers
  - *In vitro* and *ex vivo* testing of antivirals (HSV-2, SARS-CoV-2)
  - Translation into pre-clinical studies, with the design of PK and *in vivo* experiments in collaboration with CROs
- 2018 – 2021      **Safety deputy** and **BioSafety Officer**, EPFL, Switzerland  
Responsible for the compliance to safety regulations in chemical and biological lab (nano, BSL-2, BSL-3). Design of a new NanoLab. Acquisition of new equipment (80kCHF)
- 2017      **Process Engineer for Solar Cells** - Saule Technologies, Poland  
Development of inks and processes for novel flexible perovskite solar cells
- 2015 – 2016      **Intern** at Centre for Hybrid and Organic Solar Energy (CHOSE), Italy  
Development of novel inorganic layers for low-T flexible perovskite solar cells
- 2015      **Intern** at Chemical Engineering Dept at TU/e, the Netherlands  
Optimization of graphene-based ink formulation
- 2013 – 2014      **Intern** at Institute of Microelectronics and Microsystems (CNR-IMM), Italy  
Microfabrication of silicon nanotubes from sacrificial nanowires

**TECHNICAL SKILLS**

---

- Materials Science:** TEM, NMR, TGA, UV-Vis, nanomaterials synthesis, thin film deposition, profilometry, XRD, Clean Room, GloveBox, CVD, RIE, SEM, XPS.
- Biology:** Activity in BSL-2 (HSV-2), BSL-3 (SARS-CoV-2), wet lab, cell lines (VERO, HeLA), cytotoxicity, antiviral assays, qPCR, SPR.
- Innovation:** Management of Innovation, IP policy, Regulatory Affairs, Project Management (Prince2). Filing of two patents.
- IT:** GraphPad Prism, Origin, ImageJ, Illustrator, MS Office (ppt, doc, xcl), iOS

**LANGUAGES**

---

Fluent in **English** and **French**, beginner in **German**, native in **Italian**

**PATENTS**

---

"Sulfated and sulfonated dendritic polyglycerols and use thereof as broad-spectrum virucidal agents", **M. Gasbarri**, E. Mohammadifar, R. Haag, F. Stellacci, PCT/EP2021/071188, filed 28 July 2021, claiming the priority of EP 20 188 654. 6 filed 30.07.20.

"Virucidal compositions and use thereof", **M. Gasbarri**, E. Mohammadifar, R. Haag, F. Stellacci, PCT/EP2021/07990, filed 27 July 2021, claiming the priority of EP 20 188 654. 6 filed 30.07.20.

**AWARDS**

---

2015 – 2016	Award for Merit (Premio per Merito) – top 5% of the students
2011 – 2012	Award for Merit (Studenti Meritevoli) – based on average grade/credits

**PERSONAL INFORMATION**

---

29 y.o., single, Italian Citizenship, Swiss permit B, Swiss B Driving License.

In 2016, I co-founded TorPiuBella, an association focused on urban and social regeneration in my neighborhood in Rome. I have played basketball for 20 years and skied for the last 5.  
Interest in politics, culture, sport and food.

**PUBLICATIONS**

---

E. Mohammadifar<sup>+</sup>, **M. Gasbarri**<sup>+</sup>, V. Cagno, K. Achazi, C. Tapparel, R. Haag\*, F. Stellacci\*, "Polyanionic amphiphilic dendritic polyglycerols as broad-spectrum viral inhibitors with a virucidal mechanism", *submitted*.  
<sup>+</sup> EM and MG equally contributed to this work.

Ł. Richter, K. Paszkowska, U. Cendrowska, F. Olgiati, P. Silva, **M. Gasbarri**, P. Guven, J. Paczesny and F. Stellacci "Broad-spectrum nanoparticles against bacteriophage infections", *Nanoscale* (2021)

E. Canepa, D. Bochicchio, **M. Gasbarri**, D. Odino, C. Canale, R. Ferrando, F. Canepa, F. Stellacci, G. Rossi, S. Dante, A. Relini, "Cholesterol hinders passive uptake of amphiphilic nanoparticles into fluid lipid membranes", *The Journal of Physical Chemistry Letters* (2021) 12 (35), 8583-8590

A. Palika, A. Armanious, A. Rahimi, C. Medaglia, **M. Gasbarri**, S. Handschin, A. Rossi, M. Pohl, I. Busnadiego, C. Gübeli, R. Anjanappa, S. Bolisetty, M. Peydayesh, S. Stertz, B. Hale, C. Tapparel, F. Stellacci, R. Mezzenga, "An anti-viral trap made of protein nanofibrils and iron oxyhydroxide nanoparticles", *Nature Nanotechnology* (2021)

**M. Gasbarri**, P. V'kovski, G. Torriani, V. Thiel, F. Stellacci, C. Tapparel, V. Cagno, "SARS-CoV-2 inhibition by sulfonated compounds", *Microorganisms* 8 (12), 1894 (2020)

V. Cagno, **M. Gasbarri**, C. Medaglia, D. Gomes, S. Clement, F. Stellacci, C. Tapparel, "Sulfonated nanomaterials with broad-spectrum antiviral activity extending beyond heparan sulfate-dependent viruses", *Antimicrobial Agents and Chemotherapy* 64 (12) (2020)

R. Heida, Y. C. Bhide\*, **M. Gasbarri**\*, Ö. Kocabiyik, F. Stellacci, A.L.W. Huckriede, W.L.J. Hinrichs, H.W. Frijlink, "Advances in the development of entry inhibitors for sialic-acid-targeting viruses", *Drug Discovery Today* 26(1), 122-137 (2020)

S. T. Jones, V. Cagno, M. Janeček, D. Ortiz, N. Gasilova, J. Piret, **M. Gasbarri**, D. A. Constant, Y. Han, L. Vuković, P. Král, L. Kaiser, S. Huang, S. Constant, K. Kirkegaard, G. Boivin, F. Stellacci, C. Tapparel, "Modified cyclodextrins as broad-spectrum antivirals", *Science Advances* 6(5), eaax9381 (2020)

Z. P. Guven, , P.H.J. Silva, Z. Luo, U. B. Cendrowska, **M. Gasbarri**, S. T. Jones, F. Stellacci "Synthesis and Characterization of Amphiphilic Gold Nanoparticles", Journal of Visual Experiments 149, e58872, (2019)

J. Dagar, S. Castro-Hermosa, **M. Gasbarri**, A. L. Palma, L. Cinà, F. Matteocci, E. Calabrò, A. Di Carlo, T. M. Brown "Efficient Low Temperature Flexible Perovskite Module and Solar Cell Based on Solution-Processed SnO<sub>2</sub>/meso-TiO<sub>2</sub> Scaffold Electron Transport Layers", Nano Research 11 2669 (2018)

---

## PRESENTATIONS

---

03/2021	International Conference on Antiviral Research: ICAR21 (Poster)
07/2019	International Union of Pure and Applied Chemistry Conference (Invited Talk)
06/2019	Novartis FreeNovation final meeting (Talk and Poster)
05/2019	NCCR Bio-Materials Conference (Talk)
04/2019	MEGA Seminar (EPFL Mechanical Engineering Dept. Seminar) (Talk)
01/2019	Global Young Scientists Summit: GYSS19 (Poster)
09/2018	International conference on Nanomedicine and Nanobiotechnology
06/2016	Hybrid and Organic Photovoltaics:HOPV16 (Poster)

---

## FAIRES & SCHOOLS

---

01/2018	Winter School: "Nanoparticles: from Fundamentals to applications in Life Science"
09/2017	Hannover Messe (for Saule Technologies)
10/2016	Maker Faire 4.0